Charles University
Faculty of Science
Department of Experimental Plant Biology
Program: Plant Anatomy and Physiology

IST Austria
Group Plant Cell and Developmental Biology





Mgr. Matouš Glanc

Mechanisms of establishment and maintenance of PIN polarity in *Arabidopsis*

Mechanismy ustavení a udržení polarity PIN přenašečů v *Arabidopsis*

PhD Thesis

Supervisor: prof. Jiří Friml
Co-advisors: prof. Eva Zažímalová; Mgr. Matyáš Fendrych, PhD

Prague, 2018

Statement:

I hereby state that I have completed this thesis by myself and that I have properly cited all literature and other information sources I have used. Neither this thesis nor its parts have been submitted to achieve any other academic title(s).

Prohlášení:

Prohlašuji, že jsem závěrečnou práci zpracoval samostatně a že jsem uvedl všechny použité informační zdroje a literaturu. Tato práce ani její podstatná část nebyla předložena k získání jiného nebo stejného akademického titulu.

In Prague, 20.11.2018

Signature / Podpis

Abstract

Cell polarity is a key concept in plant biology. The subcellular localization of Pin-formed (PIN) auxin efflux carriers in the root of *Arabidopsis* is remarkably asymmetrical, making PINs prominent markers to study cell polarity. In spite of its developmental importance and two decades of research, the molecular basis of PIN polarity remains largely unknown. In this thesis, I employed advanced transgenic and fluorescence microscopy approaches to gain insight into several aspects of PIN polarity regulation. I participated in establishing a novel genetically encoded inhibitor of endocytosis, an invaluable tool for the study of the importance of endocytosis for various cellular processes, including PIN polarity. I demonstrated that apical polarity of PIN2 needs to be re-established after cell division and that this process depends on endocytosis, *de novo* protein secretion and the action of WAG1 and related protein kinases, but not transcytosis, cell-cell signaling or intact cytoskeleton. Finally, I identified the previously unknown role of MAB4/MEL proteins in PIN polarity, which lies in the ability of MAB4/MELs to reduce PIN lateral diffusion and thus contribute to PIN polarity maintenance. My results, besides broadening current understanding of PIN polarity regulation, identify mechanisms that appear to be crucial for plant cell polarity as such, and are therefore promising topics for future research.

Keywords: Cell polarity, *Arabidopsis*, endocytosis, cytokinesis, auxin, PIN auxin efflux carriers

Abstrakt

Buněčná polarita představuje v biologii rostlin klíčový koncept. Subcelulární lokalizace auxinových přenašečů rodiny Pin-formed (PIN) v kořeni *Arabidopsis* je výrazně asymetrická, což činí z PIN proteinů důležitý model studia mechanismů regulujících buněčnou polaritu. I přes její význam pro rostlinný vývoj a dvě dekády usilovného výzkumu toho o molekulárním principu polarity PIN proteinů víme stále velmi málo. V této práci jsem se za využití pokročilých transgenních a fluorescenčně-mikroskopických přístupů zaměřil na studium několika aspektů regulace polarity PIN proteinů. Podílel jsem se na zavedení nového genetického nástroje pro inhibici endocytózy, který se ukázal velmi užitečným pro studium role endocytózy nejen v regulaci polarity PINů. Ukázal jsem, že apikální polarita proteinu PIN2 musí být po rozdělění buněk znovu ustavena a že tento proces závisí na endocytóze, sekreci nově syntetizovných proteinů a funkci WAG1 a příbuzných proteinových kináz; nikoli však na transcytóze, mezibuněčné signalizaci či neporušeném cytoskeletu. Nakonec jsem popsal dosud neznámou roli proteinů MAB4/MEL v regulaci polarity PINů, která spočívá ve schopnosti proteinů MAB4/MEL omezit laterální difuzi PIN proteinů v plazmatické membráně a tím přispět k udržení jejich polární lokalizace. Mé výsledky, kromě přispění k současným znalostem regulace polarity PIN proteinů, identifikují mechanismy, které jak se zdá hrají důležitou roli v buněčné polaritě jako takové, a jsou tak slibnými tématy pro budoucí výzkum.

Klíčová slova: Buněčná polarita, *Arabidopsis*, endocytóza, cytokineze, auxin, PIN přenašeče auxinu

Acknowledgements

First of all, I would like to thank Jiří for his supervision. He provided me with resources to do whatever needed to be done, with independence to do what I wanted to do, with freedom to organize my work as I saw fit, with a push when I needed one and with ideas and advice when I didn't know how to move forward. The environment I experienced in Jiří's group was one of mutual respect, where occasional scientific disagreements were not projected to personal relationships and where everyone had the opportunity to grow to fulfill their potential; for this, I would like to thank not only Jiří, but also all of my colleagues. I am also grateful to my co-advisor Eva, who supported me both scientifically and emotionally especially in the beginning of my PhD when things didn't go very well. And of course, I thank Matyáš for making huge conceptual contributions to all of my projects, teaching me a lot and being my closest peer and one of my best friends. Finally, thank you Natalia, for following me to Austria, standing beside me at all times, supporting my career at the expense of your own, and taking such great care of our daughter when I have been busy with PIN polarity!

Preface

I started my PhD in October 2014 with a proposal for the project called „Roles of ER in auxin signaling and metabolism “, which focused mainly on elucidating the function of ER-localized ABP1 in plant development. Three months later, the findings by Gao et al. (Gao et al., 2015) put almost everything that had been known about ABP1, and therefore also the foundations of my project, into question. After another year, work from our as well as other laboratories confirmed that Gao et al. were right in their original assumptions that most genetic material used to obtain pre-2015 knowledge about ABP1 was invalid (Michalko et al., 2015, 2016 (Chapter 9.1); Enders et al., 2015; Dai et al., 2015). In light of these events, halfway through the second year of my PhD, I decided to completely switch my focus and the topic of my PhD project from ABP1 to regulation of PIN polarity in newly divided cells and beyond.

The findings presented in the main body of this thesis represent approximately 2,5 years of work on the latter topic. Results related to my originally proposed PhD project, as well as findings that I participated in during the course of my PhD studies, but are not directly related to either of the two projects, are appended at the end of my thesis.

I sincerely apologize to all referees that the published manuscripts (chapters 4.1, 4.2, 9.1-9.4) are embedded as bitmap images, rather than regular text-containing PDFs, hence their content cannot be commented, highlighted, copy-pasted etc. Since 2017, Charles University requires all theses to be submitted in the PDF/A format, yet it provides zero assistance in converting conventional PDFs, such as those of the published manuscripts, to PDF/A. Furthermore, the submission system does not accept files converted to PDF/A using Adobe Acrobat Pro, the world’s leading PDF-editing program and the inventor of PDF/A, as well as PDF format as such, claiming such files do not comply with the PDF/A requirements. As a results, converting published PDFs to bitmap images is the only way to include them in a thesis. In my opinion, this is a disastrous policy which I intend to publicly speak up against in the near future.

Table of Contents

1. Summary 8

2. Introduction 10

2.1. Cell and protein polarity, its establishment and maintenance as key concepts in plant cell biology 10

2.2. PIN proteins: landmark of cell polarity studies in plants 11

2.3. Selected aspects of PIN polarity regulation 12

2.3.1. Clathrin mediated endocytosis 12

2.3.2. Cytoskeleton 13

2.3.3. Lateral diffusion 14

2.3.4. Phosphorylation 16

2.3.5. PIN polarity establishment and cytokinesis 18

3. Aims of the study 20

4. Results 21

4.1. A Functional Study of AUXILIN-LIKE1 and 2, Two Putative Clathrin Uncoating Factors in *Arabidopsis* 22

4.2. Mechanistic framework for cell-intrinsic re-establishment of PIN2 polarity after cell division 51

4.3. Generation of PIN2 polarity in the absence of functional cytoskeleton 69

4.4. Arabidopsis MAB4/MEL proteins mediate PIN polarity maintenance and root gravitropism by reducing PIN lateral diffusion 75

5. Discussion 98

5.1. PIN polarity establishment – secretion or recycling? 98

5.2. MEL proteins, lateral diffusion and PIN polarity maintenance 99

5.3. Phosphorylation-dependent regulation of PIN polarity 100

5.4. Theoretical concept of cell-intrinsic re-establishment of cell polarity after cytokinesis 102

6. Conclusions and outlook 104

7. List of abbreviations 106

8. References 107

9. Appendix 111

9.1. Strong morphological defects in conditional *Arabidopsis abp1* knock-down mutants generated in absence of functional ABP1 protein 112

9.2. Gibberellin DELLA signaling targets the retromer complex to redirect protein trafficking to the plasma membrane 125

9.3. Rapid and reversible root growth inhibition by TIR1 auxin signaling 142

9.4. Relative contribution of PIN-containing secretory vesicles and plasma membrane PINs to the directed auxin transport: theoretical estimation 169

9.5. Contributions to manuscripts 190

9.6. *Curriculum Vitae* 192

1. Summary

In biology, polarity refers to structured asymmetrical distribution of components along an axis. In this respect, the bodies of most plants are polarized at least in one direction – they grow roots underground, or along gravity, and shoots including leaves and flowers above ground, against gravity. In order to achieve this polarity on the level of the whole plant, every single cell needs to be polarized as well.

In the research group led by my supervisor Jiří Friml at IST Austria, we study cell polarity on the model of the PIN proteins. PINs are transporters of the plant hormone auxin that are typically found only at one end of each cell. By their polar subcellular localization, they direct the flux of auxin throughout the plant, which is in turn instructive to many developmental processes that shape the whole plant body and help it survive under ever-changing environmental conditions.

In spite of the importance of polar PIN localization for both cell and developmental plant biology, our knowledge of the molecular mechanisms underlying its regulation is still very limited. During the course of my PhD studies, I aimed to contribute to the understanding of the fascinating PIN polar localization.

For a long time, it has been known that endocytosis, or removal of molecules from the cell surface, plays an important role in regulating PIN polarity, but the exact mechanism has been enigmatic, partly due to lack of reliable tools to study it. In chapter 4.1 (Adamowski et al., 2018), we aimed to identify novel regulators of Clathrin-mediated endocytosis through a biochemical screen for Clathrin Light Chain interactors. Among the candidates, we found a pair of closely related, previously uncharacterized proteins with similarity to animal Auxilins that we called AUXILIN-like1 and 2. Functional characterization studies revealed that conditional overexpression of either of the two proteins can be used as a powerful tool to specifically inhibit endocytosis of, among other cargos, the PIN proteins.

The fact that PIN polarity is lost during cell division has been known almost as long as PIN polarity itself, but the mechanism by which it is subsequently re-established had remained unknown. In chapter 4.2 (Glanc et al., 2018), we developed tools to study the re-establishment of apical PIN2 polarity in newly divided cells in the primary root meristem and used them to systematically assess the importance of various cellular mechanisms for the process. We found that apical-basal polarity is in this context governed by cell-intrinsic cues. We showed that while *de novo* secretion and endocytosis

are indispensable, basal-to-apical transcytosis is not required for PIN2 polarity re-establishment. Furthermore, we demonstrated that the process depends on the action of WAG1, a protein kinase that phosphorylates PIN2 and is expressed specifically in dividing epidermal cells, and its homologues PID and WAG2.

This manuscript originally included a chapter where we demonstrated that PIN2 polarity can be generated also in a situation when both components of the plant cytoskeleton, microtubules and actin microfilaments, are pharmacologically depolymerized at the same time, implying that the main mechanism of PIN polarity establishment must be independent of cytoskeleton-guided endomembrane trafficking. Despite we were forced to remove this part from the paper during the peer-review process, we are convinced it is a conclusive and important piece of data, therefore we transformed it into a stand-alone 1-figure brief communication manuscript presented here as chapter 4.3.

A family of proteins called MAB4/MEL has been implicated in regulating PIN polarity, but as in the previous cases, the details of their function were not known. In chapter 4.4., we showed that while MAB4/MEL proteins are needed for proper PIN polarity, the PINs themselves are required for MAB4/MEL association with the plasma membrane. We demonstrated that this is achieved through physical interaction between the PINs and the MAB4/MELs, and that this interaction likely depends on the phosphorylation status of the PINs. Finally, we found that MAB4/MELs contribute to PIN polarity maintenance, but not establishment, by reducing their lateral diffusion-based escape into the neighboring plasma membrane domains.

All these findings add little pieces to the still very blurry puzzle of our understanding of the molecular mechanisms that govern polar subcellular localization of the PIN proteins. Furthermore, and perhaps more importantly, they identify several topics that appear to be crucial for plant cell polarity regulation in general, and the importance of which thus extends far beyond the PINs. These include spatially regulated endocytosis, which appears to be able to generate protein polarity even in the absence of cytoskeleton-guided vesicular trafficking, and the notion that information on cell polarity is, at least in the time-frame of a single round of the cell cycle, conveyed by a cell-intrinsic cue that is inherited from the mother to the daughter cells, rather than being communicated by cell-cell signaling from the neighboring cells.

Addressing these and similar questions in future research, and hopefully understanding the underlying molecular mechanisms in detail, will likely advance our understanding of cell polarity in plants incomparably more.

2. Introduction

2.1. Cell and protein polarity, its establishment and maintenance as key concepts in plant cell biology

Polarity *sensu lato* in a biological context refers to *"persistent asymmetrical and ordered distribution of structures along an axis"* (Cove, 2000). In this respect, higher plants are, like most other multicellular organisms, polarized at all levels of organization: the whole organism, individual organs, tissues and cells. Cell polarity thus refers to spatially oriented unequal distribution of cellular components including organelles, cytoskeletal strands and proteins (Grebe et al., 2001; Kania et al., 2014); when cell polarities within a tissue layer are coordinated, the term planar polarity is used (Nakamura and Grebe, 2018). Protein polarity can then be understood as asymmetrical distribution of molecules of a given protein within the cell. Consequently, the relationship between cell polarity and protein polarity can have bidirectional causality. Polarized distribution of a particular protein can be seen as a manifestation or readout of cell polarity. But at the same time, cell polarity is defined by asymmetrical distribution of its components, and therefore, at least in some cases, protein polarity must be the defining element of cell polarity.

In order to meet the requirement of persistence according to the definition above, both cell and protein polarity need to be first established and subsequently maintained. Regulation of these two processes is a fundamental topic of cell biology (Kania et al., 2014). While the underlying molecular mechanisms are relatively well described in animal systems, our understanding of cell and protein polarity establishment and maintenance in plants remains fragmented and incomplete.

In this thesis, I will describe previously unknown mechanisms regulating the establishment and maintenance of protein polarity of the canonical polar markers, the PIN-formed (PIN) auxin efflux carriers, and discuss the implications of my findings to the broader context of cell polarity regulation in plants.

2.2. PIN proteins: landmark of cell polarity studies in plants

The existence of an unknown polarized regulator of auxin efflux from cells was predicted more than 40 years ago based on the chemiosmotic model of intercellular auxin transport (Rubery and Sheldrake, 1974). 25 years later, this factor was found in the *PIN-formed (PIN)* gene family, named after the characteristic flowerless inflorescence phenotype of the knockout mutant in its founding member *PIN1* (Gälweiler et al., 1998). *PIN* genes, present in all plant genomes analyzed to date, encode proteins with ten transmembrane helices that act as auxin efflux carriers (Petrášek et al., 2006; Zourelidou et al., 2014). The genome of *Arabidopsis* encodes 5 "canonical" (PIN1-4,7) and 3 "non-canonical" (PIN5,6,8) PIN proteins that differ mainly by the length of their central hydrophilic loop and subcellular localization (Mravec et al., 2009; Bennett et al., 2014). While the "non-canonical" PINs possess a short hydrophilic loop and localize, at least in part, to the endoplasmic reticulum (Mravec et al., 2009; Ding et al., 2012; Ganguly et al., 2014; Simon et al., 2016b), all of the "canonical" PINs have a long central hydrophilic loop and are localized at the plasma membrane (PM). Typically, their distribution within the PM is highly asymmetrical – in other words, the PINs are a prominent example of polarly localized proteins (Friml and Palme, 2002). Polar localization of activated (Barbosa et al., 2014) PINs determines the directionality of intercellular auxin transport (Wisniewska et al., 2006), which is instructive for many developmental processes, such as embryo patterning, apical meristem organization, phyllotaxis, vascular development, tropic responses and more (reviewed in Adamowski and Friml, 2015).

Ever since its discovery 20 years ago, PIN polar localization has received substantial attention: in developmental biology for being instructive to auxin-mediated developmental processes, and in cell biology for being a great model to study the mechanisms of cell and protein polarity establishment and maintenance.

The root apical meristem is a popular model system for cell biological studies of cell polarity thanks to its well-defined tissue organization and accessibility to imaging and experimental manipulations. Cells in the root apical meristem possess at least four distinct PM domains: basal, apical, outer-lateral and inner-lateral, each of which is marked by the localization of specific protein markers (Kania et al., 2014). In normal conditions, PIN1 and PIN4 localize to and mark the basal PM domain of the stele, endodermis and cortex cells, while PIN2 is localized basally in young cortex, but shows pronounced apical localization in the lateral root cap, epidermis, and older cortex cells (Müller et al., 1998; Steinmann et al., 1999; Friml et al., 2002a; Friml and Palme, 2002; Kleine-Vehn et al.,

2008b). The outer-lateral domain is marked by proteins such as PEN3, PIS1 and BOR4, and BOR1 is a characteristic marker of the inner-lateral domain (Łangowski et al., 2010; Takano et al., 2010; Łangowski et al., 2016; Nakamura and Grebe, 2018).

The fact that PIN2 shows opposite polarity in epidermis and cortex demonstrates that PIN polarity depends on the cell type. On the other hand, when PIN1 is expressed ectopically from the promoter of *PIN2*, it localizes predominantly basally also in the epidermis, therefore sequence of the particular PIN plays an equally important role in determining its polarity (Wisniewska et al., 2006). This notion is further supported by the observation that one version of the PIN1-GFP translational reporter adopts apical localization when expressed in the epidermis, presumably due to disruption of basal targeting signal(s) encoded in the primary or secondary structure by the GFP insertion (Wisniewska et al., 2006). Moreover, even the polarity of a given PIN in a given cell type can change in response to internal or external stimuli (Friml et al., 2002b, 2004, Kleine-Vehn et al., 2008b, 2010; Prát et al., 2018; Grones et al., 2018). All these findings demonstrate that the localization of PINs can change in response to different inputs without massive alterations of tissue organization. Therefore, in the root apical meristem, PIN *protein polarity* is a readout and interpretation of *cell polarity* rather than its determinant.

Many aspects of PIN biology, including their evolution, structure, function, physiological and developmental relevance and multilevel regulation of expression, activity, trafficking and localization have been covered by recent reviews (Luschnig and Vert, 2014; Adamowski and Friml, 2015; Zhou and Luo, 2018). Here, instead of providing yet another extensive overview of all known mechanisms of PIN polarity regulation, I will focus on selected aspects that i) have been studied, but not fully understood, ii) cause certain controversies in the field and iii) are most relevant for the experimental part of my thesis.

2.3. Selected aspects of PIN polarity regulation

2.3.1. Clathrin-mediated endocytosis

Early studies with the fungal toxin Brefeldin A (BFA) revealed that PINs undergo constitutive recycling between the PM and endosomal compartments (Geldner et al., 2001, 2003; Grebe et al., 2003). The internalization step of this process happens through Clathrin-Mediated Endocytosis (CME) (Dhonukshe et al., 2007; Kitakura et al., 2011). Several different experimental approaches have established that defects in CME lead to

defects in PIN polarity (Men et al., 2008; Kitakura et al., 2011). However, the mechanistic basis of CME importance for PIN polarity remains unclear.

One proposed explanation postulates that PINs are initially secreted in an apolar manner and their polarity is subsequently established through endocytosis and polarized recycling (Dhonukshe et al., 2008; Kitakura et al., 2011; Richter et al., 2014). First and main evidence for this hypothesis came from Fluorescence Recovery After Photobleaching (FRAP) experiments: after whole-cell photobleaching, recovered PIN1-GFP signal was reported to be initially apolar and only later to acquire the characteristic basal polarity (Dhonukshe et al., 2008). However attractive, this hypothesis cannot be taken for fact, since the study that first introduced it has been retracted due to irreproducibility of that very same key experiment (Dhonukshe et al., 2014); and a directly contradicting observation was made in another paper (Łangowski et al., 2016).

Another theory proposes that CME acts on its own, rather than as a necessary pre-requisite for polar recycling, in PIN polarity maintenance by removing protein molecules that escape the basal or apical PM domain by lateral diffusion. This is supported by observations that a Clathrin light chain translational reporter CLC-GFP localizes more strongly to lateral than apical and basal cell sides, that point a mutation in a putative Clathrin-coated pit sorting motif in PIN2 leads to reduction of its polarity, and by mathematical modeling (Kleine-Vehn et al., 2011). Nevertheless, conclusive evidence for higher rates of PIN endocytosis on lateral sides and its direct requirement for PIN polarity is missing, therefore also this model requires further validation.

2.3.2. Cytoskeleton

One of the principal modes of action of the cytoskeleton lies in the regulation of endomembrane trafficking, and therefore the involvement of microtubules (MTs) and actin microfilaments in the regulation of PIN polarity is a long-standing question (Geldner et al., 2001).

When actin microfilaments were pharmacologically depolymerized by the application of Cytochalasin D or Latrunculin B, relocation of PIN1 from the PM to BFA-induced compartments and vice versa upon BFA washout was reduced, suggesting that intracellular trafficking routes of PIN1 were actin-dependent. Nevertheless, PIN1 polar PM localization was only weakly affected by the actin-depolymerizing treatments in the absence of BFA (Geldner et al., 2001; Boutté et al., 2006), questioning the relevance of actin-dependent, BFA-sensitive PIN1 trafficking for its polarity. Only marginal

importance of actin-guided trafficking for basal PIN localization was confirmed by similar experiments with basally localized PIN2 in young cortex cells (Kleine-Vehn et al., 2008b). In contrast, actin depolymerization led to pronounced defects of apical PIN2 localization in the epidermis and older cortex cells, indicating stricter dependence of apical PIN targeting on intact actin microfilaments (Kleine-Vehn et al., 2008b).

Treatment with the MT-depolymerizing agent Oryzalin had, regardless of the presence or absence of BFA, no effect on PIN1 localization in most cells. Nevertheless, ectopic PIN1 accumulation in irregular endomembrane patches could occasionally be observed. Since these patches were positive for the cytokinesis-specific syntaxin KNOLLE, and both PIN1 and KNOLLE colocalized to the cell plate (CP) of untreated dividing cells, the conclusion was drawn that in contrast to actin-dependent trafficking in the interphase, CP-targeting of PIN1 during cytokinesis followed a MT-dependent route (Geldner et al., 2001). However, the data presented also allow for an alternative interpretation: since close KNOLLE and PIN1 colocalization was retained, it might have been the biogenesis and morphology of the CP itself, rather than PIN1 targeting to this compartment, that was disrupted by the lack of MTs. This interpretation would not support a specific role of MT-dependent vesicular traffic for PIN targeting.

On the other hand, defects in basal localization of both PIN2 in young cortex and PIN1 in the stele were observed upon Oryzalin treatment of a comparable duration (5 vs. 6 hours); and prolonged (12 hours) Oryzalin treatment was reported to lead even to a basal-to-apical shift of both PIN1 and PIN2 localization (Kleine-Vehn et al., 2008b). Nevertheless, PIN localization studies in the *tonneau* mutants with disorganized MT arrays, as well as under even longer Oryzalin treatments (42 hours), showed that polar PIN1 localization could still be observed, but its coordination between cells was compromised. These data suggest that MTs are required for coordination of polarities within the tissue context, or planar polarity, rather than for establishment or maintenance of PIN polarity at the level of individual cells (Boutté et al., 2006).

In summary, when it comes to the role of the cytoskeleton in regulation of PIN polarity, not only the interpretations, but even the experimental observations lack a clear consensus, and the question thus remains wide open.

2.3.3. Lateral diffusion

In epithelial cells, a classical model system for cell polarity studies in animals, apical and basolateral polar PM domains are separated by tight junctions – multiprotein

complexes that prevent the diffusion of cargoes from one polar domain to the other, and thus play a key role in polarity maintenance (Wells et al., 2006). Plant root epidermal cells possess not two, but at least four distinct polar domains, yet no structure similar to the tight junction has been described (Kania et al., 2014). Therefore, it remains conceptually unclear how is the lateral diffusion-based mixing of cargoes belonging to different PM domains prevented.

Multiple reports from different groups have agreed that the lateral diffusion of PINs is slow compared to an apolar integral PM protein LTI6b or its close homolog LTI6a (Men et al., 2008; Kleine-Vehn et al., 2011; Martinière et al., 2012). However, this comparison is problematic, given the manyfold difference in size of the two proteins (PIN2 ~ 69 kDa, LTI6b ~ 6kDa). Comparing PIN1 and PIN2 mobility to bigger and therefore more appropriate apolar membrane protein controls PIP2 or NPSN12 (both ~ 30kDa) revealed that while the mobility of all these proteins was low, the differences between PINs and other polar proteins and nonpolar controls was very mild or non-existent (Martinière et al., 2012; Łangowski et al., 2016). Therefore, slow lateral diffusion is not a unique common characteristic of polar proteins (Łangowski et al., 2016) and hence it is unlikely involved in protein polarity establishment. This does not, however, exclude the possibility that slow lateral diffusion is a necessary prerequisite for protein polarity, possibly through being an important factor for polarity maintenance once it is established by other cellular mechanisms.

Arguing for this hypothesis, a link between PIN lateral diffusion, its polarity maintenance and the cell wall has been proposed based on the phenotype of a *cellulose synthase catalytic subunit 3 (cesa3)* mutant identified in a forward genetic screen for PIN polarity regulators (Feraru et al., 2011; Korbei and Luschnig, 2011). *cesa3* plants showed a basal-to-apical polarity shift of PIN1 expressed ectopically in the epidermis, this phenotype could be phenocopied by pharmacological interference with cellulose synthesis. Plasmolytic experiments revealed that PINs are physically connected to the cell wall in their polar domains, and both plasmolysis and pharmacological disruption of the cell wall led to increased PIN2 lateral diffusion (Feraru et al., 2011; Korbei and Luschnig, 2011). Increase of lateral diffusion upon cell wall disruption was observed also with free GFP linked to the PM by a GPI anchor (Martinière et al., 2012).

In summary, the cell wall physically restricts the mobility of all PM proteins that protrude into the apoplast (Martinière et al., 2012). Limited lateral diffusion mediated by

interactions with the cell wall is probably required for the maintenance, but not establishment, of polar localization of various proteins including the PINs.

2.3.4. Phosphorylation

One of the longest-known factors regulating PIN polarity is the (de)phosphorylation of their hydrophilic loops. The AGCVIII kinase PINOID (PID) and its homologues WAG1 and WAG2 phosphorylate PINs at three conserved Serine residues known as S1, S2 and S3; this is antagonized by dephosphorylation mediated by Protein Phosphatase 2A (PP2A) (Michniewicz et al., 2007; Dhonukshe et al., 2010). Overexpression of PID leads to basal-to-apical shift in polarity of PIN1, PIN4 and PIN2 in the cortex, while apical PIN2 polarity in the epidermis is defective in the *pid wag1 wag2* triple mutant (Friml et al., 2004; Dhonukshe et al., 2010). *pp2a* mutants display similar phenotypes as PID overexpressors and these are additive (Michniewicz et al., 2007). Finally, mutating the respective serine residues to phospho-mimicking glutamates in the PIN1-GFP sequence led to partial PIN1 apicalization, while introducing non-phosphorylable alanines in the PIN2-Venus sequence instead caused it to occasionally localize basally also in the epidermis; and prevented the PID overexpression effect on PIN2 apicalization in the cortex (Kleine-Vehn et al., 2009; Dhonukshe et al., 2010). All these findings point towards a very straight forward model, in which phosphorylated PINs are targeted to apical and dephosphorylated ones to the basal PM domain. Point mutation analysis of another putative serine phosphosite in the PIN1 hydrophilic loop showed results consistent with this model, despite this residue was not phosphorylated by PID *in vitro* (Zhang et al., 2010).

Nevertheless, there are certain discrepancies between this model and recent findings about the requirement of AGCVIII kinase-mediated PIN phosphorylation for their transport activity (Zourelidou et al., 2014; Barbosa et al., 2018). It was shown that D6 protein kinase (D6PK), another member of the AGCVIII kinase clade, phosphorylates PINs at the same serine residues previously identified as PID/WAG targets (S1-S3), as well as two additional serines, designated S4 and S5. D6PK-mediated PIN phosphorylation was shown to be required for PIN transport activity in a *Xenopus* oocyte heterologous transport assay. Interestingly, PID and WAG2 had the same effect on PIN activation as D6PK (Zourelidou et al., 2014), but unlike PID or WAG2 overexpression, D6PK overexpression did not induce the basal-to-apical shift of PIN polarity (Zourelidou et al., 2009; Barbosa et al., 2018). This was first explained by the differential importance

of individual phosphosites for PIN polarity and activation, and different phosphosite preference of the two kinases: While both PID and D6PK could phosphorylate PIN1 at all five sites *in vitro*, PID phosphorylated preferentially S1, S2 and S3, which were presumably crucial for polarity regulation, while D6PK preferred S4 and S5, presumably the key activity control phosphosites (Zourelidou et al., 2014). Nevertheless, this explanation has been ruled out by *in situ* immunolocalization experiments with antibodies recognizing only S1-, resp. S4-phosphorylated PIN1, both of which behaved identically in WT as well as PID overexpressing plants and followed the general PIN1 localization pattern, rather than S1-phosphorylation being specifically enriched in the apical PM domain (Weller et al., 2017).

Overall, the body of evidence supporting the involvement of AGCVIII kinase-mediated PIN phosphorylation in the control of PIN polarity is vast, and the existence and importance of this regulatory module are beyond question. Nevertheless, extension and update of the classical model, in which phosphorylated PINs are targeted to the apical and dephosphorylated ones to the basal PM domain, seem necessary to accommodate also the most recent observations. Several such hypothetical extensions of the current model have recently been proposed, some of them involving members of the *MAB4/MEL* gene family as additional players (Barbosa et al., 2018).

The founding member of this family, *Macchi bou 4 (MAB4)* was identified in a forward genetic screen for *pid* enhancers. *MAB4* and its *Mab4/Enp1-Like1-4 (MEL1-4)* homologues encode proteins of unknown function related to NPH3, which is part of an E3 ubiquitin ligase complex that acts in phototropism (Furutani et al., 2007). A genetic interaction between MAB4/MEL and PID/WAG genes, as well as a link between MAB4/MEL function and PIN polarity, have been firmly established (Furutani et al., 2007; Cheng et al., 2008; Li et al., 2011; Furutani et al., 2011, 2014). The MAB4/MEL proteins were proposed to regulate PIN polarity either by modulating PIN endocytosis, or by acting as positive regulators of PID through their hypothetical ubiquitin-ligase activity (Furutani et al., 2011; Barbosa et al., 2018). Nevertheless, the first hypothesis is based on rather inconclusive results, while the second is entirely speculative. Therefore, until convincing experimental data to support the function of the MAB4/MEL proteins becomes available, the role of these proteins in PIN polarity regulation, as well as their relationship to PID-mediated phosphorylation, remain unresolved.

2.3.5. PIN polarity establishment and cytokinesis

Already in the first work that described PIN constitutive cycling, an observation was made that in cells undergoing cytokinesis, PIN1 localizes to the CP. This implies that upon cytokinesis completion, one of the daughter cells ends up with the protein present at both apical and basal PM domains, and therefore it must possess a mechanism for subsequent re-establishment of PIN1 polarity (Geldner et al., 2001). Symmetrical distribution of PINs on both sides of the CP, and therefore the notion that their polarity needs to be re-established after cytokinesis, was confirmed for PIN1 (Boutté et al., 2006) as well as PIN2 (Men et al., 2008; Jaillais and Gaude, 2008).

The first question related to this issue is which trafficking pathways do the CP-localized PIN molecules originate from? Localization of PM markers including PIN2 to the CP also in presence of the translation inhibitor Cycloheximide (CHX) suggested that the CP-localized PINs come mainly from endocytic recycling (Dhonukshe et al., 2006). Further support for this scenario came from experiments with PIN2 tagged with the photoconvertible fluorescent marker EosFP: after irreversible conversion of the fluorophore from green to red at the plasma membrane before a cell divided, red signal was observed at the CP (Kleine-Vehn et al., 2008a). On the other hand, pharmacological and genetic evidence was used to support a directly contradictory claim that trafficking to the CP occurs only via the secretory pathway (Reichardt et al., 2007; Richter et al., 2014).

The next, and from the polarity regulation point of view much more important, question is what is the fate of PIN molecules that end up on the "wrong" end of one of the daughter cells after cell division is completed? The process of PIN2 polarity re-establishment, as well as CME, was clearly compromised in a sterol biosynthesis mutant *cpi1-1*, suggesting that sterol-mediated endocytosis plays an important role in PIN polarity re-establishment (Men et al., 2008; Jaillais and Gaude, 2008). Dynamin-related protein 1A (DRP1a) was picked up in a biochemical screen for PIN1 interactors; this interaction was shown to take place mainly at the CP, and the *drp1a* mutant displayed similar PIN2 polarity re-establishment defects as *cpi1-1* (Mravec et al., 2011). These findings suggest that, as one would expect, endocytosis probably plays an important role in PIN polarity re-establishment after cell division. Nevertheless, given the strong pleiotropic defects of both mutants, secondary effects cannot be ruled out. Therefore, conclusive evidence for a direct causal link between CME and post-cytokinetic PIN polarity re-establishment, such as was shown for the inner-lateral marker BOR1 by a

conditional, genetically encoded endocytosis inhibitor (Yoshinari et al., 2016), is still missing.

Moreover, other important questions related to the topic have not been addressed at all: the timing of polarity re-establishment; the fate of the molecules from the "wrong" end of the cell after endocytosis (are they turned over, or recycled to the proper polar domain by transcytosis? (Kleine-Vehn et al., 2008a)); the molecular machinery that mediates the targeting switches; and the nature of the cue that re-determines *cell* polarity, necessary for PIN *protein* polarity re-establishment.

3. Aims of the study

1. To validate whether inducible overexpression of *AUXILIN-like1 and 2* in *Arabidopsis* can be used as a genetic tool to conditionally inhibit Clathrin-mediated endocytosis of, among other cargoes, the PIN proteins.
2. To develop methods to study the re-establishment of PIN2 polarity after cell division using live-cell imaging and to use these to systematically dissect the contribution of various cellular mechanisms to the process.
3. To understand by which mechanism do NPH3-like proteins encoded by the MAB4/MEL gene family contribute to PIN polarity.

4. Results

The Plant Cell, Vol. 30: 700–716, March 2018, www.plantcell.org © 2018 ASPB.

Check for updates

A Functional Study of AUXILIN-LIKE1 and 2, Two Putative Clathrin Uncoating Factors in Arabidopsis[OPEN]

Maciek Adamowski,[a] Madhumitha Narasimhan,[a] Urszula Kania,[a,b,c,1] Matouš Glanc,[a,d] Geert De Jaeger,[b,c] and Jiří Friml[a,2]

[a] IST Austria, 3400 Klosterneuburg, Austria
[b] Ghent University, Department of Plant Biotechnology and Bioinformatics, 9052 Ghent, Belgium
[c] VIB Center for Plant Systems Biology, 9052 Ghent, Belgium
[d] Department of Experimental Plant Biology, Faculty of Science, Charles University, 12844 Prague, Czech Republic

ORCID IDs: 0000-0002-8600-0671 (M.N.); 0000-0003-0619-7783 (M.G.); 0000-0001-6558-5669 (G.D.J.); 0000-0002-8302-7596 (J.F.)

Clathrin-mediated endocytosis (CME) is a cellular trafficking process in which cargoes and lipids are internalized from the plasma membrane into vesicles coated with clathrin and adaptor proteins. CME is essential for many developmental and physiological processes in plants, but its underlying mechanism is not well characterized compared with that in yeast and animal systems. Here, we searched for new factors involved in CME in *Arabidopsis thaliana* by performing tandem affinity purification of proteins that interact with clathrin light chain, a principal component of the clathrin coat. Among the confirmed interactors, we found two putative homologs of the clathrin-coat uncoating factor auxilin previously described in non-plant systems. Overexpression of AUXILIN-LIKE1 and AUXILIN-LIKE2 in Arabidopsis caused an arrest of seedling growth and development. This was concomitant with inhibited endocytosis due to blocking of clathrin recruitment after the initial step of adaptor protein binding to the plasma membrane. By contrast, *auxilin-like1/2* loss-of-function lines did not present endocytosis-related developmental or cellular phenotypes under normal growth conditions. This work contributes to the ongoing characterization of the endocytotic machinery in plants and provides a robust tool for conditionally and specifically interfering with CME in Arabidopsis.

INTRODUCTION

The endomembrane system provides a spatial organization for plant cell activities by compartmentalizing distinct biochemical processes. The endomembrane system compartments, including the plasma membrane (PM), endoplasmic reticulum, Golgi stacks, *trans*-Golgi network/early endosome, multivesicular body, and vacuole perform distinct, specialized functions. At the cell periphery, endocytosis internalizes PM-localized proteins, lipids, and extracellular material. The best-characterized endocytic mechanism in plants depends on the coat protein clathrin. More than 20 years ago, clathrin-coated pits and vesicles were observed in plant cells by electron microscopy and vesicles were purified from plant tissues (Tanchak et al., 1984; Mersey et al., 1985; Emons and Traas, 1986; Galway et al., 1993). With the advent of *Arabidopsis thaliana* as a model system and the availability of mutants and live imaging techniques in recent times, CME has been further investigated (Dhonukshe et al., 2007; Kitakura et al., 2011; Wang et al., 2013a; Konopka et al., 2008). Despite these advances, detailed descriptions of the events that comprise CME in plants are still often based on the more advanced studies of CME in animal and yeast systems (reviewed in McMahon and Boucrot, 2011).

In non-plant systems, the endocytic process is initiated by the adaptor protein complex AP-2, which acts by interacting with specific PM lipids and endocytotic cargoes and through clathrin recruitment. Proteins of the FCH domain only (FCHo) family were also proposed to be initiation factors (Henne et al., 2010). In plants, two candidates for initiation factors are the conserved AP-2 complex (Di Rubbo et al., 2013; Kim et al., 2013; Yamaoka et al., 2013; Bashline et al., 2013; Fan et al., 2013) and the recently identified TPLATE adaptor protein complex (Gadeyne et al., 2014; Zhang et al., 2015). A family of genes encoding monomeric adaptors of the AP180 N-Terminal Homology and Epsin N-Terminal Homology (ANTH/ENTH) type is present in plant genomes as well (reviewed in Zouhar and Sauer, 2014). Clathrin-coated pits grow via the recruitment, by adaptors, of clathrin triskelions. These three-legged units of the clathrin coat are each composed of three clathrin light chains and three clathrin heavy chains (CLCs and CHCs, respectively). Clathrin triskelions assemble into a regularly shaped lattice surrounding the forming lipid vesicle. The scission (separation) of a completed vesicle from the PM is mediated by dynamins, i.e., molecular scissors that mechanically constrict the neck between the clathrin-coated vesicle (CCV) and the PM. In non-plant systems, upon scission, the CCV recruits uncoating factors, which are the molecular chaperone Hsc70 and its cochaperones auxilin/cyclin G-associated kinase (GAK) (Gao et al., 1991; Ahle and Ungewickell, 1990; Ungewickell et al., 1995; Massol et al., 2006; Xing et al., 2010). The uncoating step releases the vesicle for its subsequent fusion with endosomal compartments and allows the CME machinery components to be recycled for further rounds of endocytosis. The CCV-uncoating process is virtually uncharacterized in plants, although an auxilin-like

[1] Current address: The Sainsbury Laboratory Cambridge University, Cambridge CB2 1NN, UK.
[2] Address correspondence to jiri.friml@ist.ac.at.
The author responsible for distribution of materials integral to the findings presented in this article in accordance with the policy described in the Instructions for Authors (www.plantcell.org) is: Jiří Friml (jiri.friml@ist.ac.at).
[OPEN] Articles can be viewed without a subscription.
www.plantcell.org/cgi/doi/10.1105/tpc.17.00785

protein of Arabidopsis is thought to have an uncoating function (Lam et al., 2001).

So far, endocytosis has been manipulated in plants through the use of clathrin mutants and a dominant negative version of CHC (Kitakura et al., 2011; Dhonukshe et al., 2007), lines with down-regulated expression of the endocytic adaptors (Gadeyne et al., 2014, Di Rubbo et al., 2013; Kim et al., 2013; Bashline et al., 2013; Fan et al., 2013), and mutants defective in dynamins (Yoshinari et al., 2016; Collings et al., 2008) and early endosomal components (Tanaka et al., 2013). These and similar tools allowed characterization of roles of CME in processes such as plant immunity (reviewed in Ben Khaled et al., 2015), establishment of polar auxin transport through the polarized subcellular localization of PIN-FORMED (PIN) auxin transporters (reviewed in Adamowski and Friml, 2015; Łangowski et al., 2016), and brassinosteroid signaling (Irani et al., 2012; Di Rubbo et al., 2013).

Here, our aim was to search for new proteins involved in CME in plants. To this end, we screened for proteins that bind to CLC, a fundamental component of the clathrin coat, in Arabidopsis. Based on several confirmed interactors, this study focused on two putative homologs of the uncoating factor auxilin. We found that overexpression of AUXILIN-LIKE1 and AUXILIN-LIKE2 caused an arrest of growth and development and inhibition of endocytosis, likely by preventing clathrin recruitment to endocytic pits initiated by the adaptor proteins. In contrast, loss of AUXILIN-LIKE1/2 function did not visibly interfere with development, or endocytosis, under optimal growth conditions.

RESULTS

Identification of CLC1-Associated Proteins

To search for new proteins involved in CME, we employed tandem affinity purification coupled with mass spectrometry (TAP-MS; Van Leene et al., 2014) using CLATHRIN LIGHT CHAIN1 (CLC1) as bait. We first expressed C- and N-terminal CLC1-TAP tag fusions in Arabidopsis cell suspensions, which was followed by protein isolation, affinity purification, and identification of clathrin-bound proteins by mass spectrometry. Using this technique, we identified a small number of clathrin binding proteins with sequence features indicating possible endocytic functions (Figure 1A).

The first identified were two highly homologous proteins containing DNAJ domains at their C termini. As such, they bear limited similarity to auxilins and GAKs, which also contain C-terminal DNAJ domains that are needed for Hsc70 recruitment and activation leading to clathrin uncoating (Ungewickell et al., 1995). We named the putative auxilin homologs AUXILIN-LIKE1 (AT4G12780) and AUXILIN-LIKE2 (AT4G12770). These two proteins belong to a family of seven proteins in Arabidopsis with C-terminal DNAJ domains, which can all therefore be called auxilin-likes. AUXILIN-LIKE1 is identical to the auxilin-like protein identified previously as a putative uncoating factor in Arabidopsis (Lam et al., 2001).

Second, we found CAP1, a monomeric adaptor protein that, together with its closest homolog ECA4 (Song et al., 2012), was identified based on interactions with the TPLATE endocytic adaptor protein complex (Gadeyne et al., 2014). CAP1 and ECA4 are part of a family of ANTH/ENTH adaptors that may be involved in the generation of coated vesicles at various sites of the endomembrane system (Zouhar and Sauer, 2014)

Third, we found SH3P2, a protein consisting of a central BAR domain and a C-terminal SH3 domain, the first of which acts in membrane curvature generation, while the second functions in protein-protein interactions. In animals, proteins with a similar BAR-SH3 domain composition are called endophilins and have been shown to act in a clathrin-independent endocytic pathway (Boucrot et al., 2014; Renard et al., 2014). SH3P2 belongs to a family of three proteins in Arabidopsis, the other two being SH3P1 and SH3P3 (Lam et al., 2001). SH3P2 has been implicated in the autophagy pathway (Zhuang et al., 2013, 2015), cell plate formation (Ahn et al., 2017), as well as vacuolar trafficking of ubiquitinated cargoes (Kolb et al., 2015; Nagel et al., 2017). Apart from AUXILIN-LIKE1/2, CAP1, and SH3P2, our TAP approach also identified the thioesterase DHNAT2, a peroxisome-localized enzyme (Widhalm et al., 2012), but we did not follow up on this finding. Finally, and as expected, we also identified both CHC homologs of Arabidopsis as well as two of the three homologs of CLC.

To confirm the interactions of the two auxilin-likes, CAP1, and SH3P2 with clathrin, we used bimolecular fluorescence complementation (BiFC), also known as the split-GFP assay (Kerppola, 2009). In this approach, two proteins of interest are fused to two complementary fragments of the GFP molecule and transiently coexpressed in wild tobacco (*Nicotiana benthamiana*) leaves via *Agrobacterium tumefaciens* injection. The physical proximity, or a direct interaction, of the two assayed proteins results in reconstitution of the GFP molecule and fluorescence, which is captured by confocal laser scanning microscopy (CLSM). Using this method, we confirmed the interactions of AUXILIN-LIKE1, AUXILIN-LIKE2, CAP1, and SH3P2 with CLC1 (Figure 1B). As a negative control, we probed for interactions of all these proteins with PHOSPHATIDYLINOSITOL 4,5-BISPHOSPHATE KINASE1 (PIP5K1; Tejos et al., 2014; Ischebeck et al., 2013), a peripheral PM-localized protein, and found no reconstituted GFP fluorescence (Supplemental Figure 1A). We also tested for interactions between our CLC-interacting proteins and observed interactions of AUXILIN-LIKE1/2 with SH3P2 and CAP1, but no interaction between SH3P2 and CAP1 (Supplemental Figure 1B). A summary of all BiFC interactions is presented in Figure 1C. The localization of the interacting pairs in wild tobacco cells appeared to be cytosolic. However, this is expected for soluble proteins, and we think it may not be indicative of the real interaction site of these proteins, as it is likely that reconstitution of a GFP molecule in the BiFC assay binds the two partners into stable dimers that subsequently don't exhibit normal localization and activity. Finally, SH3P2 was recently shown to interact with CHC (Nagel et al., 2017), while AUXILIN-LIKE1 was reported to interact with clathrin and with SH3P1, an SH3P2 homolog (Lam et al., 2001). These additional observations clearly support our interaction data.

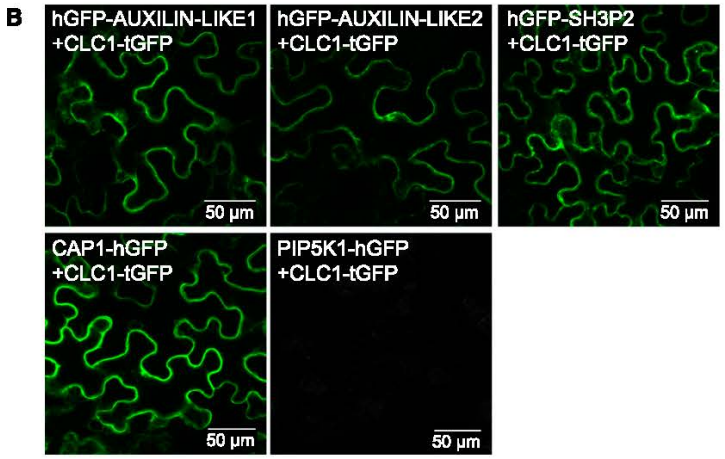
In conclusion, our TAP and split-GFP data demonstrate interactions between clathrin, AUXILIN-LIKE1/2, CAP1, and SH3P2, suggesting a common function of these proteins.

Subcellular Localization of Clathrin-Associated Proteins

Next, we addressed the subcellular localization of the newly identified clathrin interactors (Figure 2; Supplemental Figure 2).

A

AGI code	Protein name	Isolated with (no. exp.)	
		C-terminal tag	N-terminal tag
AT4G12780 / AT4G12770	AUXILIN-LIKE1/2	2	-
AT4G32285	CAP1	2	-
AT4G34660	SH3P2	1	-
AT5G48950	DHNAT2	2	2
AT3G08530	Clathrin Heavy Chain1	2	2
AT3G11130	Clathrin Heavy Chain2	2	2
AT2G20760	Clathrin Light Chain1	2	2
AT2G40060	Clathrin Light Chain2	2	-



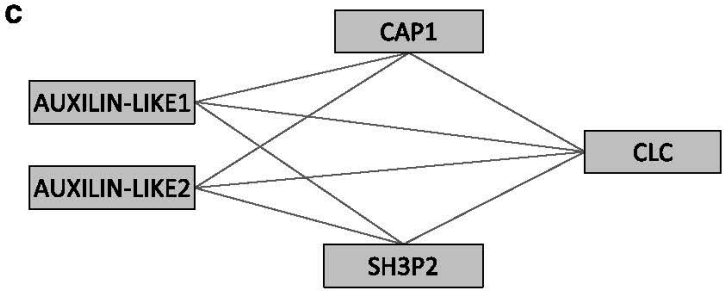


Figure 1. Identification of CLC-Interacting Proteins.

(A) TAP-MS-based isolation of proteins associated with clathrin. CLC1 in C- and N-terminal fusions with TAP tags was used as bait. Two repetitions with each construct were performed.

(B) BiFC-based interactions between CLC1 and selected interactors identified with TAP-MS. Pairs of proteins of interest fused with halves of the GFP molecule were transiently expressed in wild tobacco leaves and reconstituted GFP fluorescence was imaged in epidermis on the abaxial leaf side. PIP5K1 did not interact with any of the proteins tested and was used as a negative control.

(C) Schematic representation of all interactions detected with BiFC. Additional interactions are presented in Supplemental Figure 1.

We used CLSM on fluorescent protein fusions expressed in stable transgenic lines of Arabidopsis. We used a common model system for endomembrane trafficking studies, the epidermis of the seedling root apical meristem (RAM). To detect CAP1 localization, we cloned *CAP1*$_{pro}$*:CAP1-mCherry* and *35S*$_{pro}$*:CAP1-RFP* constructs and in both cases observed PM and cell plate binding (Figures 2A and 2B; Supplemental Figure 2A). Rarely, in ~10% of seedlings, CAP1 also showed binding to endosomal compartments (Supplemental Figure 2A). For SH3P2 localization, we used the previously published *UBQ*$_{pro}$*:SH3P2-GFP* line and cloned a *35S*$_{pro}$*:SH3P2-GFP* construct. Here too we observed PM and cell plate binding, as well as endosomal-like intracellular signals,

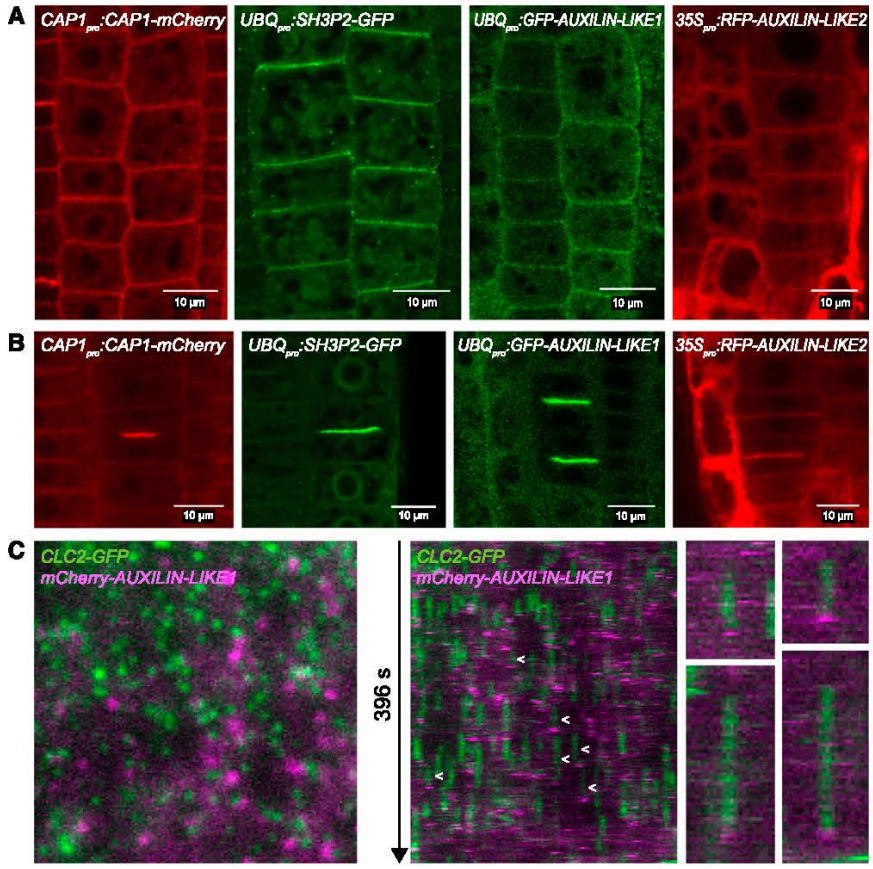


Figure 2. Subcellular Localizations of the Identified Clathrin Interactors.

(A) and **(B)** PM **(A)** and cell plate **(B)** localization of CAP1, SH3P2, AUXILIN-LIKE1, and AUXILIN-LIKE2 fluorescent protein fusions in the seedling root epidermis of stable transformants. Background cytosol staining can be observed in all lines, while CAP1 and SH3P2 also show faint nuclear staining. *35S$_{pro}$:RFP-AUXILIN-LIKE1* was identical to *35S$_{pro}$:RFP-AUXILIN-LIKE2*. Additional localization data, including colocalizations with PM markers, are presented in Supplemental Figure 2B.

(C) VAEM colocalization of clathrin (*CLC2$_{pro}$:CLC-GFP*) and AUXILIN-LIKE1 (*UBQ$_{pro}$:mCherry-AUXILIN-LIKE1*) in the hypocotyl epidermis. Kymographs (middle and right) show examples of auxilin-like1 recruitment at the end of CCP lifetime, which was observed in a small subset of all endocytic events (arrowheads). The majority of clathrin foci were lacking AUXILIN-LIKE1, and AUXILIN-LIKE1 foci without clathrin could be observed. See Supplemental Movie 1.

which were larger and more pronounced upon strong overexpression driven by the 35S promoter (Figures 2A and 2B; Supplemental Figure 2A). Our observations of SH3P2 localization are consistent with other recent reports (Ahn et al., 2017; Kolb et al., 2015; Nagel et al., 2017). We failed to clone the *AUXILIN-LIKE1/2* locus promoter region and instead prepared *UBQ10$_{pro}$:GFP-AUXILIN-LIKE1* as well as *35S$_{pro}$:RFP-AUXILIN-LIKE1* and *35S$_{pro}$:RFP-AUXILIN-LIKE2* constructs. Both auxilin-likes localized to the PM and cell plates, like CAP1 and SH3P2 (Figures 2A and 2B). Furthermore, all proteins of interest showed background cytosolic staining, while SH3P2 and CAP1 additionally weakly stained the nucleus. In summary, the localization patterns are consistent with a function of AUXILIN-LIKE1/2, CAP1, and SH3P2 in CME at the PM as well as clathrin-mediated processes at the cell plate. Additionally, SH3P2 functions at the endosomes, as has been demonstrated (Nagel et al., 2017), and the rarely observed endosomal localization of CAP1 suggests it may function there as well.

In animal cells, auxilins and GAKs are briefly recruited to clathrin-coated pits (CCPs) at the end of their lifetimes on the PM during the transition to vesicle budding (Massol et al., 2006; Lee et al., 2006). Apart from this late burst of auxilin recruitment, small and variable amounts of auxilin are present at earlier stages of CCP growth (Massol et al., 2006). Such events can be observed with total internal reflection fluorescence (TIRF) microscopy, a method that allows live imaging of the PM surface at high magnification. We wanted to address the recruitment of AUXILIN-LIKE1/2 to newly forming clathrin-coated vesicles in a similar manner. We

generated a double fluorescent reporter line, *CLC2*$_{pro}$*:CLC2-GFP* × *UBQ10*$_{pro}$*:mCherry-AUXILIN-LIKE1*, and employed variable angle epifluorescence microscopy (VAEM), a plant cell-specific TIRF-like method that allows the PM surface to be imaged through the plant cell walls, although it does not completely remove the cytoplasmic background below the PM (Konopka and Bednarek, 2008). In the epidermis of etiolated hypocotyls, AUXILIN-LIKE1 appeared as highly dynamic PM foci (Figure 2C; Supplemental Movie 1). With kymograph analysis, we observed events of brief AUXILIN-LIKE1 recruitment at the end of the lifetime of clathrin-coated pits, as previously described in non-plant systems. However, notably, we only observed this in a small fraction of all CCPs (estimated at around 5%), while the majority of clathrin-positive foci apparently did not recruit AUXILIN-LIKE1 (Figure 2C). We also regularly observed events of brief AUXILIN-LIKE1 recruitment at sites not containing clathrin. Based on these observations, we performed a control to assure that the observed colocalization events indeed represent specific late recruitment to coated pits. We looked at the kymographs for events where AUXILIN-LIKE1 signal appears not at the end, but around the beginning of a CLC2-GFP trace, which we consider to represent accidental colocalization. We found such events to be much more rare (16 versus 100 events in a single TIRF movie), which confirms that AUXILIN-LIKE1 is indeed specifically recruited at the end of the PM lifetime for at least a subpopulation of CCPs.

This observation might indicate that the majority of clathrin-coated vesicles do not use AUXILIN-LIKE1/2 for uncoating. Alternatively, perhaps AUXILIN-LIKE1/2 recruitment often takes place later after scission, when the vesicles had already moved away from the PM and thus had moved away from the variable region of VAEM detection. Some brief recruitment events could have also been missed because our method uses sequential scanning of the two fluorescent channels.

Seedling Phenotypes of AUXILIN-LIKE1/2 Overexpressors

While generating transgenic lines expressing fluorescent protein fusions of the clathrin-associated proteins, we observed that overexpressing *AUXILIN-LIKE1* and *AUXILIN-LIKE2* under the control of the 35S promoter was associated with deleterious phenotypes (Supplemental Figure 3B). In the T2 generation of *35S*$_{pro}$*:RFP-AUXILIN-LIKE1* and *35S*$_{pro}$*:RFP-AUXILIN-LIKE2* lines, we saw many seeds that did not germinate, even after prolonged culturing. Seeds that did germinate often developed slowly and exhibited relatively weak and patchy expression of RFP-AUXILIN-LIKE1/2 signals. In the T3 generation, a virtually complete silencing of the transgenes was observed. These observations reveal selection against high AUXILIN-LIKE1/2 expression levels, which was of interest to us, because overexpressing auxilins in non-plant systems can inhibit endocytosis (Zhao et al., 2001). In contrast, overexpression of CAP1 and SH3P2 in 35S-promoter-driven lines did not interfere with seed germination or seedling development (Supplemental Figure 3A). Therefore, we chose to follow up on the effects of AUXILIN-LIKE1/2 overexpression as a possible way to elucidate a clathrin-associated function of these two putative uncoating factors.

To circumvent the deleterious effects of constitutive AUXILIN-LIKE1/2 overexpression, we generated stable transgenic Arabidopsis lines overexpressing AUXILIN-LIKE1/2 under the control of chemically inducible promoters. We prepared estradiol-inducible transactivation lines overexpressing untagged AUXILIN-LIKE1 and AUXILIN-LIKE2 (*XVE»AUXILIN-LIKE1* and *XVE»AUXILIN-LIKE2*), as well as a tamoxifen-inducible transactivation line overexpressing GFP-tagged AUXILIN-LIKE1 (*INTAM»GFP-AUXILIN-LIKE1*). Depending on the strength of a particular transgenic line, upon chemical induction, we observed a spectrum of seedling phenotypes ranging from weak reduction in the rates of growth and development to a strong delay or inhibition of germination, as well as the complete inhibition of seedling growth and development if the transgene was activated later (Figures 3A and 3B; Supplemental Figure 4). Overexpression of auxilin-like genes in the lines with strong phenotypes was confirmed with qRT-PCR (Supplemental Figure 5). Using long-term, time-lapse confocal microscopy with automated root tracking (TipTracker; von Wangenheim et al., 2017), we directly compared root growth rates with AUXILIN-LIKE1 expression levels in the root tips of induced *INTAM»GFP-AUXILIN-LIKE1* seedlings (Supplemental Figure 6). GFP-AUXILIN-LIKE1 expression was first observed 1 h after induction and gradually increased until ~15 h. Following GFP-AUXILIN-LIKE1 expression, we observed a sharp decrease in growth between the 4th and 11th hour of induction. Therefore, growth inhibition appears to be a relatively direct effect of AUXILIN-LIKE1/2 overexpression.

Using light microscopy, we found that the morphology of cells in the RAM in AUXILIN-LIKE1/2-overexpressing seedlings was drastically different from that of the wild-type controls. RAM epidermis cells of *XVE»AUXILIN-LIKE1/2* lines exhibited enlarged vacuoles that filled major parts of the cell volume, while the cytosol content was reduced and the nucleus was displaced from its central location (Figures 3C and 3D). This phenomenon was typically observed after ~1 d of induction and became progressively more pronounced after 2 to 3 d.

Inhibition of Endocytosis by AUXILIN-LIKE1/2 Overexpression

Using our inducible overexpressing lines, we then assayed the effect of AUXILIN-LIKE1/2 overexpression on endocytosis. Three lines of evidence support the notion that overexpression of AUXILIN-LIKE1 and AUXILIN-LIKE2 leads to the inhibition of endocytosis: (1) imaging of the endocytic cargoes, (2) imaging of the molecular endocytic machinery, and (3) the distribution of membranes within the cell.

As a basic experiment to assay the general rates of endocytosis, we monitored the uptake of FM4-64, a membrane dye commonly used in studies of endocytosis (Aniento and Robinson, 2005; Bolte et al., 2004; Jelínková et al., 2010). After pulse staining of Arabidopsis seedlings with FM4-64, the dye is gradually taken up by the cell through the endocytic process, and over time it can be observed first at endosomal compartments and then at the tonoplast (vacuolar membrane). *XVE»AUXILIN-LIKE1/2* lines induced overnight (~16–24 h) showed an inhibition of FM4-64 uptake in a majority of the seedlings and RAM epidermis cells observed (Figure 4A). Considering the alteration of cell morphology (the enlargement of vacuoles), we monitored the cells closely in the visible light channel to recognize areas still containing the cytosol, and therefore also endosomes that FM4-64 could reach, and saw that staining was either absent from these areas or endosomes were

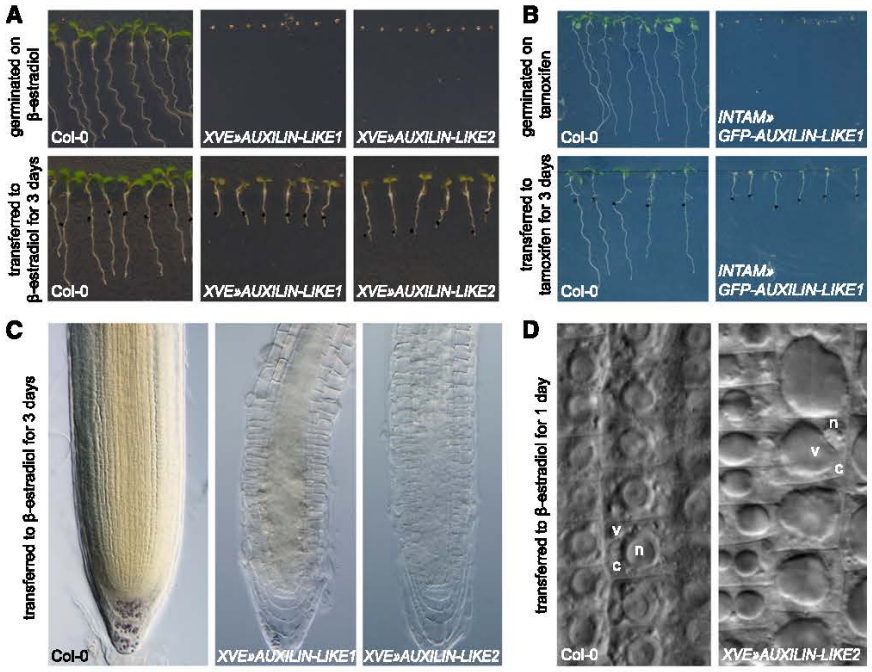


Figure 3. AUXILIN-LIKE1/2 Overexpression Causes an Arrest of Seed Germination and Seedling Growth and Alterations in Cell Morphology.

Overexpression of auxilin-likes in *XVE»AUXILIN-LIKE1/2* **(A)** or *INTAM»GFP-auxilin-like1* **(B)** lines inhibits or strongly delays seed germination and inhibits seedling growth if the transgene is induced postgermination. The RAMs of AUXILIN-LIKE1/2-overexpressing seedlings appear semitransparent **(C)** due to enlargement of vacuoles and reduction of the cytoplasmic volume **(D)**. V, vacuole; c, cytoplasm; n, nucleus.

only weakly stained compared with the controls (Supplemental Figure 7A). In these experiments, we also observed that FM4-64-stained PMs in *XVE»AUXILIN-LIKE1/2* lines often lost the normal, smooth appearance and were instead thicker and uneven, which will be explained below. We then repeated the FM4-64 uptake experiment in the *INTAM»GFP-AUXILIN-LIKE1* line at earlier stages of induction. In this line, we could monitor AUXILIN-LIKE1 expression directly due to the GFP fluorescence. We observed inhibition of FM4-64 uptake into RAM epidermis cells as early as 8 h after transgene induction (Figure 4B). The rate of endocytic tracer uptake was inversely correlated with GFP expression levels on a cell-to-cell basis, demonstrating that the endocytic inhibition by auxilin-like overexpression is cell-autonomous. Importantly, at these early stages of overexpression, the epidermal cells still exhibited normal morphology, with abundant cytosol and small, fragmented vacuoles. Finally, at an even earlier time point of 5 h of expression induction, GFP-AUXILIN-LIKE1 levels were already high in the lateral root cap, and we observed inhibition of FM4-64 uptake specifically in this tissue (Supplemental Figure 7B).

Next, we corroborated these findings by monitoring known CME cargoes, including the auxin efflux transporters of the PIN family (Nodzyński et al., 2016; Adamowski and Friml, 2015) and the syntaxin KNOLLE (Lauber et al., 1997). The endocytic trafficking of PIN proteins is classically assayed via Brefeldin A (BFA) treatments. BFA treatments lead to the deactivation of ADP-ribosylation factors (ARFs), components of the vesicle formation machinery in the endomembrane system, by directly targeting a subset of ARF activators, the guanine nucleotide exchange factors for ARFs (ARF-GEFs). As a result, certain endomembrane trafficking pathways, including GNOM ARF-GEF-dependent polar recycling of PINs to the PM, are inhibited, while others, including PIN endocytosis, are not. As a related phenomenon, agglomeration of endosomal compartments into large structures called "BFA bodies" or "BFA compartments" occurs. Therefore, after BFA treatments, the continuously internalized PIN proteins can be observed inside BFA bodies, from which they cannot be recycled back to the PM (Naramoto et al., 2014). In RAMs of *XVE»AUXILIN-LIKE1/2* seedlings induced for 16 to 24 h, immunolabeled PIN1 was rarely found in BFA bodies in the stele, while in the epidermis, PIN2-GFP was not observed in BFA bodies at all (Figures 5A and 5B), indicating that PIN1 and PIN2 endocytosis was inhibited. To assure that BFA bodies still form after auxilin-like overexpression and that they can be observed despite the enlarged vacuoles, we visualized the BFA body structures themselves using CLC2-GFP as a marker of aggregating endosomal populations (Figure 5C).

To confirm these observations without the use of BFA and to more clearly distinguish the internalization of PIN2 from its biosynthesis and secretion, we monitored the cellular turnover of PIN2 over the long term using PIN2 fused to Dendra (a green-to-red photoactivatable fluorescent protein induced by blue light). After 6 h of *XVE»AUXILIN-LIKE2* induction, we converted PIN2-Dendra from the green into the red form in whole root tips. Eighteen

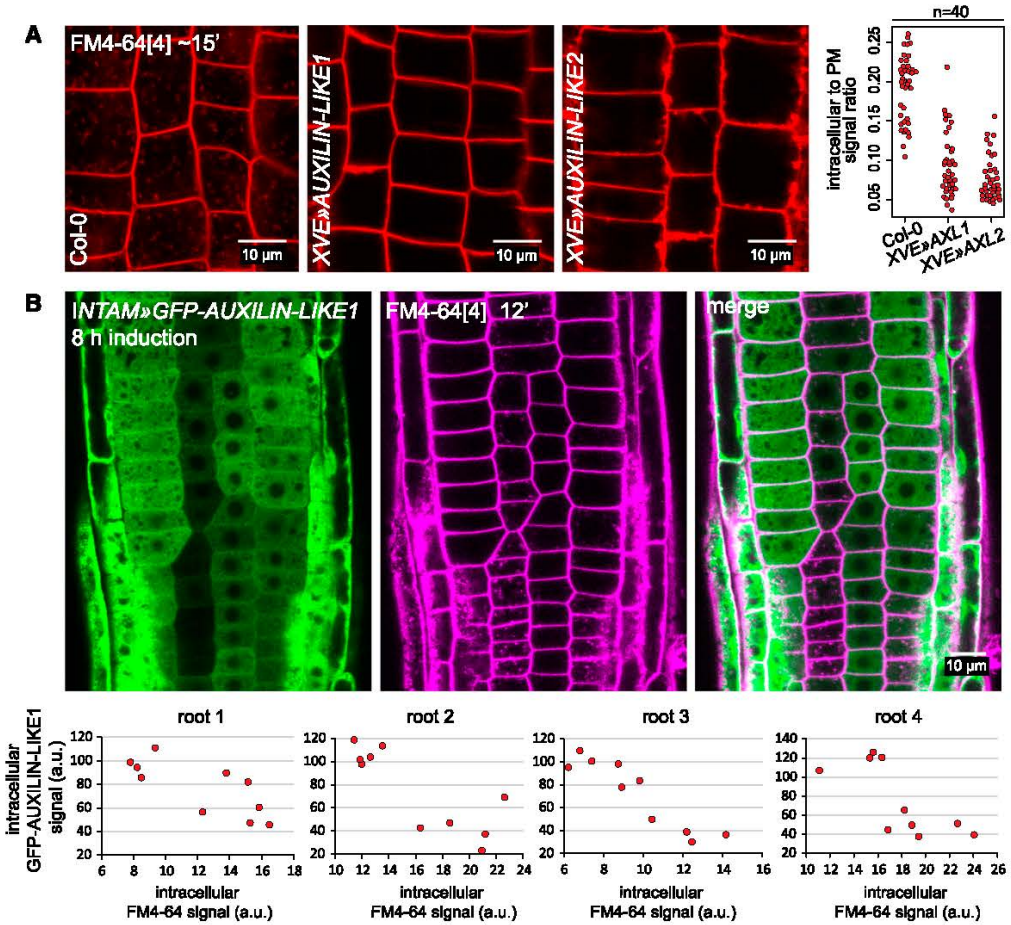


Figure 4. Inhibition of FM4-64 Endocytic Tracer Uptake by AUXILIN-LIKE1/2 Overexpression.

(A) The uptake of the endocytotic tracer FM4-64 into RAM epidermal cells in *XVE»AUXILIN-LIKE1/2* seedlings induced for 16 to 24 h is strongly reduced. At least 10 roots per genotype were imaged in three repeated experiments. The graphs shows quantification of intracellular-to-PM FM4-64 signal ratio from 40 cells coming from four roots in a representative experiment.

(B) FM4-64 uptake at early stages (8 h) of *INTAM»GFP-AUXILIN-LIKE1* induction. The degree of FM4-64 uptake correlated with GFP-AUXILIN-LIKE1 levels in individual root meristem epidermal cells. Graphs show examples of this correlation in four roots. Each data point represents an individual cell. Notice that at this stage of AUXILIN-LIKE1 overexpression, cell morphology remains normal, with abundant cytosol illuminated by GFP-AUXILIN-LIKE1 expression, and small, fragmented vacuoles seen by negative staining. a.u., arbitrary units.

hours later, AUXILIN-LIKE2-overexpressing seedlings retained significant amounts of the red PIN2-Dendra form at the PMs (Figure 5D), demonstrating inhibition of PIN2 endocytosis. In control seedlings, virtually all of the red form became internalized and degraded and was replaced by newly synthesized, green PIN2-Dendra.

In addition to PIN1 and PIN2, we monitored the endocytosis of KNOLLE. KNOLLE is a SNARE protein that is specifically expressed during cell division and targeted to the growing cell plates, where it is retained for some time after cell division is completed. The specific localization of KNOLLE to the newly formed cell membranes is dependent on the endocytic process, as inhibition of endocytosis is associated with lateral spreading of KNOLLE to the "old" PMs after the completion of cell division (Boutté et al., 2010). Similar to previous observations, overexpression of AUXILIN-LIKE1/2 also caused diffusion of KNOLLE out of the newly completed cell membranes and into the old PMs, demonstrating that endocytosis of KNOLLE was inhibited (Figure 5E).

In summary, our imaging of FM4-64 dye, as well as known CME cargoes PIN1, PIN2, and KNOLLE, supported the notion that overexpression of AUXILIN-LIKE1/2 inhibits endocytosis.

AUXILIN-LIKE1/2 Overexpression Inhibits Endocytosis at the Clathrin Recruitment Step

Next, we visualized the effect of auxilin-like overexpression on the molecular components of the endocytic machinery itself. For this

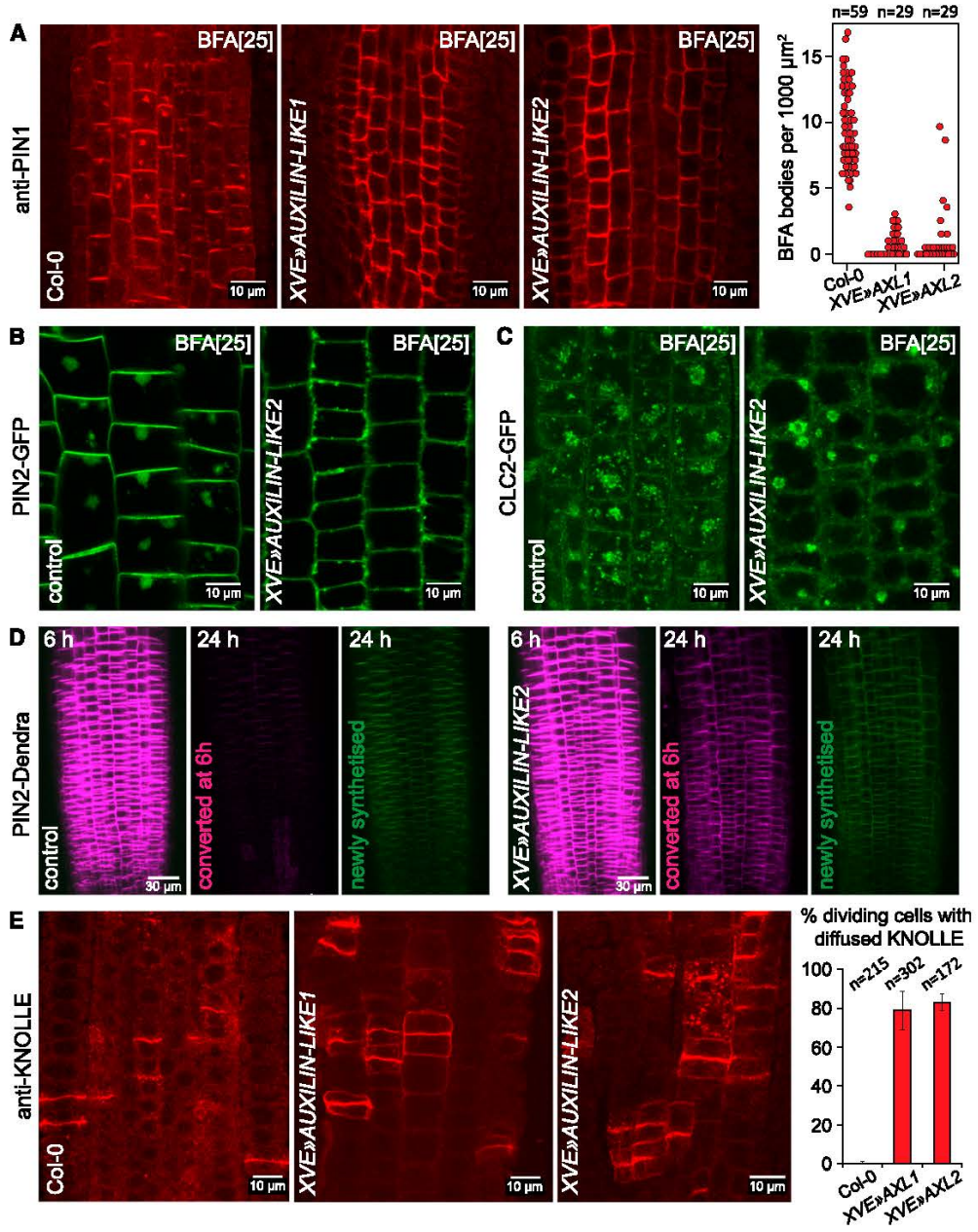


Figure 5. Inhibition of Protein Cargo Endocytosis by AUXILIN-LIKE1/2 Overexpression.

(A) Immunolocalization of PIN1 in the RAM stele after 90 min of BFA (25 µM) treatment. The BFA body number is markedly reduced, indicative of inhibition of PIN1 endocytosis. The graph shows collated results from three repetitions of the experiment. Each data point represents one root.

(B) and **(C)** Following AUXILIN-LIKE2 overexpression, PIN2-GFP does not localize to BFA-induced bodies in RAM epidermis after 90 min of BFA (25 µM) treatment **(B)**. Control experiment with CLC2-GFP used as an endosome marker **(C)** shows that BFA bodies can be easily observed in auxilin-like overexpressing seedlings despite the enlarged vacuoles.

(D) Long-term PIN2 turnover monitoring in *XVE»AUXILIN-LIKE2* with photoconvertible PIN2-Dendra fusion. PIN2-Dendra has been converted from green into red form in whole root tips at 6 h of AUXILIN-LIKE2 induction. At the 24-h time point, significant amounts of the red form have been retained at the PMs of

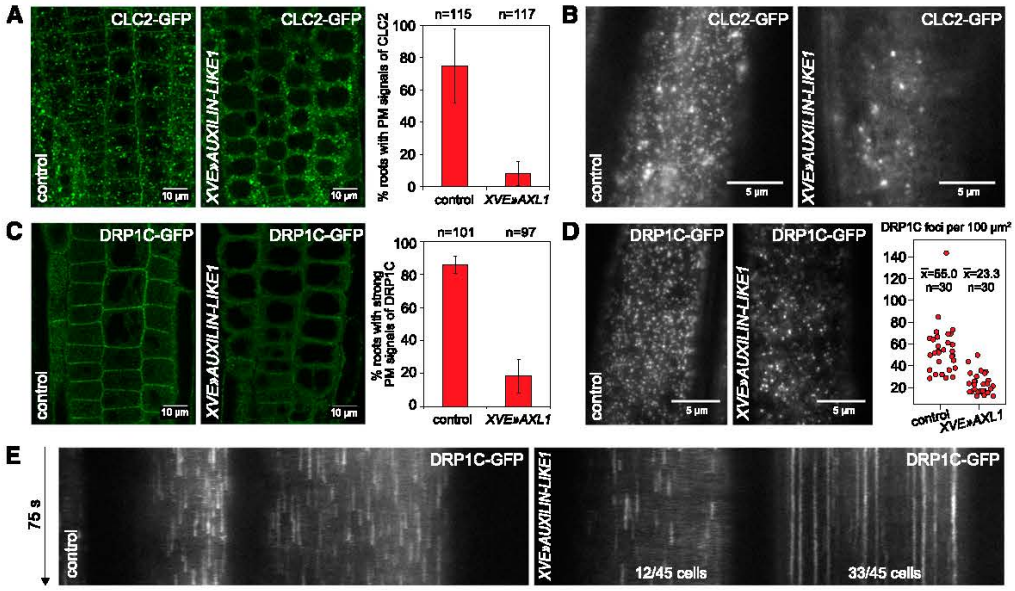


Figure 6. Loss of Clathrin and Dynamin from the PMs of *XVE»AUXILIN-LIKE1* Line.

(A) and **(B)** Following AUXILIN-LIKE1 overexpression, CLC2-GFP signals were absent from the PMs of RAM epidermis cells **(A)** and normal CLC2-GFP endocytic foci could not be observed in hypocotyl epidermis by VAEM **(B)**. The endosomal clathrin populations were retained in both tissues.
(C) to **(E)** DRP1C-GFP PM signals were markedly reduced in RAM epidermis **(C)**, and the density of DRP1C-positive PM foci was reduced in the hypocotyl epidermis **(D)**. The remaining DRP1C-positive PM foci had exceptionally long lifetimes in the majority of observed cells **(E)**.
Graphs in **(A)** and **(C)** show average ± SD percentage of roots with strong PM signals from the fluorescent markers. Graph in **(D)** shows collated measurements from three repetitions of the experiment. All experiments in this figure were performed after 16 to 24 h of *XVE»AUXILIN-LIKE1* induction.

analysis, we crossed the *XVE»AUXILIN-LIKE1* line with fluorescent reporter lines for subunits of the adaptor protein complexes AP2 and TPLATE (AP2A1-TagRFP and TPLATE-GFP), for clathrin (CLC2-GFP), and for dynamins (DRP1C-GFP). We then performed live imaging after 1 d (16–24 h) of AUXILIN-LIKE1 induction.

Through CLSM of seedling roots, we observed that clathrin signals were absent from the PMs of epidermal cells in a majority of AUXILIN-LIKE1-overexpressing seedlings (Figure 6A). These observations were confirmed in the hypocotyl epidermis, where we employed VAEM. Upon AUXILIN-LIKE1 overexpression, normal, densely distributed clathrin-positive PM foci were not observed (Figure 6B). However, we did observe CLC2 signals that were very sparse, larger than normal endocytic pits, and often laterally mobile (Supplemental Movie 2). We cannot determine whether these were clathrin structures that were attached to the PM or localized to the cytosol.

Apart from endocytosis at the PM, clathrin participates in vesicle formation at other compartments of the endomembrane system, where it likely acts with AP-1, AP-3, and AP-4 complexes to function in vacuolar, and potentially secretory, trafficking (Richter et al., 2014; Park et al., 2013; Wang et al., 2013b, 2014; Feraru et al., 2010; Fuji et al., 2016; Robinson and Pimpl, 2014; Zwiewka et al., 2011). Interestingly, it appears that the endosomal clathrin pools were not affected by auxilin-like overexpression, as CLC2-GFP signals were still bound to endosomes (observed as large, intracellular bodies) in both roots and hypocotyls (Figures 6A and 6B; Supplemental Movie 2).

The presence of dynamin (DRP1C) at the PM was also reduced, although the reduction was less pronounced than that of clathrin. In most roots, very weak PM signals of DRP1C-GFP could still be observed (Figure 6C), while VAEM in the hypocotyl epidermis showed DRP1C-positive foci of normal appearance, but at much reduced densities compared with the control (Figure 6D). These remaining DRP1C foci did not show normal dynamics in most of the cells observed, but instead exhibited very long lifetimes, suggesting that these DRP1C-containing structures may have been nonfunctional (Figure 6E).

Figure 5. (continued).

auxilin-like overexpressing seedlings, while the protein has been internalized and degraded in the mock-treated controls. Panels at 6 h show merged green and red channels, while panels at 24 h show green and red channels separately.
(E) Immunolocalization of KNOLLE in the RAM of *XVE»AUXILIN-LIKE* lines showing diffusion of KNOLLE out of the completed cell plates and into the old PM in late cytokinetic cells. The graph shows percentage of cells with diffused KNOLLE signals; error bars indicate SD between 3 experiments.
Experiments in **(A)** to **(C)** and **(E)** were performed after 16 to 24 h of *XVE»AUXILIN-LIKE1/2* induction.

Interestingly, in contrast to clathrin and dynamin, the endocytic adaptor complexes AP2 and TPLATE were not only present at the PMs of *XVE»AUXILIN-LIKE1*, but their binding was consistently stronger than in control conditions. This was most clearly observed in the RAM epidermis using CLSM (Figures 7A and 7B), but the same phenomenon occurred in the hypocotyl epidermis, as observed by VAEM (Figures 7C and 7D). Furthermore, time-resolved imaging demonstrated that these adaptor protein foci had shorter lifetimes at the PM than under control conditions (Figures 7E and 7F; Supplemental Movies 3 and 4).

In summary, live microscopy observations of clathrin, dynamin, and adaptor protein complexes suggest that auxilin-like overexpression blocks endocytosis after the initial step of adaptor protein complex binding to the PM. It appears that endocytic pits are initiated by the adaptors at high frequency, but due to the lack of clathrin binding, they are not progressing and quickly become aborted. The nature of the scarce, remaining DRP1C-positive structures with long lifetimes remains unclear.

Disturbance in Cellular Membrane Distribution Indicates Inhibited Endocytosis

Apart from cargoes and the trafficking-related molecular machinery, the endomembrane system naturally consists of the biological membranes themselves. These membranes are in a constant state of flux through the cell, moving from place to place as vesicles (e.g., secretory vesicles, CCVs, COPI, and COPII-coated vesicles) and through the maturation of compartments, examples of which include the proposed maturation of *trans*-Golgi network/early endosome into multivesicular bodies (Scheuring et al., 2011) and the *cis*-medial-*trans* progression of cisternae in the Golgi stack. Considering this overall membrane flow, one can imagine that interfering with a particular trafficking process could lead to broad changes in membrane distribution in the endomembrane system. Specifically, inhibited endocytosis should lead to the excess accumulation of the membrane at the cell periphery—the plasma membrane—and a concomitant loss of membranes from the cell interior, both occurring due to the now isolated, imbalanced activity of the secretory pathway. Indeed, upon staining the PMs in AUXILIN-LIKE1/2-overexpressing lines with the FM4-64 dye or with PIN2-GFP, we observed thick deposits of membrane at the cell periphery instead of the typical smooth, thin PMs (Figure 8). This observation provides more, although indirect, evidence for inhibited endocytosis due to AUXILIN-LIKE1/2 overexpression. Staining with propidium iodide showed that the cell wall structure was also affected (Supplemental Figure 8), as thick deposits strongly binding to propidium iodide could be seen.

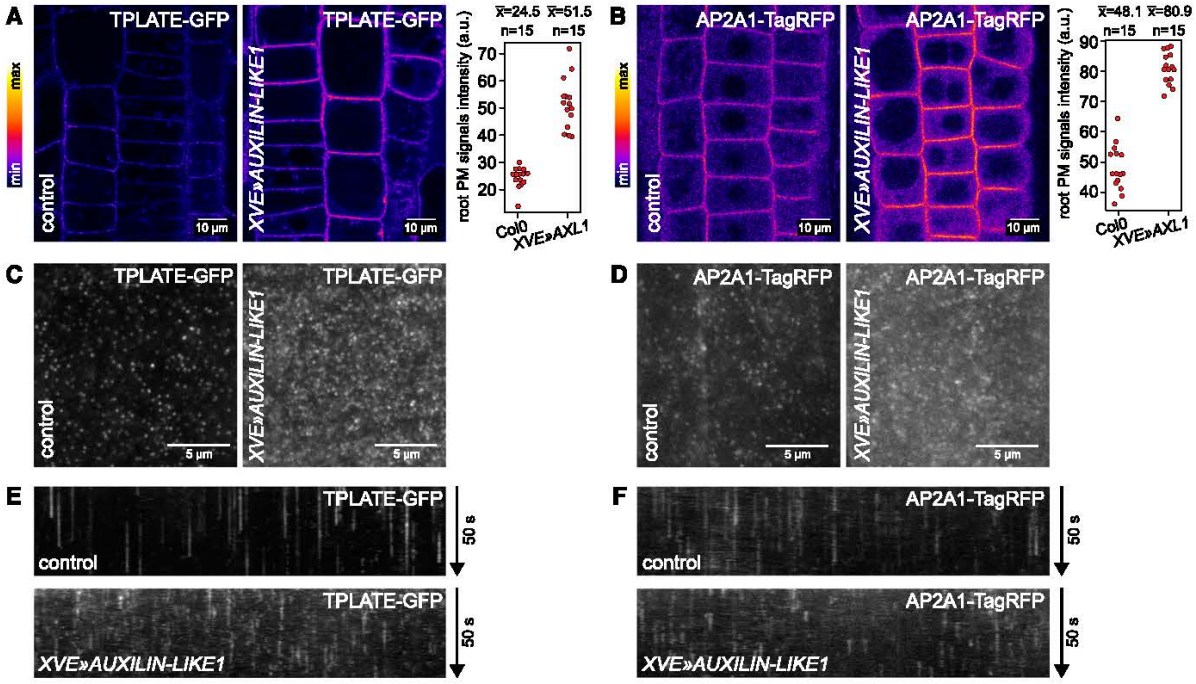


Figure 7. Increased PM Binding of Endocytic Adaptor Protein Complexes in *XVE»AUXILIN-LIKE1* Line.

Overexpression of AUXILIN-LIKE1 caused increased PM binding of TPLATE, a subunit of the TPLATE complex, as well as AP2A1, a subunit of the AP-2 complex. CLSM images from RAM epidermis (**[A]** and **[B]**) and VAEM images from hypocotyl epidermis (**[C]** and **[D]**) are shown. Graphs in **(A)** and **(B)** show PM signal intensity measurements from a representative experiment. Kymographs (**[E]** and **[F]**) show reduced lifetimes of TPLATE and AP2A1 foci in *XVE»AUXILIN-LIKE1* line, likely indicating that endocytic pits aborted after initiation. All experiments in this figure were performed after 16 to 24 h of *XVE»AUXILIN-LIKE1* induction.

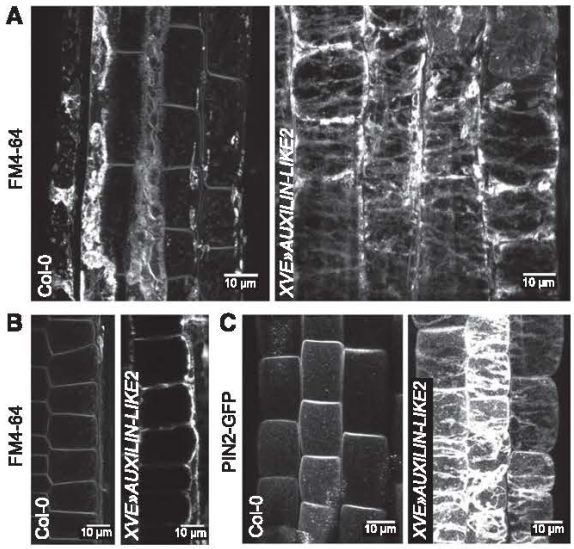


Figure 8. Excess Membrane Accumulation at the PM as a Result of Inhibited Endocytosis.

Overexpression of AUXILIN-LIKE2 caused excess deposition of membrane material at the PMs of root epidermis, as visualized with FM4-64 staining (**[A]** and **[B]**) or with PIN2-GFP **(C)**. **(A)** and **(C)** are maximum intensity projections of *z*-stacks through outer region of the epidermis, while **(B)** is a longitudinal section of epidermal cells showing membrane aggregation mainly in the outer domain. FM4-64-stained deposits in Col-0 in **(A)** are likely remnants of apoptosed lateral root cap cells.

Taken together, the imaging of endocytic cargoes, the endocytic machinery components, and the cellular distribution of membranes all demonstrated that overexpressing AUXILIN-LIKE1/2 leads to the inhibition of endocytosis. This phenomenon is analogous to the effect of overexpression of auxilin homologs in non-plant systems. However, we do not consider these data to necessarily be indicative of a vesicle-uncoating function of AUXILIN-LIKE1/2. The most parsimonious interpretation is that overexpressed AUXILIN-LIKE1/2 proteins may inhibit the recruitment of clathrin to initiating endocytic pits simply by binding to and retaining all available clathrin in the cytosol, although this simple model would not explain why the endosomal pools of clathrin remain intact (Figures 6A and 6B). While not proving a specific function in uncoating, these findings, together with our protein-protein interaction and subcellular localization data, constitute strong evidence for a clathrin-related function of AUXILIN-LIKE1/2.

AUXILIN-LIKE1/2 Loss of Function

In an attempt to address the specific molecular function of AUXILIN-LIKE1/2, we aimed to obtain *auxilin-like1/2* knockout plants. The behaviors of the two proteins in terms of interactions, localization, and the effects of overexpression were the same in our experiments, and the two proteins share very high sequence similarity. Therefore, we expected AUXILIN-LIKE1 and AUXILIN-LIKE2 to be functionally redundant, so we aimed to obtain a double mutant. *AUXILIN-LIKE1* and *AUXILIN-LIKE2* genes occupy a common locus on chromosome 4, in which their coding sequences are inversely oriented around a short, shared promoter region (Figure 9A). The genes are therefore tightly linked, making it impossible to generate double mutants by crossing single T-DNA insertion lines. Instead, we generated double knockouts by simultaneously targeting both homologs using CRISPR technology. The CRISPR method generates short (1–2 nucleotide) deletions or insertions in the target sequence, thus causing open reading frame shifts and disrupting the coding sequence. Using this approach, we isolated two double mutant combinations, *auxilin-like1/2*^{c1} and *auxilin-like1/2*^{c2}, as well as single *auxilin-like1* and *auxilin-like2* mutants (Figure 9A). To our surprise, both the single and the double mutants were phenotypically normal under standard growth conditions at the seedling and adult stages (Figure 9B). The plants also exhibited normal fertility. Furthermore, an FM4-64 uptake experiment using the RAM epidermis of *auxilin-like1/2*^{c1} seedlings did not indicate any defects in endocytosis (Figure 9C). This loss-of-function analysis revealed that Arabidopsis auxilin-like proteins are not essential for endocytosis and development, at least under optimal environmental conditions. This finding is in contrast to the results of similar analyses in animals such as mouse (*Mus musculus*), worm (*Caenorhabditis elegans*), and zebra fish (*Danio rerio*), where defects in growth and development of auxilin/GAK mutants were reported (Yim et al., 2010; Greener et al., 2001; Bai et al., 2010; Lee et al., 2008), hinting at crucial differences in the mechanism of clathrin-mediated endocytosis between plants and animals.

DISCUSSION

Here, we aimed to expand our knowledge of clathrin-mediated endocytosis in plants by searching for, and functionally characterizing, novel clathrin-associated proteins. Using a TAP-MS approach, we identified four CLC binding proteins with possible endocytic functions: CAP1, SH3P2, AUXILIN-LIKE1, and AUXILIN-LIKE2. We analyzed the binary interactions among these proteins and revealed their localization to the PM and the cell plate, two of the sites of clathrin action.

Our more detailed studies focused on characterizing the two putative uncoating factor homologs, AUXILIN-LIKE1 and AUXILIN-LIKE2. Like auxilin homologs in non-plants, we found that overexpressing AUXILIN-LIKE1/2 led to an inhibition of endocytosis. We believe that our inducible auxilin-overexpressing lines are useful and very efficient genetic tools for specifically interfering with endocytosis, with applications in studies of various clathrin-dependent processes (Ortiz-Morea et al., 2016). Our in-depth mapping of the effects of AUXILIN-LIKE1 overexpression on the molecular components of the endocytic pathway may prove interesting for researchers interested in the endocytic process itself. We note that the effect of AUXILIN-LIKE1/2 overexpression appears to be specific for the PM pool of clathrin, as we did not observe a loss of clathrin from the endosomal compartments.

The observation that membranes accumulated at the cell periphery, which we interpret as an effect of the continuation of secretion in the absence of endocytosis, tangibly demonstrates the interdependence of distinct trafficking processes in the endomembrane system. Although highly speculative, it is tempting to

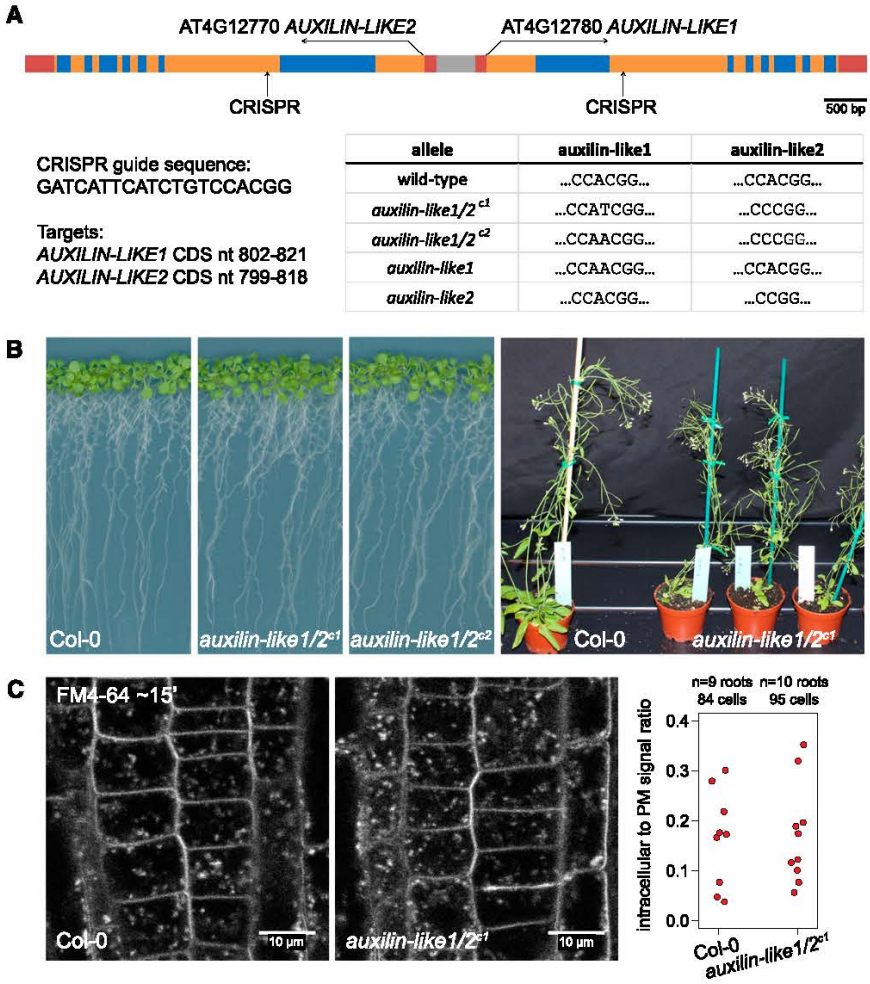


Figure 9. *auxilin-like1/2* Loss-of-Function Mutants.

(A) Isolation of *auxilin-like1/2* CRISPR mutants. Top: Overview of the *AUXILIN-LIKE1/2* genomic locus showing CRISPR target sites in the second exons of *AUXILIN-LIKE1* and *AUXILIN-LIKE2*. Bottom: Details of the CRISPR target sequence and the isolated mutant alleles.
(B) *auxilin-like1/2* double homozygous mutants, as well as single mutants, developed normally at both the seedling and adult stages.
(C) FM4-64 uptake into *auxilin-like1/2*^{c1} seedlings was comparable to that of the controls, indicating functional endocytosis.

hypothesize that the loss of cytoplasm in which the endomembrane compartments are embedded, together with the increase in vacuolar volume, as observed in AUXILIN-LIKE1/2-overexpressing lines, are also trafficking homeostasis-related phenomena, as they may represent secondary effects of the bulk loss of internal endomembrane compartments.

In an attempt to address the specific molecular function of AUXILIN-LIKE1/2, we also generated *auxilin-like1/2* mutants using CRISPR technology. We found that the loss of AUXILIN-LIKE1/2 function did not visibly affect endocytosis or plant growth and development under optimal growth conditions. This is in contrast to loss-of-function alleles of other endocytic components, which exhibit various defects in growth, development, and/or reduced fertility (Gadeyne et al., 2014; Kang et al., 2001, 2003; Collings et al., 2008; Kim et al., 2013; Kitakura et al., 2011). This observation also differs from that of auxilin loss-of-function mutants in yeast, whose growth is reduced (Ding et al., 2015), and auxilin/GAK loss-of-function mutants in animals such as mouse, worm, or zebra fish, where various aspects of development are affected (Yim et al., 2010; Greener et al., 2001; Bai et al., 2010; Lee et al., 2008).

We propose several possible interpretations for the lack of mutant phenotypes in *auxilin-like1/2*. First, it appears likely that AUXILIN-LIKE1/2 function is necessary for only a small subset of all clathrin-coated vesicles that form at the PM. This can be concluded from our VAEM colocalization analysis of clathrin and AUXILIN-LIKE1, in which we observed that a vast majority of

CCPs did not recruit AUXILIN-LIKE1. As discussed above, it is possible that auxilin-like recruitment often takes place in the cytosol, and such events could have been missed by our imaging system. However, it is also possible that most CCVs are in fact uncoated with the help of other factors, while the function of AUXILIN-LIKE1/2 is limited to only a specific subpopulation of vesicles. This appears consistent with the observation that knocking out the two genes does not visibly interfere with endocytosis, and it hints at the exciting possibility of the existence of functionally distinct populations of PM-derived CCVs in plant cells, only one of which uses the conserved auxilin-Hsc70 pathway for uncoating.

Second, the lack of evident phenotypes in *auxilin-like1/2* may be explained by a functional overlap between the closely homologous AUXILIN-LIKE1/2 pair and any of the five remaining auxilin-like proteins in Arabidopsis. However, we and others identify these proteins as auxilin-like only due to the presence of C-terminal DNAJ domains that recruit and activate the heat shock protein. The remaining portions of auxilin-likes have different lengths and bear little or no sequence similarity when comparisons are made between the closely homologous AUXILIN-LIKE1/2 pair and AUXILIN-LIKE3-7 (Supplemental Figure 9). The lack of sequence similarity, together with the specific detection of AUXILIN-LIKE1/2 but not AUXILIN-LIKE3-7 in our CLC-TAP assay, suggest a possible diversification in the functions of plant C-terminal DNAJ proteins beyond simply clathrin-related processes. An example of this is JAC1 (AUXILIN-LIKE6), which was identified in a forward genetic screen for regulators of light-dependent chloroplast relocations in the leaf (Suetsugu et al., 2005), a process, to our knowledge, not regulated by clathrin. An analysis of the effects of AUXILIN-LIKE3-7 overexpression, as well as clathrin binding assays, may help to address with more certainty whether any of these proteins could function in the endocytic process together with AUXILIN-LIKE1/2. At the moment, we hypothesize that plant cells recruit the chaperoning function of Hsc70 at various cellular locations using a suite of auxilin-like DNAJ domain proteins that act as binding adaptors between the chaperone and distinct target protein complexes.

As a final note, while it is true that some of the features of AUXILIN-LIKE1/2, such as the presence of a C-terminal DNAJ domain, the late recruitment to coated pits, and the effects of overexpression, suggest they possess a function identical to that of non-plant auxilins, our data are insufficient to draw specific conclusions about the molecular function of these auxilin-like proteins. Returning to protein sequence comparisons, when whole sequences are taken into consideration, neither AUXILIN-LIKE1/2 nor any other Arabidopsis auxilin-like are similar to non-plant auxilins; interestingly, yeast auxilin is overall not similar to animal auxilins either. Although biochemical experiments have suggested that AUXILIN-LIKE1 possesses uncoating activity in vitro (Lam et al., 2001), we believe that further investigation into the molecular function of AUXILIN-LIKE1/2 and into the uncoating of CCVs in plants, may bring more clarity. The recent finding that the yeast auxilin homolog AUX1/SWA2 not only participates in the uncoating of CCVs, but also functions with COPI and COPII-coated vesicles in the early secretory pathway (Ding et al., 2015), provides a cautionary tale against assuming that distantly similar proteins found across the tree of life possess identical molecular functions.

METHODS

Plant Materials

The following previously published *Arabidopsis thaliana* lines were used: *UBQ10$_{pro}$:SH3P2-GFP* (Zhuang et al., 2013), *PIN2$_{pro}$:PIN2-GFP* (Abas et al., 2006), *PIN2$_{pro}$:PIN2-Dendra* (Salanenka et al., 2018), *CLC2$_{pro}$:CLC2-GFP* and *DRP1C$_{pro}$:DRP1C-GFP* (Konopka and Bednarek, 2008), *INTAM:GAL4* (Friml et al., 2004), *TPLATE-GFP* × *AP2A1-TagRFP* (Gadeyne et al., 2014), and *35S$_{pro}$:PIN5-GFP* (Mravec et al., 2009).

The following lines and crosses were generated in this study: *XVE»AUXILIN-LIKE1*, *XVE»AUXILIN-LIKE2*, *XVE»AUXILIN-LIKE1×CLC2$_{pro}$:CLC2-GFP*, *XVE»AUXILIN-LIKE1×DRP1C$_{pro}$:DRP1C-GFP*, *XVE»AUXILIN-LIKE1×TPLATE-GFP*, *XVE»AUXILIN-LIKE1×AP2A1-TagRFP*, *XVE»AUXILIN-LIKE2×PIN2$_{pro}$:PIN2-GFP*, *XVE»AUXILIN-LIKE2×PIN2$_{pro}$:PIN2-Dendra*, *CAP1$_{pro}$:CAP1-mCherry*, *35S$_{pro}$:CAP1-RFP*, *35S$_{pro}$:SH3P2-GFP*, *UBQ10$_{pro}$:GFP-AUXILIN-LIKE1*, *CLC2$_{pro}$:CLC2-GFP×UBQ10$_{pro}$:mCherry-AUXILIN-LIKE1*, *35S$_{pro}$:RFP-AUXILIN-LIKE1*, *35S$_{pro}$:RFP-AUXILIN-LIKE2*, *UAS:GFP-AUXILIN-LIKE1*, *INTAM»GFP-AUXILIN-LIKE1* (*UAS:GFP-AUXILIN-LIKE1×'' INTAM:GAL4*), *auxilin-like1/2^{c1}*, *auxilin-like1/2^{c2}*, *auxilin-like1*, and *auxilin-like2*.

Unfortunately, *35S$_{pro}$:RFP-auxilin-like1/2* seeds are not available due to low yields and a high degree of silencing, but expression vectors for plant transformation can be provided instead.

Molecular Cloning

All constructs used for TAP, for generating stable Arabidopsis transgenic lines, and for BiFC assays were cloned with the Gateway system. The following Gateway entry clones were generated in this study: CLC1/pDONR221, AUXILIN-LIKE1/pENTR/D-TOPO, AUXILIN-LIKE2/pENTR/D-TOPO, AUXILIN-LIKE1/pDONRP2rP3, AUXILIN-LIKE2/pDONRP2rP3, CAP1/pENTR/D-TOPO, SH3P2/pENTR/D-TOPO (all in variants with and without stop codons), PIP5K1/pDONR221, and pCAP1/pDONRP4P1r. The coding sequences of *CLC1*, *AUXILIN-LIKE1*, *AUXILIN-LIKE2*, and *CAP1* were cloned from Arabidopsis (accession Columbia-0) cDNA, whereas those of *SH3P2* and the *CAP1* promoter were cloned from Arabidopsis Col-0 genomic DNA. The primers used are shown in Supplemental Table 1.

The expression vectors were cloned using previously published Gateway vectors (Karimi et al., 2002; Curtis and Grossniklaus, 2003; Van Leene et al., 2014). Constructs for TAP were generated by fusing CLC1 with TAP tags and with 35S promoter sequences in pKCTAP and pKCTAP destination vectors. The following constructs were cloned and used for stable transformation of Arabidopsis: *XVE»AUXILIN-LIKE1* and *XVE»AUXILIN-LIKE2* [pMDC7B(UBQ10)], *35S$_{pro}$:RFP-AUXILIN-LIKE1* and *35S$_{pro}$:RFP-AUXILIN-LIKE2* (pK7WGR2), *UAS:GFP-AUXILIN-LIKE1* (pK7m34GW), *UBQ10$_{pro}$:GFP-AUXILIN-LIKE1* (pB7m34GW,0), *UBQ10$_{pro}$:mCherry-AUXILIN-LIKE1* (pB7m34GW,0), *35S$_{pro}$:SH3P2-GFP* (pH7FWG2), *35S$_{pro}$:CAP1-RFP* (pK7RWG2), and *CAP1$_{pro}$:CAP1-mCherry* (pK7m34GW). The constructs used for the BiFC assays were cloned in p*7m34GW and p*7m24GW2 backbones (where * indicates resistance cassettes not relevant for these constructs) and consisted of fusions of N- and C-terminal parts of EGFP fused to CLC1, AUXILIN-LIKE1, AUXILIN-LIKE2, CAP1, SH3P2, and PIP5K1, all under the control of the 35S promoter.

TAP

TAP using CLC1 as bait was performed as described previously (Van Leene et al., 2014) with Arabidopsis cell cultures.

BiFC Assays

For the BiFC assays, *Nicotiana benthamiana* leaves were transiently transformed with *Agrobacterium tumefaciens*. The Agrobacterium strains carrying the BiFC constructs were grown to OD = 1, spun down, and

resuspended in infiltration buffer (10 mM $MgCl_2$, 10 mM MES, and 100 μM acetosyringone) to OD = 1.5. The suspensions were incubated at room temperature on a shaker for 2 h. Strains carrying the two assayed constructs were mixed and injected into the bottom sides of leaves. Leaves were imaged by CLSM 3 to 4 d after injection. Each interacting pair was assayed in three repeated experiments. Positive interactions displayed broad areas of GFP fluorescence throughout the injected leaf surface. Single photographs of GFP fluorescence were taken to document the results.

Growth Conditions and Chemical Induction of Transgenes

Arabidopsis seedlings were grown on half-strength Murashige and Skoog (1/2MS) medium with 1% (w/v) sucrose at 21°C under a 16-h-day/8-h-night cycle or in darkness for imaging in etiolated hypocotyls. Lights used were Philips GreenPower LED in deep red/far red/blue combination, intensity: 2100 μW ±10%. Estradiol induction of the *XVE»AUXILIN-LIKE1/2* lines was done by transferring 3-d-old seedlings to medium containing β-estradiol (Sigma-Aldrich) or solvent (ethanol) as a control. β-Estradiol concentrations used were 2.5 μg/mL (~9.18 μM) for experiments presented in Figures 3, 4, 5A to 5C, 5E, 6 to 8, and Supplemental Figure 7A and 2 μM for experiments presented in Figure 5D and Supplemental Figures 5 and 8. Induction of the *INTAM»GFP-AUXILIN-LIKE1* line was done analogously on medium supplemented with 2 μM tamoxifen (Sigma-Aldrich).

Seedling Root Morphology

For light microscopy of *XVE»AUXILIN-LIKE1/2* seedling roots, seedlings were stained in Lugol's solution for ~1 min, washed, and mounted on slides in chloral hydrate solution.

Immunostaining

An Intavis InsituPro VSi robot was used for immunostaining according to a previously published protocol (Sauer et al., 2006). The following antibodies were used: rabbit anti-PIN1 (1:1000; Paciorek et al., 2005), rabbit anti-PIN2 (1:1000; Abas et al., 2006), rabbit anti-KNOLLE (1:1000; Lauber et al. 1997), and anti-rabbit-Cy3 (1:600; Sigma-Aldrich; catalog no. C2306).

Fluorescent Imaging

CLSM imaging was done with a Zeiss LSM700, LSM800, and LSM880 confocal microscopes with Plan-Apochromat 20x/0.8 and Plan-Apochromat 40×/1.2 lenses. Long-term live imaging with root growth tracking was performed on a vertical Zeiss LSM700 as previously described (von Wangenheim et al., 2017).

VAEM imaging was performed with an Olympus IX83 inverted microscope equipped with a cell-TIRF module and an UAPON OTIRF 100× lens. For colocalization imaging of $CLC2_{pro}$*:CLC2-GFP*×$UBQ10_{pro}$*:mCherry-AUXILIN-LIKE1*, the two channels were captured sequentially.

FM4-64 and FM1-43 Staining

For FM4-64 uptake experiments, seedlings were stained in liquid 1/2MS medium with 1% (w/v) sucrose supplemented with 2 μM FM 4-64 dye (Thermo Fisher) for 5 min in the dark and on ice. Excess dye was washed off and the seedlings were mounted in 1/2MS medium with 1% (w/v) sucrose on microscopy slides at room temperature, marking the start of the internalization time measurement.

To visualize the membrane accumulation at the PMs of the *XVE»AUXILIN-LIKE2* line, and for colocalizations of fluorescent markers with PM-localized FM4-64 and FM1-43 stains, the seedlings were treated as described above but at room temperature and imaged immediately after washing. FM1-43 stain was used at 0.2 μM concentration.

BFA Treatments

Seedlings were incubated in liquid 1/2MS medium with 1% (w/v) sucrose and containing BFA (Sigma-Aldrich) at a final concentration of 25 μM. The solvent (DMSO) was added to the controls.

Propidium Iodide Staining

Propidium iodide (Sigma-Aldrich) was diluted 100× in 1/2MS medium with 1% (w/v) sucrose and roots were stained for 2 min before CLSM imaging.

Fluorescence Quantification

Quantification of CLSM and VAEM fluorescence images was performed using Fiji/ImageJ. FM4-64 uptake was quantified by comparing average PM and intracellular signal intensities in individual cells. BFA bodies stained by PIN1 were counted in circular areas 50 μm in diameter, placed in the middle of microscopic pictures. DRP1C-GFP foci at the PM in VAEM pictures were counted similarly in circular areas 120 pixels in diameter. PM signal intensities of TPLATE-GFP and AP2A1-TagRFP in root epidermis were measured on lines drawn along multiple PMs in individual microscopic pictures.

Quantitative RT-PCR

Total RNA from ~15 4-d-old seedlings induced with 2 μM β-estradiol/4-hydroxytamoxifen/solvent control (Sigma-Aldrich) for 24 h was extracted using the TRIzol reagent (Invitrogen) and purified using an RNeasy Mini Kit (Qiagen) according to manufacturer's instructions. Two micrograms of RNA was reverse-transcribed using an iScript cDNA Synthesis Kit (Bio-Rad). qRT-PCR was performed in 5-μL reactions using the LightCycler480 SYBR Green I Master Mix in a LightCycler480 II (ser. no. 5659; Roche) according to the manufacturer's instructions. Relative gene expression was calculated with the $2^{-\Delta\Delta CT}$ method (Livak and Schmittgen, 2001). The primers used are listed in Supplemental Table 1.

CRISPR Mutant Isolation

The CRISPR construct was cloned according to a published method (J. Richter, J.M. Watson, P. Stasnik, M. Borowska, J. Neuhold, P. Stolt-Bergner, V.K. Schoft, and M.T. Hauser, unpublished data). T1 plants transformed with the CRISPR construct were selected on Basta and resistant transformants genotyped for *AUXILIN-LIKE1/2* mutations by PCR amplification and sequencing of relevant gene fragments. Plants carrying mutations in auxilin-like paralogs were propagated, and the T2 progenies were PCR genotyped to find those that segregated out the CRISPR cassette (by amplification of the *Cas9* and *Bar* genes). Among them, single and double *auxilin-like* homozygotes were selected. The primers used are listed in Supplemental Table 1.

Protein Sequence Alignment

Auxilin-like protein sequences were aligned using the Geneious software package (www.geneious.com) with standard settings.

Accession Numbers

Sequence data from this article can be found in the GenBank/EMBL libraries under the following accession numbers: AUXILIN-LIKE1 (At4g12780), AUXILIN-LIKE2 (At4g12770), CAP1 (At4g32285), SH3P2 (At4g34660), CLC1 (At2g20760), CLC2 (At2g40060), CHC1 (At3g08530), CHC2 (At3g11130), DRP1C (At1g14830), TPLATE (At3g01780), AP2A1 (At5g22770), KNOLLE (At1g08560), PIN1 (At1g73590), PIN2 (At5g57090), AUXILIN-LIKE3 (At1g21660), AUXILIN-LIKE4 (At4g36520), AUXILIN-

LIKE5 (At1g75310), JAC1/AUXILIN-LIKE6 (At1g75100), AUXILIN-LIKE7 (At1g30280), PIP5K1 (At1g21980), and DHNAT2 (At5g48950).

Supplemental Data

Supplemental Figure 1. Additional BiFC interactions.

Supplemental Figure 2. Additional subcellular localization data for AUXILIN-LIKEs, SH3P2, and CAP1.

Supplemental Figure 3. Growth and development of seedlings in transgenic lines constitutively overexpressing AUXILIN-LIKE1, SH3P2, and CAP1.

Supplemental Figure 4. Uninduced controls for seed germination experiments with *XVE»AUXILIN-LIKE* lines.

Supplemental Figure 5. qPCR of inducible AUXILIN-LIKE overexpression lines.

Supplemental Figure 6. Correlation of GFP-AUXILIN-LIKE1 expression and root growth inhibition during *INTAM»GFP-AUXILIN-LIKE1* induction.

Supplemental Figure 7. Additional data on FM4-64 uptake in inducible AUXILIN-LIKE overexpression lines.

Supplemental Figure 8. Propidium iodide staining of *XVE»AUXILIN-LIKE2* roots.

Supplemental Figure 9. Protein sequence alignment of Arabidopsis AUXILIN-LIKE1-7.

Supplemental Table 1. Primers used in this study.

Supplemental Movie 1. VAEM colocalization of CLC2-GFP and mCherry-AUXILIN-LIKE1.

Supplemental Movie 2. VAEM imaging of CLC2-GFP in the *XVE»AUXILIN-LIKE1* line.

Supplemental Movie 3. VAEM imaging of TPLATE-GFP in the *XVE»AUXILIN-LIKE1* line.

Supplemental Movie 4. VAEM imaging of AP2A1-TagRFP in the *XVE»AUXILIN-LIKE1* line.

ACKNOWLEDGMENTS

We thank James Matthew Watson, Monika Borowska, and Peggy Stolt-Bergner at ProTech Facility of the Vienna Biocenter Core Facilities for the CRISPR/CAS9 construct; Anna Müller for assistance with molecular cloning; Sebastian Bednarek, Liwen Jiang, and Daniël Van Damme for sharing published material; Matyáš Fendrych, Daniël Van Damme, and Lindy Abas for valuable discussions; and Martine De Cock for help with correcting the manuscript. This work was supported by the European Research Council under the European Union Seventh Framework Programme (FP7/2007-2013)/ERC Grant 282300 and by the Ministry of Education of the Czech Republic/MŠMT project NPUI-LO1417.

AUTHOR CONTRIBUTIONS

All authors designed parts of the research. M.A., M.N., U.K., and M.G. performed experiments. M.A. and J.F. wrote the manuscript.

Received October 9, 2017; revised January 16, 2018; accepted March 5, 2018; published March 6, 2018.

REFERENCES

Abas, L., Benjamins, R., Malenica, N., Paciorek, T., Wiśniewska, J., Moulinier-Anzola, J.C., Sieberer, T., Friml, J., and Luschnig, C. (2006). Intracellular trafficking and proteolysis of the *Arabidopsis* auxin-efflux facilitator PIN2 are involved in root gravitropism. Nat. Cell Biol. **8:** 249–256.

Adamowski, M., and Friml, J. (2015). PIN-dependent auxin transport: action, regulation, and evolution. Plant Cell **27:** 20–32.

Ahle, S., and Ungewickell, E. (1990). Auxilin, a newly identified clathrin associated protein in coated vesicles fron bovine brain. J. Cell Biol. **111:** 19–29.

Ahn, G., et al. (2017). SH3P2 plays a crucial role at the step of membrane tubulation during cell plate formation in plants. Plant Cell **29:** 1388–1405.

Aniento, F., and Robinson, D.G. (2005). Testing for endocytosis in plants. Protoplasma **226:** 3–11.

Bai, T., Seebald, J.L., Kim, K.-E., Ding, H.-M., Szeto, D.P., and Chang, H.C. (2010). Disruption of zebrafish cyclin G-associated kinase (GAK) function impairs the expression of Notch-dependent genes during neurogenesis and causes defects in neuronal development. BMC Dev. Biol. **10:** 7.

Bashline, L., Li, S., Anderson, C.T., Lei, L., and Gu, Y. (2013). The endocytosis of cellulose synthase in *Arabidopsis* is dependent on μ2, a clathrin-mediated endocytosis adaptin. Plant Physiol. **163:** 150–160.

Ben Khaled, S., Postma, J., and Robatzek, S. (2015). A moving view: subcellular trafficking processes in pattern recognition receptor-triggered plant immunity. Annu. Rev. Phytopathol. **53:** 379–402.

Bolte, S., Talbot, C., Boutte, Y., Catrice, O., Read, N.D., and Satiat-Jeunemaitre, B. (2004). FM-dyes as experimental probes for dissecting vesicle trafficking in living plant cells. J. Microsc. **214:** 159–173.

Boucrot, E., Ferreira, A.P.A., Almeida-Souza, L., Debard, S., Vallis, Y., Howard, G., Bertot, L., Sauvonnet, N., and McMahon, H.T. (2014). Endophilin marks and controls a clathrin-independent endocytic pathway. Nature **517:** 460–465.

Boutté, Y., Frescatada-Rosa, M., Men, S., Chow, C.-M., Ebine, K., Gustavsson, A., Johansson, L., Ueda, T., Moore, I., Jürgens, G., and Grebe, M. (2010). Endocytosis restricts *Arabidopsis* KNOLLE syntaxin to the cell division plane during late cytokinesis. EMBO J. **29:** 546–558.

Collings, D.A., Gebbie, L.K., Howles, P.A., Hurley, U.A., Birch, R.J., Cork, A.H., Hocart, C.H., Arioli, T., and Williamson, R.E. (2008). *Arabidopsis* dynamin-like protein DRP1A: A null mutant with widespread defects in endocytosis, cellulose synthesis, cytokinesis, and cell expansion. J. Exp. Bot. **59:** 361–376.

Curtis, M.D., and Grossniklaus, U. (2003). A Gateway cloning vector set for high-throughput functional hnalysis of henes in planta. Plant Physiol. **133:** 462–469.

Dhonukshe, P., Aniento, F., Hwang, I., Robinson, D.G., Mravec, J., Stierhof, Y.D., and Friml, J. (2007). Clathrin-mediated constitutive endocytosis of PIN auxin efflux carriers in *Arabidopsis*. Curr. Biol. **17:** 520–527.

Ding, J., Segarra, V.A., Chen, S., Cai, H., Lemmon, S.K., and Ferro-Novick, S. (2015). Auxilin facilitates membrane traffic in the early secretory pathway. Mol. Biol. Cell **27:** 1–36.

Di Rubbo, S., et al. (2013). The clathrin adaptor complex AP-2 mediates endocytosis of BRASSINOSTEROID INSENSITIVE1 in *Arabidopsis*. Plant Cell **25:** 2986–2997.

Emons, A.M.C., and Traas, J.A. (1986). Coated pits and coated vesicles on the plasma membrane of plant cells. Eur. J. Cell Biol. **41:** 57–64.

Fan, L., Hao, H., Xue, Y., Zhang, L., Song, K., Ding, Z., and Botella, M.A., Wang, H., Lin, J. (2013). Dynamic analysis of *Arabidopsis* AP2 σ subunit reveals a key role in clathrin-mediated endocytosis and plant development. Development **140:** 3826–3837.

Feraru, E., Paciorek, T., Feraru, M.I., Zwiewka, M., De Groodt, R., De Rycke, R., Kleine-Vehn, J., and Friml, J. (2010). The AP-3 β-adaptin mediates the biogenesis and function of lytic vacuoles in *Arabidopsis*. Plant Cell **22:** 2812–2824.

Friml, J., et al. (2004). A PINOID-dependent binary switch in apical-basal PIN polar targeting directs auxin efflux. Science **306:** 862–865.

Fuji, K., Shirakawa, M., Shimono, Y., Kunieda, T., Fukao, Y., Koumoto, Y., Takahashi, H., Hara-Nishimura, I., and Shimada, T. (2016). The adaptor complex AP-4 regulates vacuolar protein sorting at the trans-Golgi network by interacting with VACUOLAR SORTING RECEPTOR1. Plant Physiol. **170:** 211–219.

Gadeyne, A., et al. (2014). The TPLATE adaptor complex drives clathrin-mediated endocytosis in plants. Cell **156:** 691–704.

Galway, M.E., Rennie, P.J., and Fowke, L.C. (1993). Ultrastructure of the endocytotic pathway in glutaraldehyde-fixed and high-pressure frozen/freeze-substituted protoplasts of white spruce (*Picea glauca*). J. Cell Sci. **3:** 847–858.

Gao, B., Biosca, J., Craig, E.A., Greene, L.E., and Eisenberg, E. (1991). Uncoating of coated vesicles by yeast hsp70 proteins. J. Biol. Chem. **266:** 19565–19571.

Greener, T., Grant, B., Zhang, Y., Wu, X., Greene, L.E., Hirsh, D., and Eisenberg, E. (2001). *Caenorhabditis elegans* auxilin: a J-domain protein essential for clathrin-mediated endocytosis in vivo. Nat. Cell Biol. **3:** 215–219.

Henne, W.M., Boucrot, E., Meinecke, M., Evergren, E., Vallis, Y., Mittal, R., and McMahon, H.T. (2010). FCHo proteins are nucleators of clathrin-mediated endocytosis. Science **328:** 1281–1284.

Irani, N.G., et al. (2012). Fluorescent castasterone reveals BRI1 signaling from the plasma membrane. Nat. Chem. Biol. **8:** 583–589.

Ischebeck, T., et al. (2013). Phosphatidylinositol 4,5-bisphosphate influences PIN polarization by controlling clathrin-mediated membrane trafficking in *Arabidopsis*. Plant Cell **25:** 4894–4911.

Jelínková, A., Malínská, K., Simon, S., Kleine-Vehn, J., Pařezová, M., Pejchar, P., Kubeš, M., Martinec, J., Friml, J., Zažímalová, E., and Petrášek, J. (2010). Probing plant membranes with FM dyes: tracking, dragging or blocking? Plant J. **61:** 883–892.

Kang, B.H., Busse, J.S., Dickey, C., Rancour, D.M., and Bednarek, S.Y. (2001). The *Arabidopsis* cell plate-associated dynamin-like protein, ADL1Ap, is required for multiple stages of plant growth and development. Plant Physiol. **126:** 47–68.

Kang, B.H., Rancour, D.M., and Bednarek, S.Y. (2003). The dynamin-like protein ADL1C is essential for plasma membrane maintenance during pollen maturation. Plant J. **35:** 1–15.

Karimi, M., Inzé, D., and Depicker, A. (2002). GATEWAY™ vectors for Agrobacterium-mediated plant transformation. Trends Plant Sci. **7:** 193–195.

Kerppola, T.K. (2009). Visualization of molecular interactions using analysis: Characteristics of protein fragment complementation. Chem. Soc. Rev. **38:** 2876–2886.

Kim, S.Y., Xu, Z.-Y., Song, K., Kim, D.H., Kang, H., Reichardt, I., Sohn, E.J., Friml, J., Juergens, G., and Hwang, I. (2013). Adaptor protein complex 2-mediated endocytosis Is crucial for male reproductive organ development in *Arabidopsis*. Plant Cell **25:** 2970–2985.

Kitakura, S., Vanneste, S., Robert, S., Löfke, C., Teichmann, T., Tanaka, H., and Friml, J. (2011). Clathrin mediates endocytosis and polar distribution of PIN auxin transporters in *Arabidopsis*. Plant Cell **23:** 1920–1931.

Kolb, C., Nagel, M.-K., Kalinowska, K., Hagmann, J., Ichikawa, M., Anzenberger, F., Alkofer, A., Sato, M.H., Braun, P., and Isono, E. (2015). FYVE1 is essential for vacuole biogenesis and intracellular trafficking in *Arabidopsis*. Plant Physiol. **167:** 1361–1373.

Konopka, C.A., Backues, S.K., and Bednarek, S.Y. (2008). Dynamics of *Arabidopsis* dynamin-related protein 1C and a clathrin light chain at the plasma membrane. Plant Cell **20:** 1363–1380.

Konopka, C.A., and Bednarek, S.Y. (2008). Variable-angle epifluorescence microscopy: A new way to look at protein dynamics in the plant cell cortex. Plant J. **53:** 186–196.

Lam, B.C., Sage, T.L., Bianchi, F., and Blumwald, E. (2001). Role of SH3 domain-containing proteins in clathrin-mediated vesicle trafficking in *Arabidopsis*. Plant Cell **13:** 2499–2512.

Lauber, M.H., Waizenegger, I., Steinmann, T., Schwarz, H., Mayer, U., Hwang, I., Lukowitz, W., and Jürgens, G. (1997). KNOLLE protein is a cytokinesis-specific syntaxin. Cell **139:** 1485–1493.

Lee, D.-W., Wu, X., Eisenberg, E., and Greene, L.E. (2006). Recruitment dynamics of GAK and auxilin to clathrin-coated pits during endocytosis. J. Cell Sci. **119:** 3502–3512.

Lee, D., Zhao, X., Yim, Y.-I., Eisenberg, E., and Greene, L.E. (2008). Essential role of cyclin-G-associated kinase (auxilin-2) in developing and mature mice. Mol. Biol. Cell **19:** 2766–2776.

Van Leene, J., et al. (2014). An improved toolbox to unravel the plant cellular machinery by tandem affinity purification of *Arabidopsis* protein complexes. Nat. Protoc. **10:** 169–187.

Livak, K.J., and Schmittgen, T.D. (2001). Analysis of relative gene expression data using real-time quantitative PCR and the $2-\Delta\Delta CT$ method. Methods **25:** 402–408.

Łangowski, Ł., Wabnik, K., Li, H., Vanneste, S., Naramoto, S., Tanaka, H., and Friml, J. (2016). Cellular mechanisms for cargo delivery and polarity maintenance at different polar domains in plant cells. Cell Discov. **2:** 16018.

Massol, R.H., Boll, W., Griffin, A.M., and Kirchhausen, T. (2006). A burst of auxilin recruitment determines the onset of clathrin-coated vesicle uncoating. Proc. Natl. Acad. Sci. USA **103:** 10265–10270.

McMahon, H.T., and Boucrot, E. (2011). Molecular mechanism and physiological functions of clathrin-mediated endocytosis. Nat. Rev. Mol. Cell Biol. **12:** 517–533.

Mersey, B.G., Griffing, L.R., Rennie, P.J., Fowke, L.C., Mersey, B.G., Griffing, L.R., Rennie, P.J., and Fowke, L.C. (1985). The isolation of coated vesicles from protoplasts of soybean. Planta **163:** 317–327.

Mravec, J., et al. (2009). Subcellular homeostasis of phytohormone auxin is mediated by the ER-localized PIN5 transporter. Nature **459:** 1136–1140.

Nagel, M.-K., Kalinowska, K., Vogel, K., Reynolds, G.D., Wu, Z., Anzenberger, F., Ichikawa, M., Tsutsumi, C., Sato, M.H., Kuster, B., Bednarek, S.Y., and Isono, E. (2017). *Arabidopsis* SH3P2 is an ubiquitin-binding protein that functions together with ESCRT-I and the deubiquitylating enzyme AMSH3. Proc. Natl. Acad. Sci. USA **114:** E7197–E7204.

Naramoto, S., Otegui, M.S., Kutsuna, N., de Rycke, R., Dainobu, T., Karampelias, M., Fujimoto, M., Feraru, E., Miki, D., Fukuda, H., Nakano, A., and Friml, J. (2014). Insights into the localization and function of the membrane trafficking regulator GNOM ARF-GEF at the Golgi apparatus in *Arabidopsis*. Plant Cell **26:** 3062–3076.

Nodzyński, T., Vanneste, S., Zwiewka, M., Pernisová, M., Hejátko, J., and Friml, J. (2016). Enquiry into the topology of plasma membrane-localized PIN auxin transport components. Mol. Plant **9:** 1504–1519.

Ortiz-Morea, F.A., et al. (2016). Danger-associated peptide signaling in *Arabidopsis* requires clathrin. Proc. Natl. Acad. Sci. USA **113:** 11028–11033.

Paciorek, T., Zazímalová, E., Ruthardt, N., Petrásek, J., Stierhof, Y.D., Kleine-Vehn, J., Morris, D.A., Emans, N., Jürgens, G., Geldner, N., and Friml, J. (2005). Auxin inhibits endocytosis and promotes its own efflux from cells. Nature **435:** 1251–1256.

Park, M., Song, K., Reichardt, I., Kim, H., Mayer, U., Stierhof, Y.-D., Hwang, I., and Jurgens, G. (2013). *Arabidopsis* mu-adaptin subunit AP1M of adaptor protein complex 1 mediates late secretory and vacuolar traffic and is required for growth. Proc. Natl. Acad. Sci. USA **110:** 10318–10323.

Renard, H.-F., et al. (2014). Endophilin-A2 functions in membrane scission in clathrin-independent endocytosis. Nature **517:** 493–496.

Richter, J., Watson, J.M., Stasnik, P., Borowska, M., Neuhold, J., Stolt-Bergner, P., Schoft, V.K., and Hauser, M.T. (2018). Multiplex mutagenesis with CRISPR/CAS9 exposes growth regulatory roles of four clustered CrRLK1L to metal ions. submitted.

Richter, S., Kientz, M., Brumm, S., Nielsen, M.E., Park, M., Gavidia, R., Krause, C., Voss, U., Beckmann, H., Mayer, U., Stierhof, Y.D., and Jürgens, G. (2014). Delivery of endocytosed proteins to the cell-division plane requires change of pathway from recycling to secretion. eLife **2014:** 1–16.

Robinson, D.G., and Pimpl, P. (2014). Clathrin and post-Golgi trafficking: A very complicated issue. Trends Plant Sci. **19:** 134–139.

Salanenka, Y., Verstraeten, I., Löfke, Ch., Tabata, K., Naramoto, S., Glanc, M., and Friml, J. (2018). Gibberellin DELLA signaling targets the retromer complex to redirect protein trafficking to the plasma membrane. Proc. Natl. Acad. Sci. USA **pii:** 201721760.

Sauer, M., Paciorek, T., Benková, E., and Friml, J. (2006). Immunocytochemical techniques for whole-mount *in situ* protein localization in plants. Nat. Protoc. **1:** 98–103.

Scheuring, D., Viotti, C., Kruger, F., Kunzl, F., Sturm, S., Bubeck, J., Hillmer, S., Frigerio, L., Robinson, D.G., Pimpl, P., and Schumacher, K. (2011). Multivesicular bodies mature from the trans-Golgi network/early endosome in *Arabidopsis.* Plant Cell **23:** 3463–3481.

Song, K., Jang, M., Kim, S.Y., Lee, G., Lee, G.-J., Kim, D.H., Lee, Y., Cho, W., and Hwang, I. (2012). An A/ENTH domain-containing protein functions as an adaptor for clathrin-coated vesicles on the growing cell plate in *Arabidopsis* root cells. Plant Physiol. **159:** 1013–1025.

Suetsugu, N., Kagawa, T., Wada, M., and Corporation, T. (2005). An auxilin-like J-domain protein, JAC1, regulates phototropin-mediated chloroplast movement. Plant Physiol. **139:** 151–162.

Tanaka, H., Kitakura, S., Rakusová, H., Uemura, T., Feraru, M.I., de Rycke, R., Robert, S., Kakimoto, T., and Friml, J. (2013). Cell polarity and patterning by PIN trafficking through early endosomal compartments in *Arabidopsis thaliana.* PLoS Genet. **9:** 1–9.

Tanchak, M.A., Griffing, L.R., Mersey, B.G., and Fowke, L.C. (1984). Endocytosis of cationized ferritin by coated vesicles of soybean protoplasts. Planta **162:** 481–486.

Tejos, R., Sauer, M., Vanneste, S., Palacios-Gomez, M., Li, H., Heilmann, M., van Wijk, R., Vermeer, J.E.M., Heilmann, I., Munnik, T., and Friml, J. (2014). Bipolar plasma membrane distribution of phosphoinositides and their requirement for auxin-mediated cell polarity and patterning in *Arabidopsis.* Plant Cell **26:** 2114–2128.

Ungewickell, E., Ungewickell, H., Holstein, S.E.H., Linder, R., Prasad, K., Barouch, W., Martin, B., Greene, L.E., and Eisenberg, E. (1995). Role of auxilin in uncoating clathrin-coated vesicles. Nature **378:** 632–635.

von Wangenheim, D., Hauschild, R., Fendrych, M., Barone, V., Benková, E., and Friml, J. (2017). Live tracking of moving samples in confocal microscopy for vertically grown roots. eLife **6:** 1–20.

Wang, C., Yan, X., Chen, Q., Jiang, N., Fu, W., Ma, B., Liu, J., Li, C., Bednarek, S.Y., and Pan, J. (2013a). Clathrin light chains regulate clathrin-mediated trafficking, auxin signaling, and development in *Arabidopsis.* Plant Cell **25:** 499–516.

Wang, J.-G., Li, S., Zhao, X.-Y., Zhou, L.-Z., Huang, G.-Q., Feng, C., and Zhang, Y. (2013b). HAPLESS13, the *Arabidopsis* μ1 adaptin, is essential for protein sorting at the trans-Golgi network/early endosome. Plant Physiol. **162:** 1897–1910.

Wang, X., Cai, Y., Wang, H., Zeng, Y., Zhuang, X., Li, B., and Jiang, L. (2014). Trans-Golgi network-located AP1 gamma adaptins mediate dileucine motif-directed vacuolar targeting in *Arabidopsis.* Plant Cell **26:** 4102–4118.

Widhalm, J.R., Ducluzeau, A.L., Buller, N.E., Elowsky, C.G., Olsen, L.J., and Basset, G.J.C. (2012). Phylloquinone (vitamin K1) biosynthesis in plants: Two peroxisomal thioesterases of lactobacillales origin hydrolyze 1,4-dihydroxy-2-naphthoyl-coa. Plant J. **71:** 205–215.

Xing, Y., Böcking, T., Wolf, M., Grigorieff, N., Kirchhausen, T., and Harrison, S.C. (2010). Structure of clathrin coat with bound Hsc70 and auxilin: mechanism of Hsc70-facilitated disassembly. EMBO J. **29:** 655–665.

Yamaoka, S., Shimono, Y., Shirakawa, M., Fukao, Y., Kawase, T., Hatsugai, N., Tamura, K., Shimada, T., and Hara-Nishimura, I. (2013). Identification and dynamics of *Arabidopsis* Adaptor Protein-2 complex and its involvement in floral organ development. Plant Cell **25:** 2958–2969.

Yim, Y.-I., Sun, T., Wu, L.-G., Raimondi, A., De Camilli, P., Eisenberg, E., and Greene, L.E. (2010). Endocytosis and clathrin-uncoating defects at synapses of auxilin knockout mice. Proc. Natl. Acad. Sci. USA **107:** 4412–4417.

Yoshinari, A., Fujimoto, M., Ueda, T., Inada, N., Naito, S., and Takano, J. (2016). DRP1-dependent endocytosis is essential for polar localization and boron-induced degradation of the borate transporter BOR1 in *Arabidopsis thaliana.* Plant Cell Physiol. **57:** 1985–2000.

Zhang, Y., Persson, S., Hirst, J., Robinson, M.S., van Damme, D., and Sánchez-Rodríguez, C. (2015). Change your Tplate, change your fate: Plant CME and beyond. Trends Plant Sci. **20:** 41–48.

Zhao, X., Greener, T., Al-Hasani, H., Cushman, S.W., Eisenberg, E., and Greene, L.E. (2001). Expression of auxilin or AP180 inhibits endocytosis by mislocalizing clathrin: evidence for formation of nascent pits containing AP1 or AP2 but not clathrin. J. Cell Sci. **114:** 353–365.

Zhuang, X., Cui, Y., Gao, C., and Jiang, L. (2015). Endocytic and autophagic pathways crosstalk in plants. Curr. Opin. Plant Biol. **28:** 39–47.

Zhuang, X., Wang, H., Lam, S.K., Gao, C., Wang, X., Cai, Y., and Jiang, L. (2013). A BAR-domain protein SH3P2, which binds to phosphatidylinositol 3-phosphate and ATG8, regulates autophagosome formation in *Arabidopsis.* Plant Cell **25:** 4596–4615.

Zouhar, J., and Sauer, M. (2014). Helping hands for budding prospects: ENTH/ANTH/VHS accessory proteins in endocytosis, vacuolar transport, and secretion. Plant Cell **26:** 1–13.

Zwiewka, M., Feraru, E., Möller, B., Hwang, I., Feraru, M.I., Kleine-Vehn, J., Weijers, D., and Friml, J. (2011). The AP-3 adaptor complex is required for vacuolar function in *Arabidopsis.* Cell Res. **21:** 1711–1722.

A Functional Study of AUXILIN-LIKE1 and 2, Two Putative Clathrin Uncoating Factors in Arabidopsis

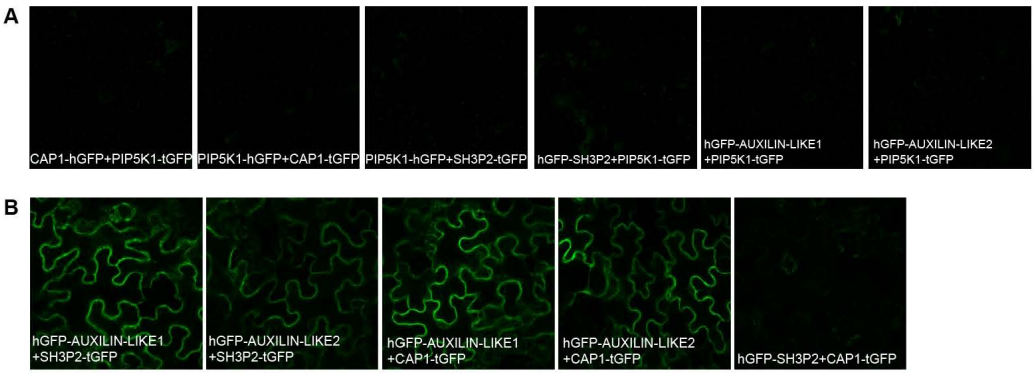
Maciek Adamowski, Madhumitha Narasimhan, Urszula Kania, Matous Glanc, Geert De Jaeger and Jirí Friml

Plant Cell 2018;30;700-716; originally published online March 6, 2018;
DOI 10.1105/tpc.17.00785

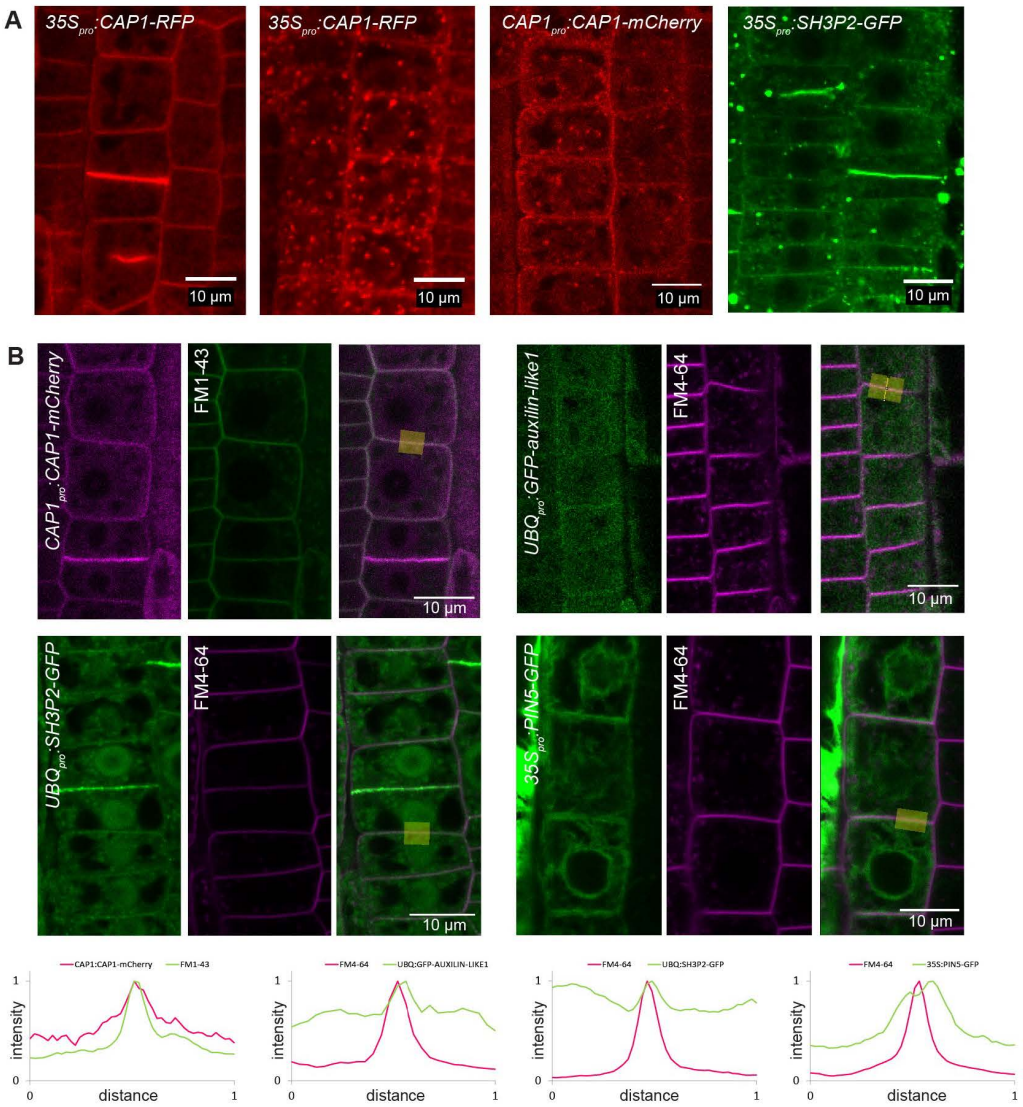
This information is current as of September 20, 2018

Supplemental Data	**/content/suppl/2018/03/06/tpc.17.00785.DC1.html**
References	This article cites 81 articles, 39 of which can be accessed free at: /content/30/3/700.full.html#ref-list-1
Permissions	https://www.copyright.com/ccc/openurl.do?sid=pd_hw1532298X&issn=1532298X&WT.mc_id=pd_hw1532298X
eTOCs	Sign up for eTOCs at: http://www.plantcell.org/cgi/alerts/ctmain
CiteTrack Alerts	Sign up for CiteTrack Alerts at: http://www.plantcell.org/cgi/alerts/ctmain
Subscription Information	Subscription Information for *The Plant Cell* and *Plant Physiology* is available at: http://www.aspb.org/publications/subscriptions.cfm

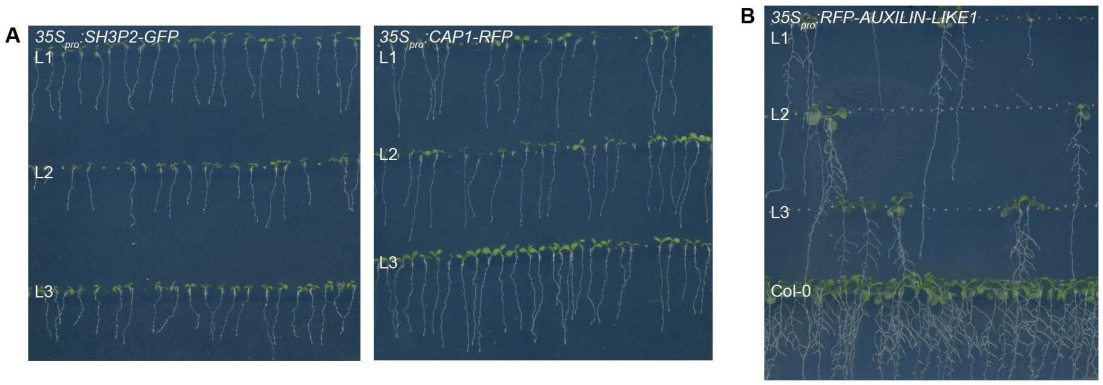
© American Society of Plant Biologists
ADVANCING THE SCIENCE OF PLANT BIOLOGY



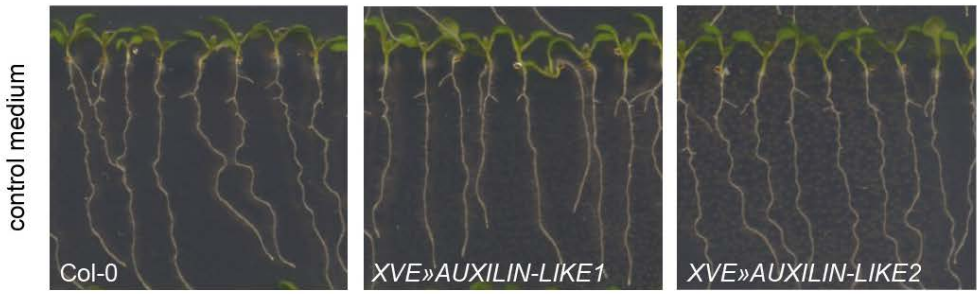
Supplemental Figure 1. Additional BiFC interactions.
(Supports Figure 1)
(A) Lack of interaction and GFP fluorescence upon coexpression of any CLC1 interactor with PIPK51.
(B) BiFC interactions among selected CLC1 interactors. AUXILIN-LIKE1/2 interacted with CAP1 and SH3P2, but no interaction was detected between SH3P2 and CAP1.



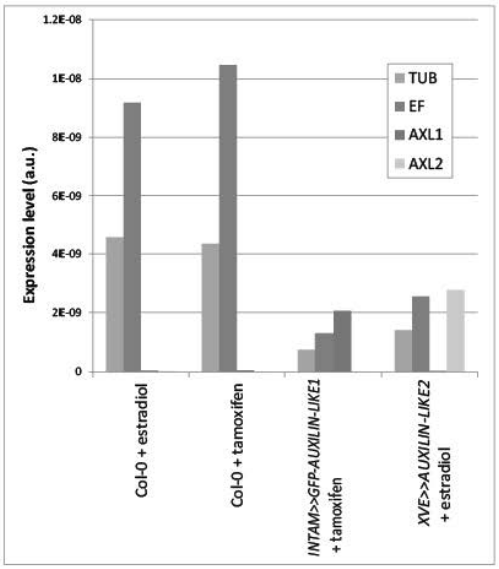
Supplemental Figure 2. Additional subcellular localisation data for AUXILIN-LIKEs, SH3P2 and CAP1. (Supports Figure 2)
(A) *35S$_{pro}$:CAP1-RFP* line showed PM and cell plate localisation with faint cytosolic background signal. In both *35S$_{pro}$:CAP1-RF*P and *CAP1$_{pro}$:CAP1-mCherry* lines, signal was detected at the endosomes in some (~10%) of the seedlings analysed. *35S$_{pro}$:SH3P2-GFP* localised to PM, cell plate and endosomes or intracellular aggregates.
(B) Colocalisation of CAP1, AUXILIN-LIKE1, and SH3P2 with the PM marked by FM4-64 and FM1-43 stains. PIN5-GFP, an ER-localised marker, was used as a negative control. Graphs show measurements of signal intensity along lines drawn across the PM and surrounding area.



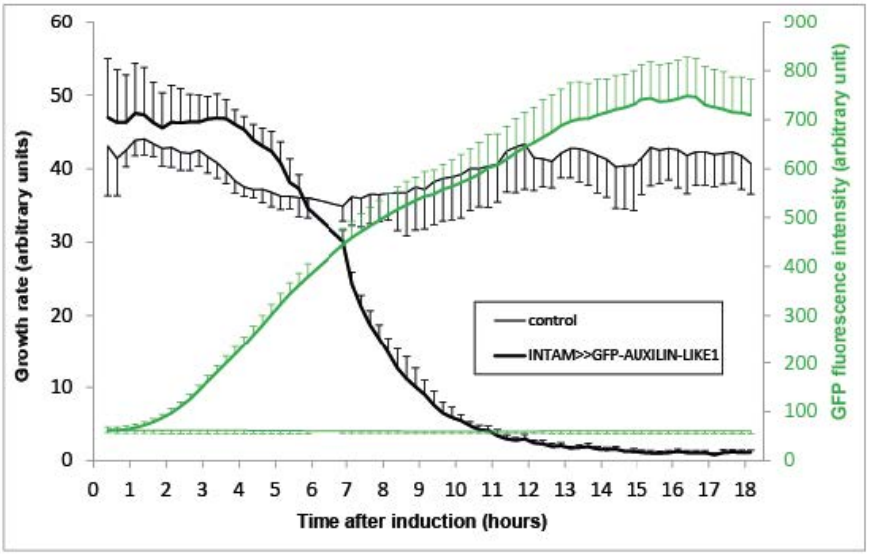
Supplemental Figure 3. Growth and development of seedlings in transgenic lines constitutively overexpressing AUXILIN-LIKE1, SH3P2, and CAP1.
(A) Normal seed germination and growth in *35S$_{pro}$:SH3P2-GFP* and *35S $_{pro}$:CAP1-RFP* lines.
(B) Germination arrest in segregating T2 populations of *35S$_{pro}$:RFP-AUXILIN-LIKE1* lines. *35S$_{pro}$:RFP-AUXILIN-LIKE2* lines behaved similarly and are not shown.
L1, L2, L3 – distinct transgenic lines.



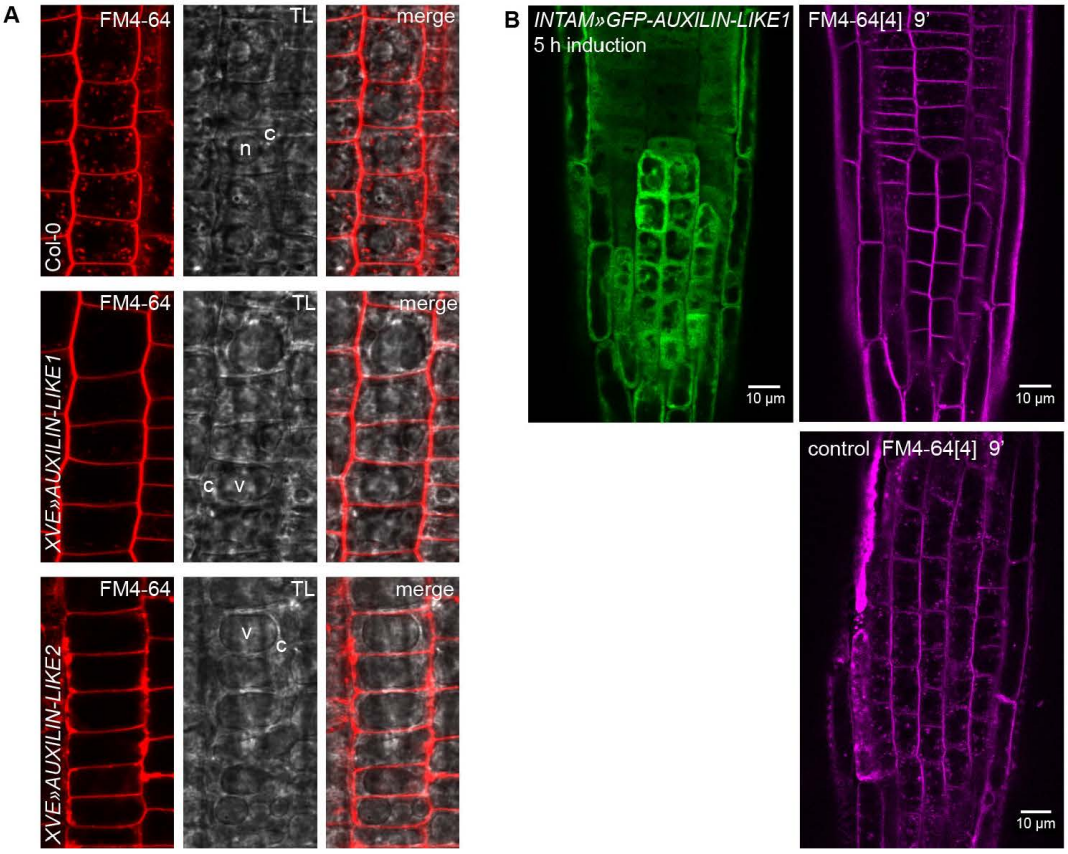
Supplemental Figure 4. Uninduced controls for seed germination experiments with *XVE»AUXILIN-LIKE* lines.
(Supports Figure 3)
Normal germination and growth of *XVE»AUXILIN-LIKE1/2* seedlings on a medium without beta-estradiol.



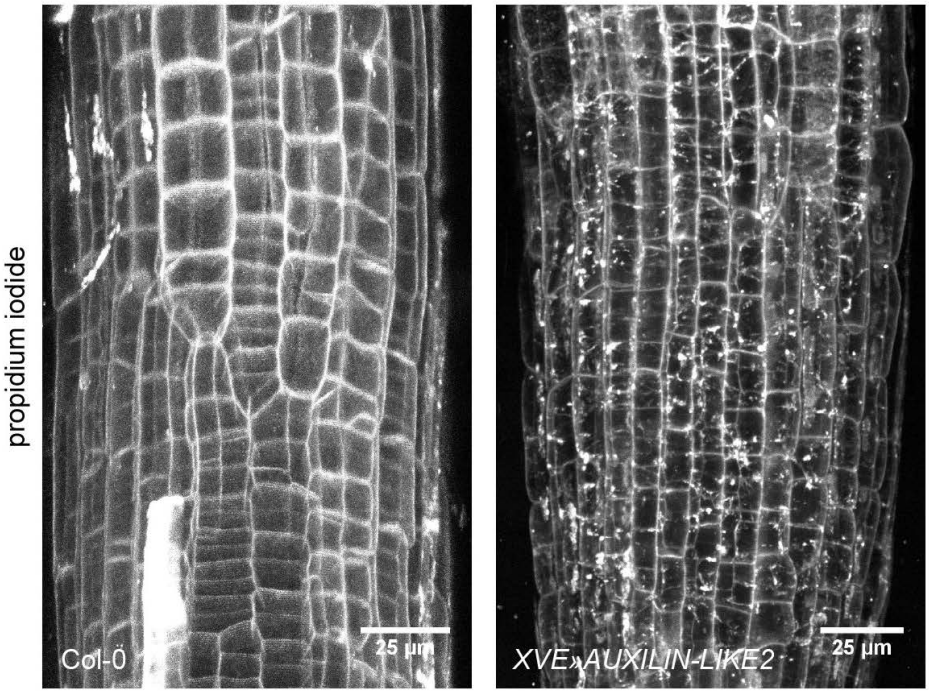
Supplemental Figure 5. qPCR of inducible AUXILIN-LIKE overexpression lines (Supports Figure 3).
Expression level of auxilin-like1 and auxilin-like2 were scored in *INTAM»GFP- AUXILIN-LIKE1* and *XVE»AUXILIN-LIKE 2* 24h after induction. Results are expressed as the average +/- standard deviation of three biological replicates (RNA isolates from three distinct pools of approx.. 15 seedlings) and three technical replicates (three qPCR reactions on each cDNA sample). Tubulin beta-chain 2 (TUB2, AT5G62690) and GTP binding Elongation factor Tu family protein (EF1, AT5G60390) were used as reference genes.



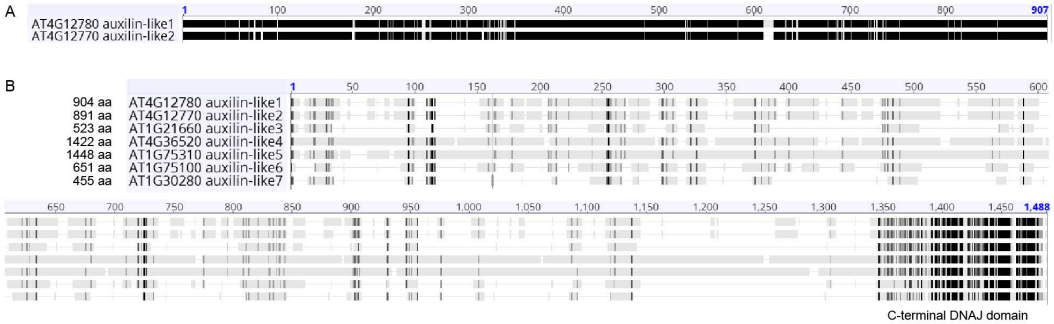
Supplemental Figure 6 . Correlation of GFP-AUXILIN-LIKE1 expression and root growth inhibition during *INTAM»GFP-AUXILIN-LIKE1* induction.
(Supports Figure 3).
Growth rates (in black) were automatically measured by TipTracker (von Wangenheim et al. 2017) during long-term live microscopy and compared with GFP-AUXILIN-LIKE1 signal intensities (in green; mean gray values of sum projections of z-stacks) in whole root tips. 6 control and 8 induced roots were analysed. Error bars for growth and GFP intensity indicate standard deviations. Only single (upper or lower) bar is drawn for clarity.



Supplemental Figure 7. Additional data on FM4-64 uptake in inducible AUXILIN-LIKE overexpression lines
(Supports Figure 4)
(A) Comparison of FM4-64 fluorescence and transmitted light channel showing areas of cytosol with faint or absent staining of endosomes in the auxilin-like1/2-overexpressing lines. V, vacuole; n, nucleus; c, cytoplasm.
(B) FM4-64 uptake into the lateral root cap was inhibited after 5h of induction in *INTAM»GFP-AUXILIN-LIKE1* line concomitant with high expression of the transgene in this tissue. Control shows FM4-64 uptake into lateral root cap in the wild type.



Supplemental Figure 8. Propidium iodide staining of *XVE»AUXILIN-LIKE2* roots.
(Supports Figure 8)
Propidium iodide staining of cell walls demonstrates aggregations in the cell wall, similar in appearance to the agglomerations of membranes observed in this line. PI staining was overall stronger in *XVE»AUXILIN-LIKE2* and the detection sensitivity had to be adjusted to achieve correctly exposed pictures.



Supplemental Figure 9. Protein sequence alignment of *A. thaliana* AUXILIN-LIKE1-7.
Protein sequence alignments highlighting high overall similarity between AUXILIN-LIKE1 and AUXILIN-LIKE2 (A) and little similarity between AUXILIN-LIKE1/2 and AUXILIN-LIKE3-7 with the exception of the C-terminal DNAJ domain (B). Gray-to-black scale represents local similarity score. Lengths of the proteins are indicated.

Supplemental Table 1. Primers used in this study.

Primers used for molecular cloning.

Construct	F primer	R primer (with stop codon)	R primer (without stop codon)
AUXILIN-LIKE1/pENTR	CACCATGGATGATTTCAC AGGATTGTT	TCAGAAGAGTTCTTCTGAGTT AAAC	GAAGAGTTCTTCTGAGTTAA ACTTG
AUXILIN-LIKE2/pENTR	CACCATGGATGATTTCAC AGGATTGTT	TCAAAAGAGTTCCTCTGAGTT GAAT	AAAGAGTTCCTCTGAGTTGA ATTTG
CAP1/pENTR	CACCATGGCGCTAAGCAT GCGA	TCAGTAAGGGTTGTTGTAGTA ATAACC	GTAAGGGTTGTTGTAGTAAT AACC
SH3P2/pENTR	CACCATGGATGCAATTAG AAAACAAGC	TCAGAAAACTTCGGACACTTT G	GAAAACTTCGGACACTTTGC TA
AUXILIN-LIKE1/pDONRP2rP3	GGGGACAGCTTTCTTGTA CAAAGTGGCCATGGATGA TTTCACAGGATTGTT	GGGGACAACTTTGTATAATAA AGTTGGTCAGAAGAGTTCTTC TGAGTTAAAC	-
AUXILIN-LIKE2/pDONRP2rP3	GGGGACAGCTTTCTTGTA CAAAGTGGCCATGGATGA TTTCACAGGATTGTT	GGGGACAACTTTGTATAATAA AGTTGGTCAAAAGAGTTCCTC TGAGTTGAAT	-
CLC1/pDONR221	GGGGACAAGTTTGTACAA AAAAGCAGGCTCGATGGC GACTTTTGATGATGGAG	GGGGACCACTTTGTACAAGAA AGCTGGGTTTCACTCCGCCTT GGTTCCCTCGGCC	GGGGACCACTTTGTACAAG AAAGCTGGGTTCTCCGCCTT GGTTCCCTCGGCC
PIP5K1/pDONR221	GGGGACAAGTTTGTACAA AAAAGCAGGCTATGAGTG ATTCAGAAGAAGA	-	GGGGACCACTTTGTACAAG AAAGCTGGGTGCCCTCTTCA ATGAAGA
pCAP1/pDONRP4P1r	GGGGACAACTTTGTATAG AAAAGTTGGGATAGGCGT TCAAATCGG	GGGGACTGCTTTTTTGTACAAACTTGGATTCCACTACTACTTAA GGATTCGAA	

Primers used for qPCR.

TUB2-F	TAACAACTGGGCCAAGGGACA
TUB2-R	ACAAACCTGGAACCCTTGGAGAC
EF1-F	TGCTGTTGTAACAAGATGGATGCC
EF1-R	GGGTTGTATCCGACCTTCTTCAGG

AXL1-F	GGGGAAGAAAGGGGCAGATA
AXL1-R	GTCCAATGGATCAGTACGGGA
AXL2-F	AACAATTTGGGGAAGAAAGAGAGTG
AXL2-R	TGGATCAGTGAACCCTCCTGT

Primers used for genotyping CRISPR mutants.

CAS9-F	TGAGAACACTCAGCTCCAGAAT
CAS9-R	TCGAAACCACCGTATTTCTTAG
BAR-F	TCTCTTACGACTCAATGACAAG
BAR-R	GTGATTTTTGCGGACTGAGCT
AXL1-CRISPR-F	GGGGAAGAAAGGGGCAGATA
AXL1-CRISPR-R	GTCCAATGGATCAGTACGGGA
AXL2-CRISPR-F	AACAATTTGGGGAAGAAAGAGAGTG
AXL2-CRISPR-R	TGGATCAGTGAACCCTCCTGT
AXL1-seq	TGCAATGTAGCATGAACTATA
AXL2-seq	AACCTAGAAGATAACTCCCAG

DispatchDate: 13.11.2018 · ProofNo: 318, p.1

nature plants

LETTERS

https://doi.org/10.1038/s41477-018-0318-3

Mechanistic framework for cell-intrinsic re-establishment of PIN2 polarity after cell division

Matouš Glanc[1,2], Matyáš Fendrych[1,2] and Jiří Friml[1]*

Cell polarity, manifested by the localization of proteins to distinct polar plasma membrane domains, is a key prerequisite of multicellular life. In plants, PIN auxin transporters are prominent polarity markers crucial for a plethora of developmental processes. Cell polarity mechanisms in plants are distinct from other eukaryotes and still largely elusive. In particular, how the cell polarities are propagated and maintained following cell division remains unknown. Plant cytokinesis is orchestrated by the cell plate—a transient centrifugally growing endomembrane compartment ultimately forming the cross wall[1]. Trafficking of polar membrane proteins is typically redirected to the cell plate, and these will consequently have opposite polarity at least in one of the daughter cells[2–5]. Here, we provide mechanistic insights into post-cytokinetic re-establishment of cell polarity as manifested by the apical, polar localization of PIN2. We show that the apical domain is defined in a cell-intrinsic manner and that re-establishment of PIN2 localization to this domain requires de novo protein secretion and endocytosis, but not transcytosis. Furthermore, we identify a PINOID-related kinase WAG1, which phosphorylates PIN2 in vitro[6] and is transcriptionally upregulated specifically in dividing cells, as a crucial regulator of post-cytokinetic PIN2 polarity re-establishment.

Cells in the *Arabidopsis* root meristem are a perfect model to study cell polarity as they possess at least four distinct plasma membrane domains marked by the asymmetric accumulation of different cargoes[7] (Fig. 1a). Among these, PIN2 in the epidermis is particularly interesting for its pronounced apical polarity, which is crucial for shootward auxin transport and root gravitropism[8,9]. It has been reported that during cytokinesis, plasma membrane cargoes, including polarly localized ones, localize to the cell plate[2–5,10]. To dissect which trafficking pathways were responsible for cell plate cargo delivery we utilized the Dendra photoconvertible marker[11]. When we photoconverted functional (Supplementary Fig. 1) PIN2-Dendra or Dendra-PIP1;4 from green to red before cytokinesis, we observed the contribution of both de novo secretion and endocytic recycling to the cell plate, (Fig. 1b,c, Supplementary Fig. 1 and Supplementary Video 1), consistently with previous findings[10]. It was reported that in newly divided cells, PIN2 is localized at both sides of the cross wall[4]. Thus, the rerouting of endomembrane trafficking during cytokinesis results in apolar localization of the otherwise strictly polar PIN2[4,12].

When is apical PIN2 localization subsequently re-established, and which cellular mechanisms are required for this process? There was no difference in PIN2 promoter activity between the daughter cells (Supplementary Fig. 1), implying post-transcriptional regulation. To address the dynamic changes of subcellular PIN2 localization, live-cell imaging is indispensable since time is the decisive variable. However, exact determination of PIN2 polar localization dynamics is difficult using *PIN2::PIN2-XFP* reporter lines, since the original apical domain is pre-occupied with molecules inherited from the mother cell, conventional microscopy cannot distinguish between adjacent newly formed plasma membranes due to the diffraction limit, and super-resolution techniques are limited in time lapse potentiality and throughput. To overcome these limitations, we expressed *PIN2-GFP* from the cytokinesis-specific *KNOLLE* promoter[13] and performed time lapse imaging. This approach enabled us to observe the trafficking fate of molecules synthesized in a narrow time window during and immediately after the cytokinetic event (Fig. 1d,e and Supplementary Video 2). In recently divided cells, the KN::PIN2-GFP signal could be observed almost exclusively at the cell plate or new plasma membrane, further confirming redirection of secretion to the cell plate during cytokinesis[12], but also afterwards (Fig. 1d,e). At 1–2 hours after cytokinesis, KN::PIN2-GFP signal was still strongest at the newly formed membrane pair but started to appear also at the apical and lateral domains of the upper cell. By 3–5 hours after cytokinesis, the signal clearly localized to the apical domains of both daughter cells, marking completed polarity re-establishment (Fig. 1e,f). *KN::PIN2-GFP* only non-significantly rescued root gravitropism in the *pin2* mutant, did not affect the phenotype of *Col-0*, and its signal intensities at newly formed plasma membranes were comparable with those in a complementing *PIN2::PIN2-GFP* line (Supplementary Fig. 1), suggesting that the observed localization was not an overexpression artefact.

Taken together, these results confirm that during and immediately after cytokinesis, virtually all membrane traffic of both daughter cells is redirected to the cell plate[12], creating a situation in which the lower cell has a correctly, that is apically localized, PIN2, but the upper daughter cell has an ectopic basally localized pool of PIN2, in addition to the apical pool inherited from the mother cell[4]. Therefore, the cell must possess a mechanism to re-establish proper localization of PIN2 and other polar proteins (Fig. 1a).

In plants, cell fate is determined by positional information conveyed by numerous intercellular signalling molecules[14]. We therefore tested whether tissue context and cell-to-cell signalling is required for re-establishment of cell polarity after cytokinesis. In other developmental contexts, for example during organogenesis or vascularization, auxin itself serves as a polarizing cue for the localization of PIN proteins[15,16]; therefore, we first tested whether post-cytokinetic polarity re-establishment is regulated by auxin levels in cells or its directional flow across the tissue. Nonetheless, PIN2 polarity developed normally in *KN::PIN2-GFP* roots when we exogenously applied the natural auxin indole-3-acetic acid (IAA) (Supplementary Figs. 2 and 6). In plants treated with the auxin transport inhibitor naphthylphthalamic acid (NPA)[17], apical polarity was

[1]IST Austria, Klosterneuburg, Austria. [2]Department of Experimental Plant Biology, Faculty of Science, Charles University, Prague, Czechia.
*e-mail: jiri.friml@ist.ac.at

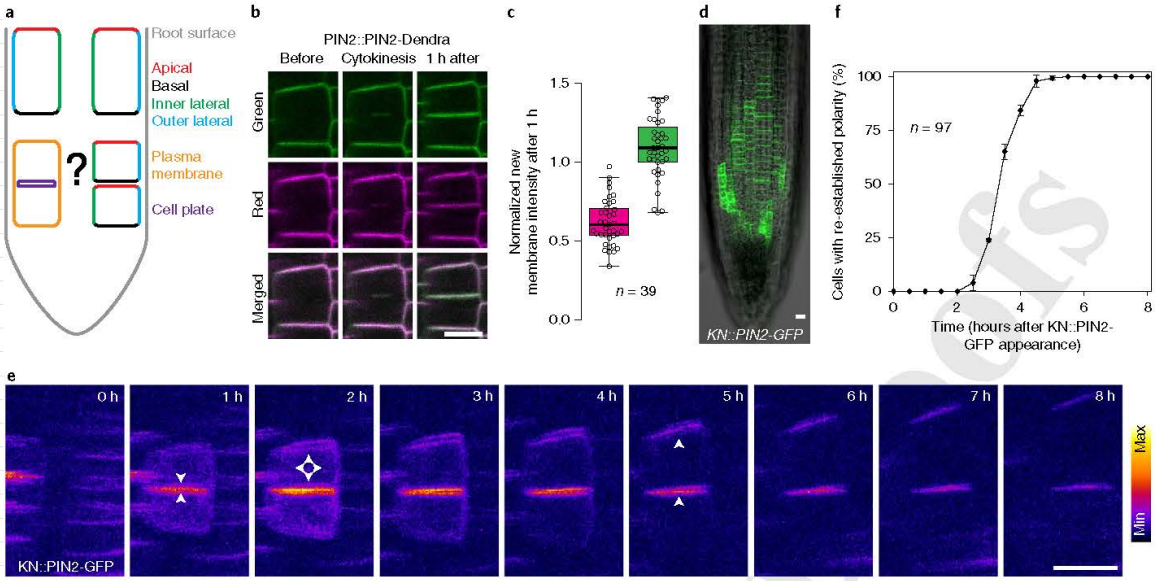


Fig. 1 | Cell polarity needs to be re-established after cytokinesis. a, Cells in the *Arabidopsis* root possess at least four distinct plasma membrane domains: apical, basal, inner lateral and outer lateral[7]. During cytokinesis, virtually all membrane traffic is redirected to the cell plate[12], implying that the daughter cells must have a mechanism to re-establish polarity afterwards. **b**, Both pre-existing (magenta) and newly synthesized (green) pools of PIN2-Dendra localize to the cell plate and newly formed plasma membrane in cells that were photoconverted before the onset of cytokinesis. **c**, Quantification of **b**. The graph shows signal intensity at the newly formed plasma membrane 1 h after cytokinesis normalized to the intensity of the neighbouring, old plasma membranes in both red and green channels; higher relative intensity of the green channel confirms predominant contribution of de novo secretion to the cell plate protein pool. The box plot represents median, 1st and 3rd quartile; the whiskers extend to data points <1.5 interquartile range away from the 1st or 3rd quartile; all data points are shown as circles. *n* indicates the number of cells from eight roots and three independent experiments. **d**, Expression pattern of the *KN::PIN2-GFP* construct in the root meristem. The experiment was repeated independently more than three times with similar results. **e**, A time series of a single newly divided cell pair expressing *KN::PIN2-GFP*. Up to 1 h after cytokinesis, signal is almost exclusively at the cell plate. At 1–3 h after cytokinesis, signal appears at all plasma membrane domains, and typical apical polar distribution pattern is re-established 2–5 h after cytokinesis. Arrowheads indicate predominant signal localization. **f**, Quantitative analysis of the dynamics of KN::PIN2-GFP polarity re-establishment. The timepoint at which both daughter cells had clearly apically localized KN::PIN2-GFP signal (between 4 and 5 h in the case of the cell pair shown in **e**) was scored for each cell pair, and the percentage of cell pairs with re-established polarity was plotted against time. The graph shows mean ±s.d. of three independent experiments, *n* indicates the total number of cell pairs. The number of roots/cell pairs analysed in each experiment was 5/47, 3/30 and 2/20, respectively. Scale bars, 10 µm.

established correctly, but with a significant delay (Fig. 2a,b,e and Supplementary Fig. 6).

To test more generally for a requirement of tissue context, we separated the *KN::PIN2-GFP* root meristematic and transition zone from, (1) the root tip, (2) the differentiation zone and the rest of the plant or (3) both. The pattern of cell division occurrence and orientation was disturbed as described before[18] but PIN2 polarity re-establishment remained unaffected (Supplementary Figs. 2 and 6), suggesting that this process does not depend on long-range cell-to-cell signalling. To address the importance of short-range signalling, we isolated small patches of cells from their neighbours by laser ablation. We could still observe normal re-establishment of apical PIN2 polarity in isolated patches of as few as three cells (Fig. 2c–e and Supplementary Fig. 6), arguing against the influence of short-range signalling.

Together, these results indicate that while auxin transport and/or signalling can affect PIN trafficking and polarity, presumably through transcriptional reprogramming[16], neither polarized auxin flow nor other cell-to-cell signalling pathways are primary cues defining apical–basal polarity in newly divided root cells. Therefore, post-cytokinetic polarity re-establishment must be governed by an unknown cell-intrinsic mechanism instead.

We next addressed the cellular machinery that executes PIN2 polarity re-establishment. To test whether the ectopic basal PIN2 molecules were delivered to the apical domain by transcytosis (trafficking-based protein translocation between polar domains)[19], we created a *KN::PIN2-Dendra* line, photoconverted newly divided cell pairs and followed them during polarity re-establishment. The apical signal distribution pattern developed in both channels showing contribution of both pre-existing PIN2 molecules (in magenta) and the de novo synthesized PIN2 (in green) (Fig. 3a,b). However, after photoconversion, when we photobleached the red signal from the endosomes and all cell sides except the new, cell plate-derived plasma membranes, we did not observe a significant apical signal in the red channel (Fig. 3c,d) which argues against a significant contribution of basal-to-apical PIN2 transcytosis to polarity establishment in this context. Furthermore, only weak, presumably lateral diffusion-based, redistribution of red signal was observed after photoconversion of the new plasma membrane domain in *PIN2::PIN2-Dendra*, and the apical signal was not restored in *KN::PIN2-GFP* cells treated with the translation inhibitor cycloheximide (Supplementary Figs. 3 and 6). Finally, treatment with the ARF GEF inhibitor brefeldin A prevented PIN2 polarity re-establishment of *KN::PIN2-GFP* in the *big3* mutant, where it inhibits secretion[12], but not in the wild type

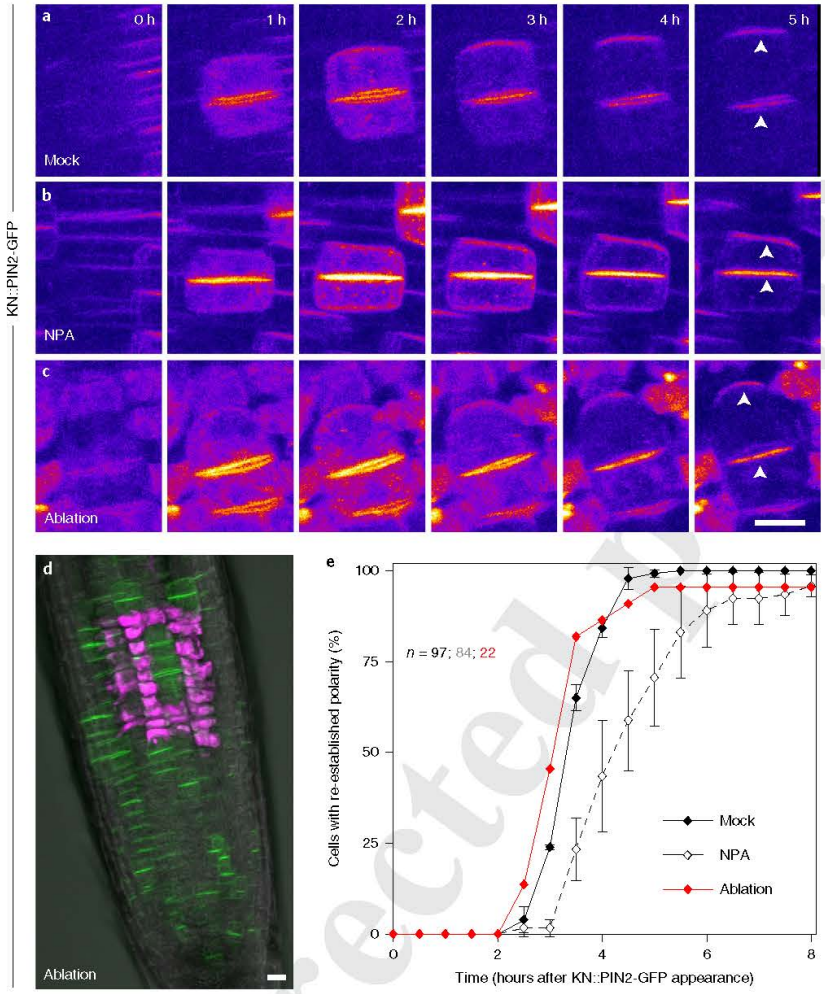


Fig. 2 | Apical–basal polarity of newly divided cells is established in a cell-intrinsic manner. a,**b**, Re-establishment of apical PIN2 polarity in *KN::PIN2-GFP* plants treated with the auxin transport inhibitor NPA, **b** is qualitatively not altered compared with the mock control **a**. **c**, Laser ablation of surrounding cells does not prevent the re-establishment of apical PIN2 polarity. **d**, *KN::PIN2-GFP* expressing root in which laser-ablated cells are marked by the uptake of propidium iodide (magenta). The experiment was repeated independently three times with similar results. **e**, Quantitative analysis of the dynamics of KN::PIN2-GFP polarity re-establishment in **a**–**c**. NPA treatment causes a delay of polarity re-establishment compared with the control, while laser ablation of surrounding cells has no effect. The control is the same as in Fig. 1f . The graph shows mean ± s.d. of three independent experiments, *n* indicates the total number of cell pairs. The number of roots/cell pairs analysed in each experiment was 4/20, 4/35 and 3/29 in **b** and 3/9, 1/5 and 4/8 in **c**, respectively. Due to the smaller sample size of **c** caused by technical limitations, values from all experiments were pooled and analysed together. Arrowheads indicate apical polar localization of PIN2-GFP. Scale bars, 10 µm.

(Supplementary Figs. 3 and 6). Taken together, these data demonstrate that re-establishment of PIN2 apical polarity depends on secretion of de novo synthesized PIN2 molecules but not on their basal-to-apical transcytosis.

Ectopic basal and lateral PIN2 molecules need to be removed from the plasma membrane during polarity re-establishment. Polarity of PINs has been linked to their slower lateral diffusion within the plasma membrane[4,20–22]. We therefore speculated that higher PIN2 mobility in the new plasma membrane domain might contribute to PIN2 removal and polarity re-establishment and tested this with fluorescence recovery after photobleaching experiments. We did observe slightly higher PIN2 fluorescence recovery after photobleaching rates in the newly formed membranes compared with the old ones; however, the differences were noticeable only in *PIN2::PIN2-GFP*, but not in *PIN2::PIN2-mCherry* (Supplementary Fig. 4). We therefore conclude that they reflected differential properties of the fluorophores rather than of the cargo, and that specific lateral diffusion properties probably do not play a major role in PIN2 polarity re-establishment.

A link between clathrin-mediated endocytosis (CME) and PIN polarity[23], as well as post-cytokinetic PIN2 polarity re-establishment, has previously been proposed[3,4]. However, strong pleiotropic defects of the mutants used in these studies make it difficult to dissect direct and indirect effects. To re-examine the role of CME in PIN2 polarity re-establishment, we conditionally inhibited endocytosis by inducible overexpression of the putative clathrin-uncoating

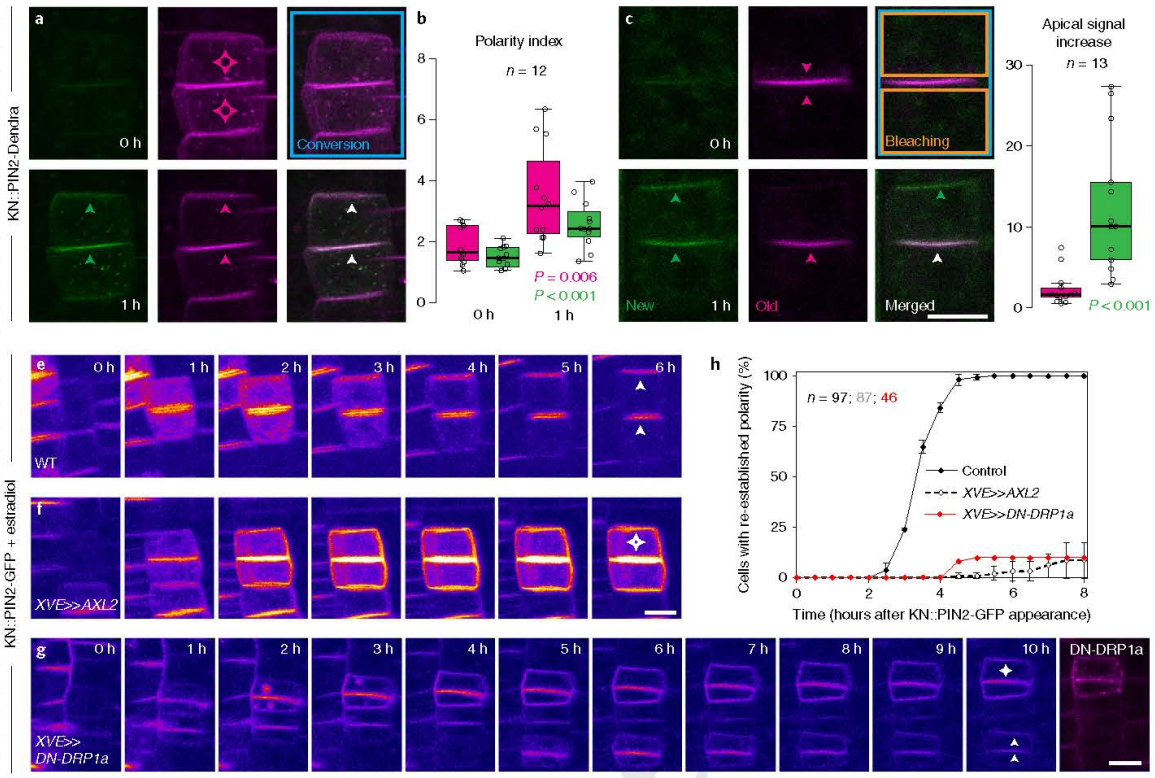


Fig. 3 | PIN2 apical polarity re-establishment requires secretion and endocytosis, but not transcytosis. a, A newly divided cell pair of *KN::PIN2-Dendra* that was photoconverted before polarity re-establishment. Within 1 h following photoconversion, apical polar distribution of both newly synthesized (green) and pre-existing (magenta) PIN2-Dendra pools can be observed. **b**, Quantitative analysis of **a**. The value of the polarity index (ratio of signal intensity at the apical plasma membrane/lateral plasma membrane of the upper cell) significantly increased in both channels within 1 h following photoconversion. $n = 12$ cell pairs from 11 roots in four independent experiments. **c**, A similar experiment as in **a** with an additional step where all signal, except that at the new membrane pair, was photobleached immediately after photoconversion. In this case, apical polarity develops only in the green channel. **d**, Quantification of **c**. The graph shows the increase in red and green signal intensity at the apical plasma membrane of the upper cell within 1 h following photoconversion and photobleaching. Thearger signal increase in the green channel indicates predominant contribution of de novo secretion to polarity re-establishment. $n = 13$ cells from nine roots in three independent experiments. Arrowheads indicate predominant localization of PIN2-Dendra in the corresponding channel; white, both channels. **e**,**f**, Inhibition of endocytosis by estradiol-inducible overexpression of Auxilin-like2 in *KN::PIN2-GFP* cells caused prolonged residence of signal at the plasma membrane and abolished the cells' ability to re-establish apical PIN2 polarity. **g**, Apical polarity re-establishment in *KN::PIN2* x *XVE»DN-DRP1a-mRFP* after estradiol treatment. Thanks to patchy expression of the construct (see the last frame), cells with high levels of DN-DRP1a-mRFP that fail to re-establish apical polarity could be seen alongside cells with low levels, where polarity re-establishment proceeded normally. **h**, Quantitative analysis of **e**–**g**. The control is the same as in Fig. 1f. The graph shows mean ± s.d. of three (**f**), mean of two (**g**) independent experiments, *n* indicates the total number of cell pairs. The number of roots/cell pairs analysed in each experiment was 4/29, 6/38 and 3/20 in **f** and 3/21 and 4/25 in **g**, respectively. Arrowheads indicate predominant localization of PIN2-GFP. Box plots represent median, 1st and 3rd quartile; the whiskers extend to data points <1.5 interquartile range away from the 1st or 3rd quartile; all data points are shown as circles. Scale bars, 10 µm.

factor Auxilin-like2[24]. In *KN::PIN2-GFP* x *XVE»AXL2* plants treated with estradiol, most cells completely lost the ability to polarize PIN2 (Fig. 3f–h, Supplementary Fig. 6 and Supplementary Video 3), while polarity re-establishment proceeded normally in estradiol-treated *KN::PIN2-GFP* (Fig. 3e) and mock-treated *KN::PIN2-GFP* x *XVE»AXL2* (data not shown) controls. Inducible overexpression of a dominant-negative version of Dynamin-related protein 1 A (DRP1a)[5] led to the same result (Fig. 3g,h and Supplementary Fig. 6), confirming the direct requirement of functional CME for post-cytokinetic PIN2 polarity re-establishment.

Multiple approaches have confirmed that (de)phosphorylation of PIN proteins by PINOID (PID) and its homologues WAG1 and WAG2 regulates their apical–basal localization[6,25–28]. PIN2 polarity re-establishment in the *KN::PIN2*^{S3A}*-GFP* with three PID-phosphorylated serines S237, S258 and S310 mutated to alanines[6] showed a delay in polarity re-establishment compared with the *KN::PIN2-GFP* control (Supplementary Figs. 5 and 6); however, introducing *KN::PIN2-GFP* into the *pid wag1 wag2* loss-of-function mutant[6] led to complete PIN2 polarity re-establishment failure (Fig. 4a–c, Supplementary Fig. 6 and Supplementary Video 4). Therefore, PID and WAG kinases mediate PIN2 polarity re-establishment by phosphorylating S237, S258 and S310, but also other PIN2 residues or additional polarity regulators[28–30]. Notably, analysis of the expression dynamics revealed that the abundance of WAG1 was strongly upregulated specifically in dividing epidermal cells (Fig. 4d,e and Supplementary Video 5).

Together, these results show that the cell cycle-regulated WAG1 and its homologues PID and WAG2 play a key role in

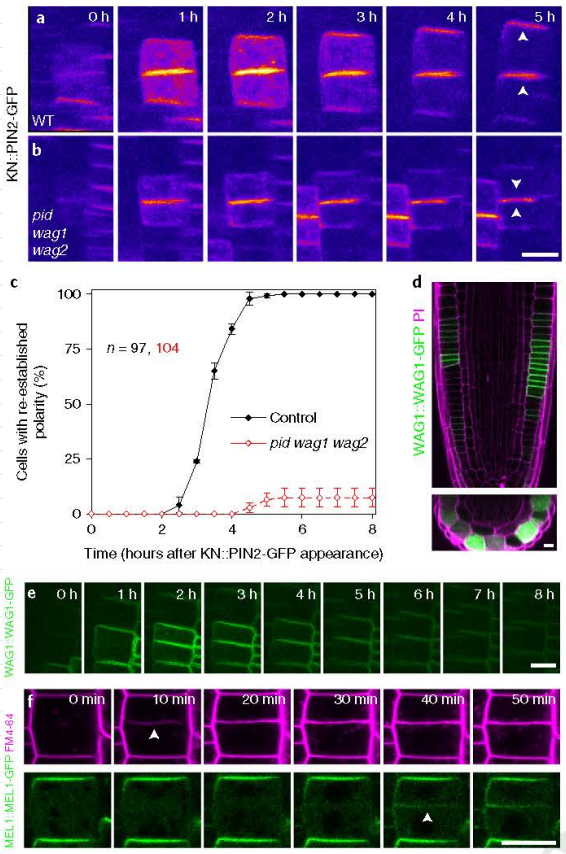


Fig. 4 | PIN apical polarity re-establishment is mediated by the AGCVIII kinase WAG1. a,**b**, *KN::PIN2-GFP* cells failed to re-establish apical polarity in the *pid wag1 wag2* triple mutant background. Arrowheads indicate predominant localization of PIN2-GFP. **c**, Quantitative analysis of **a** and **b**. The control is the same as in Fig. 1f. The graph shows mean ±s.d. of three independent experiments, *n* indicates the total number of cell pairs. The number of roots/cell pairs analysed in each experiment was 4/30, 4/38 and 4/36. **d**,**e**, Expression analysis of *WAG1::WAG1-GFP*. The signal is strongly and specifically increased in dividing cells exclusively in the epidermis. *XY* and *XZ* sections through the same root (**d**) and a time lapse of a single dividing cell from a different root (**e**) are shown. $n > 100$ cells from 16 roots in four independent experiments. **f**, Subcellular localization of MEL1::MEL1-GFP in dividing cells stained with FM4-64. MEL1-GFP never appears at the cell plate and can be detected only at the newly formed apical plasma membrane at >30 min after cell division. Arrowheads indicate the first appearance of the cell plate and of MEL1-GFP at the new plasma membrane, respectively. $n = 80$ cells from 18 roots in three independent experiments. Scale bars, 10 µm.

PIN2 post-cytokinetic polarity re-establishment, explaining the previously reported pronounced PIN2 polarity defect in the *pid wag1 wag2* roots[6].

PID/WAG kinases have been shown to interact genetically with *MEL* genes encoding NPH3-like proteins of unknown function[31]. Notably, the membrane-associated MEL proteins co-localize with PINs and polarity of PINs is reduced in higher order *mel* mutants[31]. This prompted us to analyse the dynamic localization of the *MEL1-GFP* reporter in dividing epidermal cells. We detected MEL1-GFP localization at the apical plasma membrane of the mother cell and in the cytoplasm, but not at the cell plate. MEL1-GFP first appeared at the newly formed apical domain not before 30 minutes after cell division (Fig. 4f), presumably after it had lost cell plate and acquired plasma membrane identity. This localization pattern is a manifestation of the cell-intrinsic polarity cue inherited from the mother cell during cytokinesis and defining the apical domain of the daughter cell.

Maintenance of individual cell polarities over repeated rounds of cell division is crucial for tissue polarity and proper development in multicellular organisms. We show here that redefinition of the root epidermal cell apical–basal polarity after cell division is achieved in a cell-intrinsic manner. Subsequent PIN2 polarity re-establishment requires de novo protein secretion, CME and the activity of cell cycle-regulated WAG1 and related AGCVIII kinases. On the other hand, our detailed analysis does not support a major contribution of basal-to-apical transcytosis to re-establishment of PIN2 polarity. Based on our findings, we propose the following model: (1) During cytokinesis and in the first hour thereafter, PIN2 targeting is redirected to the cell plate along with most endomembrane traffic;[12] (2) PIN2 molecules localized ectopically to the basal side of the upper cell must be endocytosed, but are gradually turned over rather than being transcytosed to the apical side; and (3) During cytokinesis, WAG1 kinase is transcriptionally upregulated and together with its homologues is required for re-establishment of PIN2 localization to the apical plasma membrane, which is marked by the presence of MEL proteins. It remains a challenge for future investigations to elucidate the precise molecular machinery responsible for differential endocytosis rates between the apical and other plasma membrane domains, and to uncover the nature of the cell-intrinsic polarity cue responsible for proper redefinition of apical–basal polarity of newly divided cells.

Methods

Plant material and growth conditions. Seeds were surface sterilized by chlorine vapour, sown on ½ MurashigeSkoog medium supplemented with 1% sucrose and 1% agar and grown in vitro under long day conditions. The transgenic lines *PIN2::PIN2-Dendra*[32], *PIN2::nls-GFP*[32], *PIN2::PIN2-GFP*[6], *PIN2::PIN2-mCherry*[32] and *WAG1::WAG1-GFP*[6] were described previously. The lines *PIN2::Dendra-PIP1;4*, *KN::PIN2-GFP*, *KN::PIN2-Dendra*, *KN::PIN2*^{S3A}*-GFP* and *MEL1::MEL1-GFP* were generated by transformation of the respective constructs into *Col-0* by the floral dip method[33]. *KN::PIN2-GFP* was introduced into the *eir1–1*[34], *XVE»AXL2*[24], *pid wag1 wag2*[6], *big3*[12] *and XVE»DN-DRP1a-mRFP*[6] backgrounds by genetic crossing. In the case of *KN::PIN2-GFP* x *pid wag1 wag2*, *pid*$^{\pm}$ *wag1 wag2* plants were used for the cross. *pid*$^{\pm}$ plants were identified by PCR-based genotyping in F1 and F2 generations, and seedlings were selected based on the no cotyledon phenotype from an F3 *KN::PIN2-GFP*$^{+}$ x *pid*$^{\pm}$*wag1*$^{-/-}$*wag2*$^{-/-}$ line for the experiments. Due to high levels of *XVE»DN-DRP1a-mRFP* silencing, the construct was retransformed in our laboratory, T1 plants were used for the cross and the resulting F1/T2 plants were used for the experiments.

Molecular cloning. All cloning was performed using the Gateway Technology (Invitrogen). To generate *KN::PIN2-GFP*, a promoter fragment 1 kilobase (kb) upstream of the KNOLLE (*At1g08560*) start codon was cloned into pDONR P4-P1r, the *PIN2-GFP* coding sequence was cloned into pDONR 221 and both entry clones were recombined into the binary vector pB7m24GW,3. *KN::PIN2-Dendra* was generated analogically. To introduce S3A mutations into the *PIN2-GFP* sequence, an N-terminal *PIN2* fragment containing the three mutations was amplified from the *PIN:: PIN2*^{S3A}*-Venus* line genomic DNA[6], fused to a C-terminal fragment containing the *GFP* tag by overlap PCR, and cloned into pDONR 221, which was used to generate *KN::PIN2*^{S3A}*-GFP*. For *MEL1::MEL1-GFP*, a 2.9 kb fragment upstream of the *MEL1* (*At4g37590*) start codon was cloned into pDONR P4-P1r, the *MEL1* coding sequence without a stop codon into pDONR 221 and the *EGFP* coding sequence into pDONR P2r-P3. All three entry clones were then recombined into pH7m34GW,0. *PIN2::Dendra-PIP1;4* was generated analogically by recombining the 1,397 base pair (bp) *PIN2* promoter in pDONR P4-P1r, the *Dendra* coding sequence without a stop codon in pDONR 221 and the *PIP1;4* coding sequence in pDONR P2r-P3 into pB7m34GW,0. Sequences of all primers used can be found in Supplementary Table 1.

Imaging and image analysis. Four-day-old seedlings were mounted on a slice of growth medium, containing the respective chemicals in case of pharmacological

experiments, placed into a chambered coverslip (Lab-Tek) and imaged with Zeiss LSM700, LSM800 or LSM880 inverted confocal microscopes; long time lapse imaging was performed using a vertically oriented LSM700 microscope as described previously[35]. To apply chemical treatments, the respective amount of compound stock solution was predissolved in 100 µl H_2O, pipetted on to a slice of growth medium and incubated for 1–2 h at room temperature to diffuse. The seedlings were then transferred into a chambered coverslip (Lab-Tek), covered with the treatment-including medium and imaged, in the case of inhibitors together with a mock control containing only the solvent. The drugs (manufacturer; stock concentration and solvent; final concentration) were as follows: naphthylphthalamic acid (Duchefa; 10 mM dimethylsulfoxide (DMSO); 10 µM), indole-3-acetic acid (Sigma-Aldrich, 10 mM ethanol; 100 nM), β-estradiol (Sigma-Aldrich; 10 mM DMSO; 10 µM), brefeldin A (Sigma-Aldrich; 50 mM DMSO; 25 µM), cycloheximide (Sigma-Aldrich; 50 mM DMSO; 25 µM), propidium iodide (Sigma-Aldrich; 1 mg ml^{-1} H_2O; 50 µg ml^{-1}), FM4–64 (Invitrogen; 2 mM H_2O; 2 µM). In tissue context disruption experiments, roots mounted on growth medium were cut manually with a razor blade under a stereomicroscope. Individual cells were ablated with a 355 nm pulsed laser at a Zeiss Observer inverted microscope equipped with an Andor iXon 897 Spinning Disk system, propidium iodide was used to mark the ablated cells. Dendra photoconversion was performed as described previously[36]. Images were handled and analysed with FIJI[37] and Adobe Photoshop. All *KN::PIN2-GFP* time lapse data are presented as maximum intensity projections of a Z stack.

Phenotypic analysis. Plates with four-day-old light-grown seedlings were scanned on an Epson Perfection V700 flatbed scanner and root vertical growth index was measured as described previously[38].

Reproducibility and statistics. The number of independent repetitions of experiments, as well as exact sample sizes, is described in the figure legends. Tukey box plots were generated with BoxPlotR (http://shiny.chemgrid.org/boxplotr/). Statistical significance was tested as described in the figure legends. For the purpose of statistical analysis of KNOLLE::PIN2-GFP experiments, any cell pair that failed to repolarize during the time course of the experiment was considered to have repolarized after 10 h.

Reporting Summary. Further information on research design is available in the Nature Research Reporting Summary linked to this article.

Data availability

The data that support the findings of this study are available from the corresponding author upon request.

Received: 6 June 2018; Accepted: 1 November 2018;

References

1. Smertenko, A. et al. Plant cytokinesis: terminology for structures and processes. *Trends Cell Biol.* **27**, 885–894 (2017).
2. Geldner, N. et al. Auxin transport inhibitors block PIN1 cycling and vesicle trafficking. *Nature* **413**, 425–428 (2001).
3. Mravec, J. et al. Cell plate restricted association of DRP1A and PIN proteins is required for cell polarity establishment in *Arabidopsis*. *Curr. Biol.* **21**, 1055–1060 (2011).
4. Men, S. et al. Sterol-dependent endocytosis mediates post-cytokinetic acquisition of PIN2 auxin efflux carrier polarity. *Nat. Cell Biol.* **10**, 237–244 (2008).
5. Yoshinari, A. et al. DRP1-dependent endocytosis is essential for polar localization and boron-induced degradation of the borate transporter BOR1 in *Arabidopsis thaliana*. *Plant Cell Physiol.* **57**, 1985–2000 (2016).
6. Dhonukshe, P. et al. Plasma membrane-bound AGC3 kinases phosphorylate PIN auxin carriers at TPRXS(N/S) motifs to direct apical PIN recycling. *Development* **137**, 3245–3255 (2010).
7. Kania, U. et al. Polar delivery in plants; commonalities and differences to animal epithelial cells. *Open Biol.* **4**, 140017 (2014).
8. Abas, L. et al. Intracellular trafficking and proteolysis of the *Arabidopsis* auxin-efflux facilitator PIN2 are involved in root gravitropism. *Nat. Cell Biol.* **8**, 249–256 (2006).
9. Baster, P. et al. SCF(TIR1/AFB)-auxin signalling regulates PIN vacuolar trafficking and auxin fluxes during root gravitropism. *EMBO J.* **32**, 260–274 (2013).
10. Dhonukshe, P. et al. Endocytosis of cell surface material mediates cell plate formation during plant cytokinesis. *Dev. Cell* **10**, 137–150 (2006).
11. Gurskaya, N. G. et al. Engineering of a monomeric green-to-red photoactivatable fluorescent protein induced by blue light. *Nat. Biotechnol.* **24**, 461–465 (2006).
12. Richter, S. et al. Delivery of endocytosed proteins to the cell-division plane requires change of pathway from recycling to secretion. *eLife* **3**, e02131 (2014).
13. Lauber, M. H. et al. The *Arabidopsis* KNOLLE protein is a cytokinesis-specific syntaxin. *J. Cell Biol.* **139**, 1485–1493 (1997).
14. Sparks, E. et al. Spatiotemporal signalling in plant development. *Nat. Rev. Genet.* **14**, 631–644 (2013).
15. Mazur, E. et al. Vascular cambium regeneration and vessel formation in wounded inflorescence stems of *Arabidopsis*. *Sci. Rep.* **6**, 33754 (2016).
16. Prát, T. et al. WRKY23 is a component of the transcriptional network mediating auxin feedback on PIN polarity. *PLoS Genet.* **14**, e1007177 (2018).
17. Simon, S. et al. Defining the selectivity of processes along the auxin response chain: a study using auxin analogues. *New Phytol.* **200**, 1034–1048 (2013).
18. Sena, G. et al. Organ regeneration does not require a functional stem cell niche in plants. *Nature* **457**, 1150–1153 (2009).
19. Kleine-Vehn, J. et al. Cellular and molecular requirements for polar PIN targeting and transcytosis in plants. *Mol. Plant* **1**, 1056–1066 (2008).
20. Kleine-Vehn, J. et al. Recycling, clustering, and endocytosis jointly maintain PIN auxin carrier polarity at the plasma membrane. *Mol. Syst. Biol.* **7**, 540 (2011).
21. Feraru, E. et al. PIN polarity maintenance by the cell wall in *Arabidopsis*. *Curr. Biol.* **21**, 338–343 (2011).
22. Martinière, A. et al. Cell wall constrains lateral diffusion of plant plasma-membrane proteins. *Proc. Natl Acad. Sci. USA* **109**, 12805–12810 (2012).
23. Kitakura, S. et al. Clathrin mediates endocytosis and polar distribution of PIN auxin transporters in *Arabidopsis*. *Plant Cell* **23**, 1920–1931 (2011).
24. Adamowski, M. et al. A functional study of AUXILIN-LIKE1 and 2, two putative clathrin uncoating factors in *Arabidopsis*. *Plant Cell* **30**, 700–716 (2018).
25. Friml, J. et al. A PINOID-dependent binary switch in apical-basal PIN polar targeting directs auxin efflux. *Science* **306**, 862–865 (2004).
26. Michniewicz, M. et al. Antagonistic regulation of PIN phosphorylation by PP2A and PINOID directs auxin flux. *Cell* **130**, 1044–1056 (2007).
27. Kleine-Vehn, J. et al. PIN auxin efflux carrier polarity is regulated by PINOID kinase-mediated recruitment into GNOM-independent trafficking in *Arabidopsis*. *Plant Cell* **21**, 3839–3849 (2009).
28. Zhang, J. et al. PIN phosphorylation is sufficient to mediate PIN polarity and direct auxin transport. *Proc. Natl Acad. Sci. USA* **107**, 918–922 (2010).
29. Huang, F. et al. Phosphorylation of conserved PIN motifs directs *Arabidopsis* PIN1 polarity and auxin transport. *Plant Cell* **22**, 1129–1142 (2010).
30. Weller, B. et al. Dynamic PIN-FORMED auxin efflux carrier phosphorylation at the plasma membrane controls auxin efflux-dependent growth. *Proc. Natl Acad. Sci. USA* **114**, E887–E896 (2017).
31. Furutani, M. et al. Polar-localized NPH3-like proteins regulate polarity and endocytosis of PIN-FORMED auxin efflux carriers. *Development* **138**, 2069–2078 (2011).
32. Salanenka, Y. et al. Gibberellin DELLA signaling targets the retromer complex to redirect protein trafficking to the plasma membrane. *Proc. Natl Acad. Sci. USA* **115**, 3716–3721 (2018).
33. Clough, S. J. & Bent, A. F. Floral dip: a simplified method for Agrobacterium-mediated transformation of *Arabidopsis thaliana*. *Plant J.* **16**, 735–743 (1998).
34. Luschnig, C. et al. EIR1, a root-specific protein involved in auxin transport, is required for gravitropism in *Arabidopsis thaliana*. *Genes Dev.* **12**, 2175–2187 (1998).
35. von Wangenheim, D. et al. Live tracking of moving samples in confocal microscopy for vertically grown roots. *eLife* **6**, e26792 (2017).
36. Jásik, J. et al. PIN2 turnover in *Arabidopsis* root epidermal cells explored by the photoconvertible protein Dendra2. *PLoS ONE* **8**, e61403 (2013).
37. Schindelin, J. et al. Fiji: an open-source platform for biological-image analysis. *Nat. Methods* **9**, 676–682 (2012).
38. Grabov, a et al. Morphometric analysis of root shape. *New Phytol.* **165**, 641–651 (2005).

Acknowledgements

We thank N. Geldner, C. Luschnig, G. Jürgens, R. Offringa and Y. Takano for sharing published material. We would also like to acknowledge M. Adamowski, U. Kania and C. Cuesta for providing entry clones, and the Biomaging Facility at IST Austria for providing excellent imaging service and assistance. The research leading to these results has received funding from the European Research Council under the European Union's Seventh Framework Programme/ERC grant agreement no. 742985. Additionally, funding was received from the Ministry of Education of the Czech Republic/MŠMT project NPUI -LO1417.

Author contributions

M.G. designed experiments, performed experiments, analysed data and wrote the manuscript. M.F. designed experiments, analysed data and edited the manuscript. J.F. initiated the project, acquired funding, designed experiments and wrote the manuscript.

Competing interests

The authors declare no competing interests.

Additional information

Supplementary information is available for this paper at https://doi.org/10.1038/s41477-018-0318-3.

Reprints and permissions information is available at www.nature.com/reprints.

Correspondence and requests for materials should be addressed to J.F.

Publisher's note: Springer Nature remains neutral with regard to jurisdictional claims in published maps and institutional affiliations.

© The Author(s), under exclusive licence to Springer Nature Limited 2018

Uncorrected proofs

nature research

Corresponding author(s): Jiří Friml

Reporting Summary

Nature Research wishes to improve the reproducibility of the work that we publish. This form provides structure for consistency and transparency in reporting. For further information on Nature Research policies, see Authors & Referees and the Editorial Policy Checklist.

Statistical parameters

When statistical analyses are reported, confirm that the following items are present in the relevant location (e.g. figure legend, table legend, main text, or Methods section).

n/a	Confirmed	
☐	☒	The exact sample size (*n*) for each experimental group/condition, given as a discrete number and unit of measurement
☐	☒	An indication of whether measurements were taken from distinct samples or whether the same sample was measured repeatedly
☐	☒	The statistical test(s) used AND whether they are one- or two-sided *Only common tests should be described solely by name; describe more complex techniques in the Methods section.*
☒	☐	A description of all covariates tested
☐	☒	A description of any assumptions or corrections, such as tests of normality and adjustment for multiple comparisons
☐	☒	A full description of the statistics including central tendency (e.g. means) or other basic estimates (e.g. regression coefficient) AND variation (e.g. standard deviation) or associated estimates of uncertainty (e.g. confidence intervals)
☒	☐	For null hypothesis testing, the test statistic (e.g. *F*, *t*, *r*) with confidence intervals, effect sizes, degrees of freedom and *P* value noted *Give P values as exact values whenever suitable.*
☒	☐	For Bayesian analysis, information on the choice of priors and Markov chain Monte Carlo settings
☒	☐	For hierarchical and complex designs, identification of the appropriate level for tests and full reporting of outcomes
☒	☐	Estimates of effect sizes (e.g. Cohen's *d*, Pearson's *r*), indicating how they were calculated
☐	☒	Clearly defined error bars *State explicitly what error bars represent (e.g. SD, SE, CI)*

Our web collection on statistics for biologists may be useful.

Software and code

Policy information about availability of computer code

Data collection	The TipTracker script that was used to collect data was described previously (von Wangenheim et al., 2017; https://doi.org/10.7554/eLife.26792.022)
Data analysis	Following software was used to analyze data: FIJI / ImageJ v 1.51w; Microsoft Excel 2010 and 2016; BoxPlotR (http://shiny.chemgrid.org/boxplotr/); RStudio 1.1.383. Figures were assembled using Adobe Photoshop CS5, Adobe Illustrator CS5 and CC, and LibreOffice Draw 6.1.0.3.

For manuscripts utilizing custom algorithms or software that are central to the research but not yet described in published literature, software must be made available to editors/reviewers upon request. We strongly encourage code deposition in a community repository (e.g. GitHub). See the Nature Research guidelines for submitting code & software for further information.

Data

Policy information about availability of data

All manuscripts must include a data availability statement. This statement should provide the following information, where applicable:

- Accession codes, unique identifiers, or web links for publicly available datasets
- A list of figures that have associated raw data
- A description of any restrictions on data availability

The datasets generated during and/or analysed during the current study are available from the corresponding author on reasonable request.

Field-specific reporting

Please select the best fit for your research. If you are not sure, read the appropriate sections before making your selection.

☒ Life sciences ☐ Behavioural & social sciences ☐ Ecological, evolutionary & environmental sciences

For a reference copy of the document with all sections, see nature.com/authors/policies/ReportingSummary-flat.pdf

Life sciences study design

All studies must disclose on these points even when the disclosure is negative.

Sample size	No statistical methods were used to predetermine sample size; sample size was determined empirically throughout experiments as an optimal trade-off between sample size, image quality and feasibility in each particular epxeriment. The sample sizes were considered sufficient sice all observed trends were consistent between samples within an experiment as well as between independent experimental replicates.
Data exclusions	No data was excluded from the analysis
Replication	Each experiment was repeated 2-4 times and all attempts at replication were successful
Randomization	Selecting seedlings for mock/experimental treatments and/or imaging from a plate containing at least one order of magnitude more individuals than needed for the experiment was inherently random; no other randomization method was used.
Blinding	Blinding was not possible due to the effects of each mutation/treatment on the growth and/or morphology of the plants that were obvious at first sight.

Reporting for specific materials, systems and methods

Materials & experimental systems

n/a	Involved in the study
☐	☒ Unique biological materials
☒	☐ Antibodies
☒	☐ Eukaryotic cell lines
☒	☐ Palaeontology
☒	☐ Animals and other organisms
☒	☐ Human research participants

Methods

n/a	Involved in the study
☒	☐ ChIP-seq
☒	☐ Flow cytometry
☒	☐ MRI-based neuroimaging

Unique biological materials

Policy information about availability of materials

Obtaining unique materials	All unique biological materials (Arabidopsis transgenic lines and DNA constructs) are available from the corresponding author with the exception of the KN::PIN2-GFP x XVE>>DRP1a-mRFP line, since F1 seeds were used in this case and their amount is thus very limited. Upon request, KN::PIN2-GFP seeds and XVE>>DRP1a-mRFP expression clone (also available from Yunpei Takano, corresponding author of Yoshinari et al., 2016, where the construct was described) can be provided instead so that the line can be re-created as described in Materials and Methods.

nature plants

SUPPLEMENTARY INFORMATION

https://doi.org/10.1038/s41477-018-0318-3

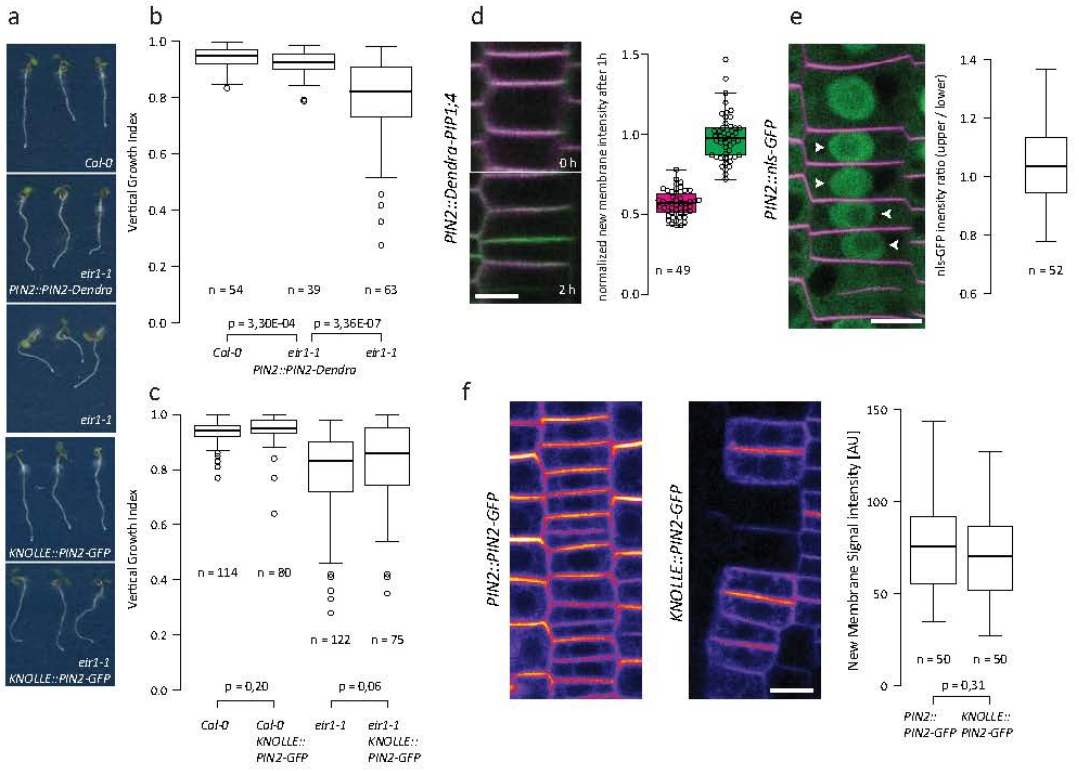
In the format provided by the authors and unedited.

Mechanistic framework for cell-intrinsic re-establishment of PIN2 polarity after cell division

Matouš Glanc[1,2], Matyáš Fendrych[1,2] and Jiří Friml[1*]

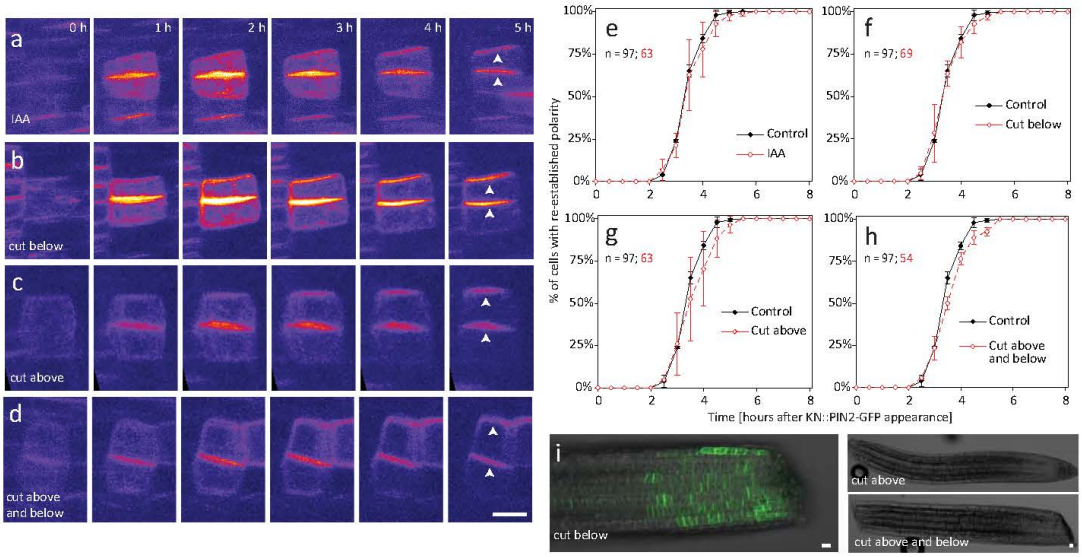
[1]IST Austria, Klosterneuburg, Austria. [2]Department of Experimental Plant Biology, Faculty of Science, Charles University, Prague, Czechia.
*e-mail: jiri.friml@ist.ac.at

Uncorrected proofs



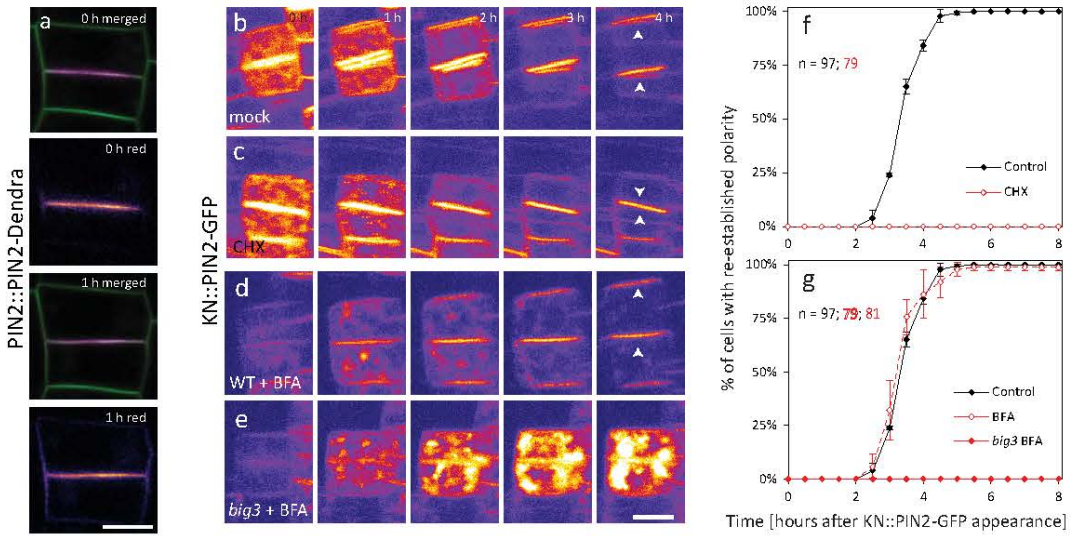
Supplementary Figure 1, related to Figure 1

a: Phenotype of 4-day-old seedlings of the genotypes *Col-0, PIN2::PIN2-Dendra / eir1-1, eir1-1, KNOLLE::PIN2-GFP and KNOLLE::PIN2-GFP / eir1-1.* **b:** quantitative analysis of the rescue of *eir1-1 (pin2)* root agravitropic phenotype by *PIN2::PIN2-Dendra*. n indicates the number of roots in one experiment; the experiment was repeated 3 times. **c**: quantitative analysis of the effect of *KNOLLE::PIN2-GFP* on root gravitropism in *Col-0* and *eir1-1*. n indicates the pooled number of roots from two experiments; the experiment was repeated 4 times. **d:** Both pre-existing (magenta) ad newly synthesized (green) pools of Dendra-PIP1;4 contribute to the signal at the newly formed PM. The graph shows signal intensity at the newly formed PM 1h after cytokinesis normalized to the intensity of the neighboring old PMs in both red and green channels; higher relative intensity of the green channel confirms predominant contribution of *de novo* secretion to the CP protein pool. n indicates the number of cells from 12 roots and 3 independent experiments. **e**: PIN2::nls-GFP signal intensity does not differ between the upper and lower newly divided daughter cells (marked by arrows). PM is stained with FM4-64. Quantification of the upper/lower daughter cell ratios is shown on the right; n indicates the number of cell pairs from 6 roots; the experiment was repeated three times. **f:** *PIN2::PIN2-GFP* and *KNOLLE::PIN2-GFP* images acquired side-by-side with identical microscope settings. Quantification of the signal intensity on the post-cytokinetic membrane is shown on the right; n indicates the number of membranes from 10 roots; the experiment was repeated 3 times. All box-plots represent median, 1st and 3rd quartile; the whiskers extend to data points <1,5 interquartile range away from the 1st/3rd quartile; Outliers (b,c) or all data points (d) are shown as circles. P-values were calculated using two-tailed two-sample T-test with unequal variance. Scale bars = 10 µm



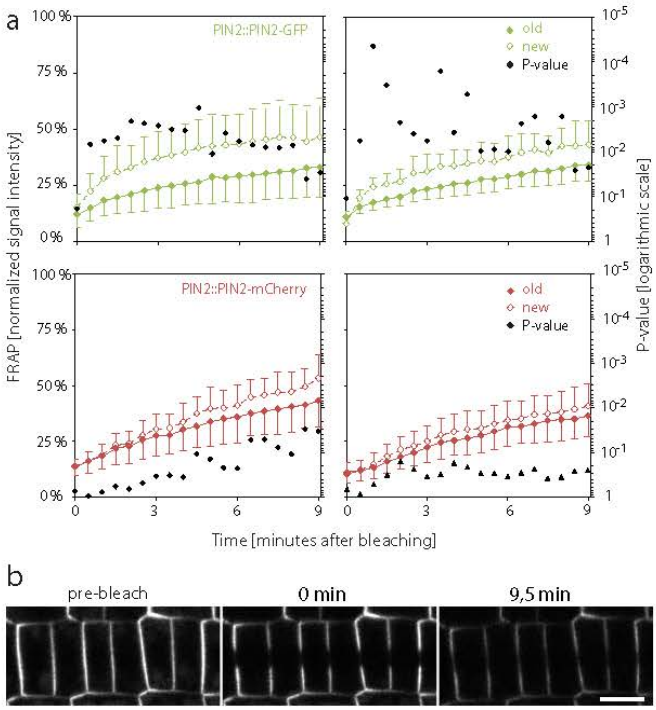
Supplementary Figure 2, related to Figure 2

a: Re-establishment of apical PIN2 polarity in *KN::PIN2-GFP* plants treated with the natural auxin IAA is not altered compared to the mock control (Fig.2a) **b-d**: Re-establishment of apical PIN2 polarity in *KN::PIN2-GFP* roots after incision below the meristem, above it, or both**. e-h:** quantitative analysis of **a**-**d**. Neither of the manipulations affected the dynamics of KN::PIN2-GFP polarity re-establishment. The controls are the same as in **1f**. The graphs show mean +/- SD of 3 independent experiments, n indicates the total number of cell pairs. The number of roots/cell pairs analyzed in each experiment was 3/13, 3/21 and 3/29 in **e;** 3/28, 2/20 and and 2/21 in **f**; 2/22, 3/19 and 2/22 in **g**; 2/15, 4/21 and 6/18 in **h**, respectively. **i:** Representative illustrations of incised roots that were used in **b-d**. The experiment was repeated independently 3 times with similar results. Arrows indicate predominant KN::PIN2-GFP localization. Scale bars = 10 µm



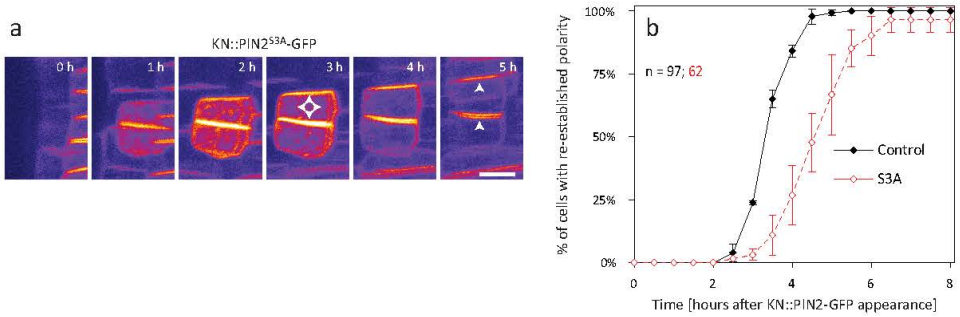
Supplementary Figure 3, related to Figure 3

a: 1 hour after local photoconversion of PIN2::PIN2-Dendra signal at the new PM, only weak, presumably lateral-diffusion based redistribution of the red signal was observed. n = 21 cell pairs from 10 roots in 3 independent experiments. **b-c:** Apical signal does not appear in *KN::PIN2-GFP* roots treated with the translation inhibitor CHX. **d-e:** The ARF-GEF inhibitor BFA prevents apical polarity re-establishment only in the *big3* mutant (**e**), where it blocks both secretion and recycling, but not in *WT* (**d**), where it only inhibits recycling. **f-g:** quantitative analysis of **b-e**. The controls are the same as in **1f**. The graphs show mean +/- SD of 3 independent experiments, n indicates the total number of cell pairs. The number of roots/cell pairs analyzed in each experiment was 4/20, 4/21 and 6/38 in **f;** 4/21, 3/29 and 3/29 in **g** (BFA); 4/32, 3/21 and 3/28 in **g** (big3 + BFA), respectively. Arrows indicate predominant KN::PIN2-GFP localization. Scale bars = 10 µm



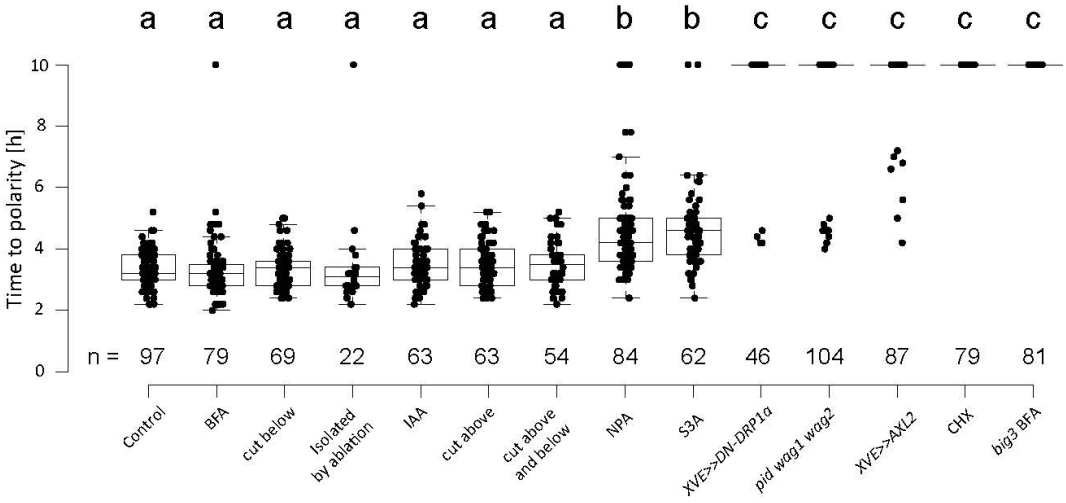
Supplementary Figure 4, related to Figure 3

a: FRAP analysis of PIN2 mobility in *PIN2::PIN2-GFP* and *PIN2::PIN2-mCherry.* The graphs show mean signal recovery in the bleached ROI after background subtraction and normalization to photobleaching due to iterative imaging +/- SD and P-values for each timepoint of 4 independent experiments, each consisting of 15,19,15,15 old membranes and 15,13,13,13 new membranes from 3 different roots, respectively. P-values were calculated using two-tailed two-sample T-test with unequal variance. **b:** representative image from **a**. Scale bar = 10 µm



Supplementary Figure 5, related to Figure 4

a: Apical polarity re-establishment of *KN::PIN2^{S3A}-GFP* cells. **b**: quantitative analysis of **a**. The control is the same as in **1f**. The graph shows mean +/- SD of 3 independent experiments, n indicates the total number of cell pairs. The number of roots/cell pairs analyzed in each experiment was 2/22, 6/19 and 2/21, respectively. Arrows indicate predominant KN::PIN2^{S3A}-GFP localization. Scale bars = 10 µm



Supplementary Figure 6: Statistical analysis of all KN::PIN2-GFP experiments

Boxplot representation and statistical analysis of the timing of *KN::PIN2-GFP* apical polarity re-establishment under all conditions tested throughout the manuscript. Box-plots represent median, 1st and 3rd quartile; the whiskers extend to data points <1,5 interquartile range away from the 1st/3rd quartile, all data points are shown as circles. n = total number of cell pairs analysed in all roots and repetitions of each experiment. Conditions with the same letter (a,b,c) are not significantly different from each other, but are significantly different from conditions with a different letter. Statistical significance was tested with Kruskal-Wallis Rank Sum Test (post hoc analysis: alpha: 0,01, p-value adjustment: bonferroni).

Supplementary movie legends

Movie S1: PIN2::PIN2-Dendra dynamics in dividing cells. The experiment was repeated independently 3 times with similar results.

Movie S2: KN::PIN2-GFP dynamics in dividing cells. The experiment was repeated independently >3 times with similar results.

Movie S3: Effect of *AXL2* overexpression on KN::PIN2-GFP dynamics. The experiment was repeated independently 3 times with similar results.

Movie S4: KN::PIN2-GFP dynamics in *pid wag1 wag2* mutant background. The experiment was repeated independently 3 times with similar results.

Movie S5: WAG1::WAG1-GFP dynamics in dividing cells. The experiment was repeated independently 3 times with similar results.

Supplementary table 1: Primers used in this study

pKN_attB_F	GGGGACAACTTTGTATAGAAAAGTTGcatttttcaagcattacaga
pKN_attB_R	GGGGACTGCTTTTTTGTACAAACTTGcttttcacctgaaagtcaa
PIN2_attb_F	ggggacaagtttgtacaaaaaagcaggctccATGATCACCGGCAAAGACAT
PIN2stop_attb_R	ggggaccactttgtacaagaaagctgggtcTTAAAGCCCCAAAAGAACGTAGTAGA
DEN_attB1_F	GGGGACAAGTTTGTACAAAAAAGCAGGCTTAATGAATCTCATCAAGGAAGA
DEN_attB2_R	GGGGACCACTTTGTACAAGAAAGCTGGGTTCCAAACCTGTGATGGGAGAG
W138_attB2r_F	GGGGACAGCTTTCTTGTACAAAGTGGTAATGGAAGGCAAAGAAGAAGA
W138_attB3_R	GGGGACAACTTTGTATAATAAAGTTGTCTAACTCTTGCTCTTGAAAG
PIN2_1004-F	ACAACAATAATAGTGTTCCGTCGTACCCAC
PIN2_1004-R	GTGGGTACGACGGAACACTATTATTGTTGT
pMEL1-attB-F	GGGGACAACTTTGTATAGAAAAGTTGTCgtggagtttgacagctaaac
pMEL1-attB-R	GGGGACTGCTTTTTTGTACAAACTTGAgatgaagaagaaactgatag
MEL1-attB-F	GGGGACAAGTTTGTACAAAAAAGCAGGCTTCATGAAGTTCATGAAACTTG
MEL1-attB-R	GGGGACCACTTTGTACAAGAAAGCTGGGTAATGCTTCTTGCTTGTGGAAG
big3_F	AAACTCTCCACTGGCTAAGCC
big3_R	GCAAGTTTTCTTGCGCAATAC
pid14_F	ATGTTACGAGAATCAGACGGTG
pid14_R	TCAAAAGTAATCGAACGCCGCTGG
wag1_F	ATGGAAGACGACGGTTATTACC
wag1_R	GGAGAAACAACCGCCACCACG
wag2_F	CTCCGCAGCAACGGAGAAGCAAC
wag2_R	GAACTCTCTGCCTCAAAGACACAC
LBb1.3	ATTTTGCCGATTTCGGAAC
eir1-1_F	ggcaattgcttgatgttgttgatcattttatgggaca
eir1-1_R	aagcaccaaagactataacta

Generation of PIN2 polarity in *Arabidopsis* in the absence of intact cytoskeleton

Matouš Glanc[a,b]*, Matyáš Fendrych*[a,b] *and Jiří Friml*[a,]*

[a]IST Austria, 3400 Klosterneuburg, Austria

[b]Department of Experimental Plant Biology, Faculty of Science, Charles University, 12844 Prague, Czechia

*correspondence to: jiri.friml@ist.ac.at

Cell polarity is crucial for the coordinated development of all multicellular organisms. In plants, this is exemplified by the PIN-formed (PIN) efflux carriers of the phytohormone auxin: the polar subcellular localization of the PINs is instructive to the directional intercellular auxin transport, and thus to a plethora of auxin-regulated growth and developmental processes [1]. Endomembrane trafficking has been considered one of the main factors mediating PIN polar localization. Movement of endomembrane vesicles depends on the cytoskeleton, and accordingly, pharmacological interference with actin or microtubules (MTs) has been linked to defects in PIN subcellular dynamics [2,3]. However, opinions on the importance of the cytoskeleton for PIN polarity *per se* differ [3,4]. Here, we analyzed the effect of cytoskeleton-depolymerizing agents on the generation of apical PIN2 polarity in *Arabidopsis* roots using time-lapse imaging of advanced fluorescent reporters. We found, surprisingly, that the correctly polarized subcellular PIN distribution can be achieved in the absence of both intact actin and MTs. Our findings imply that that the primary PIN polarization mechanism is independent of cytoskeleton-mediated endomembrane trafficking.

During cytokinesis of *Arabidopsis* root cells, PIN polarity is transiently lost and subsequently re-established [2,4,5]. We have recently shown that in combination with temporally-restricted expression of PIN2-GFP from the cytokinesis-specific *KNOLLE* promoter, the dividing cells can be used as a suitable model to study PIN polarity establishment *in vivo* [5]. Here, we employed this system together with the well-established actin- and MT-depolymerizing drugs Latrunculin B (LatB) and Oryzalin (Ory), respectively, to test the importance of the cytoskeleton for the establishment of PIN polarity.

Application of either of the two drugs caused severe cytokinetic defects ranging from division plane misorientationation to complete cell plate formation failure, consistently with both actin and MTs playing key roles in multiple steps of cell division [6] and providing a good internal control that the treatments indeed disrupted the respective cytoskeletal network (Fig. 1a-c). In both cases, KNOLLE::PIN2-GFP signal was partly mislocalized to abnormal endomembrane compartments, providing further evidence of functionality of the drugs. In spite of the disturbed cytoskeleton, however, apical polarity of the plasma-membrane (PM) localized signal was in both cases eventually achieved, albeit with a considerable delay (Fig. 1b-c,g). Notably, in case of the Ory treatment, establishment of apical polarity was preceded by apolar distribution of the PM signal (Fig. 1c).

We next applied both LatB and Ory at the same time. This co-treatment led to efficient depolymerization of both actin and MTs, as visualized by the respective markers Fimbrin-GFP and GFP-MAP4 (Fig.1e-f), and completely abolished the cells' ability to divide (Fig. 1d). Under these conditions, much of KNOLLE::PIN2-GFP localized to ectopic endomembrane aggregates that displayed only slow random movement and never reached the PM, indicating that PIN2-GFP trafficking was indeed severely disrupted (Fig. 1d). Nevertheless, part of the signal was localized at the PM, initially in an apolar manner, as in the case of the Ory treatment alone. Nonetheless, surprisingly, apical polarity of the PM-bound signal was eventually correctly established, albeit significantly later compared to the mock-treated control or either of the treatments alone (Fig.1d,g). This shows that the cellular mechanism that establishes apical PIN2 apical polarity is independent of the intact cytoskeletal network.

To validate our findings outside of the context of (unsuccessfully) dividing cells, we generated an *RPS5a::LOX:nls-mCherry:lox::PIN2-GFP* construct and introduced it into the *HS::CRE* background. In the resulting plants, a mild heat shock led to the onset of Cre/Lox recombination-mediated expression of PIN2-GFP only in a few random and therefore often isolated cells, thus allowing to observe the dynamic generation of PIN2 polarity also in interphase cells (Fig. 1h-i). Consistently with previous results, the LatB + Ory cotreatment did not prevent apical PIN2-GFP polarity generation in this experiment either (Fig. 1j).

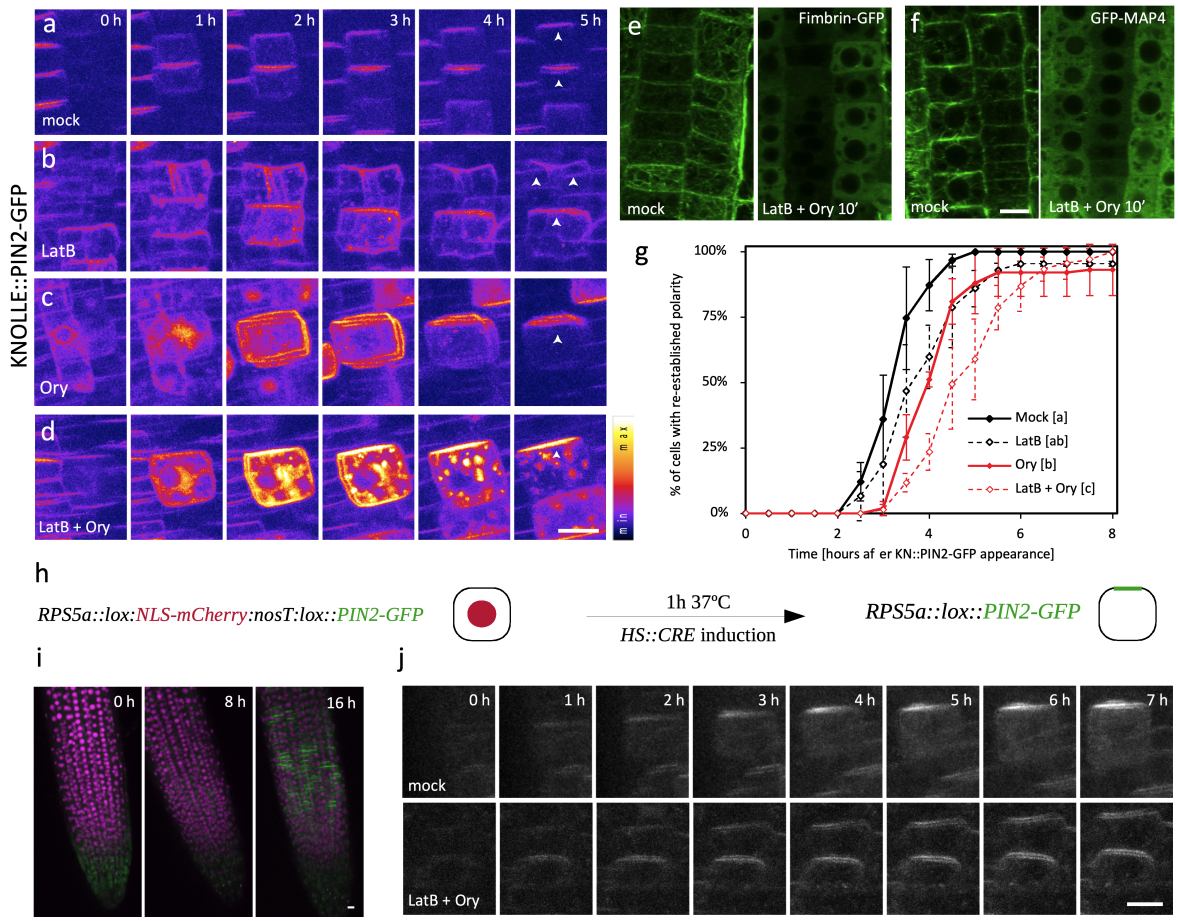


Figure 1: PIN2 polarity establishment does not require intact cytoskeleton
a-d: Establishment of PIN2 polarity in root epidermal cells visualized by dynamic localization of PIN2-GFP expressed from the mitosis-specific *KNOLLE* promoter. **a** In a control situation, the signal localizes initially to the cell plate-derived new PM pair, and the apical polar distribution typical for PIN2 is reestablished 2-5 hours afterwards [5]. n = 51 cells from 6 roots in 3 independent experiments. **b** In LatB treated cells, part of the signal localizes to ectopic endomembrane compartments, but the distribution dynamics of PM signal is similar to the control if the CP is formed (upper cell); and apical polar distribution develops also in cells where the treatment leads to cytokinetic failure (lower cell). n = 87 cells from 11 roots in 3 independent experiments. **c** In oryzalin treated cells, the signal is initially localized to a ball-shaped endomembrane aggregate that forms instead of the cell plate. Most of the signal is subsequently relocalized to the PM initially in an apolar manner, followed by development of apical polarity. n = 90 cells from 11 roots in 3 independent experiments. **d** Cells treated with both inhibitors at the same time display strict cytokinetic failure and signal localization to large, mostly immobile endomembrane aggregates in addition to the PM. Nevertheless, apical polarity of PM-bound signal is eventually achieved also in this case. n = 83 cells from 9 roots in 3 independent experiments. **e-f** The markers Fimbrin-GFP (**e**) and GFP-MAP4 (**f**) confirm that the LatB + Ory cotreatment leads to fast and efficient depolymerizatin of both actin and MTs, respectively. n = 19-20 roots from 3 independent experiments per line and treatment. **g** quantification of the data presented in **a-d**. The timepoint of KNOLLE::PIN2-GFP apical signal polarity establishment was marked for each cell, and the percentage of cells with established polarity in each condition was plotted against time. Mean of 3 independent experiments, each consisting of >20 cells from 2-4 different roots (see n values in **a-d**), +/- SD is shown. The letters [a-c] indicate statistical significance based on Kruskal-Wallis Rank Sum Test (post hoc analysis: alpha: 0.01, p-value adjustment: Bonferroni); the data points from all three experimental replicates were pooled for the purpose of statistical analysis. **h** Schematic depiction of the *RPS5a::lox:NLS-mCherry:nosT:lox::PIN2-GFP* construct generated to monitor PIN2-GFP polarity establishment in interphase cells. **i** Merged red and green channels of an *RPS5a::lox:NLS-mCherry:nosT:lox::PIN2-GFP*-expressing root 0, 8 and 16h after the heatshock induction of CRE recombinase expression. **j** Establishment of PIN2 polarity in Mock- and LatB + Ory – treated *RPS5a::lox:NLS-mCherry:nosT:lox::PIN2-GFP* cells. The green channel is shown, t0 = the last timepoint before PIN2-GFP signal appeared. n > 30 cells from 6 different roots in 2 independent experiments. Scale bars = 10µm.

In both experiments, depolymerization of actin, MTs or both at the same time led to partial PIN2-GFP mislocalization to abnormal endomembrane compartments. This again confirms that both cytoskeletal components are involved in PIN intracellular trafficking as previously proposed [2–4]. Moreover, the polar distribution of KNOLLE::PIN2-GFP appeared later under all treatments, demonstrating that cytoskeleton-guided trafficking contributes to PIN polar *targeting*. Nevertheless, the *establishment* of PIN2-GFP polarity was cytoskeleton-independent in both mitotic and interphase cells, supporting similar conclusions drawn in the past for PIN1 [4]. This suggests that actin- and MT-guided endomembrane trafficking stabilizes cell polarity by reinforcing asymmetrical distribution of polar cargoes including the PINs. However, both actin and MTs act downstream of an unknown, cytoskeleton-independent polarity establishment mechanism.

Therefore, cytoskeleton-dependent polarized exocytosis, either secretory or recycling, cannot be the main mechanism of PIN polarity generation as hypothesized previously [7]. It has been theoretically predicted and experimentally verified that clathrin-mediated endocytosis plays a key role in PIN polarity regulation [5,8,9]. An endocytosis-dependent, cytoskeleton-independent system based on differential rates of PIN endocytosis at different PM domains is therefore a prime candidate for the main mechanism of PIN polarity establishment. In case of apically localized PIN2, such a mechanism might in principle work in two different ways, or their combination: A) Endocytosis machinery might be generally less active at the apical PM compared to the rest of the cell, or B) PIN2 molecules in the apical domain could be specifically "protected" from endocytosis by an unknown factor. The observation that CLC-GFP signal is enhanced at the lateral PM domains has already indirectly hinted at A) [8], while the existence or nature of any factor specifically modulating PIN2 endocytosis in a domain-specific manner predicted in B) is so far elusive. It was proposed that NPH3-like proteins encoded by *MAB4/MEL* gene family might possess this function, but the evidence presented to support this claim is far from conclusive [10].

In conclusion, we have demonstrated that apical PIN2 polarity can be generated in the absence of intact actin and MTs in both mitotic and interphase cells. In combination with previous results with PIN1 [4], this excludes any cytoskeleton-guided vesicular trafficking-based mechanism as the main driving force of PIN polarity establishment. This finding, together with recent evidence that endocytosis plays a central role in PIN polarity [5,9], necessitates that regulation of PIN endocytosis, and specifically its rates at

different PM domains, be subjected to detailed analyses, as these will likely shed light on the still enigmatic mechanisms of cell polarity establishment in plants.

References

1. Adamowski, M., and Friml, J. (2015). PIN-Dependent Auxin Transport: Action, Regulation, and Evolution. Plant Cell Online *27*, 20–32.
2. Geldner, N., Friml, J., Stierhof, Y.-D.D., Jürgens, G., and Palme, K. (2001). Auxin transport inhibitors block PIN1 cycling and vesicle trafficking. Nature *413*, 425–428.
3. Kleine-Vehn, J., Łangowski, L., Wisniewska, J., Dhonukshe, P., Brewer, P.B., and Friml, J. (2008). Cellular and molecular requirements for polar PIN targeting and transcytosis in plants. Mol. Plant *1*, 1056–66.
4. Boutte, Y., Crosnier, M.-T., Carraro, N., Traas, J., and Satiat-Jeunemaitre, B. (2006). The plasma membrane recycling pathway and cell polarity in plants: studies on PIN proteins. J. Cell Sci. *119*, 1255–1265.
5. Glanc, M., Fendrych, M., and Friml, J. (2018). Mechanistic framework for cell-intrinsic re-establishment of PIN2 polarity after cell division. Nat. Plants *in press*.
6. Smertenko, A., Assaad, F., Baluška, F., Bezanilla, M., Buschmann, H., Drakakaki, G., Hauser, M.T., Janson, M., Mineyuki, Y., Moore, I., *et al.* (2017). Plant Cytokinesis: Terminology for Structures and Processes. Trends Cell Biol. *27*, 885–894.
7. Dhonukshe, P., Tanaka, H., Goh, T., Ebine, K., Mähönen, A.P., Prasad, K., Blilou, I., Geldner, N., Xu, J., Uemura, T., *et al.* (2008). Generation of cell polarity in plants links endocytosis, auxin distribution and cell fate decisions. Nature *456*, 962–966.
8. Kleine-Vehn, J., Wabnik, K., Martinière, A., Łangowski, Ł., Willig, K., Naramoto, S., Leitner, J., Tanaka, H., Jakobs, S., Robert, S., *et al.* (2011). Recycling, clustering, and endocytosis jointly maintain PIN auxin carrier polarity at the plasma membrane. Mol. Syst. Biol. *7*, 540.
9. Adamowski, M., Narasimhan, M., Kania, U., Glanc, M., De Jaeger, G., and Friml, J. (2018). A Functional Study of AUXILIN-LIKE1 and 2, Two Putative Clathrin Uncoating Factors in Arabidopsis. Plant Cell *30*, 700–716.
10. Furutani, M., Sakamoto, N., Yoshida, S., Kajiwara, T., Robert, H.S., Friml, J., and Tasaka, M. (2011). Polar-localized NPH3-like proteins regulate polarity and endocytosis of PIN-FORMED auxin efflux carriers. Development *138*, 2069–78.

Supplemental Information

Experimental procedures

Seeds were grown on ½ Murashige-Skoog medium with 1% sucrose and 1% agar and grown *in vitro* for 4 days under long day conditions. The transgenic lines *KNOLLE::PIN2-GFP* [5], *35S::AtFIM1-GFP* [11] and *35S:: GFP-MAP4* [12] were described previously. The *RPS5a::LOX:nls-mCherry:lox::PIN2-GFP* construct was generated using the Gateway cloning thechnology (Invitrogen) as follows: *RPS5a* promoter fragment was cloned into pDonrP4-P1r, a fragment comprising a *LOX* site, *mCherry* with an N-terminal nuclear localization signal, a *NOS* terminator and another *LOX* site was commercially synthesized (Eurofins Genomics) and cloned into pDonr221, and the *PIN2-GFP* fragment was cloned into pDonr P2r-P3. All three entry clones were recombined into the pB7m34GW,0 destination vector and the resulting expression clone was transformed into the *HS::CRE* [13] background using the floral dip method [14]. 20μM LatrunculinB and 40μM Oryzalin (both Sigma) were applied from 20mM or 40mM DMSO stocks, respectively, in small slices of agar medium as described previously [5]. Heat-shock induction of CRE recombinase expression was performed by placing the seedlings mounted in chambered coverslips (LabTek) into a 37°C incubator for 1 hour. *KNOLLE::PIN2-GFP* and *RPS5a::LOX:nls-mCherry:lox::PIN2-GFP* time-lapse imaging was performed on a vertically oriented Zeiss LSM700 confocal microscope as described previously [5,15]; imaging of *35S::AtFIM1-GFP and 35S:: GFP-MAP4* controls was performed on inverted Zeiss LSM700 or LSM880 miscroscopes.

Supplemental references

11. Wang, Y.-S., Motes, C.M., Mohamalawari, D.R., and Blancaflor, E.B. (2004). Green fluorescent protein fusions to *Arabidopsis* fimbrin 1 for spatio-temporal imaging of F-actin dynamics in roots. Cell Motil. Cytoskeleton *59*, 79–93.
12. Marc, J., Granger, C., Brincat, J., Fisher, D., Kao, T., McCubbin, A., and Cyr, R. (1998). A GFP-MAP4 reporter gene for visualizing cortical microtubule rearrangements in living epidermal cells. Plant Cell *10*, 1927–40.
13. Dubrovsky, J.G., Sauer, M., Napsucialy-Mendivil, S., Ivanchenko, M.G., Friml, J., Shishkova, S., Celenza, J., and Benková, E. (2008). Auxin acts as a local morphogenetic trigger to specify lateral root founder cells. Proc. Natl. Acad. Sci. U. S. A. *105*, 8790–4.
14. Clough, S.J., and Bent, A.F. (1998). Floral dip: a simplified method forAgrobacterium-mediated transformation ofArabidopsis thaliana. Plant J. *16*, 735–743.
15. von Wangenheim, D., Hauschild, R., Fendrych, M., Barone, V., Benková, E., and Friml, J. (2017). Live tracking of moving samples in confocal microscopy for vertically grown roots. Elife *6*, e26792.

Arabidopsis MAB4/MEL proteins mediate PIN polarity maintenance by reducing PIN lateral diffusion

Matouš Glanc[1,2], David Domjan[1], Lindy Abas[3], Lukas Hörmayer[1], Ludmila Včelařová[1], Robert Hauschild[1], Shutang Tan[1], Lesia Rodriguez-Solovey[1], Matyáš Fendrych[1,2] and Jiří Friml[1,#]

[1]Institute of Science and Technology Austria (IST Austria), 3400 Klosterneuburg, Austria
[2]Department of Experimental Plant Biology, Faculty of Science, Charles University, 12844 Prague, Czechia
[3]Department of Applied Genetics and Cell Biology, University of Natural Resources and Life Sciences – BOKU, 1190 Vienna, Austria
[#]Correspondence to: jiri.friml@ist.ac.at

Abstract

The mechanisms of cell polarity maintenance in plants remain conceptually unclear, since plant cells lack tight junctions and therefore their polar plasma membrane domains are not physically delineated. Polarly localized PIN auxin efflux carriers represent a prime model to study cell polarity in plants. NPH3-like proteins of unknown function encoded by the *MAB4/MEL* gene family were previously implicated in the regulation of PIN polarity, but the mechanistic basis of their importance remained unknown. Here, we demonstrate that MAB4/MELs are involved in PIN polarity maintenance rather than establishment. MAB4/MEL proteins are recruited to the PM by a physical interaction with the PINs, likely in a PIN phosphorylation-dependent manner, and reduce PIN mobility within the plasma membrane, thereby limiting lateral diffusion-based escape of the PINs from their respective polar domain. These findings provide a conceptual advance in the understanding of PIN polarity maintenance, and of cell polarity regulation in plants in general.

Introduction

Cell polarity, its establishment and maintenance are pivotal topics of cell biology across kingdoms and model organisms. In animal systems such as the epithelial cells, plasma membrane (PM) domains are delimited by tight junctions – multiprotein complexes that act as physical barriers preventing cargos to escape from their respective polar domain by lateral diffusion and thus playing a key role in polarity maintenance (Wells et al., 2006). In plants, no similar structure has been described, and hence the mechanisms of polarity maintenance remain conceptually unclear (Kania et al., 2014).

PIN-FORMED (PIN) auxin efflux carriers are a popular model to study cell polarity in the model plant *Arabidopsis* due to their remarkably asymmetrical subcellular localization as well as a key role in polar auxin transport-mediated developmental processes (Adamowski and Friml, 2015). Nevertheless, our knowledge of molecular mechanisms underlying PIN polarity is fragmented and incomplete.

The importance of slow lateral diffusion in PIN polarity maintenance is supported by experimental data and mathematical modeling (Feraru et al., 2011; Kleine-Vehn et al., 2011), but since this feature is neither universal (Łangowski et al., 2016) nor unique (Martinière et al., 2012) to polar membrane proteins, the mechanistic basis of its role is yet to be discovered.

One of the better-characterized PIN polarity regulators is the Ser/Thr AGCVIII kinase PINOID (PID), which regulates the polar localization of PINs by directly phosphorylating them (Friml et al., 2004; Michniewicz et al., 2007; Dhonukshe et al., 2010). However, the exact nature of the link between PIN polarity and its phosphorylation by the apolarly localized PID is missing (Barbosa et al., 2018). The gene *MACCHI-BOU 4 (MAB4;* also known as *Enhancer of pinoid 1 /ENP1/* or *Naked Pins in Yucca mutants 1 /NPY1/)*, the founding member of the *MAB4/MEL (Macchi-bou 4/Enhancer of pinoid 1-Like)* family, was identified in a forward genetic screen as an enhancer of *pid* mutants (Furutani et al., 2007) and multiple members of both *MAB4/MEL* and *PID* gene families were shown to act in the same pathway based on their genetic interactions in multiple developmental contexts (Cheng et al., 2008; Furutani et al., 2011, 2014; Li et al., 2011). MAB4/MEL proteins colocalize with PINs and PIN polarity is compromised in higher order *mab4/mel* mutants (Furutani et al., 2011, 2014). Additionally, several findings hinted at the existence of a feedback mechanism co-regulating PIN and MAB4/MEL polarity (Furutani et al., 2011). However, the mechanism by which MAB4/MELs regulate PIN polarity, as

well as the nature of the interaction between *MAB4/MEL* and *PID* genes, remains unknown.

Here, we show that PINs recruit MEL1 to the plasma membrane by a physical protein-protein interaction that likely depends on the phosphorylation status of the PINs by PID and other AGCVIII kinases. Furthermore, we show that the interaction with MAB4/MELs contributes to PIN polarity maintenance by reducing PIN lateral diffusion. Our findings, besides identifying the role of MAB4/MEL proteins in PIN polarity, provide a conceptual advance in the understanding of polarity maintenance in plant cells.

Results

MEL1 plasma membrane association depends on the presence of PINs

To test the inter-dependence of MAB4/MEL and PIN polarity, we generated translational reporters *MEL1::MEL1-GFP* and *PIN2::MEL1-mCherry*. Both constructs rescued the *mel1234* quadruple mutant to a similar extent (Fig. S1), demonstrating that they were functional, but also that MEL absence specifically from the *PIN2* expression domain is responsible for the reduced gravitropism phenotype of the *me1234* mutant (Furutani et al., 2011). Notably, when introduced into the *pin2* null allele *eir1-1*, the subcellular localization of both reporters was severely disrupted in the epidermis. Instead of the apical PM domains, the signal localized to the cytoplasm or ectopic membrane

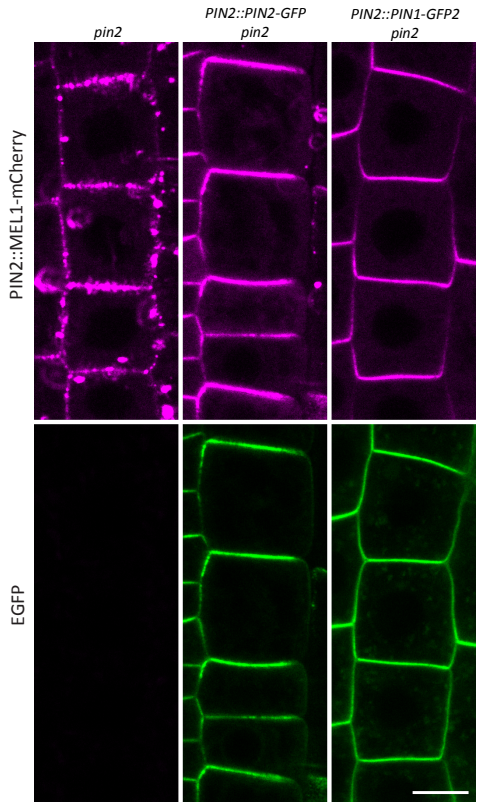


Figure 1: PINs recruit MEL1 to the plasma membrane
PIN2::MEL1-mCherry translational reporter localized to ectopic membrane aggregations in the epidermal cells of the *pin2* mutant, instead of the apical PM as in *WT* (See figure S1). Introducing *PIN2::PIN2-GFP* into *PIN2::MEL1-mCherry/pin2* restored *WT*-like apical PM localization of MEL1-mCherry, while introducing the basally localized *PIN2::PIN1-GFP2* caused MEL1-mCherry to localize basally, demonstrating that MEL1 localization depends on PIN localization. Images are representative of 18, 15 and 20 roots from 4 independent experiments, respectively. Scale bar = 10 µm.

aggregates, while its localization was not affected in the inner cell files where other PINs are expressed (Fig. 1, S1). The different mislocalization pattern was presumably caused by a difference in strength of the two promoters. A cross of *MEL1::MEL1-GFP/pin2* and *PIN2:MEL1-mCherry/pin2* lines back into Col-0, or of *PIN2:MEL1-mCherry/pin2* into *PIN2::PIN2-GFP/pin2 or PIN2::PIN2-Venus/pin2,* was sufficient to restore apical PM localization of both reporters in epidermal cells (Fig. 1, 3a, S1), suggesting that MEL1 localization depends on PIN localization. To ultimately test this hypothesis, we crossed *PIN2:MEL1-mCherry* with *PIN2::PIN1-GFP2,* where PIN1-GFP shows basal localization in the epidermis (Wisniewska et al., 2006). As expected, MEL1-mCherry adopted pronounced basal polar localization in the epidermal cells in the resulting *PIN2::MEL1-mCherry* x *PIN2::PIN1-GFP2/pin2* line (Fig 1). Together, these data demonstrate that PIN presence at the PM is required and sufficient for MEL1 polar PM association.

MEL1 physically interacts with PIN2

Next, we examined the distribution of PIN2-GFP and MEL1-mCherry signal within the PM with Airyscan superresolution imaging. PIN2-GFP signal was highly clustered in agreement with previous findings (Kleine-Vehn et al., 2011). Notably, the distribution of MEL1-mCherry signal was highly heterogeneous as well, and both signals colocalized almost perfectly into the same clusters (Fig. 2a-b). This remarkable co-localization of MEL1 with PIN2 prompted us to test whether they could physically interact. To this end, we employed two different pulldown assays. In a fully *in vitro* setup, recombinant MEL1-His clearly co-sedimented with GST-PIN2 hydrophilic loop (PIN2HL), but not with the GST control alone, upon incubation with glutathione agarose beads (Fig. 2c). In a parallel *semi-in vitro* approach, soluble MEL1-GFP from a *MEL1::MEL1-GFP* plant extract partly co-sedimented with the microsomal fraction of suspension cultured cells; the amount of MEL1-GFP that was pulled down this way was ca. 2x higher when *35S::PIN* cell cultures were used, compared to the WT control (Fig. S2).

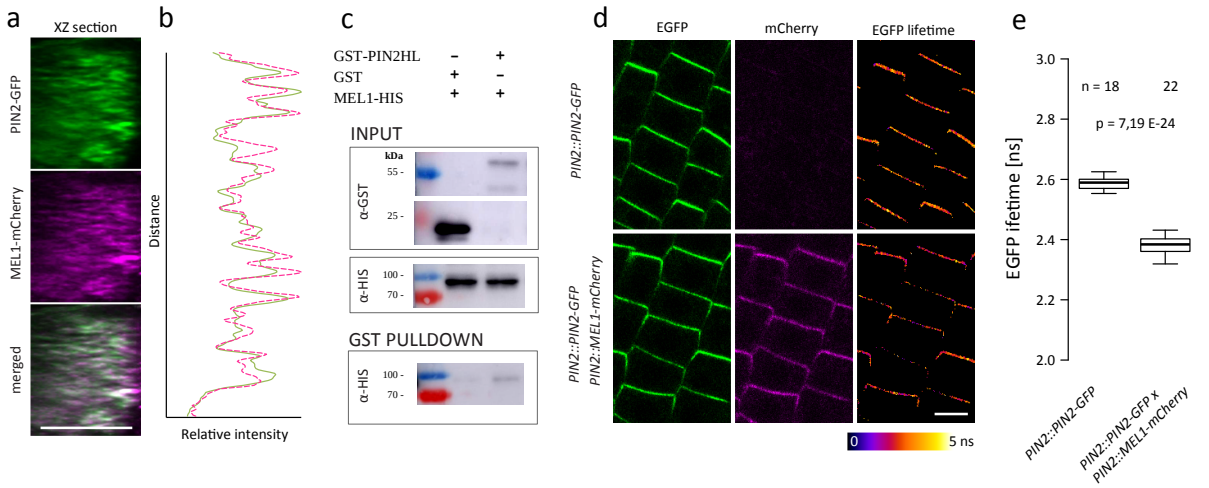


Figure 2: MEL1 physically interacts with PIN2
a: XZ optical section through a multichannel Airyscan superresolution image of a *PIN2::PIN2-GFP x PIN2::MEL1-mCherry* epidermal cell. Both PIN2-GFP and MEL1-mCherry signals are distributed in highly co-localized clusters. The image is representative of 48 cells from 6 roots in 2 independent experiments. **b**: Intensity profile along a line through the image shown in **a** confirms the close co-localization of PIN2-GFP and MEL1-mCherry. **c**: Western blot of an *in vitro* pulldown assay between recombinant GST-PIN2HL and MEL1-HIS. After incubation with MEL1−HIS, GST-PIN2HL and a GST negative control were pulled down with glutathione agarose beads. MEL1-His clearly co-sedimented with GST-PIN2HL, while its co-sedimentation with GST alone was negligible, despite the amount of GST in the reaction was much higher than that of GST-PIN2HL. **d:** FLIM-FRET imaging of PIN2::PIN2-GFP in the presence and absence of PIN2::MEL1-mCherry. PIN2-GFP fluorescence lifetime was reduced in the presence of MEL1-mCherry, indicating the occurrence of FRET and hence physical interaction between the two proteins. **e:** Quantitative analysis of **d**. n indicates the total number of roots from 3 independent experiments; P-value was calculated using two-tailed two-sample T−test with unequal variance. The box-plot represents median, 1st and 3rd quartile; the whiskers extend to data points <1,5 interquartile range away from the 1st/3rd quartile. Scale bars = 10 µm.

Finally, we performed FLIM-FRET imaging to test the PIN2-MEL1 interaction *in vivo*. Fluorescence lifetime of PIN2-GFP was consistently and significantly reduced in plants co-expressing MEL1-mCherry, indicating the occurrence of FRET and thus physical interaction between PIN2-GFP and MEL1-mCherry (Fig. 2 d-e). A similar experiment with MEL1-GFP and PIN2 hydrophilic loop (P2HL-mCherry) transiently expressed in suspension culture protoplasts yielded comparable results (Fig. S2). Together, these findings demonstrate that PIN2 physically interacts with MEL1 through its hydrophilic loop.

PIN-MEL interaction depends on PIN phosphorylation status

We hypothesized that the genetic interaction between *MAB4/MELs* and *PID/WAGs* might be explained by the requirement of PID/WAG-mediated phosphorylation of the PINs for their physical interaction with MAB4/MELs. When we introduced *PIN2::PIN2^{S3A}-Venus*, which has three main serine targets of *PID/WAG*-mediated phosphorylation mutated to alanines (Dhonukshe et al., 2010), into *PIN2:MEL1-mCherry/pin2*, the rescue of MEL1-

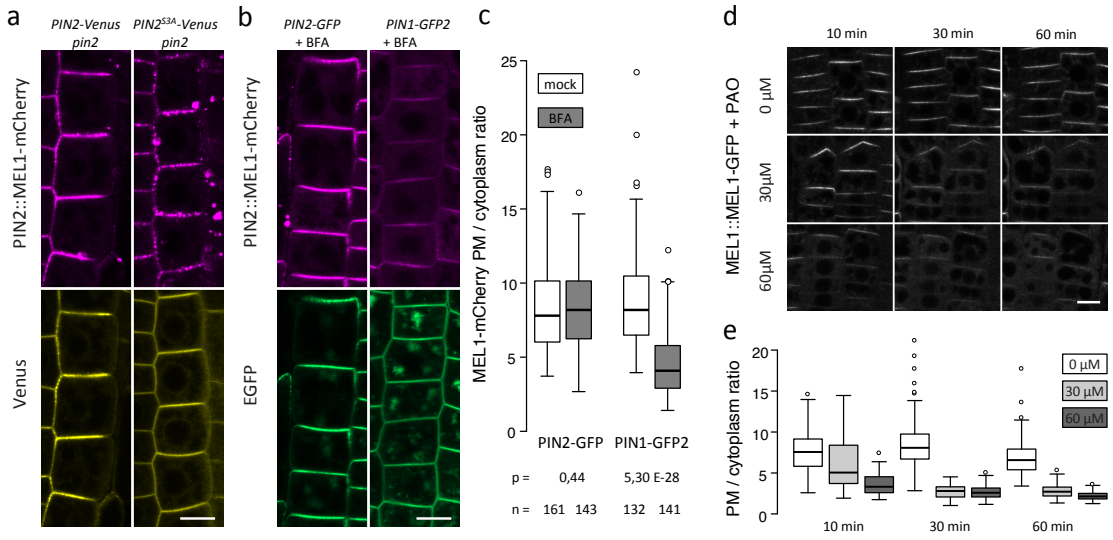


Figure 3: MEL1 interacts with phosphorylated PINs
a: PIN2::MEL1-mCherry was localized to the apical PM in the *PIN2::PIN2-Venus/pin2* background, similarly as in *PIN2::PIN2-GFP/pin2* or *Col-0*. However, the *PIN2::PIN2^{S3A}-Venus* construct harboring point mutations in three PID/WAG-targeted Ser residues in the PIN2 cental hydrophilic loop failed to restore apical PM localization of PIN2::MEL1-mCherry (compare to Fig. 1). The images are representative of 16 roots from 3 independent experiments. **b**: BFA treatment (50µM, 1h) had no effect on apically localized PIN2::MEL1-mCherry localization in the *PIN2::PIN2-GFP* background, as reported previously (Furutani et al., 2011). However, basally localized PIN2::MEL1-mCHerry in the *PIN2::PIN1-GFP2* background was largely dissociated from the PM upon BFA treatment (compare to Fig. 1). **c:** quantification of **b**.The graph shows the ratios of PM/cytoplasm signal intensities. n indicates the number of cells from 4 different roots; P-values were calculated using two-tailed two-sample T−test with unequal variance. The experiment was independently repeated twice with comparable results. **d**: MEL1::MEL1-GFP was dissociated from the PM upon PAO treatment with time- and dose-dependence similar to PID (Simon et al., 2016). **e:** quantification of **c**. The graph shows the ratios of PM/cytoplasm signal intensities. n = 60 cells from 6 different roots. The experiment was repeated twice with comparable results. The box-plots represent median, 1st and 3rd quartile; the whiskers extend to data points <1,5 interquartile range away from the 1st/3rd quartile; outliers are shown as circles. Scale bars = 10 µm.

mCherry PM localization was strongly reduced compared to the *PIN2::PIN2-Venus* control (Fig. 3a, compare to Fig. 1). Next, we made use of the fact that basally, but not apically localized PINs are quickly and efficiently dephopsohrylated upon treatment with the fungal toxin Brefeldin-A (BFA) due to differential BFA-sensitivity of PID and D6PK kinases (Weller et al., 2017). Coincidentally, apically localized MEL1-mCherry and MEL1-GFP were insensitive to BFA as reported before (Furutani et al., 2011). However, both basally localized PIN2::MEL1-mCherry in epidermal cells of *PIN2::PIN1-GFP2* and MEL1::MEL1-GFP in endodermis and pericycle cells of the WT (Fig. S3) dissociated from the PM upon BFA treatment (Fig 3b-c, compare to Fig. 1). Interestingly, in basal PIN-containing cortex cells, BFA treatment led to apicalization rather than PM-dissociation of MEL1-GFP (Fig S3). Finally, PID association with the PM, and therefore presumably also apical PIN phosphorylation, was shown to be sensitive to the phosphoinositol-phospate kinase inhibitor Phenyl-arsine Oxide (PAO) (Simon et al., 2016). MEL1-GFP apical PM localization was sensitive to PAO in a time- and

concentration-dependent manner very similar to PID (Fig. 3d-e). Taken together, these results suggest that the PIN-dependent association of MEL1 with the PM depends on the phosphorylation status of the PINs.

MAB4/MEL proteins mediate PIN polarity maintenance by reducing their lateral diffusion rate

Having established physical, likely phosphorylation-dependent interaction with PINs as a requirement for MAB4/MEL association with the PM, we wanted to know by which mechanism do MAB4/MELs regulate PIN polarity? The fact that MEL1 localization was determined by PIN localization, and not vice-versa, suggested that MAB4/MELs were involved in PIN polarity maintenance, but not its establishment. To verify this, we introduced our recently developed *KNOLLE::PIN2-GFP* reporter (Glanc et al., 2018) into the *mel1234* mutant and followed its localization pattern in newly divided cells over time. In the *KNOLLE::PIN2-GFP x mel1234* line, apical polarity of KNOLLE::PIN2-GFP

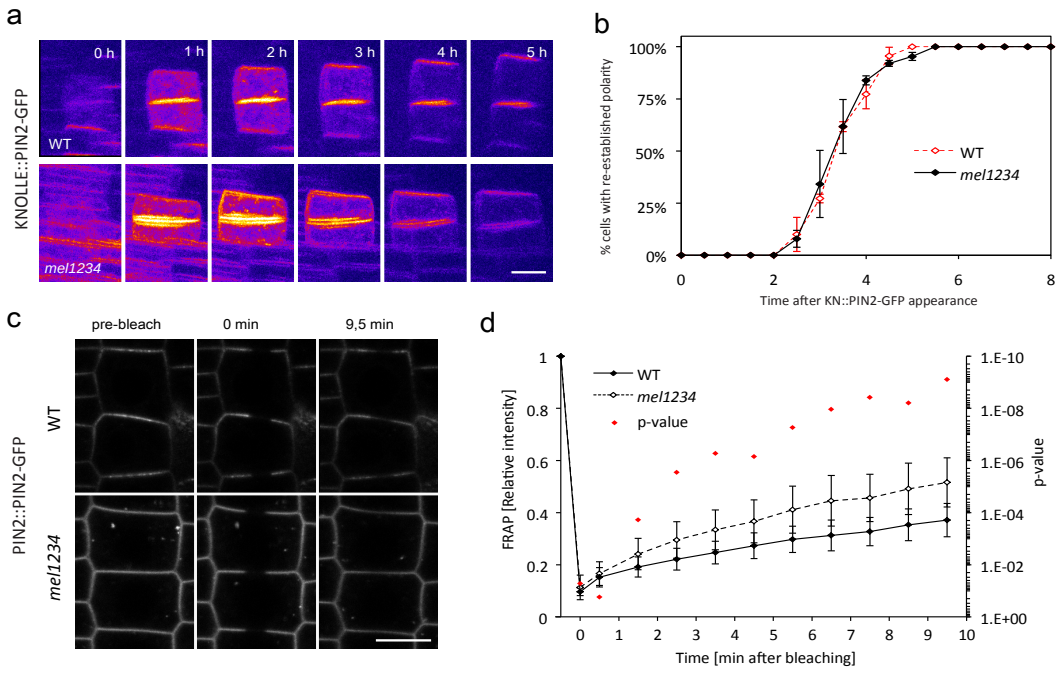


Figure 4: MAB4/MEL proteins maintain PIN polarity by reducing PIN lateral diffusion
a: Post-cytokinetic polarity re-establishment of PIN2-GFP expressed from the *KNOLLE* promoter was not obviously defective in the *mel1234* quadruple mutant compared to *Col-0*. Maximum intensity projections of a Z-stack are shown. **b**: quantitative analysis of **a.** Mean +/- SD of three independent experiments is shown, the total number of cells/roots analyzed was 70/7 (*WT*), resp. 87/8 (*mel1234*). **c-d**: FRAP dynamics of PIN2::PIN2-GFP in *Col-0* and *mel1234* background revealed significantly faster lateral diffusion of PIN2-GFP in the quadruple mutant. The graph shows mean normalized signal recovery +/- SD after background subtraction and correction to photobleaching caused by iterative imaging. n = 35 (*WT*), resp. 34 (*mel1234*) cells from three different roots, P-values were calculated using two-tailed two-sample T−test with unequal variance. The experiment was repeated independently 3 times with comparable results. Scale bars = 10 µm.

molecules synthesized in a narrow time window around a cytokinetic event developed normally (Fig. 4a-b), confirming that the reduced PIN polarity of the *mel1234* mutant was caused by defects in its maintenance rather than establishment. PIN polarity maintenance has previously been linked to limited PIN mobility within the PM (Feraru et al., 2011; Kleine-Vehn et al., 2011; Martinière et al., 2012; Łangowski et al., 2016). We therefore hypothesized that MAB4/MEL proteins might contribute to PIN polarity maintenance by reducing their lateral diffusion rates and thus reducing their escape from the respective polar domain. Test this hypothesis, we analyzed PIN2-GFP mobility by a Fluorescence Recovery After Photobleaching (FRAP) experiment in *WT* and *mel1234* background. In contradiction with previously reported results (Furutani et al., 2011), we observed significantly higher PIN2-GFP FRAP rate in the *mel1234* mutant (Fig. 4c-d), suggesting that MAB4/MEL proteins contribute to PIN polarity maintenance by limiting their lateral diffusion. Two manipulations that caused MEL1 dissociation from the PM, phosphodead PIN mutations in the PIN2 loop and the PAO treatment, concomitantly also led to an increase in PIN2 mobility (Fig. S4). This supports the hypothesis that PIN phosphorylation is a pre-requisite for their binding with MAB4/MELs. Together, these data indicate that the contribution of MAB4/MELs to PIN2 polarity lies in mediating its maintenance through reducing PIN2 lateral diffusion, likely in a PIN2 phosphorylation-dependent manner.

Discussion

In the present study, we found that in root epidermal cells, MEL1 is recruited to the PM through a physical interaction with PIN2, and that this interaction is important for low PIN2 lateral diffusion and hence its polarity maintenance. The fact that the presence of MEL1 in the PIN2 expression domain was sufficient to rescue gravitropic growth of the *mel1234* roots demonstrates that the lack of MEL-mediated PIN2 polarity maintenance is directly responsible for the agravitropic phenotype of the mutant. Although we focused on the model of MEL1 and PIN2 in the epidermis, we consider it likely that a similar mode of action applies also to other MAB4/MEL and PIN proteins in different cell types and developmental contexts, given the substantial functional redundancy within both respective protein families (Cheng et al., 2008; Furutani et al., 2011; Li et al., 2011; Vieten et al., 2005).

Whether PIN polarity depends on MAB4/MEL polarity or vice versa has previously been referred to as a “chicken or egg” question (Furutani et al., 2011). In light of the findings

presented here (Fig. 1, 4), it appears that PIN polarity is established first in a MAB4/MEL-independent manner and MAB4/MEL proteins are subsequently recruited to PIN-containing polar PM domains to maintain PIN polarity through reducing their lateral diffusion.

The result of our FRAP analysis of PIN2-GFP lateral diffusion rate directly contradicts previously published findings (Furutani et al., 2011). Unlike us, Furutani et al. performed the experiments in presence of translation and energy inhibitors; this should however not affect the result, since it was shown that this treatment does not affect PIN2-GFP FRAP dynamics in the given time scale (Men et al., 2008; Łangowski et al., 2016). In our opinion, the most likely explanation of the discrepancy is that in the experiment presented by Furutani et al., the difference between WT and mutant was masked by noise due to a small sample size (n=10 cells).

Despite an unequivocal proof is missing, several independent lines of evidence suggest that MAB4/MELs only interact with PINs phosphorylated by PID or related AGCVIII kinases, which would elegantly explain the previously identified genetic interaction between MAB4/MELs and PID. Nevertheless, this explanation doesn't fit with the situation in dividing cells, where the PID homologue WAG1 is strongly upregulated and localized at the cell plate together with PIN2, while MEL1 first appears at the mature apical PM >30 min after cytokinesis (Glanc et al., 2018). Existence of a hypothetic PID/WAG co-factor required for the efficient phosphorylation of PINs (Barbosa et al., 2018; Weller et al., 2017), present at the mature PM but absent from the cell plate, would explain this discrepancy.

In a very attractive hypothesis, such a co-factor could be the MAB4/MEL protein itself. In that case, MAB4/MELs recruited to phosphorylated PINs would promote their polarity maintenance and further phosphorylation by PID/WAGs. Hence, all three components would constitute a feed-forward regulatory loop with the potential to quickly reinforce and maintain small initial differences in PIN density and thus to substantially contribute to PIN polarity.

If both these assumptions, (preferential phosphorylation of apical PINs by PID/WAG and existence of a feed forward loop between PIN phosphorylation and their MAB4/MEL-mediated polarity maintenance) were correct, this model would among others explain the previously observed, yet not fully understood apicalization of basally localized PINs after PID overexpression or prolonged BFA treatment (Friml et al., 2004; Kleine-Vehn et al., 2008), since in both cases, apical PINs would be phosphorylated more efficiently than

basal ones (due to a simple change of PID:D6PK stoichiometry towards PID in the first and D6PK dissociation from the PM in the second).
In conclusion, we have shown that while PIN polarity is established in a MAB4/MEL-independent manner, PINs recruit MAB4/MELs to the PM, and MAB4/MELs in turn contribute to PIN polarity maintenance by limiting their lateral diffusion. These findings explain how polar localization of membrane cargoes can be maintained in the absence of physical diffusion barriers such as the tight junctions. Detailed analysis of the inter-dependence between the PIN-MEL interaction and PID-mediated PIN phosphorylation, as well as studies of the molecular mechanism by which the MAB4/MEL-mediated reduction of PIN lateral diffusion is achieved, will likely advance our understanding of plant cell polarity even further.

Materials and Methods

Plant material and growth conditions

Seeds were surface-sterilized by chlorine vapor, sown on ½ Murashige-Skoog medium supplemented with 1% sucrose and 1% agar and grown *in vitro* under long day conditions. The transgenic and mutant lines *eir1-1*(Luschnig et al., 1998), *PIN2::PIN2-GFP* (Xu and Scheres, 2005), *PIN2::PIN2-GFP/eir1-4* (Abas et al., 2006), *PIN2::PIN1-GFP2*, *PIN2::PIN1-GFP-3* (Wisniewska et al., 2006), *PIN2::PIN2-Venus, PIN2::PIN2^{S3A}-Venus* (Dhonukshe et al., 2010), *KNOLLE::PIN2-GFP*, *MEL1::MEL1-GFP* (Glanc et al., 2018), *mel1234* and *PIN2::PIN2-GFP/mel1234* (Furutani et al., 2011) have been described previously. The lines *KNOLLE::PIN2-GFP/mel1234*, *MEL1::MEL1-GFP/mel1234*, *MEL1::MEL1-GFP/eir1-1, PIN2::MEL1-mCherry*, *PIN2::MEL1-mCherry/eir1-1, PIN2::MEL1-mCherry/mel1234* were obtained by transforming the constructs into the respective background by the floral dip method (Clough and Bent, 1998). MEL1::MEL1-GFP/eir1-1 and PIN2::MEL1-mCherry/eir1-1 were crossed with Col-0 and the respective PIN1/PIN2-XFP/pin2 lines described above and F1 seeds heterozygous for each of the two fluorescent reporters and homozygous for the *eir1-1* mutation (or *eir1-1 eir1-4* biallelic) were used. For the *in planta* FLIM-FRET experiments, homozygous *PIN2::PIN2-GFP* and segregating T2 *PIN2::MEL1-mCherry* lines were used, resulting in a 1:1 ratio of plants expressing only the donor and both the donor and acceptor fluorescent markers. Phenotype analysis was performed as described previously (Glanc et al., 2018).

Molecular cloning

Cloning of plant expression constructs was performed using the Gateway technology (Invitrogen). *PIN2::MEL1-mCherry* was obtained by recombination of the entry clones *pPIN2(pDonrP4-P1r)* (Salanenka et al., 2018), *MEL1(pDonr221)* (Glanc et al., 2018) and *mCherry(pDonrP2r-P3)* (Adamowski et al., 2018) into the destination vector *pH7m34GW,0*. *MEL1(pDonr221)* was recombined with *PK7FWG2* to yield *35S::MEL1-GFP*. To generate *35S::PIN2HL-mCherry*, the PIN2 central hydrophilic loop sequence (corresponding to amino acid residues 157 - 484) was cloned into *pDonr221* and subsequently recombined into *p2GWCh7,0* (Yu et al., 2015). Constructs for recombinant expression of GST-PIN2HL and MEL1-HIS were generated by inserting the *PIN2HL* and *MEL1* fragments into *pGEX-4T-1* and *pET-32a*, respectively, via the EcoRI – SalI sites. Empty *pGEX-4T-1* was used to express free GST. The sequence of all primers used can be found in Supplementary table 1.

Transient expression in protoplasts

Preparation and transient expression in protoplasts was carried out as described previously (Meskiene et al., 2003; Fülöp et al., 2005) with minor modifications. Briefly: 3-day-old *Arabidopsis* root suspension culture cells were pelleted, resuspended in GM buffer (Murashige-Skoog Basal Salt Mixture 4.4 g/l, 0.17M glucose, 0.17M mannitol, pH5.5) with 1% cellulase and 0.2% macerozyme and incubated for 4h in darkness with gentle shaking. Protoplasts were separated by sucrose gradient centrifugation, concentration-adjusted to 10^8 cells/ml, and incubated for 1h in darkness with 12-15 μg of plasmid DNA in the presence of PEG, followed by a wash and overnight incubation in GM buffer.

Imaging and image analysis

Confocal imaging was performed on 4-day-old, chambered coverslip (Lab-Tek)-mounted seedlings using Zeiss LSM700, LSM800 or LSM880 inverted microscopes. Immunofluorescence staining was performed as described previously (Sauer et al., 2006); following antibodies were used at the dilutions indicated: rabbit αPIN1, 1:1000; rabbit αPIN2, 1:1000; rabbit αPIN4, 1:250; mouse αGFP (Sigma), 1:1000; Alexa Fluor 488-conjugated goat αMouse IgG (Thermo Fisher), 1:600; Cy5-conjugated goat αRabbit IgG (Thermo Fisher), 1:600. BFA and PAO (both Sigma) treatments were applied by transferring the seedlings onto a small slice of agar medium containing the respective chemical as described previously (Glanc et al., 2018); the DMSO stock solution and final concentrations were 50mM/50μM (BFA) and 60mM/30 or 60 μM (PAO).

FRAP experiments and assessment of PIN2 polarity re-establishment from time-lapse imaging of *KNOLLE::PIN2-GFP*-expressing plants were performed as described previously (Glanc et al., 2018).

FLIM-FRET experiments were performed using a TriM Scope II inverted 2-photon microscope equipped with a FLIM X16 TCSPC detector for time correlated single photon counting (LaVision BioTec). Fluorescence lifetime image stacks (150 slices, with 0,082ns time interval) were acquired, and a threshold mask was created from the sum projection of each stack in FIJI (Schindelin et al., 2012) to segment the apical PM domains. All pixels within the masked area were then pooled and averaged at each time point of the FLIM stack. The intensity at t=0 was normalized and a simple exponential decay [I(t)=exp(-t/lambda)+offset] was fitted to the data. The MatLab code that generates a single lifetime value for each image based on the source FLIM stack and the threshold mask can be found at https://datarep.app.ist.ac.at/id/eprint/113.

Pulldown assays and western blotting

Recombinant protein expression was induced by 0,5 mM IPTG at 17° C for 24h in *E. coli* strain BL21. The cells were then transferred to TBS buffer (pH7,5) and sonicated. The MEL1-His lysate was incubated together with the GST-PIN2HL or free GST lysate, respectively, for 12 h at 4° C and 150 rpm before Pierce Glutathione Agarose (Thermo Fisher) was added to the reactions, followed by another 1,5 h incubation (4° C, 150 rpm). Finally, the agarose beads were collected and washed, and proteins were eluted with TBS buffer with reduced glutathione (pH 7,5). Samples were then run on SDS-PAGE and blotted, blots were probed with αGST and αHis HRP-conjugated antibodies (both Agrisera).

Membrane and soluble protein fractions were prepared from roots of *mel1234* and *MEL1::MEL1-GFP/mel1234* as described previously (Abas and Luschnig, 2010). Membrane protein fractions were also prepared from suspension cultures derived from *Col-0* and *35S::PIN1* and *35S::PIN2* lines. The membrane fractions were resuspended in 50 mM TRIS-HCl pH 7, 10% v/v glycerol, 5 mM EDTA pH 8, 0.05% casein and protease inhibitors. Western blots using mouse monoclonal αGFP antibodies (Roche clones 7.1 /13.1 and Clontech JL8) showed that MEL-1GFP was present in both membrane and soluble fractions but was approximately 2-3 times more abundant in the soluble fraction. The soluble fraction from *mel1234* and *MEL1::MEL1-GFP/mel1234* (corresponding to 9 mg original root material) was mixed with the membrane fraction from *Col, 35S::PIN1 or 35S::PIN2* (corresponding to 2 mg Col, 0.8 mg 35SPIN1/35SPIN2 cell pellet) in a total

volume of 60 µl. Samples were incubated at room temperature for 30 min. Samples were then diluted with 1.5 volumes of water and spun at 21000 g/4°C/30 min. The supernatant was removed and the pellet washed with 100 µl of TE buffer. Both supernatant and pellet fractions were precipitated with chloroform/methanol, run on SDS-PAGE and blotted. Blots were probed with αGFP (as above), rabbit αPIN1 and rabbit αPIN2 (Abas and Luschnig, 2010).

References

Abas, L., and Luschnig, C. (2010). Maximum yields of microsomal-type membranes from small amounts of plant material without requiring ultracentrifugation. Anal. Biochem. *401*, 217–227.

Abas, L., Benjamins, R., Malenica, N., Paciorek, T., Wiśniewska, J., Wirniewska, J., Moulinier-Anzola, J.C., Sieberer, T., Friml, J.J., Luschnig, C., et al. (2006). Intracellular trafficking and proteolysis of the Arabidopsis auxin-efflux facilitator PIN2 are involved in root gravitropism. Nat. Cell Biol. *8*, 249–256.

Adamowski, M., and Friml, J. (2015). PIN-Dependent Auxin Transport: Action, Regulation, and Evolution. Plant Cell Online *27*, 20–32.

Adamowski, M., Narasimhan, M., Kania, U., Glanc, M., De Jaeger, G., and Friml, J. (2018). A Functional Study of AUXILIN-LIKE1 and 2, Two Putative Clathrin Uncoating Factors in Arabidopsis. Plant Cell *30*, 700–716.

Barbosa, I.C.R., Hammes, U.Z., and Schwechheimer, C. (2018). Activation and Polarity Control of PIN-FORMED Auxin Transporters by Phosphorylation. Trends Plant Sci. *23*, 523-538.

Cheng, Y., Qin, G., Dai, X., and Zhao, Y. (2008). NPY genes and AGC kinases define two key steps in auxin-mediated organogenesis in Arabidopsis. Proc. Natl. Acad. Sci. U. S. A. *105*, 21017–21022.

Clough, S.J., and Bent, A.F. (1998). Floral dip: a simplified method forAgrobacterium-mediated transformation ofArabidopsis thaliana. Plant J. *16*, 735–743.

Dhonukshe, P., Huang, F., Galvan-Ampudia, C.S., Mähönen, A.P., Kleine-Vehn, J., Xu, J., Quint, A., Prasad, K., Friml, J., Scheres, B., et al. (2010). Plasma membrane-bound AGC3 kinases phosphorylate PIN auxin carriers at TPRXS(N/S) motifs to direct apical PIN recycling. Development *137*, 3245–3255.

Feraru, E., Feraru, M.I., Kleine-Vehn, J., Martinière, A., Mouille, G., Vanneste, S., Vernhettes, S., Runions, J., and Friml, J. (2011). PIN Polarity Maintenance by the Cell Wall in Arabidopsis. Curr. Biol. *21*, 338–343.

Friml, J., Yang, X., Michniewicz, M., Weijers, D., Quint, A., Tietz, O., Benjamins, R., Ouwerkerk, P.B.F., Ljung, K., Sandberg, G., et al. (2004). A PINOID-dependent binary switch in apical-basal PIN polar targeting directs auxin efflux. Science *306*, 862–865.

Fülöp, K., Pettkó-Szandtner, A., Magyar, Z., Miskolczi, P., Kondorosi, É., Dudits, D., and Bakó, L. (2005). The Medicago CDKC;1-CYCLINT;1 kinase complex phosphorylates the carboxy-terminal domain of RNA polymerase II and promotes transcription. Plant J. *42*, 810–820.

Furutani, M., Kajiwara, T., Kato, T., Treml, B.S., Stockum, C., Torres-Ruiz, R.A., and Tasaka, M. (2007). The gene MACCHI-BOU 4/ENHANCER OF PINOID encodes a NPH3-like protein and reveals similarities between organogenesis and phototropism at the molecular level. Development *134*, 3849–3859.

Furutani, M., Sakamoto, N., Yoshida, S., Kajiwara, T., Robert, H.S., Friml, J., and Tasaka, M. (2011). Polar-localized NPH3-like proteins regulate polarity and endocytosis of PIN-FORMED auxin efflux carriers. Development *138*, 2069–2078.

Furutani, M., Nakano, Y., and Tasaka, M. (2014). MAB4-induced auxin sink generates local auxin gradients in Arabidopsis organ formation. Proc. Natl. Acad. Sci. U. S. A. *111*, 1198–1203.

Glanc, M., Fendrych, M., and Friml, J. (2018). Mechanistic framework for cell-intrinsic re-establishment of PIN2 polarity after cell division. Nat. Plants *in press*.

Kania, U., Fendrych, M., and Friml, J. (2014). Polar delivery in plants; commonalities and differences to animal epithelial cells. Open Biol. *4*, 140017.

Kleine-Vehn, J., Langowski, L., Wisniewska, J., Dhonukshe, P., Brewer, P.B., and Friml, J. (2008). Cellular and molecular requirements for polar PIN targeting and transcytosis in plants. Mol. Plant *1*, 1056–1066.

Kleine-Vehn, J., Wabnik, K., Martinière, A., Łangowski, Ł., Willig, K., Naramoto, S., Leitner, J., Tanaka, H., Jakobs, S., Robert, S., et al. (2011). Recycling, clustering, and endocytosis jointly maintain PIN auxin carrier polarity at the plasma membrane. Mol. Syst. Biol. *7*, 540.

Łangowski, Ł., Wabnik, K., Li, H., Vanneste, S., Naramoto, S., Tanaka, H., and Friml, J. (2016). Cellular mechanisms for cargo delivery and polarity maintenance at different polar domains in plant cells. Cell Discov. *2*, 16018.

Li, Y., Dai, X., Cheng, Y., and Zhao, Y. (2011). NPY genes play an essential role in root gravitropic responses in Arabidopsis. Mol. Plant *4*, 171–179.

Luschnig, C., Gaxiola, R. a, Grisafi, P., and Fink, G.R. (1998). EIR1, a root-specific protein involved in auxin transport, is required for gravitropism in Arabidopsis thaliana. Genes Dev. *12*, 2175–2187.

Martinière, A., Lavagi, I., Nageswaran, G., Rolfe, D.J., Maneta-Peyret, L., Luu, D.-T., Botchway, S.W., Webb, S.E.D., Mongrand, S., Maurel, C., et al. (2012). Cell wall constrains lateral diffusion of plant plasma-membrane proteins. Proc. Natl. Acad. Sci. U. S. A. *109*, 12805–12810.

Men, S., Boutté, Y., Ikeda, Y., Li, X., Palme, K., Stierhof, Y.-D., Hartmann, M.-A., Moritz, T., and Grebe, M. (2008). Sterol-dependent endocytosis mediates post-cytokinetic acquisition of PIN2 auxin efflux carrier polarity. Nat. Cell Biol. *10*, 237–244.

Meskiene, I., Baudouin, E., Schweighofer, A., Liwosz, A., Jonak, C., Rodriguez, P.L., Jelinek, H., and Hirt, H. (2003). Stress-induced protein phosphatase 2C is a negative regulator of a mitogen-activated protein kinase. J. Biol. Chem. *278*, 18945–18952.

Michniewicz, M., Zago, M.K., Abas, L., Weijers, D., Schweighofer, A., Meskiene, I., Heisler, M.G., Ohno, C., Zhang, J., Huang, F., et al. (2007). Antagonistic regulation of PIN phosphorylation by PP2A and PINOID directs auxin flux. Cell *130*, 1044–1056.

Salanenka, Y., Verstraeten, I., Löfke, C., Tabata, K., Naramoto, S., Glanc, M., and Friml, J. (2018). Gibberellin DELLA signaling targets the retromer complex to redirect protein trafficking to the plasma membrane. Proc. Natl. Acad. Sci. *115*, 3716–3721.

Sauer, M., Paciorek, T., Benková, E., and Friml, J. (2006). Immunocytochemical techniques for whole-mount in situ protein localization in plants. Nat. Protoc. *1*, 98–103.

Schindelin, J., Arganda-Carreras, I., Frise, E., Kaynig, V., Longair, M., Pietzsch, T., Preibisch, S., Rueden, C., Saalfeld, S., Schmid, B., et al. (2012). Fiji: an open-source platform for biological-image analysis. Nat. Methods *9*, 676–682.

Simon, M.L.A., Platre, M.P., Marquès-Bueno, M.M., Armengot, L., Stanislas, T., Bayle, V., Caillaud, M.-C., and Jaillais, Y. (2016). A PtdIns(4)P-driven electrostatic field controls cell membrane identity and signalling in plants. Nat. Plants *2*, 16089.

Vieten, A., Vanneste, S., Wisniewska, J., Benková, E., Benjamins, R., Beeckman, T., Luschnig, C., and Friml, J. (2005). Functional redundancy of PIN proteins is accompanied by auxin-dependent cross-regulation of PIN expression. Development *132*, 4521–4531.

Weller, B., Zourelidou, M., Frank, L., Barbosa, I.C.R., Fastner, A., Richter, S., Jürgens, G., Hammes, U.Z., and Schwechheimer, C. (2017). Dynamic PIN-FORMED auxin efflux carrier phosphorylation at the plasma membrane controls auxin efflux-dependent growth. Proc. Natl. Acad. Sci. U. S. A. *114*, E887–E896.

Wells, C.D., Fawcett, J.P., Traweger, A., Yamanaka, Y., Goudreault, M., Elder, K., Kulkarni, S., Gish, G., Virag, C., Lim, C., et al. (2006). A Rich1/Amot complex regulates the Cdc42 GTPase and apical-polarity proteins in epithelial cells. Cell *125*, 535–548.

Wisniewska, J., Xu, J., Seifertová, D., Brewer, P.B., Ruzicka, K., Blilou, I., Rouquié, D., Benková, E., Scheres, B., and Friml, J. (2006). Polar PIN localization directs auxin flow in plants. Science *312*, 883.

Xu, J., and Scheres, B. (2005). Dissection of Arabidopsis ADP-RIBOSYLATION FACTOR 1 function in epidermal cell polarity. Plant Cell *17*, 525–536.

Yu, H., Zhang, Y., Moss, B.L., Bargmann, B.O.R., Wang, R., Prigge, M., Nemhauser, J.L., and Estelle, M. (2015). Untethering the TIR1 auxin receptor from the SCF complex increases its stability and inhibits auxin response. Nat. Plants *1*, 14030.

Arabidopsis MAB4/MEL proteins mediate PIN polarity maintenance by reducing PIN lateral diffusion

Matouš Glanc[1,2], David Domjan[1], Lindy Abas[3], Lukas Hörmayer[1], Ludmila Včelařová[1], Robert Hauschild[1], Shutang Tan[1], Lesia Rodriguez-Solovey[1], Matyáš Fendrych[1,2] and Jiří Friml[1,#]

[1]Institute of Science and Technology Austria (IST Austria), 3400 Klosterneuburg, Austria
[2]Department of Experimental Plant Biology, Faculty of Science, Charles University, 12844 Prague, Czechia
[3]Department of Applied Genetics and Cell Biology, University of Natural Resources and Life Sciences – BOKU, 1190 Vienna, Austria
[#]Correspondence to: jiri.friml@ist.ac.at

Supplementary information

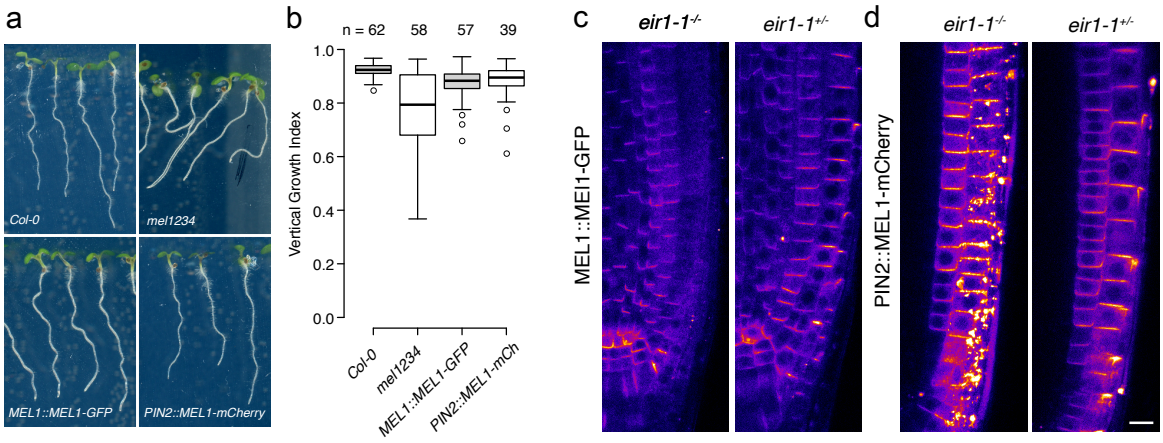


Figure S1, Related to figure 1

a: Phenotype of 5-day-old seedlings of the genotypes *Col-0, mel1234, MEL1::MEL1-GFP/mel1234* and *PIN2::MEL1-mCherry/mel1234*. **b**: Root Vertical Growth Index of the seedlings shown in **a**. n indicates the number of roots; the experiment was repeated independently 3 times with comparable results. The box-plot represents median, 1st and 3rd quartile; the whiskers extend to data points <1,5 interquartile range away from the 1st/ 3rd quartile; outliers are shown as circles. **c**: Expression pattern and subcellular localization of *MEL1::MEL1-GFP* in the *eir1-1 (pin2)* background and after a backcross into *Col-0*. The images are representative of 8, resp. 9 roots from 3 independent experiments. **d**: Expression pattern and subcellular localization of *PIN2::MEL1-mCherry* in the *eir1-1 (pin2)* background and after a backcross into *Col-0*. The images are representative of 9, resp. 6 roots from 2 independent experiments. Scale bar = 10 μm.

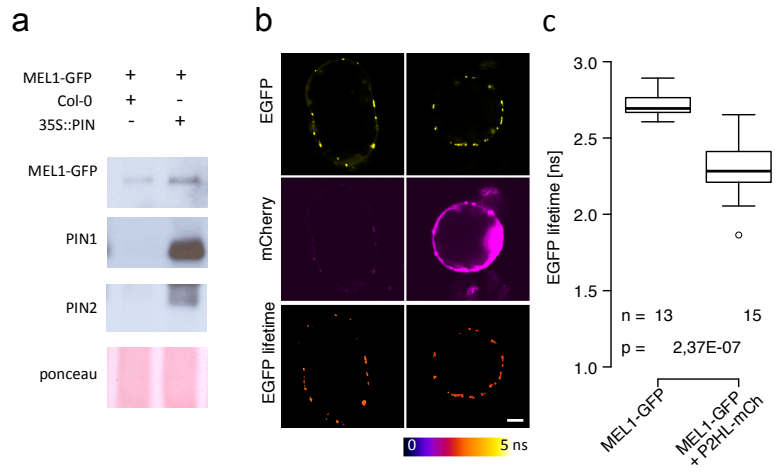


Figure S2, Related to figure 2

a: Western blot of the membrane fraction after incubation of the soluble fraction of a *MEL1::MEL1-GFP* plant extract with the microsomal fraction isolated from *Col-0* or *35S::PIN1 + 35S::PIN2* suspension cultured cells. The *35S::PIN1+2* membranes pull down ca. 2x more MEL1::MEL1-GFP than the Col-0 membranes, suggesting that MEL1 physically interacts with PIN1 and/or PIN2. **b**: FLIM-FRET imaging of suspension culture protoplasts transiently expressing *35S::MEL1-GFP* with and without *35S::PIN2HL-mCherry*. MEL1-GFP fluorescence lifetime is reduced in the presence of PIN2HL-mCherry, indicating the occurrence of FRET and hence physical interaction between the two proteins. Scale bar = 10 μm. **c:** Quantitative analysis of **b**. n indicates the total number of protoplasts from 2 independent experiments; P-value was calculated using two-tailed two-sample T-test with unequal variance. The box-plot represents median, 1st and 3rd quartile; the whiskers extend to data points <1,5 interquartile range away from the 1st/3rd quartile, outliers are shown as circles.

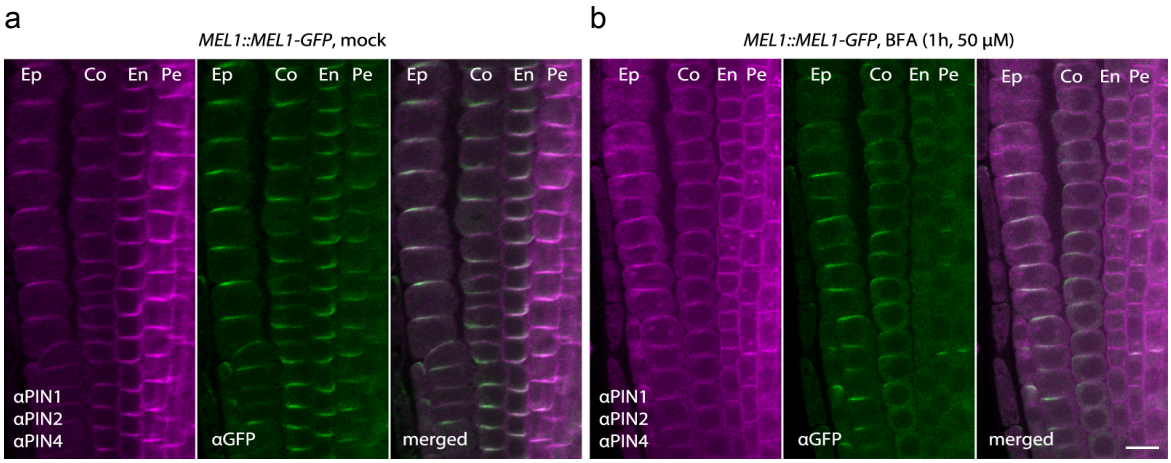


Figure S3, Related to figure 3

a: Immunofluorescence staining of PIN1, PIN2 and PIN4 (magenta) and MEL1-GFP (green) in a DMSO-treated *MEL1::MEL1-GFP* root. MEL1-GFP colocalizes with the PINs at the apical PM in the epidermis (Ep) and the basal PM in the cortex (Co), endodermis (En) and pericycle (Pe) cells. **b**: The same staining of a BFA-treated root. In addition to the PM, PIN signals can be observed in BFA bodies. MEL1-GFP signal mostly disappeared from the PM in endodermis and pericycle cells, while it is not affected in the epidermis. Notably, in cortex cells, MEL1-GFP is localized to the apical, instead of basal PM. The images are representative of 13, resp. 14 roots analyzed. Scale bar = 10 µm.

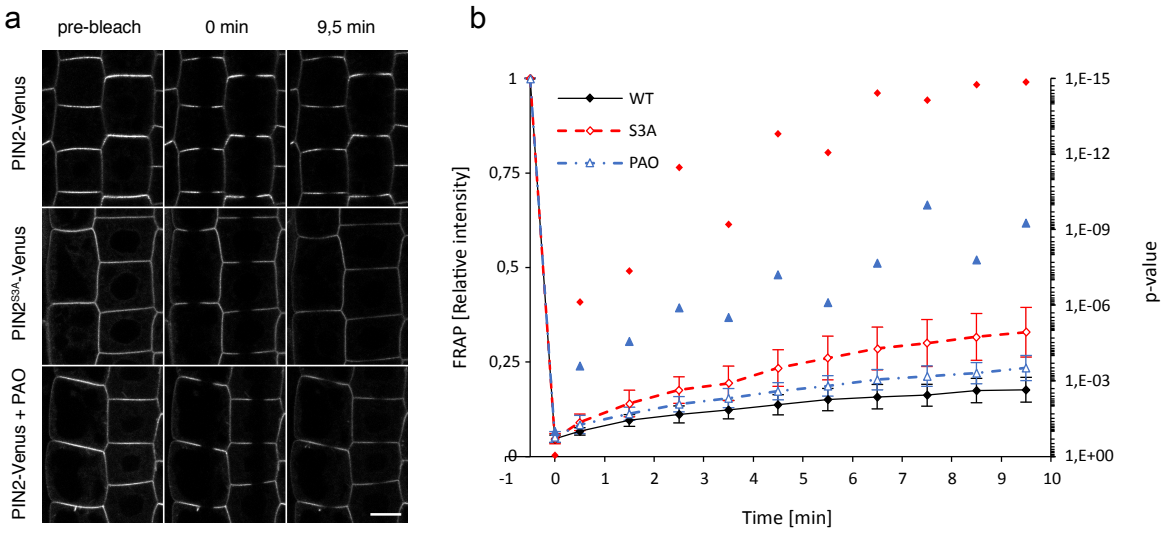


Figure S4, Related to figure 4

a-b: FRAP dynamics of PIN2::PIN2-Venus, PIN2::PIN2^{S3A}-Venus and PAO-treated (60μM, 1h) PIN2::PIN2-Venus. The graph shows mean normalized signal recovery +/- SD after background subtraction and correction to photobleaching caused by iterative imaging. n = 39 (control), resp. 33 (S3A mutant, PAO treatment) cells from three different roots, P-values (shown as full markers of the corresponding color on the secondary logarithmic axis) were calculated using two-tailed two-sample T-test with unequal variance. The experiment was repeated independently twice with comparable results. Scale bar = 10 μm.

Table S1: Primers used in this study

mel1-1_LP	GGAAGAACAAAACCACAAAGG
mel1-1_RP	ATGTAACCGCAAAAGCATCAG
mel2-1_LP	TCGGATTTACAAAGCAAGTGG
mel2-1_RP	CTCTTGCAGGATCCATAGCAG
mel3-1_LP	TGCAGGTTCCCAAACTTCTAC
mel3-1_RP	TTGATGCTTGCAAAACTGATG
mel4-1_LP	TCCAACTACGGAAGATGGTTG
mel4-1_RP	GCAGGAAAGATGCAACTTTTG
eir1-4_F	CAACGCGAAGAATGCTATGA
eir1-1_F	GGCAATTGCTTGATGTTGTTGATCATTTTATGGGACA
eir1-1/4_R	AAGCACCAAAGACTATAACTA
GABI-8409	ATATTGACCATCATACTCATTGC
LBb1.3	ATTTTGCCGATTTCGGAAC
PIN2HL_start_B1	GGGGACAAGTTTGTACAAAAAAGCAGGCTTCATGGCTAAGCTTCTCATCTCCGA
PIN2HL_nostop_B2	GGGGACCACTTTGTACAAGAAAGCTGGGTAACTCGCCGGCGGCATCTGCT
MEL1_EcoF	CCGAATTCATGAAGTTCATGAAACTTGGATCC
MEL1_SalR	GGGTCGACATGCTTCTTGCTTGTGGAA
P2HL_Eco-F	TGGAATTCGCTAAGCTTCTCATCTCCGAGC
P2HL_Sal-R	CCGGTCGACACTCGCCGGCGGCATCTGCTG

5. Discussion

5.1. PIN polarity establishment – secretion or recycling?

It has been known for a long time that endocytosis plays an important role in regulating PIN polarity; nevertheless, its detailed mechanistic role is still elusive (see chapter 2.3.1). We have confirmed the causality of the relationship between endocytosis and PIN polarity by showing that conditionally inhibiting CME by inducible overexpression of AUXILIN-like1 or 2 leads to PIN polarity defects (see chapter 4.1 - Adamowski et al., 2018). By combining AUXILIN-like2 overexpression, as well as a similar genetic tool based on a dominant-negative version of DRP1a (Yoshinari et al., 2016), with time-lapse imaging of PIN2-GFP expressed from the mitosis-specific *KNOLLE* promoter, we have shown that CME is required already for the establishment of PIN2 polarity after cell division (see chapter 4.2 – Glanc et al., 2018). Nevertheless, our findings also demonstrate that PIN2 molecules that end up at the "wrong" end of the cell due to reorganization of vesicular trafficking during cytokinesis (Richter et al., 2014) are upon endocytosis gradually turned over, rather than being recycled to the apical domain by transcytosis (see chapter 4.2 – Glanc et al., 2018). This finding speaks against the previously proposed mechanism of polarity establishment, in which PIN molecules are initially secreted in an apolar manner, and their polar localization is achieved only through polarized endocytic recycling (Dhonukshe et al., 2008; Richter et al., 2014).

Alternatively, PIN polarity establishment could be mediated directly by polarized secretion of newly synthesized protein (Łangowski et al., 2016). Directional vesicular trafficking of various cargoes including PINs relies largely on actin and/or MT cytoskeleton (Geldner et al., 2001), therefore one would expect that if PIN polarity establishment relied on targeted secretion, it would be greatly impaired upon interference with cytoskeletal dynamics. In support of this scenario, it was previously reported that application of either actin- or MT-depolymerizing drugs led to defects in PIN trafficking (Geldner et al., 2001; Kleine-Vehn et al., 2008b). However, more in-depth analysis employing different model systems, longer treatments and genetic evidence suggested that PIN polarity in the context of individual cells is cytoskeleton-independent (Boutté et al., 2006). Our data supports the latter notion, since we could show that pharmacologically induced depolymerization of actin, MTs, or even both at the same time delays, but does not prevent generation of PIN2 polarity in newly divided or interphase cells (See chapter 4.3).

Therefore, while cytoskeleton regulates intracellular PIN dynamics and targeted exocytosis probably contributes to PIN polar localization, our findings imply that the main PIN polarity-generating mechanism is independent of directional vesicle trafficking, but strictly requires functional CME.

One conceivable way such a mechanism might work is by reducing the rate of PIN endocytosis in its respective polar domain (Luschnig and Vert, 2014). Even if there was initially no domain preference of secretory and recycling PIN exocytosis, reduced PIN endocytosis in one of the domains would result in higher PIN density in that domain. Even a small asymmetry generated this way might subsequently be reinforced by a feed-forward mechanism involving reduced lateral diffusion (see chapter 4.4) or polarized exocytosis (Kleine-Vehn et al., 2011; Łangowski et al., 2016) to generate a stable, highly polarized PIN distribution pattern.

Moreover, strict requirement of functional endocytosis, but not of intact cytoskeleton, seem to apply to the establishment of lateral polarity as well: CME inhibition compromised the establishment of inner-lateral polarity of BOR1 (Yoshinari et al., 2016); and depolymerization of MTs had no effect on outer-lateral polarity of PEN3, while pharmacological or genetic interference with actin dynamics resulted in defects in PEN3 trafficking, but not polarity *per se* (Mao et al., 2016). Therefore, identifying molecular players involved in the regulation of endocytosis of multiple polar membrane proteins will likely advance our understanding of cell and protein polarity establishment in general, and should therefore be of utmost priority in further studies.

5.2. MEL proteins, lateral diffusion and PIN polarity maintenance

MAB4/MEL proteins were previously shown to be important for PIN polarity, colocalize with the PINs in their respective polar domain, and they were proposed to play a role in modulating PIN endocytosis (Furutani et al., 2011), making them prime candidates for the hypothetical factor that would limit PIN endocytosis in the respective polar domain and thus contribute to PIN polarity establishment. This assumption was further supported by our observation that MEL1-GFP did not localize to the CP and its appearance at the mature apical PM preceded re-establishment of PIN2 polarity in the newly divided cell pair (see chapter 4.2 - Glanc et al., 2018), which suggested that MAB4/MEL polarity might be a pre-requisite of PIN polarity.

Nevertheless, several lines of evidence speak against this hypothesis: 1) PIN2 polarity is re-established normally in the *mel1234* quadruple mutant (see chapter 4.4); 2)

preliminary PIN2::PIN2-Dendra photoconversion experiments didn't reveal any difference in the rate of PIN2 endocytosis between the *mel1234* mutant and wild type; and 3) PIN polarity is a pre-requisite of MEL polarity rather than vice versa (See chapter 4.4).

On the other hand, our results indicate that MAB4/MEL proteins play a role in regulating PIN2 lateral diffusion and therefore its polarity maintenance. This is in direct contradiction with previously published findings that PIN2 lateral diffusion is unaffected in the *mel1234* mutant background (Furutani et al., 2011). As discussed in chapter 4.4, we are convinced the discrepancy can most likely be explained by a difference in sample size and that our result better reflects the biological reality.

All together, these findings indicate that MAB4/MEL proteins are most likely not the hypothetical factor that limits endocytosis of PINs in their respective polar domain and hence contributes to PIN polarity establishment. Instead, we propose that MAB4/MELs are recruited to the PM by PINs, whose polarity had already been established, and participate in their polarity maintenance by limiting their lateral diffusion-based escape into the neighboring domains. Together with PIN phosphorylation mediated by PID and related AGCVIII kinases, MAB4/MELs might also be part of a feed-forward mechanism to propagate and stabilize initial asymmetry in PIN distribution generated by the endocytosis-based mechanism of PIN polarity establishment.

5.3. Phosphorylation-dependent regulation of PIN polarity

It has been firmly established by independent approaches and research groups that PID activity and PIN phosphorylation are involved in the regulation of PIN polarity (Friml et al., 2004; Michniewicz et al., 2007; Kleine-Vehn et al., 2009; Dhonukshe et al., 2010; Weller et al., 2017; chapter 4.2. - Glanc et al., 2018). For a long time, all available data fit into a straight-forward model in which phosphorylated PIN molecules were targeted preferentially to the apical, and dephosphorylated ones to the basal PM domain. However, several recent findings call for an extension of this model: D6PK phosphorylates PINs at the same residues as PID, but it's overexpression, unlike the overexpression of PID, does not lead to basal-to-apical shifts in PIN polarity (Zourelidou et al., 2014); basally and apically localized PIN1 did not show any difference in phosphorylation (Weller et al., 2017); and introducing phosphodead mutations to the PID-phosphorylated residues did not phenocopy the *pid wag1 wag2* triple mutant in the assay

to monitor PIN2 polarity re-establishment after cell division (Chapter 4.2 - Glanc et al., 2018).

One possible explanation of these discrepancies is that PID and WAG kinases, but not D6PK, phosphorylate other targets involved in PIN polarity regulation in addition to the PINs themselves, and phosphorylation of both the PIN and the putative polarity regulator is required for PIN apical polarity. In this scenario, PIN phosphorylation would be required, but not sufficient for its apical targeting. In fact, the hypothesis that PID might phosphorylate an unknown PIN polarity regulator was postulated before (Michniewicz et al., 2007), but since PINs have been established as *bona fide* PID phosphorylation targets in the very same paper, it has never been properly tested.

Another interpretation of the data is that PID and WAG kinases phosphorylate preferentially apically localized PINs, for which they possibly require an unknown additional regulator (Barbosa et al., 2018), and that PIN phosphorylation is involved in a feed-forward mechanism that propagates initial small asymmetries in the amount of (phosphorylated) PINs into pronounced polar distribution patterns, as proposed in chapter 4.4. In this case, it wouldn't be the change in PID activity and PIN phosphorylation, but rather the ratio between the activities of PID and D6PK that would cause the PIN polarity changes: a shift of this ratio towards PID activity, as in PID overexpression, would lead to the observed (Friml et al., 2004) apicalization of basally localized PINs. Concomitantly, a shift towards D6PK activity, such as in the *pid wag1 wag2* mutant or phospho-dead mutations in the S1-S3 sites that are preferred by PINOID, would lead to increased basal targeting of otherwise apical PINs, again as observed (Dhonukshe et al., 2010). This model would also explain one more described, but not fully understood aspect of PIN polarity changes. It was reported that prolonged BFA treatments led to basal-to-apical shifts in PIN polarity; this observation was explained by a difference in BFA sensitivity of the basal (sensitive) and apical (resistant) PIN targeting pathways (Kleine-Vehn et al., 2008a). However, if phosphorylation reinforced and stabilized PIN localization to either of the two polar domains, also this phenomenon could be explained by the shift of the AGCVIII kinase activity ratio towards PID, since BFA treatment leads to dissociation of D6PK, but not PID, from the PM (Barbosa et al., 2014, Weller et al., 2017).

5.4. Theoretical concept of cell-intrinsic re-establishment of cell polarity after cytokinesis

We demonstrated that post-cytokinetic re-establishment of apical PIN2 polarity in root epidermal cells requires neither cell-to-cell signaling between the divided cells and their immediate neighbors, nor intact root meristem tissue context (See chapter 4.2 - Glanc et al., 2018). Despite it can't be formally ruled out that polarity re-establishment in the epidermis depends on communication with adjacent cortex cells, we don't consider this likely, since it is not clear how transversal signaling could direct longitudinal polarity. Since PIN polarity is downstream of cell polarity (see Chapter 2.2), this implies that after cell division, the cue that instructs the re-establishment of cell polarity itself must be cell intrinsic.

In yeast, and to a large extent also in animals, cell polarity is controlled by the small GTPase Cdc42 (Wells et al., 2006; Chiou et al., 2017), which acts as a "Master Polarity Regulator (MPR)". Therefore, existence of an unknown asymmetrically localized protein with a similar role in apical/basal polarity regulation can be expected also in plants. However, this assumption is purely speculative, as the polarity cue could instead be conveyed by a membrane lipid, a cell wall component, or virtually any other biological molecule; or by an asymmetry in post-translational (in case of a protein) or other modification of an otherwise symmetrically distributed molecule. Alternatively, plants might possess no master polarity regulator at all, and plant cell polarity might depend on a principally different mechanism.

Nevertheless, assuming that a plant MPR exists, it must be inherited from the mother to the daughter cells during cytokinesis regardless of its nature (See chapter 4.2 - Glanc et al., 2018). Here, I propose a simple, mechanistically plausible model that would explain this hypothetical phenomenon.

The model presumes that apical-basal polarity of a cell is defined by the presence of the MPR in either its apical or basal pole, and its absence in the other one. For clarity, only the scenario with the MPR present in the apical and absent in the basal pole will be considered (despite it works identically in the opposite case). Therefore, when a cell divides anticlinally, the upper daughter inherits the apical, MPR-containing pole of the mother, and the lower daughter inherits the basal pole and therefore it lacks any MPR-conveyed polarity information. However, immediately after CP insertion, the apical PM domain of the lower cell still has (at least partial) CP identity, unlike all other PM domains inherited from the mother. Hence, if upon cytokinesis the new, CP-derived PM

domain of the lower daughter cell is marked with the MPR, both daughter cells will end up with correct MPR-conveyed apical-basal polarity. To achieve this, the cells would need to follow only a very simple, mechanistically plausible algorithm: *If MPR is present, do nothing. If it is absent, insert it into the new, CP-derived PM* (Fig. 1a). The algorithm is robust towards cell division plane orientation: if a cell divides periclinally or radially, the apical PM domain is partitioned between the two daughters and therefore MPR-conveyed polarity information is kept in both of them without the need of polarity re-establishment in either one (Fig. 1b). Apart from the existence of the MPR, differential composition and identity of the PM and the CP is pivotal to this model. Unlike the existence of MPR, this requirement is not purely assumptive, since it has been demonstrated experimentally that the two kinds of membrane differ in their phosphoinostide composition (Simon et al., 2016a).

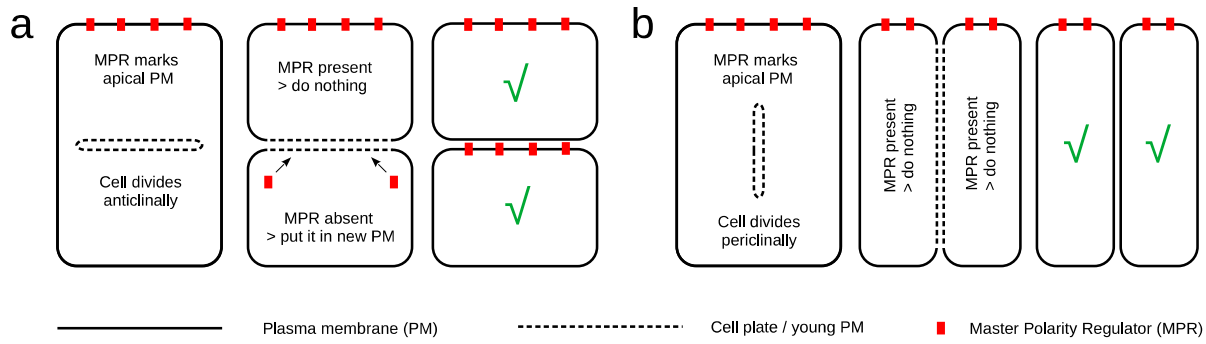


Figure 1: Theoretical concept of cell-intrinsic re-establishment of cell polarity after cytokinesis
a: Presuming that the apical PM domain of each cell is marked by a hypothetical Master Polarity Regulator (MPR), cell polarity re-establishment after anticlinal cell division could be achieved by the cells following a simple algortithm: *if MPR is present, keep it where it is and do nothing; if it is absent, put it in the new, CP-derived PM domain*. **b:** Following the same algorithm, daughter cells would inherit correct polarity information also if the mother divided periclinally; the algorithm is hence robust towards division plane orientation. The model would work identically if MPR marked the basal rather than apical PM domain.

Unfortunately, it will be very challenging to experimentally test this hypothesis, since removing a single cell from the root meristem, flipping it vertically, returning to its original place, waiting for it to divide and observing the re-establishment of polarity of a marker such as PIN2 is technically, and probably also biologically, impossible.

6. Conclusions and outlook

Cell polarity plays a crucial role in plant biology, nevertheless its regulation remains poorly understood. In this thesis, I aimed to uncover new mechanisms of establishment and maintenance of the polar localization of the PIN auxin efflux carriers by setting out 3 specific objectives: **i)** to validate whether a newly developed genetic tool can be used to study the importance of endocytosis for PIN polarity; **ii)** to dissect which cellular processes are required for the re-establishment of PIN2 polarity after cell division; and **iii)** to identify the mechanism by which MAB4/MEL proteins contribute to PIN polarity (see chapter 3 for details).

I have successfully completed these objectives by showing that **i)** Inducible overexpression of AUXILIN-like1 and 2 leads to efficient conditional inhibition of PIN2 endocytosis (see chapter 4.1 - Adamowski et al., 2018); **ii)** PIN2 polarity re-establishment after cell division requires endocytosis, *de novo* secretion and the action of PID/WAG kinases, but not transcytosis, cell-to-cell signaling or intact cytoskeleton (see chapters 4.2 Glanc et al., 2018 and 4.3); and **iii)** MAB4/MEL proteins contribute to PIN polarity maintenance by limiting their lateral diffusion rates (See chapter 4.4).

The new findings presented in my work move our knowledge of PIN polarity regulation a few steps forward. In addition, and perhaps more importantly, I believe I have in places come close to the core cell polarity regulating machinery, and my work provides hints that might be valuable in designing future experiments to ultimately understand the regulation of cell polarity establishment and maintenance in plants.

I have confirmed that CME plays a key role in PIN polarity establishment (see chapters 4.1 – Adamowski et al., 2018, 4.2 – Glanc et al., 2018), but my results also suggest that this process cannot be explained by targeted recycling of endocytic PIN cargoes (see chapter 4.2 – Glanc et al., 2018 and 4.3). Therefore, detailed inquiries into the regulation of PIN endocytosis should be of utmost priority, since understanding PIN endocytosis might be the key to understanding PIN polarity. The same holds true also for non-PIN markers of other polar domains, since CME appears to be required for protein

polarity in general (Yoshinari et al., 2016; Nakamura and Grebe, 2018). This places endocytosis into the center of cell polarity regulation as such, making it even more important to understand.

My findings reinforce the notion that apart from endocytosis, the action of PID/WAG kinases plays a central role in PIN polarity establishment, nevertheless they also support the need to refine and extend the current model of phosphorylation-dependent regulation of PIN polarity (See chapter 4.2 – Glanc et al., 2018). I provide several such hypothetical extensions. Testing these with studies of PID/WAG *in situ* activity regulation, as well as un unbiased screen for potential novel PID/WAG phosphorylation targets, might help consolidate some discrepancies currently surrounding phosphorylation-mediated regulation of PIN polarity.

One of these models proposes the existence of a feed-forward loop between PIN phosphorylation and its interaction with MAB4/MEL proteins (See chapter 4.4). My findings support the contribution of MAB4/MELs to PIN polarity by regulating PIN lateral diffusion rather than endocytosis as proposed previously (Furutani et al., 2011). Nevertheless, understanding the MAB4/MELs in more detail, such as in identifying their structure, novel interaction partners, or cellular requirements for proper functionality might also contribute to substantial advances in the PIN and cell polarity regulation field.

Finally, my data suggests that the primary cue that defines and coordinates cell polarities within the root meristem over iterative rounds of cell division is inherited, rather than being conveyed by positional information, and I propose a theoretical model how this might be achieved. While testing this hypothesis will require truly ingenious experimental design, it might, if successful, shed light on the very core of the still mostly elusive regulation of cell polarity in plants.

THE END.

7. List of abbreviations

ABP1	Auxin Binding Protein 1
BFA	Brefeldin A
Cesa3	Cellulose synthase catalytic subunit 3
CME	Clathrin-Mediated Endocytosis
CP	Cell Plate
Cpi1	Cyclopropylsterol isomerase 1
D6PK	D6 protein kinase
Drp1a	Dynamin-related protein 1A
ER	Endoplasmic Reticulum
FRAP	Fluorescence Recovery After Photobleaching
GFP	Green Fluorescent Protein
GPI	Glycosylphosphatidylinositol
MAB4/MEL	Macchi Bou 4/MAB4/ENP1-Like
MPR	Master polarity regulator
MT	Microtubule
NPH3	Non-phototropic hypocotyl 3
PID	Pinoid
PIN	PIN-formed auxin efflux carrier
PM	Plasma Membrane
PP2A	Protein phosphatase 2A
WT	Wild type

8. References

Adamowski, M. et al. (2015). PIN-Dependent Auxin Transport: Action, Regulation, and Evolution. Plant Cell Online **27**: 20–32.

Adamowski, M. et al. (2018). A Functional Study of AUXILIN-LIKE1 and 2, Two Putative Clathrin Uncoating Factors in Arabidopsis. Plant Cell **30**: 700–716.

Barbosa, I.C.R. et al. (2018). Activation and Polarity Control of PIN-FORMED Auxin Transporters by Phosphorylation. Trends Plant Sci. **23**: 523-538.

Barbosa, I.C.R. et al. (2014). D6 PROTEIN KINASE Activates Auxin Transport-Dependent Growth and PIN-FORMED Phosphorylation at the Plasma Membrane. Dev. Cell **29**: 674–685.

Bennett, T. et al. (2014). Paralogous radiations of PIN proteins with multiple origins of noncanonical PIN structure. Mol. Biol. Evol. **31**: 2042–60.

Boutté, Y. et al. (2006). The plasma membrane recycling pathway and cell polarity in plants: studies on PIN proteins. J. Cell Sci. **119**: 1255–1265.

Cheng, Y. et al. (2008). NPY genes and AGC kinases define two key steps in auxin-mediated organogenesis in Arabidopsis. Proc. Natl. Acad. Sci. U. S. A. **105**: 21017–22.

Chiou, J. et al. (2017). Cell Polarity in Yeast. Annu. Rev. Cell Dev. Biol. **33**: 77–101.

Cove, D.J. (2000). The generation and modification of cell polarity. J. Exp. Bot. **51**: 831–838.

Dai, X. et al. (2015). Embryonic lethality of Arabidopsis abp1-1 is caused by deletion of the adjacent BSM gene. Nat. Plants **1**: 15183.

Dhonukshe, P. et al. (2008). Generation of cell polarity in plants links endocytosis, auxin distribution and cell fate decisions. Nature **456**: 962–966.

Dhonukshe, P. et al. (2014). Retraction: Generation of cell polarity in plants links endocytosis, auxin distribution and cell fate decisions. Nature **511**: 370–370.

Dhonukshe, P. et al. (2007). Clathrin-Mediated Constitutive Endocytosis of PIN Auxin Efflux Carriers in Arabidopsis. Curr. Biol. **17**: 520–527.

Dhonukshe, P. et al. (2006). Endocytosis of Cell Surface Material Mediates Cell Plate Formation during Plant Cytokinesis. Dev. Cell **10**: 137–150.

Dhonukshe, P. et al. (2010). Plasma membrane-bound AGC3 kinases phosphorylate PIN auxin carriers at TPRXS(N/S) motifs to direct apical PIN recycling. Development **137**: 3245–55.

Ding, Z. et al. (2012). ER-localized auxin transporter PIN8 regulates auxin homeostasis and male gametophyte development in Arabidopsis. Nat. Commun. **3**: 941.

Enders, T. A. et al. (2015). Genome Sequencing of Arabidopsis abp1-5 Reveals Second-Site Mutations That May Affect Phenotypes. Plant Cell **27**: 1820-1826

Feraru, E. et al. (2011). PIN Polarity Maintenance by the Cell Wall in Arabidopsis. Curr. Biol. **21**: 338–343.

Friml, J. et al. (2004). A PINOID-dependent binary switch in apical-basal PIN polar targeting directs auxin efflux. Science **306**: 862–865.

Friml, J. et al. (2002a). AtPIN4 Mediates Sink-Driven Auxin Gradients and Root Patterning in Arabidopsis. Cell **108**: 661–673.

Friml, J. and Palme, K. (2002). Polar auxin transport – old questions and new concepts ? Plant Mol. Biol. **49**: 273–284.

Friml, J. et al. (2002b). Lateral relocation of auxin efflux regulator PIN3 mediates tropism in Arabidopsis. Nature **415**: 806–809.

Furutani, M. et al. (2007). The gene MACCHI-BOU 4/ENHANCER OF PINOID encodes a NPH3-like protein and reveals similarities between organogenesis and

phototropism at the molecular level. Development **134**: 3849–59.
Furutani, M., . et al. (2014). MAB4-induced auxin sink generates local auxin gradients in Arabidopsis organ formation. Proc. Natl. Acad. Sci. U. S. A. **111**: 1198–203.
Furutani, M. et al. (2011). Polar-localized NPH3-like proteins regulate polarity and endocytosis of PIN-FORMED auxin efflux carriers. Development **138**: 2069–78.
Gälweiler, L. et al. (1998). Regulation of Polar Auxin Transport by AtPIN1 in Arabidopsis Vascular Tissue. Science **282**: 2226–2230.
Ganguly, A. et al. (2014). Functional Analysis of the Hydrophilic Loop in Intracellular Trafficking of Arabidopsis PIN-FORMED Proteins. Plant Cell **26**: 1570–1585.
Gao, Y. et al. (2015). Auxin binding protein 1 (ABP1) is not required for either auxin signaling or *Arabidopsis* development. Proc. Natl. Acad. Sci. **112**: 2275–2280.
Geldner, N. et al. (2003). The Arabidopsis GNOM ARF-GEF mediates endosomal recycling, auxin transport, and auxin-dependent plant growth. Cell **112**: 219–30.
Geldner, N. et al. (2001). Auxin transport inhibitors block PIN1 cycling and vesicle trafficking. Nature **413**: 425–428.
Glanc, M. et al. (2018). Mechanistic framework for cell-intrinsic re-establishment of PIN2 polarity after cell division. Nat. Plants **in press**.
Grebe, M. et al. (2003). Arabidopsis sterol endocytosis involves actin-mediated trafficking via ARA6-positive early endosomes. Curr. Biol. **13**: 1378–87.
Grebe, M. et al. (2001). Cell axiality and polarity in plants — adding pieces to the puzzle. Curr. Opin. Plant Biol. **4**: 520–526.
Grones, P. et al. (2018). PID/WAG-mediated phosphorylation of the Arabidopsis PIN3 auxin transporter mediates polarity switches during gravitropism. Sci. Rep. **8**: 10279.
Jaillais, Y. and Gaude, T. (2008). Plant Cell Polarity: Sterols Enter into Action after Cytokinesis. Dev. Cell **14**: 318–320.
Kania, U. et al. (2014). Polar delivery in plants; commonalities and differences to animal epithelial cells. Open Biol. **4**: 140017.
Kitakura, S. et al. (2011). Clathrin mediates endocytosis and polar distribution of PIN auxin transporters in Arabidopsis. Plant Cell **23**: 1920–31.
Kleine-Vehn, J. et al. (2011). Recycling, clustering, and endocytosis jointly maintain PIN auxin carrier polarity at the plasma membrane. Mol. Syst. Biol. **7**: 540.
Kleine-Vehn, J. et al. (2008a). ARF GEF-dependent transcytosis and polar delivery of PIN auxin carriers in Arabidopsis. Curr. Biol. **18**: 526–531.
Kleine-Vehn, J. et al. (2010). Gravity-induced PIN transcytosis for polarization of auxin fluxes in gravity-sensing root cells. Proc. Natl. Acad. Sci. **107**: 22344–22349.
Kleine-Vehn, J. et al. (2009). PIN auxin efflux carrier polarity is regulated by PINOID kinase-mediated recruitment into GNOM-independent trafficking in Arabidopsis. Plant Cell **21**: 3839–49.
Kleine-Vehn, J. et al. (2008b). Cellular and molecular requirements for polar PIN targeting and transcytosis in plants. Mol. Plant **1**: 1056–66.
Korbei, B. and Luschnig, C. (2011). Cell polarity: PIN it down! Curr. Biol. **21**: R197-9.
Łangowski, L. et al. (2010). Trafficking to the outer polar domain defines the root-soil interface. Curr. Biol. **20**: 904–8.
Łangowski, Ł. et al. (2016). Cellular mechanisms for cargo delivery and polarity maintenance at different polar domains in plant cells. Cell Discov. **2**: 16018.
Li, Y. et al. (2011). NPY genes play an essential role in root gravitropic responses in Arabidopsis. Mol. Plant **4**: 171–9.
Luschnig, C. and Vert, G. (2014). The dynamics of plant plasma membrane proteins: PINs and beyond. Development **141**: 2924–2938.
Mao, H. et al. (2016). A Framework for Lateral Membrane Trafficking and Polar Tethering of the PEN3 ATP-Binding Cassette Transporter. Plant Physiol. **172**: 2245–

2260.
Martinière, A. et al. (2012). Cell wall constrains lateral diffusion of plant plasma-membrane proteins. Proc. Natl. Acad. Sci. U. S. A. **109**: 12805–10.
Men, S. et al. (2008). Sterol-dependent endocytosis mediates post-cytokinetic acquisition of PIN2 auxin efflux carrier polarity. Nat. Cell Biol. **10**: 237–244.
Michalko, J. et al. (2015). Embryo-lethal phenotypes in early abp1 mutants are due to disruption of the neighboring BSM gene. F1000Research **4**: 1104.
Michalko, J. et al. (2016). Strong morphological defects in conditional Arabidopsis abp1 knock-down mutants generated in absence of functional ABP1 protein. F1000Research **5**: 86.
Michniewicz, M. et al. (2007). Antagonistic regulation of PIN phosphorylation by PP2A and PINOID directs auxin flux. Cell **130**: 1044–1056.
Mravec, J. et al. (2011). Cell Plate Restricted Association of DRP1A and PIN Proteins Is Required for Cell Polarity Establishment in Arabidopsis. Curr. Biol. **21**: 1055–1060.
Mravec, J. et al. (2009). Subcellular homeostasis of phytohormone auxin is mediated by the ER-localized PIN5 transporter. Nature **459**: 1136–40.
Müller, A. et al. (1998). AtPIN2 defines a locus of Arabidopsis for root gravitropism control. EMBO J. **17**: 6903–11.
Nakamura, M. and Grebe, M. (2018). Outer, inner and planar polarity in the Arabidopsis root. Curr. Opin. Plant Biol. **41**: 46–53.
Petrášek, J. et al. (2006). PIN proteins perform a rate-limiting function in cellular auxin efflux. Science **312**: 914–8.
Prát, T. et al. (2018). WRKY23 is a component of the transcriptional network mediating auxin feedback on PIN polarity. PLOS Genet. **14**: e1007177.
Reichardt, I. et al. (2007). Plant Cytokinesis Requires De Novo Secretory Trafficking but Not Endocytosis. Curr. Biol. **17**: 2047–2053.
Richter, S. et al. (2014). Delivery of endocytosed proteins to the cell-division plane requires change of pathway from recycling to secretion. Elife **2014**: 1–16.
Rubery, P.H. and Sheldrake, A.R. (1974). Carrier-mediated auxin transport. Planta **118**: 101–121.
Simon, M.L.A. et al. (2016a). A PtdIns(4)P-driven electrostatic field controls cell membrane identity and signalling in plants. Nat. Plants **2**: 16089.
Simon, S. et al. (2016b). PIN6 auxin transporter at endoplasmic reticulum and plasma membrane mediates auxin homeostasis and organogenesis in Arabidopsis. New Phytol. **211**: 65–74.
Steinmann, T. et al. (1999). Coordinated polar localization of auxin efflux carrier PIN1 by GNOM ARF GEF. Science **286**: 316–318.
Takano, J. et al. (2010). Polar localization and degradation of Arabidopsis boron transporters through distinct trafficking pathways. Proc. Natl. Acad. Sci. U. S. A. **107**: 5220–5.
Weller, B. et al. (2017). Dynamic PIN-FORMED auxin efflux carrier phosphorylation at the plasma membrane controls auxin efflux-dependent growth. Proc. Natl. Acad. Sci. U. S. A. **114**: E887–E896.
Wells, C.D. et al. (2006). A Rich1/Amot complex regulates the Cdc42 GTPase and apical-polarity proteins in epithelial cells. Cell **125**: 535–48.
Wisniewska, J. et al. (2006). Polar PIN localization directs auxin flow in plants. Science **312**: 883.
Yoshinari, A. et al. (2016). DRP1-Dependent Endocytosis is Essential for Polar Localization and Boron-Induced Degradation of the Borate Transporter BOR1 in Arabidopsis thaliana. Plant Cell Physiol. **57**: 1985–2000.
Zhang, J. et al. (2010). PIN phosphorylation is sufficient to mediate PIN polarity and

direct auxin transport. Proc. Natl. Acad. Sci. U. S. A. **107**: 918–22.
Zhou, J.-J. and Luo, J. (2018). The PIN-FORMED Auxin Efflux Carriers in Plants. Int. J. Mol. Sci. **19**: 2759.
Zourelidou, M. et al. (2014). Auxin efflux by PIN-FORMED proteins is activated by two different protein kinases, D6 PROTEIN KINASE and PINOID. Elife **3**: 1–25.
Zourelidou, M. et al. (2009). The polarly localized D6 PROTEIN KINASE is required for efficient auxin transport in Arabidopsis thaliana. Development **136**: 627–636.

9. Appendix

Check for updates

RESEARCH ARTICLE

Strong morphological defects in conditional *Arabidopsis abp1* knock-down mutants generated in absence of functional ABP1 protein [version 1; referees: 1 approved, 2 approved with reservations]

Jaroslav Michalko[1,2*], Matouš Glanc[1,3*], Catherine Perrot-Rechenmann[4], Jiří Friml[1]

[1]Institute of Science and Technology Austria, Klosterneuberg, Austria
[2]Institute of Plant Genetics and Biotechnology, Slovak Academy of Sciences, Nitra, Slovakia
[3]Department of Experimental Plant Biology, Faculty of Sciences, Charles University, Prague, Czech Republic
[4]Institut Jean-Pierre Bourgin, INRA, AgroParisTech, CNRS, Université Paris-Saclay , Versailles, France

* Equal contributors

v1 **First published:** 20 Jan 2016, **5**:86 (doi: 10.12688/f1000research.7654.1)
Latest published: 20 Jan 2016, **5**:86 (doi: 10.12688/f1000research.7654.1)

Abstract

The Auxin Binding Protein 1 (ABP1) is one of the most studied proteins in plants. Since decades ago, it has been the prime receptor candidate for the plant hormone auxin with a plethora of described functions in auxin signaling and development. The developmental importance of ABP1 has recently been questioned by identification of *Arabidopsis thaliana abp1* knock-out alleles that show no obvious phenotypes under normal growth conditions. In this study, we examined the contradiction between the normal growth and development of the *abp1* knock-outs and the strong morphological defects observed in three different ethanol-inducible *abp1* knock-down mutants (*abp1-AS, SS12K, SS12S*). By analyzing segregating populations of *abp1* knock-out vs. *abp1* knock-down crosses we show that the strong morphological defects that were believed to be the result of conditional down-regulation of ABP1 can be reproduced also in the absence of the functional ABP1 protein. This data suggests that the phenotypes in *abp1* knock-down lines are due to the off-target effects and asks for further reflections on the biological function of ABP1 or alternative explanations for the missing phenotypic defects in the *abp1* loss-of-function alleles.

Open Peer Review

Referee Status: ? ✓ ?

	Invited Referees 1	2	3
version 1 published 20 Jan 2016	? report	✓ report	? report

1 **Lars Ostergaard**, John Innes Centre UK

2 **Richard M. Napier**, University of Warwick UK

3 **Christian Luschnig**, University of Natural Resources and Life Sciences Austria

Discuss this article

Comments (0)

Corresponding author: Jiří Friml (jiri.friml@ist.ac.at)

How to cite this article: Michalko J, Glanc M, Perrot-Rechenmann C and Friml J. **Strong morphological defects in conditional *Arabidopsis abp1* knock-down mutants generated in absence of functional ABP1 protein [version 1; referees: 1 approved, 2 approved with reservations]** *F1000Research* 2016, **5**:86 (doi: 10.12688/f1000research.7654.1)

Copyright: © 2016 Michalko J *et al*. This is an open access article distributed under the terms of the Creative Commons Attribution Licence, which permits unrestricted use, distribution, and reproduction in any medium, provided the original work is properly cited. Data associated with the article are available under the terms of the Creative Commons Zero "No rights reserved" data waiver (CC0 1.0 Public domain dedication).

Grant information: This work was supported by ERC Independent Research grant (ERC-2011-StG-20101109-PSDP to JF). JM internship was supported by the grant "Action Austria – Slovakia". MG was supported by the scholarship "Stipendien der Stipendienstiftung der Republik Österreich". Work by EH and CPR were supported by ANR blanc ANR-14-CE11-0018.

Competing interests: No competing interests were disclosed.

First published: 20 Jan 2016, **5**:86 (doi: 10.12688/f1000research.7654.1)

Introduction

The naturally occurring auxin, indole-3-acetic acid, plays a central role in plant growth and development alone or in orchestration with other plant hormones. Proper sensing and interpretation of fluctuating cellular auxin signals is necessary for mediating a diverse range of developmental and cell biology responses (Enders & Strader, 2015; Grunewald & Friml, 2010; Paciorek *et al.*, 2005; Petrasek *et al.*, 2006). In the early screens for auxin receptors, Auxin Binding Protein 1 (ABP1) has been identified based on its ability to bind auxin with high affinity (Hertel *et al.*, 1972; Löbler & Klämbt, 1985) and soon became a prime candidate for an extracellular auxin receptor based mainly on electrophysiological studies utilizing antibodies against ABP1 that showed rapid ABP1-mediated modulation of plasma membrane ion transport in an early step of auxin action (Barbier-Brygoo *et al.*, 1989; Leblanc *et al.*, 1999). Over the next decades, the auxin-binding activity of ABP1 has been characterized in detail by biochemical studies (Batt *et al.*, 1976; Napier *et al.*, 2002; Napier & Venis, 1995; Ray *et al.*, 1977) and its protein structure including the auxin-binding pocket has been revealed (Woo *et al.*, 2002). Phylogenetic studies have shown that ABP1 homologues are present in the genomes of all plant species from bryophytes to flowering plants (Tromas *et al.*, 2010) with more than one copy present e.g. in the genome of maize, rice, poplar or the moss *Physcomitrella patens* (http://phytozome.jgi.doe.gov/pz/portal.html).

Since its discovery, however, the biological importance of the ABP1 protein as a plasma membrane auxin receptor has been a matter of debates, in part because of its predominant subcellular localization in the endoplasmic reticulum (ER) in maize where the conditions for auxin binding are unfavorable (Habets & Offringa, 2015; Napier *et al.*, 2002). Recently, these discussions were revived by the isolation of two new *Arabidopsis abp1* knock-out alleles, *abp1-c1* and *abp1-TD1* (Gao *et al.*, 2015) that show no obvious phenotypes under standard growth conditions. The contradiction between this observation and the previously published embryo-lethal phenotypes of *abp1* mutants (Chen *et al.*, 2001; Tzafrir *et al.*, 2004) has recently been clarified by proving that the embryo-lethality of the originally reported alleles *abp1-1* and *abp1-1s* was caused by disruption of the tightly-linked neighboring gene *BELAYA SMERT (BSM)* rather than knock-out of *ABP1* (Dai *et al.*, 2015; Michalko *et al.*, 2015). This correction and the demonstration of normal embryo development in the *abp1* knock-outs (Michalko *et al.*, 2015) suggest that ABP1 plays no essential role in early *Arabidopsis* embryogenesis.

The ongoing discussion focuses on the relevance of *ABP1* in auxin signaling and other post-embryonic auxin-related biological processes that have been demonstrated using different genetic tools, namely the conditional knock-down (KD) lines, the *abp1-5* weak allele harboring a point mutation in the ABP1 auxin-binding pocket and gain-of-function alleles, all of which often provided internally consistent results (Braun *et al.*, 2008; Čovanová *et al.*, 2013; David *et al.*, 2007; Grones *et al.*, 2015; Robert *et al.*, 2010; Sassi *et al.*, 2014; Tromas *et al.*, 2013; Xu *et al.*, 2010; Xu *et al.*, 2014).

Conditional *ABP1* KD lines *SS12S6*, *SS12K9* and *abp1-AS* have been generated using two fundamentally different approaches of gene or protein down-regulation. In the *SS12S6* and *SS12K9* lines, ABP1 was inactivated by inducible over-expression of a recombinant immunoglobulin fragment termed single-chain fragment variable (scFv) (Conrad & Fiedler, 1998). This construct, consisting of the heavy- and light-chain variable domains of a well-characterized anti-ABP1 monoclonal antibody mAb12 (David & Perrot-Rechenmann, 2001; David *et al.*, 2007; Leblanc *et al.*, 1999) linked by a flexible peptide was additionally fused to the sequence encoding the 3'KDEL motif to mediate scFv ER-retention in the *SS12K9* line, while the *SS12S*-encoded scFv12 was meant to be secreted to the apoplast. *In planta*-produced scFv12 was able to pull down ABP1, and reciprocally immunoprecipitation of ABP1 using another antibody was shown to pull down scFv12 (Tromas *et al.*, 2009). An antisense approach was utilized in the *abp1-AS* line, where inducible over-expression of full-length *ABP1* antisense cDNA led to the formation of duplexes with its sense mRNA, thus preventing ABP1 translation, and potentially also transcription by RNA interference mechanism (Meister & Tuschl, 2004; Tufarelli *et al.*, 2003). Both antibody- and antisense-based lines use the ethanol-inducible system, which is well established and widely used for the conditional expression of plant genes (Deveaux *et al.*, 2003; Roslan *et al.*, 2001).

These three *abp1* knock-down lines have been instrumental to connect ABP1 function to multiple cellular and developmental processes. For example, they showed defects in shoot and root growth (Braun *et al.*, 2008; Tromas *et al.*, 2009), cell wall re-modeling (Paque *et al.*, 2014) or clathrin-mediated endocytosis of PIN auxin efflux carriers (Dhonukshe *et al.*, 2007; Robert *et al.*, 2010). In contrast, the *abp1* gain-of-function transformants promote PIN internalization both in tobacco and *Arabidopsis* (Grones *et al.*, 2015; Robert *et al.*, 2010). Contrasting effects of *ABP1* KD and gain-of-function lines were shown also in the case of auxin effect on the control of leaf epidermal pavement cells morphogenesis (Braun *et al.*, 2008; Nagawa *et al.*, 2012) on ROP GTPase activation (Xu *et al.*, 2010) and on microtubule rearrangement (Chen *et al.*, 2014; Xu *et al.*, 2014). Furthermore, analysis of ABP1 variants with mutations in the auxin-binding pocket demonstrated the importance of auxin-binding to ABP1 for its gain-of-function phenotypes (Grones *et al.*, 2015). Altogether, these studies provided an internally consistent picture showing involvement of ABP1 signaling in multiple physiological and cellular processes. These observations were further supported by the finding that loss-of-function mutants in *TMK* receptor-like protein kinases, that were recently shown to interact with ABP1 in an auxin-inducible manner, show similar phenotypes with *abp1* KD mutants (Xu *et al.*, 2014) which was consistent with the importance of the ABP1/TMK complex-mediated auxin perception in plant development. Recent identification of wild-type looking *Arabidopsis abp1* loss-of-function alleles by Gao *et al.* (2015) thus questions the interpretation of data obtained in the aforementioned studies.

Here, we address the missing phenotypes in the true *abp1* null alleles in relation to the strong and consistent morphological defects observed in the conditional *abp1* knock-down lines. We show that the morphological phenotypes in *SS12S6, SS12K9* and *abp1-AS* can be generated in the absence of functional ABP1 protein and we discuss possible underlying causes of this.

Material and methods

Plant material and growth conditions

Arabidopsis thaliana mutants used in this study were: *abp1-c1*, *abp1-TD1* (Gao *et al.*, 2015), *abp1-AS*, *SS12K9*, *SS12S6* (Braun *et al.*, 2008; David *et al.*, 2007). *A. thaliana* Col-0 wild type seeds were obtained from The Nottingham *Arabidopsis* Stock Centre (NASC, http://www.arabidopsis.info). For *in vitro* experiments, seeds were surface-sterilized with chlorine vapor, vernalized for 2 days in the dark at 4°C and grown on 1/2 MS 0.8% agar medium with or without 1% w/v sucrose (pH 5.9) on vertical Petri dishes under long day conditions (16 h light/8 h dark) or in complete darkness at 21°C. A sterilized microtube with 500 µl 5% ethanol was placed at the bottom of the plate to induce expression of *abp1-AS*, *SS12K9* and *SS12S6* constructs before germination. Plates with 5-day old etiolated or 7-day old light-grown seedlings were scanned on a flatbed scanner, phenotyped by visual examination and used for DNA/RNA extraction.

Genotyping mutants

Ethanol-inducible ABP1 down-regulating lines (*abp1-AS*, *SS12K9*, *SS12S6*) were genotyped for the presence of the *alcR* gene encoding the transcriptional regulator of the ethanol-inducible system using primers *alcR_for* and *alcR_rev* (Table 1). Fragments amplified from *abp1-c1* with primer pairs ABP1-U409F + ABP1-586R or ABP1-5P + ABP1-586R were digested with *BslI*, which cuts the WT fragment once and does not cut the mutant fragment; *abp1-TD1* was genotyped as described previously (Gao *et al.*, 2015). Genomic DNA was isolated using the CTAB extraction method. GoTaq G2 polymerase (Promega) and Bio-Rad T100 Thermal Cycler were used for PCR under following conditions: initial denaturation 5 min 98°C; 35–45 cycles (denaturation 30 s at 98°C; annealing 30 s at 55°C, elongation 1 min at 72°C); final elongation 5 min at 72°C. Restriction analysis was performed by adding the restriction enzyme directly to unpurified PCR reaction. Alternatively, Phire Plant Direct PCR Kit (Thermo Scientific by Finnzymes) and QIAquick Gel Extraction Kit (QIAGEN) were used following manufacturer's instructions to genotype the *SS12K9 x abp1-c1* line.

Quantitative RT-PCR

Total RNA from approximately twenty 8-day old seedlings frozen in liquid nitrogen was extracted using the TRIzol reagent (Invitrogen, Carlsbad, CA, USA) and purified using RNeasy Mini Kit (Qiagen) according to manufacturer's instructions. 2 µg of purified total RNA were used for a reverse transcription reaction using the iScript cDNA Synthesis Kit (BioRad). qRT-PCR was performed using the LightCycler 480 SYBR Green I Master chemistry (Roche) in a LightCycler480 II thermal cycler (Ser. no. 5659, Roche) according to manufacturer's instructions. cDNA diluted 1:10 in water was used as a template to prepare 5 µL reaction mixture (final volume). Primers used for the quantitative RT-PCR were designed using QuantPrime (http://www.quantprime.de). The *ABP1* cDNA fragment (84 bp in length) was amplified with ABP1-2E and ABP1-586R primers. *Arabidopsis Tubulin beta chain 2* (*TUB2*, At5g62690) amplified with TUB2-F and TUB2-R primers was used as a reference gene (Dataset 1). Gene expression was calculated with the $2^{-\Delta\Delta CT}$ method (Livak & Schmittgen, 2001). Results are expressed as the average +/- standard deviation of 2 biological and three technical replicates. Sequences of primers used for genotyping and qRT-PCR analysis are listed in Table 1.

Table 1. Primer sequences used in this study.

ABP1-U409F	CCTCATCACACAACAAAGTCACTC
ABP1-586R	GGAGCCAGCAACAGTCATGTG
ABP1-5P	ATGATCGTACTTTCTGTTGGTTCC
ABP1-2E	TTGCCAATCGTGAGGAATATTAG
pSKTAIL-L3	ATACGACGGATCGTAATTTGTCG
AlcR F	AGAACAAAGAAAGCCAGGA
AlcR R	GCGTGAGAGAAAAGATGA
TUB2 F	TAACAACTGGGCCAAGGGACAC
TUB2 R	ACAAACCTGGAACCCTTGGAGAC

Results

Dataset 1. Scans of ethanol-induced F2 seedlings of crosses (A) *SS12S6* × *abp1-c1*, (B) *SS12S6* × *abp1-TD1*, (C) *abp1-AS* × *abp1-c1*, (D) *abp1-AS* × *abp1-TD1*, (E) *SS12K9* × *abp1-c1* and (F) *SS12K9* × *abp1-TD1* that were used for phenotyping and genotyping (Figure 1 and Figure 2)

http://dx.doi.org/10.5256/f1000research.7654.d110722

Dataset 2. Agarose gel images from the PCR genotyping of the F2 crosses (A) *SS12S6* × *abp1-c1*, (B) *SS12S6* × *abp1-TD1*, (C) *abp1-AS* × *abp1-c1*, (D) *abp1-AS* × *abp1-TD1*, (E) *SS12K9* × *abp1-c1* and (F) *SS12K9* × *abp1-TD1* (Figure 3)

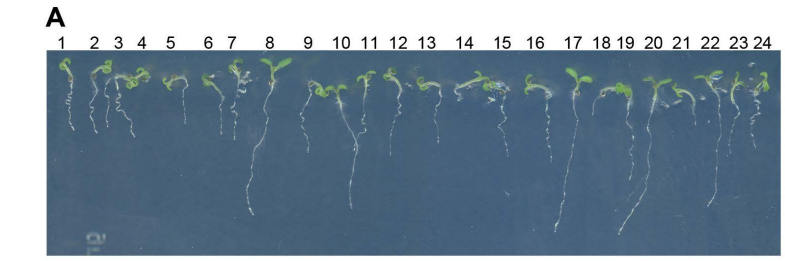
http://dx.doi.org/10.5256/f1000research.7654.d110723

All crosses were genotyped for the presence of the *alcR* transcriptional regulator (first row of the gel images) which is an integral part of the ethanol-inducible cassette in *abp1* knock-down lines. The presence of point mutation in *abp1-c1* crosses was genotyped by restriction analysis of *ABP1* PCR product as described in Gao *et al.* (2015) (second row of the gel images of *abp1-c1* crosses). The presence of the T-DNA insertion in *abp1-TD1* crosses was genotyped according to Gao *et al.* (2015) (second and third row of gel images of *abp1-TD1* crosses). GeneRuler DNA ladder mix #0331 (Thermo Scientific) was used as a fragment size standard to determine the approximate size of DNA fragments. Fragment sizes of 1000 bp and 500 bp are indicated.

Dataset 3. Source qPCR data (Figure 3c)

http://dx.doi.org/10.5256/f1000research.7654.d110724

Individual samples are annotated with their position on a 384-well plate (column A), the cDNA (column B) and primer pair (column C); the Cp value of each sample is shown in column D. The experiment was performed in two biological (1 or 2 at the last position in column B) and three technical replicates. Figure 3c shows gene expression calculated with the $2^{-\Delta\Delta CT}$ method (Livak & Schmittgen, 2001) from values of ABP1-2E and TUB as a reference gene; using ABP1-5P and/or EF as a reference gene instead gave similar results.

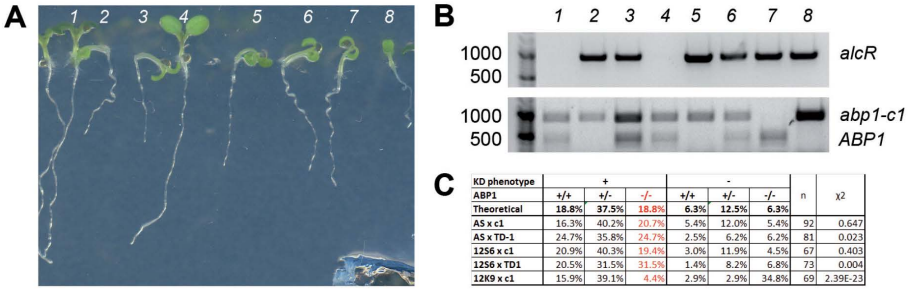


C

KD phenotype	+	-
AS x c1	71	21
	130	47
12S6 x c1	54	13
	155	38
12K9 x c1	41	28
	204	58

KD phenotype	++	+	-
AS x TD-1	49	72	32
	100		99
12S6 x TD1	45	87	37
	88		91
12K9 x TD1	22	43	13
	107		160

Figure 1. Strong morphological defects in conditional *abp1* knock-down lines correlate with the presence of the ethanol-inducible cassette and segregate normally when crossed with *abp1-c1* knock-out allele. (**A**) *abp1-AS* × *abp1-c1* F2 plants grown for 7 days in the presence of 5% ethanol segregate strong morphological defects characteristic of the *abp1* conditional knock-down (KD) alleles approximately in a 3:1 ratio. (**B**) *alcR*-specific PCR bands amplified from the genomic DNA of *abp1-AS* × *abp1-c1* F2 plants shown in (**A**) demonstrate that the KD phenotype is caused by the presence of the ethanol-inducible insertion. (**C**) Phenotypes of the scFv12-based KD lines segregate similarly in F2 crosses with *abp1-c1*, while altered segregation ratios can be observed in F2 of all three KD alleles crossed to *abp1-TD1*, which is most apparent in seedlings grown for 5 days in the dark (grey background).



C

KD phenotype	+			-			n	χ2
ABP1	+/+	+/-	-/-	+/+	+/-	-/-		
Theoretical	18.8%	37.5%	18.8%	6.3%	12.5%	6.3%		
AS x c1	16.3%	40.2%	20.7%	5.4%	12.0%	5.4%	92	0.647
AS x TD-1	24.7%	35.8%	24.7%	2.5%	6.2%	6.2%	81	0.023
12S6 x c1	20.9%	40.3%	19.4%	3.0%	11.9%	4.5%	67	0.403
12S6 x TD1	20.5%	31.5%	31.5%	1.4%	8.2%	6.8%	73	0.004
12K9 x c1	15.9%	39.1%	4.4%	2.9%	2.9%	34.8%	69	2.39E-23

Figure 2. Mendelian segregation of strong ethanol-inducible phenotypes in the F2 generation of *abp1* knock-out × knock-down crosses is independent of *abp1* mutant background. (**A**) Representative *abp1-AS* × *abp1-c1* F2 plants, (**B**) PCR products amplified from their genomic DNA and (**C**) segregation ratios from all crosses show that the ethanol-inducible phenotypes segregate independently of the presence of *abp1* knock-out alleles following approximately Mendelian rules for di-hybrid crosses. Homozygous *abp1* knock-out mutants with the inducible KD phenotype could be found in all crosses (plants 2,5,8 in (**A**) and (**B**), red numbers in (**C**)), suggesting that the phenotype does not require a functional *ABP1* gene. Strong deviations from the expected Mendelian segregation were detected in the *SS12K9* x *abp1-c1* cross, indicating genetic linkage between *ABP1* locus and the inserted ethanol-inducible scFv construct.

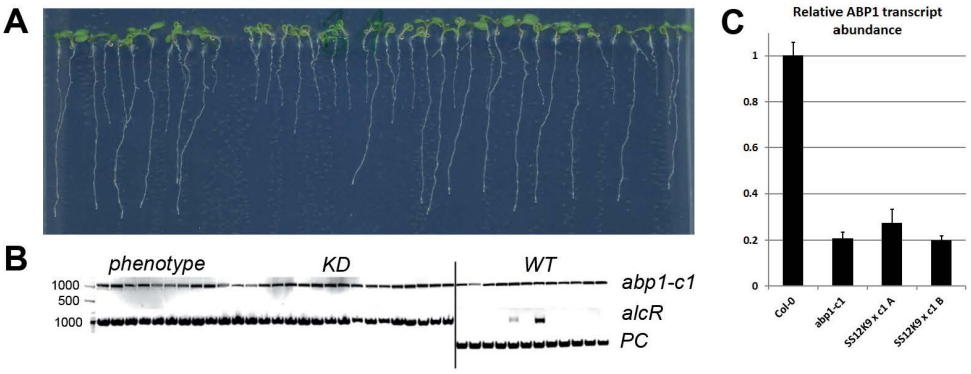


Figure 3. Strong inducible knock-down phenotypes in the absence of functional *ABP1* gene confirmed in the *SS12K9* × *abp1-c1* F3 progeny. (**A**) Representative seedlings of the ethanol-induced F3 progeny of one of the *SS12K9* × *abp1-c1* F2 plants (plant A) that showed KD phenotype in the absence of the functional *ABP1*. All F3 seedlings manifesting KD phenotype were homozygous for *abp1-c1* mutation. (**B**) Genotyping of the plants shown in **A**. The image is assemled from different regions of two gels that were copy-pasted next to each other in order to save space. (**C**) qRT-PCR analysis of KD-phenotype positive F3 seedlings of both lines revealed that *ABP1* transcript levels are reduced by about 80% like in the original *abp1-c1* mutant. Altogether these data confirm that in the *abp1* down-regulating lines the KD phenotype can be manifested without the ABP1 function. In (**C**) average of two biological and three technical replicates +/- SD is shown. PC- positive control.

Segregation of strong morphological defects in conditional *abp1* knock-down alleles crossed with *abp1-TD1* and *abp1-c1* knock-out alleles

To investigate the contradiction between missing phenotypic defects in the loss-of-function *abp1* alleles and strong morphological defects of conditional *ABP1* down-regulating lines (knock-down; KD), we decided to cross both types of lines to test three possible scenarios: 1) The absence of the strong morphological defects in the *abp1-c1* or *abp1-TD1* alleles is caused by an adaptation of the plants to the permanent loss of the ABP1 function, which compensates for this deletion; 2) the strong morphological phenotypes induced in the KD lines do not require functional ABP1 and are caused by off-target effects; or 3) both *abp1-TD-1* and *abp1-c1* lines contain background mutation(s) that suppress the phenotypes caused by the absence of ABP1.

We crossed each of the conditional lines with *abp1*-TD1 and *abp1*-c1 null mutants and with an ABP1-WTc1 line as a control and analyzed seedling phenotypes of ethanol induced F2 segregating plants (Figure 1a). We hypothesized that in case of an adaptive process, the conditional *abp1* KD phenotypes (short wavy roots and epinastic cotyledons) would not be manifested in homozygous *abp1* null background, resulting in a 9/16 KD and 7/16 WT phenotype segregation ratio. If the inducible phenotypes in the KD lines are independent of ABP1, these phenotypes will be manifested even in the absence of the functional *ABP1* gene, thus resulting in a classic Mendelian 3/4 KD and 1/4 WT phenotype segregation ratio. In case of the presence of background suppressive mutation(s), the KD phenotype segregation ratio would lie anywhere between 3/16 (dominant suppressor mutation closely linked to the *ABP1* locus) and 3/4 (recessive mutation with low penetrance and no linkage to *ABP1*) (Supplementary Figure 1).

Segregation of the morphological phenotypes in the F2 plants from different crosses is summarized in Figure 1b. These observations show that strong phenotypes in both the *abp1* antisense-based and the scFv12-based conditional knock-down lines segregate approximately 75% in the F2 crosses with *abp1-c1*. This observation favors the scenario that the strong morphological defects in the KD lines are not influenced by the presence or absence of the functional *ABP1* gene copy. The F2 phenotypic segregation is however shifted in favor of WT-looking plants in all three KD lines crossed to *abp1-TD1*. This segregation shift may be ascribed to partial transcriptional silencing of the ethanol-inducible constructs due to the presence of multiple 35S promoters/enhancers in the constructs themselves as well as the tandem T-DNA insertion in *abp1-TD1*.

We genotyped all analyzed F2 plants for the presence of the *alcR* transcriptional regulator, which is an integral part of the ethanol-inducible system and verified that the observed morphological defects were indeed correlating with the presence of the *ABP1* KD constructs (Figure 1c). About 5% of seedlings from all lines showed WT phenotype despite being positive for the presence of *alcR* or vice versa. As this phenomenon was independent of *ABP1* genetic background and could not be reproduced in F3 progeny (Supplementary Figure 2), we put it down to biological variability and/or occasional silencing of the ethanol-inducible constructs.

Strong morphological defects in conditional *abp1* knock-down alleles can be manifested in homozygous *abp1* knock-out alleles

To investigate whether the *abp1* KD phenotypes can be observed in the absence of a functional copy of the At4g02980 *ABP1* gene we further genotyped the respective *abp1* mutations in F2 seedlings of all crosses (Figure 2). As summarized in Figure 2c, in all crosses

we were able to identify multiple homozygous *abp1* mutants that showed the strong KD phenotype following ethanol induction. This analysis demonstrates that strong morphological phenotypes in *abp1* antisense-based (*abp1-AS*) and scFv12 antibody-based (*SS12S6, SS12K9*) conditional KD lines can be generated also in a null *abp1* background.

In case of the crosses *SS12K9* × *abp1-c1* and *SS12K9* × *abp1-TD1* we observed a lower level of allelic segregation between the *abp1* mutations and the KD construct in their F2 progeny (Figure 2c). Out of 28 genotyped plants with WT phenotype, 24 (85.7%) were homozygous for *abp1* mutation and did not contain the ethanol-inducible KD cassette. These results point towards genetic linkage between these two loci, most likely caused by the positional effect of the KD cassette located close to the *ABP1* locus on the chromosome 4. Nevertheless, some level of genetic recombination was happening between the two loci in the crosses as demonstrated by the identification of three F2 *SS12K9* × *abp1-c1* plants showing KD phenotype that were homozygous for *abp1-c1* mutation (Figure 2c). This analysis confirms that also *SS12K9* conditional KD construct can generate strong morphological phenotypes in the homozygous *abp1* knock-out alleles despite the insertion position being linked to the *ABP1* locus. Altogether these data are consistent with results obtained by the other crosses and further support that morphological phenotypes in the *abp1* knock-down lines can be generated in the absence of the functional ABP1.

Analysis of F3 generation confirms *SS12K9*-induced strong morphological defects in absence of ABP1 function

Next we tested the occurrence of the strong KD-induced morphological phenotypes in the absence of the functional ABP1 in the next generation by analyzing the F3 progeny of two *SS12K9* × *abp1-c1* plants showing strong KD phenotype. We confirmed that the F3 progeny was homozygous for the *abp1-c1* mutation and segregated the ethanol-inducible construct approximately in a 3:1 ratio (Figure 3b). After induction with ethanol, the analyzed F3 population of the *SS12K9* × *abp1-c1* plant A segregated into 27 plants (67.5%) with KD phenotype and 13 WT looking plants (32.5%) (Figure 3). The F3 population of plant B segregated into 18 plants with KD phenotype (81.2%) and 4 WT looking plants (18.2%) (data not shown). Genotyping of all F3 plants with ethanol-inducible phenotypes revealed that they contain KD construct in the homozygous *abp1-c1* background (Figure 3b). Notably, among the 17 analyzed WT looking F3 seedlings we also identified two plants that contain the ethanol-inducible construct in homozygous *abp1-c1* background (Figure 3b) suggesting that in these plants the functionality of the construct was affected, most probably by its silencing. Nonetheless, the majority of the plants containing the ethanol-inducible construct generated the strong morphological phenotypes even in the $abp1^{-/-}$ homozygous background.

We also analyzed the *ABP1* expression in WT, *abp1-c1* and SS12K9 × *abp1-c1* F3 seedlings by quantitative RT-PCR just to verify that introducing KD alleles does not influence, in any way, the *ABP1* expression (Figure 3c). We observed *ca.* 80% decrease in *ABP1* transcript levels in *abp1-c1*. We assume that this difference - somewhat surprising, since the *CRISPR*-induced small deletion does not necessarily decrease transcript levels - is probably caused by the decreased stability of the mutant *mRNA*. SS12K9 × *abp1-c1* F3 plants positive for the KD phenotype and homozygous for *abp1-c1* showed the same 80% decrease in *ABP1* transcription.

In summary, the phenotypic, genotypic and expression analyses consistently showed that all three conditional *abp1* knock-down alleles can generate strong morphological defects also in the absence of the functional ABP1 protein.

Discussion

Strong morphological phenotypes in *abp1* conditional knock-down alleles are not caused by ABP1 down-regulation

All three available conditional *abp1* knock-down alleles have been extensively characterized and used to link number of developmental and cellular processes to the ABP1-mediated signaling (for overview, see Grones & Friml, 2015). They are based on two unrelated strategies for down-regulation of the protein's functionality: the antisense (*abp1-AS*) and the scFv12 monoclonal antibody expression (*SS12S6, SS12K9*), which suppress the protein functionality by entirely different mechanisms and at different levels (Tromas *et al.*, 2009). All three lines showed consistent and reproducible results in a number of different laboratories and a number of developmental, physiological and cellular processes.

Nonetheless, our analysis, made possible by the newly available *abp1* knock-out lines (Gao *et al.*, 2015), strongly suggests that these observed and described effects are not caused by conditional down-regulation of the ABP1. This is supported by the fact that all three constructs show the same strong conditional phenotypes in two different homozygous *abp1* null alleles. This means that even in the absence of the functional ABP1 protein, the ethanol-inducible constructs are inducing phenotypic defects that were originally ascribed to the down-regulation of ABP1. Therefore, results generated using these lines need to be critically re-interpreted.

Possible modes of action of *abp1* conditional knock-down lines

All three types of *abp1* KD *Arabidopsis* lines generate indistinguishable morphological phenotypes. How it is possible that independent lines using fundamentally different approaches for functional down-regulation of a unique target would have in fact the same off-target effects; we do not know. One possible explanation is that the morphological defects are an artifact of the ethanol-inducible expression system. However, control lines generated in parallel using the same vector and expressing the *UIDA* reporter gene did not exhibit any significant growth and developmental alterations (Braun *et al.*, 2008). Furthermore, a number of authors have used the same ethanol-inducible system to control the expression of distinct genes and to the best of our knowledge, there are no reports describing similar phenotypes by using the ethanol-inducible system for other genes in other studies (Battaglia *et al.*, 2006; Deveaux *et al.*, 2003; Laufs *et al.*, 2003; Peaucelle *et al.*, 2008; Roslan *et al.*, 2001). This system was also used to successfully rescue mutant defects after ethanol induction of gene expression e.g. for LEAFY (Maizel & Weigel, 2004) or for N-myristoyltransferase (Pierre *et al.*, 2007) indicating that it is not responsible per se of the phenotypes observed with the ethanol inducible ABP1 AS

and scFv12 constructs. In tobacco plants and BY-2 cells, tetracycline de-repressible promoter-driven expression of the *SS12S* and *SS12K* constructs resulted in similar growth defects as their ethanol-inducible expression in *Arabidopsis* (Braun *et al.* 2008; David *et al.*, 2007), suggesting that the observed phenotypes are tightly correlated to the scFv12 action. The expression of the scFv12 in the cytosol had however no effect on cell proliferation in BY2 cells indicating that expression of scFv12 *per se* is not sufficient to generate severe phenotypes whatever its cellular localisation and that scFv12 effects are correlated to its secretion and/or retention in the ER that are known location of ABP1 (David *et al.*, 2007).

Another possibility is that both the antisense- and antibody-based lines have off-target(s) either on the very same gene(s) or elements of a common genetic pathway. Such a hypothesis would be supported by strict similarities in the phenotypes resulting from ABP1 antisense and scFv12 expression and by the fact that opposite and auxin-related defects were observed in both constitutive and conditional gain-of-function *Arabidopsis* transgenic plants as well as transitionally expressing tobacco cells (Grones *et al.*, 2015; Robert *et al.*, 2010). ABP1 is placed within the superfamily of cupins based on the presence of cupin-like motifs $HXH(X)_{111}G$ and $P(X)_4H(X)_3N$ (where X is any amino-acid residue) and a β-barrel jellyroll fold subunit structure (Dunwell *et al.*, 2004; Woo *et al.*, 2002). The epitope recognized by the scFv12 might be present in proteins belonging to this functionally highly diverse protein superfamily. On the other hand, the sequence similarity of even the closest *ABP1* homologues in *Arabidopsis* does not seem to be sufficiently high to be targeted by the *abp1-AS* constructs, thus this explanation is unlikely as well.

We also cannot completely rule out that the WT phenotype of the *abp1* knock-out mutants is caused by suppressor mutation(s). However, we do not consider it very likely, as this would imply that the similar mutation(s) or mutations with similar effects are present in the genetic background of both *abp1-c1* and *abp1-TD1,* which are independent alleles from independent mutant collections.

In summary, we do not understand how it is possible that the used *abp1* knock-down alleles generate the similar strong morphological phenotypes also in absence of the functional ABP1 protein. All possible explanations we could come up with are unlikely, including common off-targets in *abp1* antisense and antibody KD lines or common suppressor mutations in two different *abp1* knock-out alleles. Thus, more experimentation is needed to figure out what really happens in the different *abp1* KD lines and how it is possible that they independently generate phenotypes that are so consistent. Whatever the explanation at the end will be, in light of the presented data it seems obvious that these lines do not act solely by down-regulating the ABP1 function, despite the accumulation of well-fitting data from independent and complementary approaches. It is a sobering realization that even when you use independent approaches with all standard controls performed, there is no real guarantee that the observations will not lead you amiss.

Data availability

F1000Research: Dataset 1. Scans of ethanol-induced F2 seedlings of crosses (A) *SS12S6* × *abp1-c1*, (B) *SS12S6* × *abp1-TD1*, (C) *abp1-AS* × *abp1-c1*, (D) *abp1-AS* × *abp1-TD1*, (E) *SS12K9* × *abp1-c1* and (F) *SS12K9* × *abp1-TD1* that were used for phenotyping and genotyping (Figure 1 and Figure 2)., 10.5256/f1000research.7654.d110722 (Michalko *et al.*, 2016a).

F1000Research: Dataset 2. Agarose gel images from the PCR genotyping of the F2 crosses (A) *SS12S6* × *abp1-c1*, (B) *SS12S6* × *abp1-TD1*, (C) *abp1-AS* × *abp1-c1*, (D) *abp1-AS* × *abp1-TD1*, (E) *SS12K9* × *abp1-c1* and (F) *SS12K9* × *abp1-TD1* (Figure 3), 10.5256/f1000research.7654.d110723 (Michalko *et al.*, 2016b).

F1000Research: Dataset 3. Source qPCR data (Figure 3c), 10.5256/f1000research.7654.d110724 (Michalko *et al.*, 2016c).

Author contributions

JF, JM, CP and MG designed the experiments and wrote the manuscript, JM and MG performed most experiments and analyzed the data. All authors have seen and agreed to the final content of the manuscript.

Competing interests

No competing interests were disclosed.

Grant information

This work was supported by ERC Independent Research grant (ERC-2011-StG-20101109-PSDP to JF). JM internship was supported by the grant "Action Austria – Slovakia". MG was supported by the scholarship "Stipendien der Stipendienstiftung der Republik Österreich". Work by EH and CPR were supported by ANR blanc ANR-14-CE11-0018.

Acknowledgements

We would like to thank Mark Estelle and Yunde Zhao for providing *abp1-c1*, *abp1-TD1* and *abp1-WTc1* seeds. We thank Emeline Huault for technical assistance.

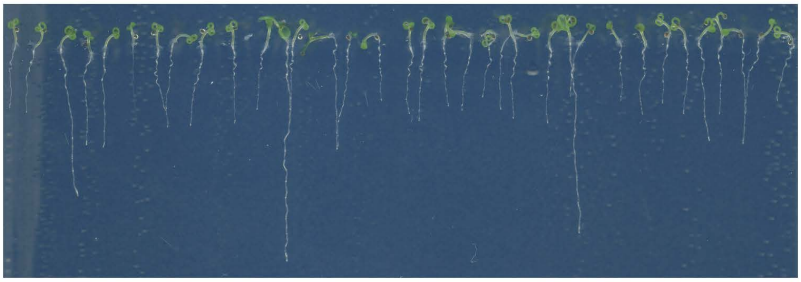
Supplementary material

1st scenario (adaptation)			
SSAA	SSAa	SsAA	SsAa
SSAa	SSaa	SsAa	Ssaa
SsAA	SsAa	ssAA	ssAa
SsAa	Sscc	ssAa	ssaa

2nd scenario (off-targets)			
SSAA	SSAa	SsAA	SsAa
SSAa	SSaa	SsAa	Ssaa
SsAA	SsAa	ssAA	ssAa
SsAa	Sscc	ssAa	ssaa

3rd scenario (suppressor mutations)			
SSAA	SSAa	SsAA	SsAa
SSAa	SSaa	SsAa	Ssaa
SsAA	SsAa	ssAA	ssAa
SsAa	Sscc	ssAa	ssaa

Supplementary Figure 1. Theoretical genotype and phenotype segregation in F2 progeny of the *abp1* knock-out × knock-down cross. Expected genotype and phenotype segregation ratios for three possible scenarios are shown. S/s = ethanol-inducible cassette positive/negative, A/a = wild-type *ABP1*/*abp1* knock-out. Genotypes manifesting wild-type phenotype are shown on white background, KD phenotype on green background, genotypes that might exhibit both WT and KD phenotypes are on pale green background.



Supplementary Figure 2. Restoration of the ethanol-inducible phenotype in the progeny of the F2 WT-looking plant from the cross *SS12K9* × *abp1-c1* containing knock-down cassette and wild-type *ABP1* version. In the presence of 5% ethanol, F3 progeny show homogenous KD phenotype indicating that silencing of the construct might be responsible for wild-type phenotype of this plant in the F2 generation.

References

Barbier-Brygoo H, Ephritikhine G, Klämbt D, *et al.*: **Functional evidence for an auxin receptor at the plasmalemma of tobacco mesophyll protoplasts.** *Proc Natl Acad Sci U S A.* 1989; **86**(3): 891–895.
PubMed Abstract | Publisher Full Text | Free Full Text

Batt S, Wilkins MB, Venis MA: **Auxin binding to corn coleoptile membranes: Kinetics and specificity.** *Planta.* 1976; **130**(1): 7–13.
PubMed Abstract | Publisher Full Text

Battaglia R, Brambilla V, Colombo L, *et al.*: **Functional analysis of mads-box genes controlling ovule development in *Arabidopsis* using the ethanol-inducible *alc* gene-expression system.** *Mech Dev.* 2006; **123**(4): 267–276.
PubMed Abstract | Publisher Full Text

Braun N, Wyrzykowska J, Muller P, *et al.*: **Conditional repression of AUXIN BINDING PROTEIN1 reveals that it coordinates cell division and cell expansion during postembryonic shoot development in *Arabidopsis* and tobacco.** *Plant Cell.* 2008; **20**(10): 2746–2762.
PubMed Abstract | Publisher Full Text | Free Full Text

Chen JG, Ullah H, Young JC, *et al.*: **ABP1 is required for organized cell elongation and division in *Arabidopsis* embryogenesis.** *Genes Dev.* 2001; **15**(7): 902–911.
PubMed Abstract | Publisher Full Text | Free Full Text

Chen X, Grandont L, Li H, *et al.*: **Inhibition of cell expansion by rapid ABP1-mediated auxin effect on microtubules.** *Nature.* 2014; **516**(7529): 90–3.
PubMed Abstract | Publisher Full Text | Free Full Text

Conrad U, Fiedler U: **Compartment-specific accumulation of recombinant immunoglobulins in plant cells: an essential tool for antibody production and immunomodulation of physiological functions and pathogen activity.** *Plant Mol Biol.* 1998; **38**(1–2): 101–109.
PubMed Abstract | Publisher Full Text

Čovanová M, Sauer M, Rychtář J, *et al.*: **Overexpression of the auxin binding protein1 modulates PIN-dependent auxin transport in tobacco cells.** *PLoS One.* 2013; **8**(7): e70050.
PubMed Abstract | Publisher Full Text | Free Full Text

Dai X, Zhang Y, Zhang D, *et al.*: **Embryonic lethality of *Arabidopsis abp1-1* is caused by deletion of the adjacent bsm gene.** *Nat Plants.* 2015; **1**: 15183.
Publisher Full Text

David KM, Couch D, Braun N, *et al.*: **The auxin-binding protein 1 is essential for the control of cell cycle.** *Plant J.* 2007; **50**(2): 197–206.
PubMed Abstract | Publisher Full Text

David KM, Perrot-Rechenmann C: **Characterization of a tobacco Bright Yellow 2 cell line expressing the tetracycline repressor at a high level for strict regulation of transgene expression.** *Plant Physiol.* 2001; **125**(4): 1548–1553.
PubMed Abstract | Publisher Full Text | Free Full Text

Deveaux Y, Peaucelle A, Roberts GR, *et al.*: **The ethanol switch: a tool for tissue-specific gene induction during plant development.** *Plant J.* 2003; **36**(6): 918–930.
PubMed Abstract | Publisher Full Text

Dhonukshe P, Aniento F, Hwang I, *et al.*: **Clathrin-mediated constitutive endocytosis of PIN auxin efflux carriers in *Arabidopsis*.** *Curr Biol.* 2007; **17**(6): 520–527.
PubMed Abstract | Publisher Full Text

Dunwell JM, Purvis A, Khuri S: **Cupins: the most functionally diverse protein superfamily?** *Phytochemistry.* 2004; **65**(1): 7–17.
PubMed Abstract | Publisher Full Text

Enders TA, Strader LC: **Auxin activity: Past, present, and future.** *Am J Bot.* 2015; **102**(2): 180–196.
PubMed Abstract | Publisher Full Text

Gao Y, Zhang Y, Zhang D, *et al.*: **Auxin binding protein 1 (ABP1) is not required for either auxin signaling or *Arabidopsis* development.** *Proc Natl Acad Sci U S A.* 2015; **112**(7): 2275–2280.
PubMed Abstract | Publisher Full Text | Free Full Text

Grones P, Chen X, Simon S, *et al.*: **Auxin-binding pocket of ABP1 is crucial for its gain-of-function cellular and developmental roles.** *J Exp Bot.* 2015; **66**(16): 5055–5065.
PubMed Abstract | Publisher Full Text

Grones P, Friml J: **Auxin transporters and binding proteins at a glance.** *J Cell Sci.* 2015; **128**(1): 1–7.
PubMed Abstract | Publisher Full Text

Grunewald W, Friml J: **The march of the PINs: developmental plasticity by dynamic polar targeting in plant cells.** *EMBO J.* 2010; **29**(16): 2700–2714.
PubMed Abstract | Publisher Full Text | Free Full Text

Habets ME, Offringa R: **Auxin Binding Protein 1: A Red Herring After All?** *Mol Plant.* 2015; **8**(8): 1131–1134.
PubMed Abstract | Publisher Full Text

Hertel R, Thomson KS, Russo VE: ***In-vitro* auxin binding to particulate cell fractions from corn coleoptiles.** *Planta.* 1972; **107**(4): 325–340.
PubMed Abstract | Publisher Full Text

Laufs P, Coen E, Kronenberger J, *et al.*: **Separable roles of *UFO* during floral development revealed by conditional restoration of gene function.** *Development.* 2003; **130**(4): 785–796.
PubMed Abstract | Publisher Full Text

Leblanc N, David K, Grosclaude J, *et al.*: **A novel immunological approach establishes that the auxin-binding protein, Nt-abp1, is an element involved in auxin signaling at the plasma membrane.** *J Biol Chem.* 1999; **274**(40): 28314–28320.
PubMed Abstract | Publisher Full Text

Livak KJ, Schmittgen TD: **Analysis of relative gene expression data using real-time quantitative PCR and the $2^{-\Delta\Delta C_T}$ method.** *Methods.* 2001; **25**(4): 402–408.
PubMed Abstract | Publisher Full Text

Löbler M, Klämbt D: **Auxin-binding protein from coleoptile membranes of corn (*Zea mays* L.). I. Purification by immunological methods and characterization.** *J Biol Chem.* 1985; **260**(17): 9848–9853.
PubMed Abstract

Maizel A, Weigel D: **Temporally and spatially controlled induction of gene expression in *Arabidopsis thaliana*.** *Plant J.* 2004; **38**(1): 164–71.
PubMed Abstract | Publisher Full Text

Meister G, Tuschl T: **Mechanisms of gene silencing by double-stranded RNA.** *Nature.* 2004; **431**(7006): 343–349.
PubMed Abstract | Publisher Full Text

Michalko J, Dravecká M, Bollenbach T, *et al.*: **Embryo-lethal phenotypes in early *abp1* mutants are due to disruption of the neighboring *BSM* gene [version 1; referees: 3 approved].** *F1000Res.* 2015; **4**: 1104.
PubMed Abstract | Publisher Full Text | Free Full Text

Michalko J, Glanc M, Perrot-Rechenmann C, *et al.*: **Dataset 1 in: Strong morphological defects in conditional *Arabidopsis abp1* knock-down mutants generated in absence of functional ABP1 protein.** *F1000Research.* 2016a.
Data Source

Michalko J, Glanc M, Perrot-Rechenmann C, *et al.*: **Dataset 2 in: Strong morphological defects in conditional *Arabidopsis abp1* knock-down mutants generated in absence of functional ABP1 protein.** *F1000Research.* 2016b.
Data Source

Michalko J, Glanc M, Perrot-Rechenmann C, *et al.*: **Dataset 3 in: Strong morphological defects in conditional *Arabidopsis abp1* knock-down mutants generated in absence of functional ABP1 protein.** *F1000Research.* 2016c.
Data Source

Nagawa S, Xu T, Lin D, *et al.*: **ROP GTPase-dependent actin microfilaments promote PIN1 polarization by localized inhibition of clathrin-dependent endocytosis.** *PLoS Biol.* 2012; **10**(4): e1001299.
PubMed Abstract | Publisher Full Text | Free Full Text

Napier RM, David KM, Perrot-Rechenmann C: **A short history of auxin-binding proteins.** *Plant Mol Biol.* 2002; **49**(3–4): 339–348.
PubMed Abstract | Publisher Full Text

Napier RM, Venis MA: **Auxin action and auxin-binding proteins.** *New Phytol.* 1995; **129**(2): 167–201.
Publisher Full Text

Paciorek T, Zazímalová E, Ruthardt N, *et al.*: **Auxin inhibits endocytosis and promotes its own efflux from cells.** *Nature.* 2005; **435**(7046): 1251–1256.
PubMed Abstract | Publisher Full Text

Paque S, Mouille G, Grandont L, *et al.*: **AUXIN BINDING PROTEIN1 links cell wall remodeling, auxin signaling, and cell expansion in *Arabidopsis*.** *Plant Cell.* 2014; **26**(1): 280–295.
PubMed Abstract | Publisher Full Text | Free Full Text

Peaucelle A, Louvet R, Johansen JN, *et al.*: ***Arabidopsis* phyllotaxis is controlled by the methyl-esterification status of cell-wall pectins.** *Curr Biol.* 2008; **18**(24): 1943–48.
PubMed Abstract | Publisher Full Text

Petrásek J, Mravec J, Bouchard R, *et al.*: **PIN proteins perform a rate-limiting function in cellular auxin efflux.** *Science.* 2006; **312**(5775): 914–918.
PubMed Abstract | Publisher Full Text

Pierre M, Traverso JA, Boisson B, *et al.*: ***N*-myristoylation regulates the SnRK1 pathway in *Arabidopsis*.** *Plant Cell.* 2007; **19**(9): 2804–2821.
PubMed Abstract | Publisher Full Text | Free Full Text

Ray PM, Dohrmann U, Hertel R: **Characterization of naphthaleneacetic Acid binding to receptor sites on cellular membranes of maize coleoptile tissue.** *Plant Physiol.* 1977; **59**(3): 357–364.
PubMed Abstract | Publisher Full Text | Free Full Text

Robert S, Kleine-Vehn J, Barbez E, *et al.*: **ABP1 mediates auxin inhibition of clathrin-dependent endocytosis in *Arabidopsis*.** *Cell.* 2010; **143**(1): 111–121.
PubMed Abstract | Publisher Full Text | Free Full Text

Roslan HA, Salter MG, Wood CD, *et al.*: **Characterization of the ethanol-inducible *alc* gene-expression system in *Arabidopsis thaliana*.** *Plant J.* 2001; **28**(2): 225–35.
PubMed Abstract | Publisher Full Text

Sassi M, Ali O, Boudon F, *et al.*: **An auxin-mediated shift toward growth isotropy promotes organ formation at the shoot meristem in *Arabidopsis*.** *Curr Biol.* 2014; **24**(19): 2335–2342.
PubMed Abstract | Publisher Full Text

Tromas A, Braun N, Muller P, *et al.*: **The AUXIN BINDING PROTEIN 1 is required for differential auxin responses mediating root growth.** *PLoS One.* 2009; **4**(9): e6648.
PubMed Abstract | Publisher Full Text | Free Full Text

Tromas A, Paponov I, Perrot-Rechenmann C: **AUXIN BINDING PROTEIN 1: functional and evolutionary aspects.** *Trends Plant Sci.* 2010; **15**(8): 436–446.
PubMed Abstract | Publisher Full Text

Tromas A, Paque S, Stierlé V, *et al.*: **Auxin-binding protein 1 is a negative regulator of the $SCF^{TIR1/AFB}$ pathway.** *Nat Commun.* 2013; **4**: 2496.
PubMed Abstract | Publisher Full Text

Tufarelli C, Stanley JA, Garrick D, *et al.*: **Transcription of antisense RNA leading to gene silencing and methylation as a novel cause of human genetic disease.** *Nat Genet.* 2003; **34**(2): 157–165.
PubMed Abstract | Publisher Full Text

Tzafrir I, Pena-Muralla R, Dickerman A, *et al.*: **Identification of genes required for embryo development in *Arabidopsis*.** *Plant Physiol.* 2004; **135**(3): 1206–1220.
PubMed Abstract | Publisher Full Text | Free Full Text

Woo EJ, Marshall J, Bauly J, *et al.*: **Crystal structure of auxin-binding protein 1 in complex with auxin.** *EMBO J.* 2002; **21**(12): 2877–2885.
PubMed Abstract | Publisher Full Text | Free Full Text

Xu T, Dai N, Chen J, *et al.*: **Cell surface ABP1-TMK auxin-sensing complex activates ROP GTPase signaling.** *Science.* 2014; **343**(6174): 1025–1028.
PubMed Abstract | Publisher Full Text | Free Full Text

Xu T, Wen M, Nagawa S, *et al.*: **Cell surface- and rho GTPase-based auxin signaling controls cellular interdigitation in *Arabidopsis*.** *Cell.* 2010; **143**(1): 99–110.
PubMed Abstract | Publisher Full Text | Free Full Text

Open Peer Review

Current Referee Status: ? ✔ ?

Version 1

Referee Report 09 February 2016

doi:10.5256/f1000research.8243.r12003

? **Christian Luschnig**
Department of Applied Genetics and Cell Biology, University of Natural Resources and Life Sciences, Vienna, Austria

In their m/s, the authors present an analysis of genetic interactions between published *ABP1* knockdown lines (based on antisense and immune-suppression approaches) and the *Arabidopsis ABP1* locus. After crossing three different knockdown lines into recently described *abp1* knockout alleles, followed by segregation analysis of resulting F2 and F3 progeny, the authors came to the conclusion that growth defects of their knockdown lines do not depend on a functional *ABP1* locus.

These findings represent a valuable contribution to ongoing attempts, trying to clarify *ABP1* issues. Nevertheless, off-target loci recognized in the knockdown lines remain mysterious. Are there any ABP1-related loci (cupins?), expression of which could be affected by these knockdown lines? Perhaps this could be tested in the *abp1-AS* line.

Phenotypes of the knockdown lines are reminiscent of mutants with altered auxin responses. Did the authors look into expression of some of the characterized auxin-related loci? This could give us a better idea about the genetic determinants, causing the phenotypes in these knockdown lines.

I have read this submission. I believe that I have an appropriate level of expertise to confirm that it is of an acceptable scientific standard, however I have significant reservations, as outlined above.

Competing Interests: No competing interests were disclosed.

Referee Report 05 February 2016

doi:10.5256/f1000research.8243.r12004

✔ **Richard M. Napier**
School of Life Sciences, University of Warwick, Coventry, UK

The authors have produced a very thorough analysis of a set of well-known conditional ABP1 knock-down Arabidopsis lines. Using crosses with the recently-described abp1 knock-out lines from the work of Gao *et al.* (2015), the manuscript reveals that the phenotypes previously associated with loss of ABP1 can be induced even in genetic backgrounds that lack ABP1. These findings cover results from the two

independent strategies used to create the conditional knock-down phenotypes, conditional immunosuppression and conditional antisense expression.

The assay used for this work was Arabidopsis root growth, not the very detailed phenotypes described recently from the conditional lines such as PIN endocytosis, ROP GTPase activation or microtubule rearrangement. However, impaired root growth was part of the initial suite of phenotypes associated with induced knock-down. The assays show very clearly that growth impairment correlates with the inheritance of the inducible cassette even in the absence of a functional ABP1 gene. We can surmise that the detailed subcellular phenotypes listed above are associated with the gross morphological changes recorded here. There is clearly some intriguing physiology associated with the switch induced by ethanol treatment, but ABP1 is not part of that story.

The title and abstract are appropriate (but see note below*), the work is done well, the data is presented clearly and fully, the text is very well structured and is easy to follow. There is a thorough introduction which explains how and why experimentation developed to tackle tangible problems linked to existing knowledge and understanding of ABP1 genetic resources. It is shown that the science was not misled by carelessness or device, that a spectrum of consistencies coloured the hypotheses covering ABP1 activity, and that these hypotheses have now been proven incorrect thanks to improved technologies, vigilance and critical reappraisal.

*The abstract ends with a sentence "…asks for further reflections on the biological function of ABP1 or alternative explanations for the missing phenotypic defects in the abp1 loss-of-function alleles." I think that this would be better if it read "… AND alternative explanations for the intriguing phenotypes previously associated with loss of ABP1 activity". Or similar. I understand that there is a requirement on all sides of the debate to be objective and critical about their data and no harm is done by registering this. However, the balance of probabilities needs to be recognised and, in my view, much more has to be gained from encouraging discovery of the root cause of the many fascinating phenotypes thrown up by the ABP1 KD lines than by searching absent defects. Therefore a small rewording at the end of the abstract is recommended. Otherwise I have no changes to suggest.

I have read this submission. I believe that I have an appropriate level of expertise to confirm that it is of an acceptable scientific standard.

Competing Interests: No competing interests were disclosed.

Referee Report 26 January 2016

doi:10.5256/f1000research.8243.r12006

Lars Ostergaard
Department of Crop Genetics, John Innes Centre, Norwich, UK

In this manuscript, Michalko *et al.* investigates the basis of the developmental phenotypes observed in knock-down (KD) lines of the *Arabidopsis ABP1* gene. By analysing segregation of defects in root elongation in the F2 and F3 generation of crosses between three KD *abp1* alleles and two recently reported *abp1* knock-out (KO) alleles, they conclude that the previously reported phenotypes of the KD lines are not due to loss of ABP1 function. The manuscript is clearly written and the experiments are thoroughly carried out providing an important contribution to the ABP1 saga.

Although I sympathise with the authors difficulty in identifying an explanation for how the KD lines can lead to the observed abnormalities, one experiment that should be done would in my opinion be a test of the expression of the closest *ABP1*-like genes that can be identified.

I have read this submission. I believe that I have an appropriate level of expertise to confirm that it is of an acceptable scientific standard, however I have significant reservations, as outlined above.

Competing Interests: No competing interests were disclosed.

Gibberellin DELLA signaling targets the retromer complex to redirect protein trafficking to the plasma membrane

Yuliya Salanenka[a], Inge Verstraeten[a], Christian Löfke[b], Kaori Tabata[a], Satoshi Naramoto[c], Matouš Glanc[a,d], and Jiří Friml[a,1]

[a]Institute of Science and Technology Austria, 3400 Klosterneuburg, Austria; [b]Gregor Mendel Institute of Molecular Plant Biology, 1030 Vienna, Austria; [c]Department of Biomolecular Sciences, Graduate School of Life Sciences, Tohoku University, 980-8577 Sendai, Miyagi, Japan; and [d]Department of Experimental Plant Biology, Faculty of Science, Charles University, 12844 Prague, Czech Republic

Edited by Natasha V. Raikhel, Center for Plant Cell Biology, Riverside, CA, and approved January 30, 2018 (received for review January 9, 2018)

The plant hormone gibberellic acid (GA) is a crucial regulator of growth and development. The main paradigm of GA signaling puts forward transcriptional regulation via the degradation of DELLA transcriptional repressors. GA has also been shown to regulate tropic responses by modulation of the plasma membrane incidence of PIN auxin transporters by an unclear mechanism. Here we uncovered the cellular and molecular mechanisms by which GA redirects protein trafficking and thus regulates cell surface functionality. Photoconvertible reporters revealed that GA balances the protein traffic between the vacuole degradation route and recycling back to the cell surface. Low GA levels promote vacuolar delivery and degradation of multiple cargos, including PIN proteins, whereas high GA levels promote their recyding to the plasma membrane. This GA effect requires components of the retromer complex, such as Sorting Nexin 1 (SNX1) and its interacting, microtubule (MT)-associated protein, the Cytoplasmic Linker-Associated Protein (CLASP1). Accordingly, GA regulates the subcellular distribution of SNX1 and CLASP1, and the intact MT cytoskeleton is essential for the GA effect on trafficking. This GA cellular action occurs through DELLA proteins that regulate the MT and retromer presumably via their interaction partners Prefoldins (PFDs). Our study identified a branching of the GA signaling pathway at the level of DELLA proteins, which, in parallel to regulating transcription, also target by a nontranscriptional mechanism the retromer complex acting at the intersection of the degradation and recycling trafficking routes. By this mechanism, GA can redirect receptors and transporters to the cell surface, thus coregulating multiple processes, including PIN-dependent auxin fluxes during tropic responses.

gibberellin | DELLA | polar auxin transport | microtubules | vesicle trafficking

Because plants have a sessile lifestyle, they constantly need to adapt to a changing environment. Through hormonal signaling, environmental cues can be integrated and developmental programs are modified accordingly. Increasing evidence supports the idea that the signaling crosstalk between different hormonal pathways, rather than specific activity of a single hormone, determines the final signaling outcome (1, 2).

Auxin and gibberellic acid (GA) are prominent growth regulators, and their signaling pathways positively interact in the regulation of cell expansion and tissue differentiation (3). In roots, auxin promotes GA responses via the degradation of major components of the GA pathway, namely, DELLA transcriptional repressors (4), and via transcriptional activation of GA biosynthesis (5). On the other hand, DELLAs have been proposed to negatively regulate polar auxin transport (PAT) by a multistep inhibition of the transcription of PIN auxin transporters (6). Moreover, during gravitropic responses, GA regulates the transcription of the *indole-3-acetic acid 19/MASSAGU2* repressor of auxin signaling (7).

Notably, the developmental output of the auxin pathway can also be modulated by the GA effect on the abundance of PIN transporters (8, 9) that are important for the formation and maintenance of the developmentally crucial local auxin gradients and maxima (10, 11). Generally, GA-deficient conditions lead to increased vacuolar trafficking and reduced incidence of PINs at the plasma membrane (PM) (8, 9). Conversely, high GA levels inhibit PIN vacuolar delivery and promote PIN incidence at the PM (9). The precise mechanism of PIN trafficking to the vacuole and its regulation is unclear, but it depends on sorting nexin (SNX1) components associated with the retromer complex (12). A direct association between SNX1 and CLASP1 (one of MT-associated proteins) suggests that cortical MT-decorating CLASP1 increases the residency time of SNX-positive vesicles close to the PM to promote recycling of cargos back to the PM (13). PIN trafficking regulation by GA appears to be developmentally relevant, e.g., during root gravitropic bending, which is regulated by GA signaling and during which asymmetric GA distribution has been detected (9).

Here we show that GA regulates the cell surface incidence of proteins by specifically targeting the SNX1-mediated switch between vacuolar trafficking and recycling to the PM. This reveals a cellular mechanism, by which GA controls auxin transport-mediated development and other cell surface-based regulations.

Results and Discussion

GA Modulates the Balance Between Vacuolar Trafficking and Exocytosis. To dissect the cellular GA-targeted processes that regulate PIN levels at the PM, we used the photoconvertible *pPIN2::PIN2-*

Significance

This study identifies and outlines a nontranscriptional branch of the canonical GA signaling pathway that redirects protein traffic from the vacuolar degradation route to the plasma membrane. As a result, the amount of receptors and transporters, such as PIN transporters for the plant hormone auxin, is functionally regulated at the cell surface. The identified branching occurs at the level of DELLA proteins that, besides transcriptional regulation, also target the microtubule (MT) network and protein trafficking. In this work, we provide multiple lines of evidence that DELLA proteins act via their interacting partners Prefoldins and that a downstream MT/CLASP1 module regulates the activity of the retromer complex that directs protein trafficking at the intersection of the vacuolar and recycling pathways.

Author contributions: Y.S., C.L., and J.F. designed research; Y.S., I.V., K.T., S.N., and M.G. performed research; Y.S. analyzed data; and Y.S. and J.F. wrote the paper.

The authors declare no conflict of interest.

This article is a PNAS Direct Submission.

This open access article is distributed under Creative Commons Attribution-NonCommercial-NoDerivatives License 4.0 (CC BY-NC-ND).

[1]To whom correspondence should be addressed. Email: jiri.friml@ist.ac.at.

This article contains supporting information online at www.pnas.org/lookup/suppl/doi:10.1073/pnas.1721760115/-/DCSupplemental.

Dendra line. The irreversible conversion of the Dendra fluorochrome from green to red allowed us to follow the subcellular fate of the already present PIN2 in GA-deficient and GA-treated conditions. Conceptually, GA can enhance PIN levels at the PM by (*i*) inhibiting PIN endocytosis, (*ii*) promoting its exocytosis, or (*iii*) inhibiting PIN vacuolar delivery and degradation.

In the nonphotoconverted situation, a GA synthesis inhibitor, paclobutrazol (PAC) (14), strongly decreased the total PIN2-Dendra signal, whereas GA treatment rapidly reverted this effect (Fig. 1 *A–D*). Therefore, PIN2-Dendra reacted identically to PAC and GA treatments as PIN2-GFP, the regulation of which by GA has been verified both by microscopy (Fig. S1 *A–D*) and Western blot analysis (Fig. S1 *E–H*). However, when PIN2-Dendra was photoconverted into its red form and its depletion from the PM was followed, the decrease in the red signal over time was not affected by PAC pretreatment (Fig. 1 *E–H* and *O*), suggesting that PIN2 internalization from the PM is not affected by GA availability and, thus, that the observed PIN2 depletion from the PM in GA-deficient conditions (8) is not due to enhanced PIN2 endocytosis. To assess the alternative scenario of GA promoting exocytosis, we photoconverted PIN2-Dendra and monitored the green signal recovery at the PM, which reflects the delivery of de novo synthesized PIN2-Dendra proteins (Fig. 1*Q*). Notably, in GA optimal conditions, the green signal intensity increased up to 40% within 5 h (Fig. 1 *I*, *J*, and *O*). On the contrary, in PAC-treated roots, the recovery was severely inhibited, reaching only ~5% (Fig. 1 *K*, *L*, and *O*). GA treatment was sufficient to revert the PAC effect and to recover the green PIN2-Dendra at the PM (Fig. 1 *M*, *N*, and *P*). Treatment with Brefeldin A (BFA), an established inhibitor for PIN delivery to the PM (15, 16), had no obvious effect on PAC- and GA-modulated PIN2 recovery at the PM (Fig. S2 *A–D* and *G*). This illustrates a BFA-insensitive delivery of newly synthesized PIN2 to the apical membranes of root epidermis cells, consistent with previous studies (17, 18).

Next, we confirmed the PIN2-Dendra observations by the fluorescence recovery after photobleaching (FRAP) and live imaging of PIN2-mCherry. The PIN2-mCherry fluorescence was almost completely bleached in the whole cellular region, so that the signal recovery indicated predominantly the delivery of de novo synthesized PIN2. As shown for PIN2-Dendra, PAC treatment decreased the PM PIN2-mCherry recovery with a concomitantly increased vacuolar delivery (Fig. S2 *E*, *F*, and *H–K*).

In summary, the photoconversion and FRAP experiments revealed that GA-deficient conditions have little effect on PIN2 endocytosis but lead to a strong inhibition of PIN2 delivery to the PM and trafficking redirection to the vacuole. GA treatment is sufficient to completely revert this effect by inhibiting vacuolar targeting and recovering PIN2 at the PM. This suggests that GA signaling targets processes balancing PIN2 vacuolar trafficking and its recycling back to the PM.

Nontranscriptional GA Mechanism Regulates Trafficking of Multiple Cargoes. We performed several experiments to confirm that GA increases PIN2 delivery to the PM but not through the regulation of PIN2 transcription or protein synthesis (Fig. S3). Quantitative reverse transcription PCR (qRT-PCR) showed that *PIN2* transcription was not influenced by PAC or GA treatments (Fig. S3 *A* and *B*). Moreover, real-time recording of *PIN2* promoter activity (in *pPIN2::NLS-GFP* roots) showed no differences between mock, PAC, and PAC+GA treatments (Fig. S3 *C–E*). *PIN2* promoter activity-independent action of GA was confirmed by the observation that PIN2 and PIN1 distributions in estradiol-inducible and 35S-driven lines were regulated by GA in a similar way as protein fusions under their native promoters (Fig. S3 *H–K*). Furthermore, PIN2-GFP levels were monitored microscopically following GA and PAC cotreatments with cycloheximide (CHX), an inhibitor of protein synthesis. Whereas CHX significantly decreased the level of PIN2 at the PM, PAC treatment led to an additional drop in PIN2 abundance, which was reversed by GA even in the presence of CHX (Fig. S3 *G* and *F*). These observations confirm that not only GA regulates PIN abundance independently of transcription but also that the GA effect itself utilizes a nontranscriptional mechanism.

To test the specificity of these GA effects on PIN proteins, we examined vacuolar targeting of different cargo proteins in GA-deficient conditions. The vacuolar degradation increased not only for PIN2 but also for several other PM proteins, such as Boron transporter 1 (BOR1), Brassinosteroid insensitive 1 (BRI1), P-glycoprotein 19 (PGP19), and PM intrinsic protein 1;4 (PIP1;4) (Fig. S4 *A–I*). These findings are not consistent with previous observations that GA did not visibly affect PM stability of AUX1, PGP19, and PIP2 (9). This discrepancy might be explained by a different evaluation method: GA effect on the PM proteins abundance (9) versus the dark-visualized protein vacuolar delivery, which seems to be more sensitive (12). Using the dark conditions or concanamycin A treatment, we detected a pronounced PIN2 vacuolar degradation following PAC treatment, which was reversed by GA (Fig. S4 *J–O*).

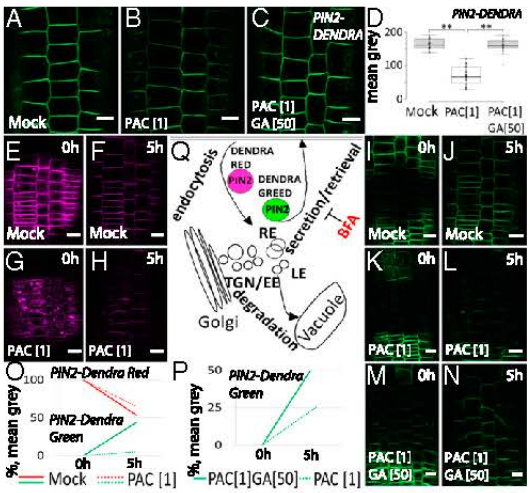


Fig. 1. GA effects on PIN2 vacuolar trafficking and exocytosis. (*A–C*) Decrease of total PIN2-Dendra signal at PM in seedlings pretreated with 1 μM paclobutrazol (PAC) for 1 d (*B*) that was rescued by 50 μM GA treatment for 4 h (*C*) compared with nontreated seedlings (*A*). (*D*) PIN2-Dendra signal quantification. A rectangular region of interest (ROI) at the PM was used for PM signal intensity quantification, and the PM signal was measured in 16 epidermal cells, including tricholasts and atrichoblasts in eight individual roots. (*E–H*) Photoconversion of PIN2-Dendra into its red form induced by illuminating the region of interest and the depletion of the red signal over time followed in nontreated seedlings (*E* and *F*) versus seedlings pretreated with 1 μM PAC (*G* and *H*). Note the increased PIN2-Dendra vacuolar delivery in PAC-treated samples (*G*). (*I–N*) Green signal recovery at the PM after photoconversion reflects the delivery of de novo synthesized protein in nontreated seedlings (*I* and *J*), pretreated with 1 μM PAC (*K* and *L*), and treated with 50 μM GA for 5 h after 1 μM PAC pretreatment (*M* and *N*). Note the faster accumulation of de novo PIN2 at the PM in seedlings untreated versus PAC treatment (*I* and *J*) and treated with GA (*M* and *N*). (*O* and *P*) Decrease in PIN2-Dendra red signal and increase in the green signal 5 h after photoconversion, reflecting the rate of endocytosis and exocytosis, respectively. The percentage of the increase in the green signal intensity was measured after 5 h, revealing the exocytosis rate in untreated epidermal cells versus 1 μM PAC treated (*O*) and roots pretreated with 1 μM PAC and followed by 50 μM GA treatment (*P*). Note the increase in the exocytosis rate of PIN2 in roots upon GA application. (*Q*) Schematic representation of PIN2-Dendra red internalization reflects the rate of endocytosis and delivery of a newly synthesized green PIN2-Dendra to the PM linked to the exocytosis rate. (Scale bar: 10 μm.)

Similar differences in vacuolar accumulation of cargo proteins like BOR1 or PGP19 were observed despite the absence of obvious differences in abundance at the PM (Fig. S4 *A*, *B*, *F*, and *G*). qRT-PCR for these proteins in identical conditions showed no significant difference in mRNA levels following PAC or GA treatment, with the exception of PIP1;4 (Fig. S5).

These results imply a nontranscriptional mechanism of GA regulation of the balance between vacuolar trafficking and recycling back to the PM of multiple PM cargoes.

Gibberellin Targets the Retromer Complex for Trafficking Modulation. The evolutionarily conserved retromer complex that functions at the interface of exocytosis/recycling and vacuolar trafficking mediates the recovery of proteins from the vacuolar degradation pathway back to the recycling pathway (19). As shown previously (20, 21), SNX1 and other components of the retromer complex are involved in PIN protein sorting from the prevacuolar compartment to make them again available for recycling to the PM (12). To test whether SNX1-dependent protein retrieval is required for GA action on PIN2 trafficking, we analyzed the GA sensitivity of *snx1* mutants. In PAC-pretreated *snx1-1* seedling roots, GA application was largely ineffective to restore PIN2-GFP levels at the PM (Fig. 2 *A–D*, *Q*, and *R*). Moreover, *snx1-1* seedlings were less sensitive to the application of PAC because we observed a less pronounced decrease of the total PM PIN2 in the *snx1-1* mutant in comparison with the control (Fig. S6 *A–D*, *G*, and *H*). Similar observations were made in the *protein affected trafficking 3* (*pat3*) mutant defective in the VACUOLAR PROTEIN SORTING35A (VPS35A), another subunit of the retromer complex (21). Also in *pat3-3* roots, GA was unable to restore PIN2-GFP incidence at the PM (Fig. S7 *A*, *B*, and *E*), confirming the importance of the retromer function for GA effect on PIN trafficking. However, in mutants generally defective in vacuolar trafficking and function, such as *pat4* (22), the sensitivity to GA was not affected (Fig. S7 *C–E*). This observation together with previously shown GA-insensitive PIN2 accumulation in Wortmannin bodies (9) indicates that the GA regulation of the PM protein accumulation is not due to decreased transit into prevacuolar compartments of PIN2 but is regulated more upstream and specifically requires the retromer complex components.

In addition, we observed a pronounced GA effect on SNX1-positive endosomal compartments. PAC treatments resulted in the appearance of abnormally enlarged SNX1-GFP bodies, distinct from the punctuated SNX1-GFP–labeled endosomes (Fig. 2 *G–O*); however, the total number of SNX1-GFP endosomes was not significantly changed (Fig. 2*P*). Prolonged PAC treatments led to an increased cytosolic SNX1-GFP signal (Fig. S7 *F* and *G*). GA application resulted in reduced numbers of these abnormal endosomes (Fig. S7 *H* and *I*). Overall, it has been common to observe in one root treated with PAC both patterns —cells with enlarged SNX1-GFP endosomes and the cells with SNX1-GFP in the cytosol. Western blots of root samples confirmed a decrease of SNX1-GFP protein in the membrane (microsomal) fraction following PAC treatment (Fig. 2*I*). When other markers for the endosomal compartments, such as VHA-GFP or FYVE-GFP, were studied, no such effects occurred (Fig. S7 *J–M*), which hinted at a more specific GA effect on the retromer-related compartments.

The observations that mutants defective specifically in retromer components are insensitive to GA in terms of regulation of trafficking together with GA effects on the SNX1-labeled endomembranes suggest that GA targets the retromer or related components to balance vacuolar trafficking and PM delivery.

Gibberellin Effect on Trafficking Requires CLASP1 Activity. The MT-associated protein CLASP1 has been shown to interact directly with SNX1 and this interaction is important for retromer-mediated trafficking regulation (13). Therefore, we assessed the

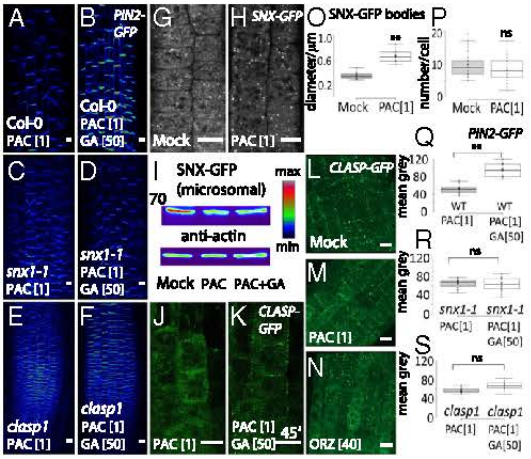


Fig. 2. GA action on PIN2 requires SNX1 and its associated protein CLASP1. (*A–F*) PIN2-GFP (*A* and *B*), *snx1-1*×PIN2-GFP (*C* and *D*), and *clasp1*×PIN2-GFP (*E* and *F*) seedlings pretreated with 1 µM PAC and subsequently treated with 50 µM GA. Reduced sensitivity to GA was observed in *snx1-1* (*C* and *D*) and *clasp1* (*E* and *F*) mutant seedlings in comparison with wild type (*A* and *B*). (*G* and *H*) SNX1-GFP-labeled endomembranes in the root epidermis of untreated seedlings (*G*) and treated with 1 µM PAC (*H*). Note the abnormally enlarged SNX1-GFP–labeled bodies in the PAC-treated seedlings (*H*) in comparison with the punctate bodies in untreated seedlings (*G*). (*I*) Decrease in microsomal (membrane) SNX1 protein upon PAC treatment and increase upon GA in *Arabidopsis* root tips by Western blot analysis. (*J* and *K*) GFP-CLASP1 association with the cell edges at 0 min (*J*) and after 45 min (*K*) of GA application in epidermal cells. Note the gradual enrichment of the GFP-CLASP1 at the cell edges starting 45 min after GA application (*K*). (*L–N*) Cellular localization of GFP-CLASP1 in untreated seedlings (*L*), treated with 1 µM PAC (*M*) and treated with 40 µM oryzalin (*N*). Note that PAC-treated roots have less cell edge-localized GFP-CLASP1 but more GFP-CLASP1 accumulated in the cytoplasm (*M*) compared with mock (*L*), whereas oryzalin treatment entirely removed GFP-CLASP1 from the cell edges, and most of it localized in cytoplasm and vesicles (*N*). (*O* and *P*) Quantification of the size of SNX1-GFP–labeled bodies (*O*) and total amount of endosomes (*P*). (*Q–S*) Quantified relative increase of PIN2-GFP signals after GA treatment in the root epidermis of wild type (*Q*), *snx1-1* (*R*), and *clasp1* (*S*). Measurements were performed as described in Fig. 1. Color code was used for PIN2-GFP intensity visualization. (Scale bar: 10 µm.)

potential contribution of CLASP1 in GA-mediated regulation of PIN2 trafficking. The *clasp1* mutant was less sensitive to PAC treatment in terms of PIN2 depletion from the PM (Fig. S6 *E*, *F*, and *I*), and more importantly, GA treatment was ineffective to recover PIN2 at the PM (Fig. 2 *E*, *F*, and *S*), suggesting that both retromer complex and CLASP1 activity are necessary for the GA effect on trafficking.

Next, we used GFP-CLASP1 fusion protein driven by its endogenous promoter to visualize the subcellular CLASP1 distribution. PAC-treated roots showed slightly but significantly fewer cells with cell edge-localized GFP-CLASP1 compared with mock (Fig. 2 *L* and *M*). PAC treatment also led to an increase of the GFP-CLASP1 cytosolic signal, similarly to our observations when MTs were depolymerized by oryzalin. The complete MT depolymerization with oryzalin removed GFP-CLASP1 from cell edges entirely (Fig. 2*N*). By using time lapse imaging following GA treatment, we perceived a gradual enrichment of GFP-CLASP1 association with the cell edges, starting as early as 45 min after GA application (Fig. 2 *J* and *K*). These observations suggest that GA targets both the retromer complex and its associated protein CLASP1, further strengthening the notion that

PLANT BIOLOGY

these regulators are part of the mechanism by which GA regulates PIN2 trafficking.

The Gibberellin Effect on Trafficking Needs Intact and Dynamic Microtubules. Because CLASP1 is known to be associated with MTs in different eukaryotes (23–25), we tested the role of MTs in the GA effect on PIN2 trafficking. The effect of GA on MT orientation is well described, and in the majority of the studies, GA promotes the transversal orientation of MTs (26, 27). Taking into account that SNX1 and CLASP1 might be involved in the GA effect on trafficking, we studied MT behavior after PAC treatment. We used live imaging of different MT reporter lines (such as MAP4-GFP, VENUS-TUA6, and EB1b-GFP) and found that PAC treatment resulted in the transition of the MT array from a more organized pattern with a distinctive bundled network to a more randomized pattern with fewer MTs per area unit (Fig. S8 *A* and *B*). Using an Eb1b-GFP marker line, we recorded the enrichment in longitudinally or obliquely oriented MTs in the roots treated with PAC (Fig. S8 *E–H*). Similarly, as observed for SNX1-GFP and GFP-CLASP1, we found that prolonged PAC treatment led to an overall decrease in the MT network labeled with VENUS-TUA6 and an increase in fluorescent signal in the cytoplasm (Fig. S8 *C* and *D*). Overall, we observed that at the early stages of GA deficiency, MT network stayed intact although it reoriented randomly or longitudinally coinciding with mostly cell-edge localized CLASP1, and SNX1 present in enlarged endosomes. At later stages, polymerization of MTs was visibly affected correlating with an increase in the cytosolic CLASP1 and SNX1.

To identify a possible requirement for MT cytoskeleton in GA-modulated PIN2 stability at the PM, we used oryzalin to disrupt the MTs (28, 29) and tested whether GA was still able to restore PIN2 abundance in PAC-grown roots. Whereas GA readily restored PIN2 at the PM in the mock control (Fig. 3 *A* and *B*), this effect was abolished when MTs were depolymerized by oryzalin (Fig. 3 *C–E*). Also, when MTs were stabilized by taxol (30), the GA effect on the PM restoration of PIN2 was abolished (Fig. 3 *F–I*). Oryzalin and taxol treatments themselves resulted in a decrease of PIN2 at the PM compared with control plants (Fig. S8 *I–N*). To test if genetic interference with MTs also changes PIN2 responses to GA, we used the *katanin 1* (*ktn1*) mutant known to be compromised in severing MTs and proper formation of cortical MT arrays (31, 32). Notably, in *ktn1* roots pretreated with PAC, GA application was not able to restore PIN2 at PM (Fig. 3 *K–O*) or to decrease vacuolar PIN2 degradation (Fig. S9 *A–E*). In general, *ktn1* mutants contained less abundant PIN2 at PM, which was not further affected by PAC application (Fig. S8 *O–Q*). Furthermore, *tortifolia 1* (*tor1*), another mutant defective in MTs (33), showed an unusual response to PAC, which rather increased instead of decreasing PIN2 incidence at the PM (Fig. S9 *F–M*).

The pharmacological and genetic interferences with MTs revealed that an intact, dynamic MT cytoskeleton is essential for GA effect on PIN2 trafficking. Thus, GA regulation of trafficking requires retromer activity, MT cytoskeleton, and CLASP1 protein, which directly links these cellular structures.

The DELLA Components of GA Signaling Mediate GA Effect on Trafficking. Next, we assessed which GA signaling mechanism acts upstream of MTs and retromer to regulate PIN trafficking. DELLA proteins are key components of GA signaling, and they are typically viewed as nucleus-based transcriptional modulators of downstream genes (34–36). Additionally, a supplementary mode of DELLA action has recently been proposed based on the DELLA interaction with Prefoldins (37), which are important factors of tubulin folding in the cytoplasm (38).

To test the involvement of DELLA proteins in trafficking regulation by GA, we used lines with deficient or modified DELLA activity. First, we studied the GA sensitivity of PIN2 trafficking in the quintuple *della* knockout mutant. Notably, in the quintuple *della*

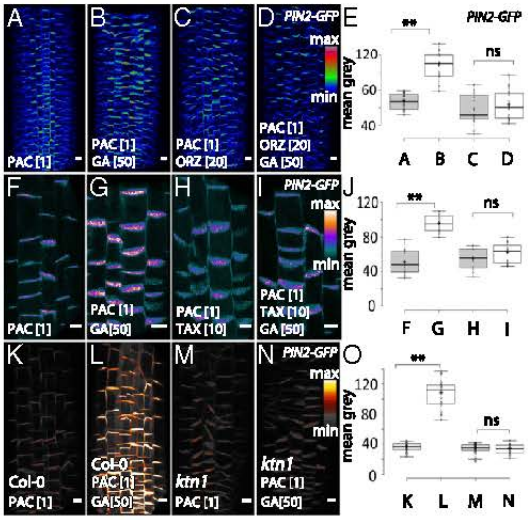


Fig. 3. Regulation of GA-dependent PIN2 trafficking by MTs. (*A–E*) Depolymerization of MTs with 20 μM oryzalin prevented GA (50 μM) effect on PIN2 restoration at the PM in PAC-treated seedlings (*C* and *D*) compared with the oryzalin-free mock (*A* and *B*). Quantifications (*E*). (*F–J*) Ability of GA to increase PIN2 at the PM of PAC-treated seedlings was abolished by 10 μM of MT-stabilizing agent taxol (*H* and *I*) compared with the taxol-free mock (*F* and *G*). Quantifications (*J*). (*K–O*) Efficiency of GA to increase PAC-compromised PIN2 amount (*K* and *L*) reduced in the *ktn1* mutant (*M* and *N*). Quantifications (*O*). Color code was used for PIN2-GFP intensity visualization. (Scale bar: 10 μm.)

roots, PAC-based interference with GA biosynthesis did not result in a substantial decrease in PIN2 at the PM, and more importantly, GA treatment was ineffective in up-regulating PIN2 levels at the PM (Fig. 4 *A–H*). Furthermore, the dominant-negative DELLA mutant *gaiΔ17* roots showed less PIN2 abundance in comparison with wild type or *della* knockout mutant (Fig. S10 *A–C* and *E*), similarly to the previous observations for PIN1 (9). Also, the *gaiΔ17* mutant roots were insensitive to GA treatment such that it failed to restore the PIN2 levels (Fig. S10 *D* and *E*). Finally, we introduced PIN2-GFP into the *GAI:gai-1-GR* line, which after induction by the synthetic glucocorticoid dexamethasone (DEX) targets a dominant DELLA mutant protein from the cytosol to the nucleus (37). In this line, the DEX treatment resulted in a significant down-regulation of PIN2 levels at the PM (Fig. 4 *I–L*). Concurrent GA application and DEX induction did not recover PIN2 levels at the PM (Fig. 4*K*). Collectively, these experiments demonstrated that GA effect on PIN2 trafficking strictly requires the DELLA function.

A possible mechanism for DELLA proteins to regulate MTs and trafficking is through the tubulin-folding factors Prefoldins (PFDs) that are known to control MT folding and dynamics in nonplant organisms (39, 40) and have been shown to interact with DELLAs in plants (37). Indeed, the *pfd6* mutant had clearly reduced levels of PIN2 at the PM (Fig. S10 *F–H*). To further confirm the role of PFDs in GA action on PIN2 trafficking, we analyzed GA sensitivity of the *pfd5 pfd6* double mutant. In PAC-pretreated *pfd5 pfd6* seedling roots, GA application was ineffective in restoring PIN2-GFP levels at the PM (Fig. 4 *M–Q*). Moreover, *pfd5 pfd6* double mutants were less sensitive to PAC treatment in terms of PIN2 decrease in the PM (Fig. S10 *I–L*). This observation supports the hypothesis that the DELLA interacting partner PFD mediates GA-dependent regulation of PIN2 trafficking.

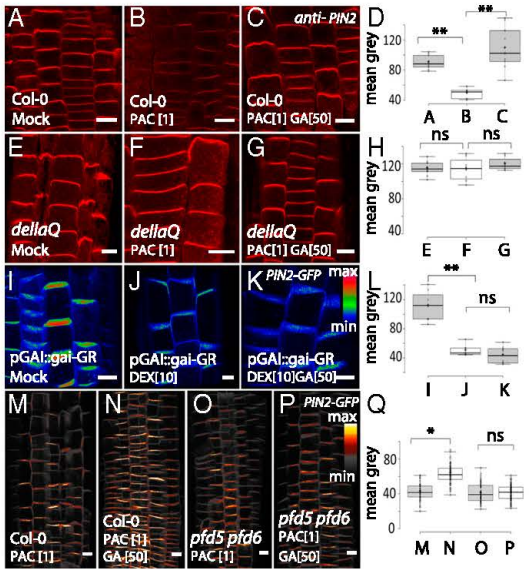


Fig. 4. DELLA proteins and their PFD interactors mediating GA effects on PIN2. (*A–H*) Immunolocalization of PIN2 at the PM in nontreated wild-type (*A–C*) and *della* knockout mutant (*E–G*) seedlings. Note reduced sensitivity of *della* knockout seedlings to 1 μM PAC and 50 μM GA (*F* and *G*) in comparison with wild type (*B* and *C*). Quantifications (*D* and *H*). (*I–L*) GAI::gai-1-GR induced in seedlings by treatment with 10 μM DEX. After induction of dominant-negative DELLA, PIN2 amount at the PM was significantly reduced (*J*), and GA treatment did not restore PIN2 levels at the PM (*K*). Quantifications (*L*). (*M–Q*) Reduced efficiency of 50 μM GA to increase PIN2 level at the PM in 1 μM PAC- treated seedlings of *pfd5 pfd6* (*O* and *P*) mutant seedlings in comparison with wild type (*M* and *N*). Color code was used for PIN2-GFP intensity visualization. The 3D Z stacks are presented. Quantifications (*Q*). (Scale bar: 10 μm.)

Conclusion

Gibberellin is a classical plant hormone that plays a crucial role in plant development and in response to environmental stimuli. Besides its traditionally studied roles in processes, such as germination, elongation growth, and flowering time (41), GA also modulates processes typically regulated by the plant hormone auxin, such as organ formation and gravitropism, by modulating trafficking and cell surface incidence of PIN auxin transporters (8, 9). Here we established the cellular mechanism and key molecular components of the GA-dependent trafficking of PIN auxin transporters and other proteins.

Live imaging and the use of photoconvertible cargos revealed that GA promotes the exocytic delivery of both newly synthesized and recycled cargos and, concomitantly, diminishes vacuolar trafficking and subsequent degradation. In contrast, GA deficiency had an opposite effect by promoting vacuolar degradation and diminishing cell surface cargo delivery, suggesting that GA targets processes at the intersection of exocytosis and vacuolar trafficking.

The retromer complex acts on retrieval of cargos, including PIN proteins from the degradation route back to the exocytic track (12, 20). This crucial switch between trafficking routes seems to be a specific target of GA signaling because mutants in different subunits of the retromer complex are insensitive to GA in terms of trafficking regulation, and GA deficiency modifies the intracellular distribution of the SNX1 retromer component. To further strengthen the link to the retromer, GA action on trafficking depends on the dynamic MTs, in line with previous observations that MT depolymerization affects both SNX1 distribution and PIN trafficking (13). This mechanism would be similar to that in animals, in which MTs and their associated motor proteins govern the endosomal trafficking and balance between recycling and degradation of PM receptors (42).

In plants, the connection between the endomembrane trafficking and MTs is mediated by the MT-associated protein CLASP1, which has been proposed to control tethering of endosomal vesicles to MTs via direct interaction with SNX1 (13). Again, CLASP1 activity is required for the GA effect on trafficking. Moreover, CLASP1 localization at sharp edges of the cells depends on GA availability. Therefore, our analysis suggests that retromer, MTs, and CLASP1 protein are linked as main targets of GA regulation of trafficking.

How can these evolutionarily conserved cell structures and functions be regulated by plant-specific signals, such as GA? The upstream processes involve the established components of GA signaling—the nuclear DELLA proteins, because manipulations with DELLA activity have an immediate effect on GA-mediated trafficking regulation. DELLAs can execute their effect on MTs and the retromer via their interactors, the PFDs (37), because in the double *pfd* mutants, PIN2 cell surface abundance is diminished, and this mutant is largely insensitive to GA. The exact role of PFDs in endomembrane trafficking has not been established yet, but they have been identified in a screen for exocytosis regulators in yeast (43). Given the tight association between MT and actin cytoskeletons (44) as well as the proposed role of PFD in both MT and actin polymerization (45) it is likely that GA as well influences actin-related processes. Whether it is in any way related to the reported auxin effect on actin-mediated vacuolar morphology and function (46) remains to be seen.

Based on these findings, we put forward a model (Fig. 5) in which the GA signaling pathway branches at the level of DELLA

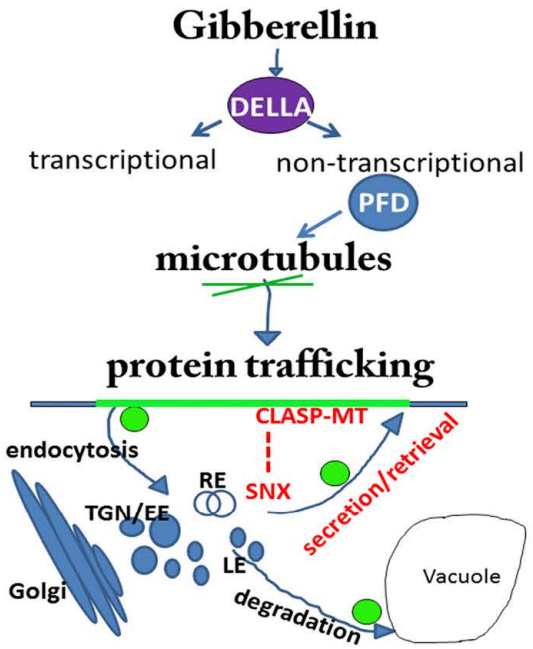


Fig. 5. Model summarizing the mechanism of GA action on PIN protein abundance. CLASP1, CLIP170-associated protein 1; LE, late endosomes; MT, microtubules; RE, recycling endosomes; SNX, sorting nexin; TGN/EE, trans-Golgi network/early endosomes.

proteins that, besides their well-established role in transcriptional regulation, would, via their interacting partners, the PFDs, and the downstream MT/CLASP1 module, regulate the retromer activity and redirect protein trafficking from the vacuolar pathway to the PM. By this mechanism, GA can regulate, in addition to transcription, also the relocation of transporters and receptors to and from the cell surface, thus controlling a wide array of cell processes, including cell expansion for growth regulation.

Materials and Methods

Plant Material and Constructs. The *pfd5×PIN2-GFP*, *pfd6×PIN2-GFP*, and *pGAI::gai-1-GR×PIN2-GFP* lines were obtained by manual hand-pollination of individual lines.

pPIN2::PIN2:DENDRA was generated by replacing the *GFP* fragment of the *pPIN2::PIN2:GFP* construct (47) with *DENDRA*. *pPIN2::PIN2:mCherry* was generated by replacing of the *Venus* tag with *mCherry*. To generate *pPIN2::NLS-GFP* and *UBQ::VENUS:TUA6* the Gateway cloning system was used. For detailed information, see *SI Materials and Methods*.

Drug Application and Experimental Conditions. Exogenous drugs were applied in solid agar-based or liquid Murashige and Skoog (MS) medium or by spraying 5-d-old seedlings. For treatments, 1 μM paclobutrazol and 50 μM GA_3 were used. The confocal laser scanning microscopes (Zeiss CLSM 700 and 800) were used to image fluorescently labeled proteins in live or fixed plant cells. For detailed information, see *SI Materials and Methods*.

Protein Extraction, Western Blot Analysis, and Protein Immunolocalization. For Western blotting, 15–20 mg of root material (4–5 d after germination) was homogenized and processed as described in ref. 48. Whole-mount immunolocalization in *Arabidopsis thaliana (L.) Heyhn.* roots was performed as described in ref. 49.

qRT-PCR. RNA was extracted with the RNeasy mini kit (Qiagen) from excised root tips of 5-d-old seedlings. All PCRs were performed in technical triplicates. For detailed information, see *SI Materials and Methods*.

ACKNOWLEDGMENTS. We gratefully acknowledge M. Blázquez (Instituto de Biología Molecular y Celular de Plantas), M. Fendrych, C. Cuesta Moliner (Institute of Science and Technology Austria), M. Vanstraelen, M. Nowack (Center for Plant Systems Biology, Ghent), C. Luschnig (Universitat fur Bodenkultur Wien, Vienna), S. Simon (Central European Institute of Technology, Brno), C. Sommerville (Carnegie Institution for Science), and Y. Gu (Penn State University) for making available the materials used in this study; M. Muszkowski and M. Adamowski for help with data analysis; *Arabidopsis* Stock Centre for providing seed stocks; M. Fendrych for scientific discussions and technical help in confocal imaging; and M. De Cock for help in preparing the manuscript. The research leading to these results has received funding from the European Research Council (ERC) under the European Union's Seventh Framework Programme (FP7/2007-2013)/ERC Grant Agreement 282300.

1. Bennett M, Bellini C, Van Der Straeten D (2005) Integrative biology: Dissecting cross-talk between plant signalling pathways. *Physiol Plant* 123:109.
2. Benková E, Hejátko J (2009) Hormone interactions at the root apical meristem. *Plant Mol Biol* 69:383–396.
3. Weiss D, Ori N (2007) Mechanisms of cross talk between gibberellin and other hormones. *Plant Physiol* 144:1240–1246.
4. Fu X, Harberd NP (2003) Auxin promotes *Arabidopsis* root growth by modulating gibberellin response. *Nature* 421:740–743.
5. Nemhauser JL, Hong F, Chory J (2006) Different plant hormones regulate similar processes through largely nonoverlapping transcriptional responses. *Cell* 126:467–475.
6. Moubayidin L, et al. (2010) The rate of cell differentiation controls the *Arabidopsis* root meristem growth phase. *Curr Biol* 20:1138–1143.
7. Gallego-Bartolomé J, Kami C, Fankhauser C, Alabadí D, Blázquez MA (2011) A hormonal regulatory module that provides flexibility to tropic responses. *Plant Physiol* 156:1819–1825.
8. Willige BC, Isono E, Richter R, Zourelidou M, Schwechheimer C (2011) Gibberellin regulates PIN-FORMED abundance and is required for auxin transport-dependent growth and development in *Arabidopsis thaliana*. *Plant Cell* 23:2184–2195.
9. Löfke C, et al. (2013) Asymmetric gibberellin signaling regulates vacuolar trafficking of PIN auxin transporters during root gravitropism. *Proc Natl Acad Sci USA* 110:3627–3632.
10. Adamowski M, Friml J (2015) PIN-dependent auxin transport: Action, regulation, and evolution. *Plant Cell* 27:20–32.
11. Vanneste S, Friml J (2009) Auxin: A trigger for change in plant development. *Cell* 136:1005–1016.
12. Kleine-Vehn J, et al. (2008) Differential degradation of PIN2 auxin efflux carrier by retromer-dependent vacuolar targeting. *Proc Natl Acad Sci USA* 105:17812–17817.
13. Ambrose C, et al. (2013) CLASP interacts with sorting nexin 1 to link microtubules and auxin transport via PIN2 recycling in *Arabidopsis thaliana*. *Dev Cell* 24:649–659.
14. Rademacher W (2000) Growth retardants: Effects on gibberellin biosynthesis and other metabolic pathways. *Annu Rev Plant Physiol Plant Mol Biol* 51:501–531.
15. Geldner N, Friml J, Stierhof Y-D, Jürgens G, Palme K (2001) Auxin transport inhibitors block PIN1 cycling and vesicle trafficking. *Nature* 413:425–428.
16. Dhonukshe P, et al. (2007) Clathrin-mediated constitutive endocytosis of PIN auxin efflux carriers in *Arabidopsis*. *Curr Biol* 17:520–527.
17. Kleine-Vehn J, et al. (2008) ARF GEF-dependent transcytosis and polar delivery of PIN auxin carriers in *Arabidopsis*. *Curr Biol* 18:526–531.
18. Kleine-Vehn J, et al. (2008) Cellular and molecular requirements for polar PIN targeting and transcytosis in plants. *Mol Plant* 1:1056–1066.
19. Seaman MNJ (2012) The retromer complex–Endosomal protein recycling and beyond. *J Cell Sci* 125:4693–4702.
20. Jaillais Y, et al. (2007) The retromer protein VPS29 links cell polarity and organ initiation in plants. *Cell* 130:1057–1070.
21. Nodzyński T, et al. (2013) Retromer subunits VPS35A and VPS29 mediate prevacuolar compartment (PVC) function in *Arabidopsis*. *Mol Plant* 6:1849–1862.
22. Zwiewka M, et al. (2011) The AP-3 adaptor complex is required for vacuolar function in *Arabidopsis*. *Cell Res* 21:1711–1722.
23. Carvalho P, Tirnauer JS, Pellman D (2003) Surfing on microtubule ends. *Trends Cell Biol* 13:229–237.
24. Akhmanova A, Hoogenraad CC (2005) Microtubule plus-end-tracking proteins: Mechanisms and functions. *Curr Opin Cell Biol* 17:47–54.
25. Ambrose JC, Shoji T, Kotzer AM, Pighin JA, Wasteneys GO (2007) The *Arabidopsis CLASP* gene encodes a microtubule-associated protein involved in cell expansion and division. *Plant Cell* 19:2763–2775.
26. Shibaoka H (1993) Regulation by gibberellins of the orientation of cortical microtubules in plant cells. *Aust J Plant Physiol* 20:461–470.
27. Shibaoka H (1994) Plant hormone-induced changes in the orientation of cortical microtubules: Alterations in the cross-linking between microtubules and the plasma membrane. *Annu Rev Plant Physiol Plant Mol Biol* 45:527–544.
28. Morejohn LC (1991) The molecular pharmacology of plant tubulin and microtubules. *The Cytoskeletal Basis of Plant Growth and Form*, ed Lloyd CW (Academic, San Diego), pp 29–43.
29. Nakamura M, Naoi K, Shoji T, Hashimoto T (2004) Low concentrations of propyzamide and oryzalin alter microtubule dynamics in *Arabidopsis* epidermal cells. *Plant Cell Physiol* 45:1330–1334.
30. Morejohn LC, Fosket DE (1991) The biochemistry of compounds with anti-microtubule activity in plant cells. *Pharmacol Ther* 51:217–230.
31. Lin D, et al. (2013) Rho GTPase signaling activates microtubule severing to promote microtubule ordering in *Arabidopsis*. *Curr Biol* 23:290–297.
32. Nakamura M, Ehrhardt DW, Hashimoto T (2010) Microtubule and katanin-dependent dynamics of microtubule nucleation complexes in the acentrosomal *Arabidopsis* cortical array. *Nat Cell Biol* 12:1064–1070.
33. Buschmann H, et al. (2004) Helical growth of the *Arabidopsis* mutant *tortifolia1* reveals a plant-specific microtubule-associated protein. *Curr Biol* 14:1515–1521.
34. Peng J, et al. (1997) The *Arabidopsis GAI* gene defines a signaling pathway that negatively regulates gibberellin responses. *Genes Dev* 11:3194–3205.
35. Silverstone AL, et al. (2001) Repressing a repressor: Gibberellin-induced rapid reduction of the RGA protein in Arabidopsis. *Plant Cell* 13:1555–1566.
36. Harberd NP (2003) Botany. Relieving DELLA restraint. *Science* 299:1853–1854.
37. Locascio A, Blázquez MA, Alabadí D (2013) Dynamic regulation of cortical microtubule organization through prefoldin-DELLA interaction. *Curr Biol* 23:804–809.
38. Hartl FU, Hayer-Hartl M (2002) Molecular chaperones in the cytosol: From nascent chain to folded protein. *Science* 295:1852–1858.
39. Le Bot N, Tsai M-C, Andrews RK, Ahringer J (2003) TAC-1, a regulator of microtubule length in the *C. elegans* embryo. *Curr Biol* 13:1499–1505.
40. Lundin VF, Srayko M, Hyman AA, Leroux MR (2008) Efficient chaperone-mediated tubulin biogenesis is essential for cell division and cell migration in *C. elegans*. *Dev Biol* 313:320–334.
41. Ueguchi-Tanaka M, Nakajima M, Motoyuki A, Matsuoka M (2007) Gibberellin receptor and its role in gibberellin signaling in plants. *Annu Rev Plant Biol* 58:183–198.
42. Hoepfner S, et al. (2005) Modulation of receptor recycling and degradation by the endosomal kinesin KIF16B. *Cell* 121:437–450.
43. Proszynski TJ, et al. (2005) A genome-wide visual screen reveals a role for sphingolipids and ergosterol in cell surface delivery in yeast. *Proc Natl Acad Sci USA* 102:17981–17986.
44. Sampathkumar A, et al. (2011) Live cell imaging reveals structural associations between the actin and microtubule cytoskeleton in Arabidopsis. *Plant Cell* 23:2302–2313.
45. Simons CT, et al. (2004) Selective contribution of eukaryotic prefoldin subunits to actin and tubulin binding. *J Biol Chem* 279:4196–4203.
46. Scheuring D, et al. (2016) Actin-dependent vacuolar occupancy of the cell determines auxin-induced growth repression. *Proc Natl Acad Sci USA* 113:452–457.
47. Leitner J, et al. (2012) Lysine63-linked ubiquitylation of PIN2 auxin carrier protein governs hormonally controlled adaptation of Arabidopsis root growth. *Proc Natl Acad Sci USA* 109:8322–8327.
48. Abas L, Luschnig C (2010) Maximum yields of microsomal-type membranes from small amounts of plant material without requiring ultracentrifugation. *Anal Biochem* 401:217–227.
49. Friml J, Benková E, Mayer U, Palme K, Muster G (2003) Automated whole mount localisation techniques for plant seedlings. *Plant J* 34:115–124.

Supporting Information

Salanenka et al. 10.1073/pnas.1721760115

SI Materials and Methods

Lines. *PIN2::PIN2-GFP* (1), *pat4-1, pat4-1×PIN2-GFP* (2), *snx1-1, SNX-GFP* (3), *snx1-1×PIN2-GFP* (4), *pat3-3, pat3-3×PIN2-GFP* (5), *FYVE-GFP* (6), *ARA7-GFP* (7), *BRI1::BRI1-GFP* (8), *PGP19::PGP19-GFP* (9), *UBQ::PIP1;4-mCherry* (10), *clasp1* (11), *MAP4-GFP* (12), *EB1b-GFP* (13), *GFP-CLASP1, clasp1xPIN2-GFP* (14), quintuple *della* mutant, *pGAI::gai-1-GR* (15), *gaiΔ17* (16), *pfd3* and *pfd5* (17), *pfd6* (18), and *eir1-1* (19) were described previously. The *ktn1* (SAIL_343_D12) mutant was purchased from the *Arabidopsis* Biological Resource Center, and *tor1-1* (N378) was purchased from the Nottingham *Arabidopsis* Stock Centre.

Growth Conditions. Three percent chlorine gas was used to sterilize seeds overnight. Plants were grown vertically on half-strength MS medium, including vitamins (Duchefa), with 1% (wt/vol) sucrose and 0.5 g/L 2-(*N*-morpholino) ethanesulfonic acid (pH 5.7), under a 16-h light/8-h dark photoperiod at 22/18 °C. All experiments were carried out in the light period.

Plasmid Constructs and Plant Transformation. *UBQ::VENUS:TUA6* was created using the Gateway cloning system by introducing the coding sequence of the *TUA6* gene (At4g14960) with stop codon into the pDONR P2r-P3 vector (Invitrogen). The *UBQ10* promoter was created by cloning 2 kb upstream of the start codon of the *UBIQUITIN 10* gene (AT4G05320) into the pDONRP4-P1r vector (Invitrogen). The *VENUS* sequence was cloned into pDONR221 (Invitrogen). These three fragments were then assembled into the pK7m34GW destination vector (https://gateway.psb.ugent.be/). Col-0 plants were transformed using standard floral dip procedures and transgenic plants were selected on MS medium +1% sucrose plates containing 50 μg/mL kanamycin. In the T2 generation, fluorescent lines that segregated as single locus were selected and propagated into the T3 generation. *pPIN2::PIN2:DENDRA* was generated by replacing the *GFP* fragment of the *pPIN2::PIN2:GFP* construct (20) with *DENDRA*. Mutant *eir1-1* plants were used for transformation and selected on BASTA. To generate *pPIN2::NLS-GFP*, 1,397 bp *PIN2* promoter sequence was cloned into pDONRP4-P1r and *NLS-GFP* coding sequence into pENTR-L1-L2. Both entry clones were assembled in pB7m24GW,3 (https://gateway.psb.ugent.be/) to generate the *pPIN2::NLS-GFP* expression clone, which was transformed into Col-0 plants by floral dip; positive T1 transformants and single-insert T2 lines were selected on BASTA. *pPIN2::PIN2:mCherry* was generated by replacing of the *Venus* tag with *mCherry* by cloning it via NaeI/AvrII into *pPZP-PIN2::PIN2:Venus* (20). Confirmed clones were transformed into *eir1-4* plants, and resulting T2/T3 progeny was tested for complementation and reporter expression. To generate estradiol-inducible *XVE>>PIN2-GFP*, PIN2-GFP fragment was cloned into pDONR221 (Invitrogen) and via LR reaction introduced into Gateway vector pMDC7 (21).

Immunolocalization of the PIN2 Protein. Antibodies were diluted as follows: 1:1,000 for anti-PIN2 serum and incubated for 4 h (1) and 1:600 for CY3-conjugated goat/anti-rabbit secondary antibody (Dianova) and incubated for 4 h. The PM signal was measured and quantified in 16 cells per root in eight individual seedlings.

Drug Application and Experimental Conditions. Paclobutrazol [1 μM final concentration (f.c.)], GA_3 (50 μM f.c.), oryzalin (20 μM and 10 μM f.c.), BFA (50 μM f.c.), and DEX (10 μM f.c.) were used for treatments. Mock treatments were done with equal amounts of solvent (DMSO/ethanol). Double drug treatments with taxol, oryzalin, or BFA were carried out with a 30-min pretreatment followed by a concomitant drug treatment for the indicated duration. All independent experiments were done at least in triplicate, with a minimum of eight individual plants.

Dark treatments to visualize the vacuolar degradation of PIN2 were done as described previously (4). To evaluate the PIN2 amount in lytic vacuoles, a square of the size of a cell, excluding the PM, was used for quantification. Images were collected at the transition zone.

Fluorescent measurements were done on the original CLSM image files. A rectangular ROI at the PM was used for PM signal intensity quantification, and the PM signal was measured in 16 epidermal cells, including trichoblasts and atrichoblasts in eight individual roots. The intensity of the fluorescent signals was measured with the Fiji software, and the images were processed in Adobe Photoshop CS5.1 (Adobe systems). Graphs were generated with BoxPlotR (shiny.chemgrid.org/boxplotr/) or Microsoft Excel. Data represent means of eight or more roots per treatment and 16 cells per root; Student's test was used to evaluate significant differences, $*P \leq 0.05$, $**P \leq 0.005$.

Western Blotting. The PIN2 and SNX1 protein abundance in membrane and soluble fractions were evaluated as previously described in ref. 22. For Western blot analysis of PIN2 in Col-0 plants, affinity purified rabbit anti-PIN2 serum in dilution 1:2,000 was used. A mouse monoclonal GFP antibody in dilution 1:2,000 (JL-8; Clontech) was used for GFP-tagged PIN2 and SNX1 proteins. Detection was performed using anti-rabbit or anti-mouse horseradish peroxidase-conjugated secondary antibodies (1:10,000) and enhanced chemiluminescence substrate (SuperSignal West Femto, Maximum sensitivity substrate; Thermo Scientific). Mouse anti-actin antibody (Sigma) in 1:5,000 dilution was used as an internal control. Blots were recorded on a Peqlab Fusion SL Advance Imager. The intensity of the chemiluminescent signals was measured with the Fiji software.

Quantitative RT-PCR. RNA was extracted with the RNeasy mini kit (Qiagen) from excised root tips of 5-d-old seedlings. A DNase treatment with the RNase-free DNase (Qiagen) was carried out for 15 min at 25 °C. Poly(dT) cDNA was prepared from 1 μg of total RNA with the iScript cDNA Synthesis Kit (Biorad) and analyzed on a LightCycler 480 II (SW1.5.1 Version; Roche Diagnostics) with the SYBR Green I Master kit (Roche Diagnostics) according to the manufacturer's instructions. Targets were quantified with specific primer pairs designed with the Beacon Designer 4.0 (Premier Biosoft International). All PCRs were performed in technical triplicates. Expression levels were first normalized to UBQ10 or PP2A expression levels and then to the respective expression levels in mock. The primers used to quantify gene expression levels are listed in Fig. S5*E*.

1. Abas L, et al. (2006) Intracellular trafficking and proteolysis of the *Arabidopsis* auxin-efflux facilitator PIN2 are involved in root gravitropism. *Nat Cell Biol* 8:249–256, and correction (2006) 8:424.
2. Zwiewka M, et al. (2011) The AP-3 adaptor complex is required for vacuolar function in *Arabidopsis*. *Cell Res* 21:1711–1722.
3. Jaillais Y, Fobis-Loisy I, Miège C, Rollin C, Gaude T (2006) AtSNX1 defines an endosome for auxin-carrier trafficking in *Arabidopsis*. *Nature* 443:106–109.
4. Kleine-Vehn J, et al. (2008) Differential degradation of PIN2 auxin efflux carrier by retromer-dependent vacuolar targeting. *Proc Natl Acad Sci USA* 105:17812–17817.
5. Nodzyński T, et al. (2013) Retromer subunits VPS35A and VPS29 mediate prevacuolar compartment (PVC) function in *Arabidopsis*. *Mol Plant* 6:1849–1862.
6. Vermeer JEM, et al. (2006) Visualization of PtdIns3*P* dynamics in living plant cells. *Plant J* 47:687–700.
7. Ueda T, Yamaguchi M, Uchimiya H, Nakano A (2001) Ara6, a plant-unique novel type Rab GTPase, functions in the endocytic pathway of *Arabidopsis thaliana*. *EMBO J* 20:4730–4741.
8. Geldner N, Hyman DL, Wang X, Schumacher K, Chory J (2007) Endosomal signaling of plant steroid receptor kinase BRI1. *Genes Dev* 21:1598–1602.

9. Mravec J, et al. (2008) Interaction of PIN and PGP transport mechanisms in auxin distribution-dependent development. *Development* 135:3345–3354.
10. Boursiac Y, et al. (2005) Early effects of salinity on water transport in Arabidopsis roots. Molecular and cellular features of aquaporin expression. *Plant Physiol* 139:790–805.
11. Ambrose JC, Shoji T, Kotzer AM, Pighin JA, Wasteneys GO (2007) The *Arabidopsis CLASP* gene encodes a microtubule-associated protein involved in cell expansion and division. *Plant Cell* 19:2763–2775.
12. Marc J, et al. (1998) A *GFP-MAP4* reporter gene for visualizing cortical microtubule rearrangements in living epidermal cells. *Plant Cell* 10:1927–1940.
13. Chan J, Calder GM, Doonan JH, Lloyd CW (2003) EB1 reveals mobile microtubule nucleation sites in *Arabidopsis*. *Nat Cell Biol* 5:967–971.
14. Ambrose C, Allard JF, Cytrynbaum EN, Wasteneys GO (2011) A CLASP-modulated cell edge barrier mechanism drives cell-wide cortical microtubule organization in Arabidopsis. *Nat Commun* 2:430.
15. Locascio A, Blázquez MA, Alabadí D (2013) Dynamic regulation of cortical microtubule organization through prefoldin-DELLA interaction. *Curr Biol* 23:804–809.
16. Peng J, et al. (1997) The *Arabidopsis GAI* gene defines a signaling pathway that negatively regulates gibberellin responses. *Genes Dev* 11:3194–3205.
17. Rodríguez-Milla MA, Salinas J (2009) Prefoldins 3 and 5 play an essential role in *Arabidopsis* tolerance to salt stress. *Mol Plant* 2:526–534.
18. Gu Y, et al. (2008) Prefoldin 6 is required for normal microtubule dynamics and organization in *Arabidopsis*. *Proc Natl Acad Sci USA* 105:18064–18069.
19. Xu J, Scheres B (2005) Dissection of Arabidopsis ADP-RIBOSYLATION FACTOR 1 function in epidermal cell polarity. *Plant Cell* 17:525–536.
20. Leitner J, et al. (2012) Lysine63-linked ubiquitylation of PIN2 auxin carrier protein governs hormonally controlled adaptation of Arabidopsis root growth. *Proc Natl Acad Sci USA* 109:8322–8327.
21. Curtis MD, Grossniklaus U (2003) A gateway cloning vector set for high-throughput functional analysis of genes in planta. *Plant Physiol* 133:462–469.
22. Abas L, Luschnig C (2010) Maximum yields of microsomal-type membranes from small amounts of plant material without requiring ultracentrifugation. *Anal Biochem* 401:217–227.

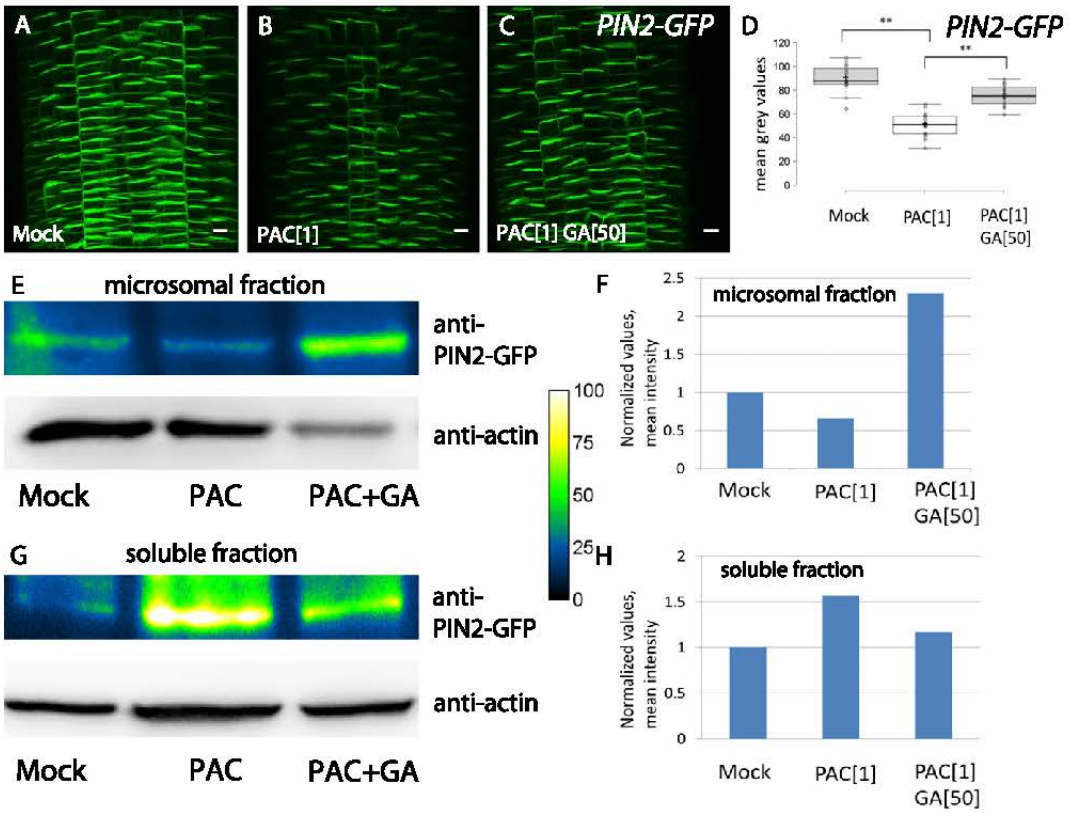


Fig. S1. GA availability led to PIN2-GFP abundance changes detected by confocal microscopy and Western blot. (*A–C*) PIN2-GFP signal at the PM in untreated seedlings (*A*), pretreated with 1 μM PAC (*B*) and treated with 50 μM GA for 4 h after PAC pretreatment (*C*). (*D*) Quantification of PIN2-GFP signals in the root epidermis (*A–C*). (*E–H*) Changes in PIN2-GFP protein levels detected by Western blot. Decrease in microsomal (membrane) PIN2-GFP protein upon PAC treatment and increase upon GA in *Arabidopsis* root tips (*E*). Enrichment of PIN2-GFP in soluble fraction coincided with PAC treatment and was reversed by GA (*G*). Western blot quantifications (*F* and *H*). Color code was used for PIN2-GFP amount visualization on Western blots. (Scale bar: 10 μm.)

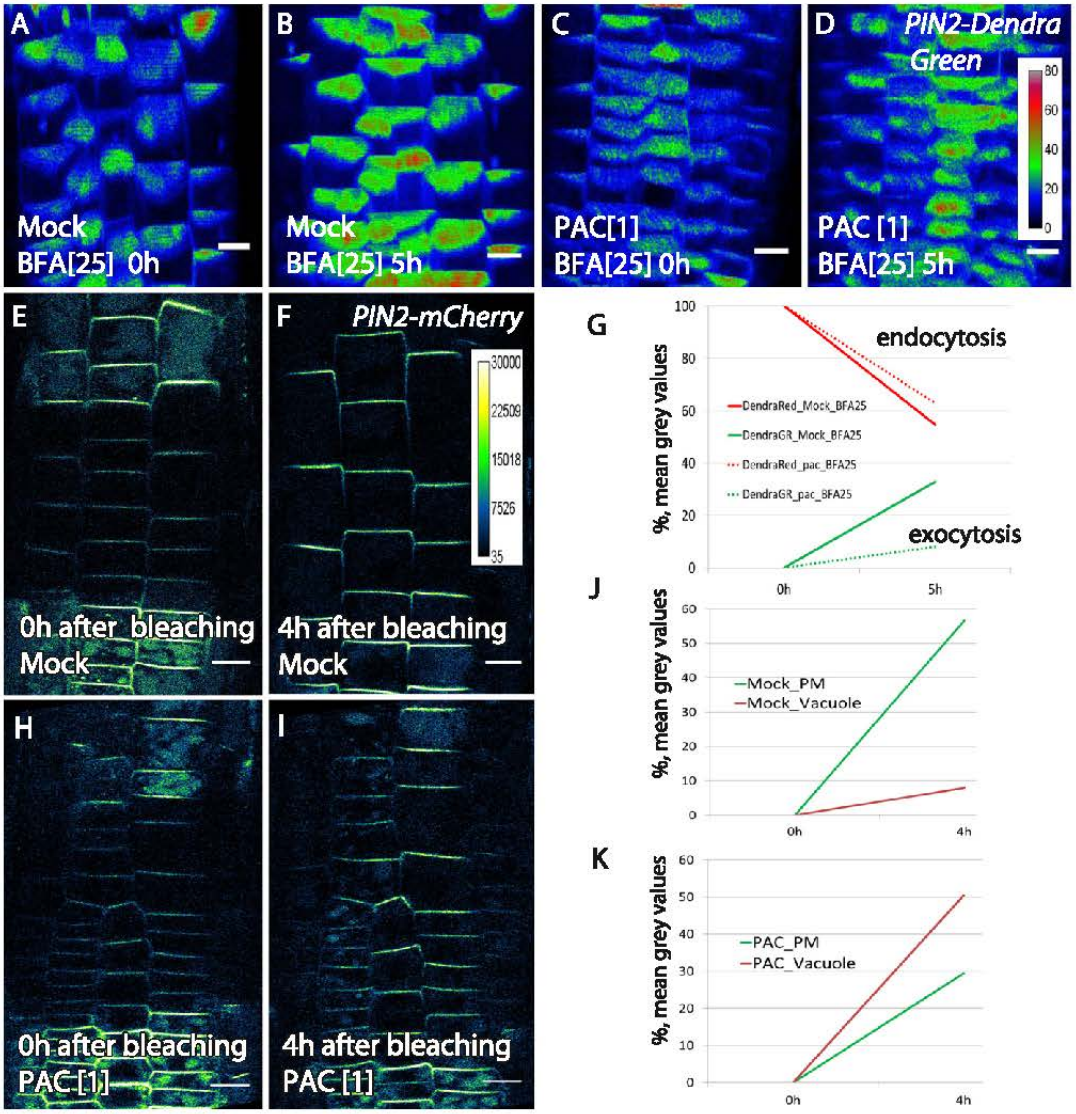


Fig. S2. GA effects on vacuolar delivery and recycling of the PM-located and de novo synthesized PIN2. (*A–D*) GA effects on the PIN2 vacuolar trafficking and exocytosis independent of BFA action. Photoconversion of PIN2-Dendra on seedlings grown on control medium (*A* and *B*) or 1 μM PAC (*C* and *D*) plates and pretreated for 30 min with 25 μM BFA. After 5 h of treatment with BFA, seedlings were imaged. Green signal recovery at the PM reflects de novo PIN2 delivery. Note the faster accumulation of de novo PIN2 at the PM in untreated (*A* and *B*) versus PAC-treated (*C* and *D*) seedlings. (*G*) Evaluation based on PIN2-Dendra red and green endocytosis and exocytosis rates in BFA-treated seedlings. (*E*, *F*, *H*, and *I*) PM localization of PIN2-mCherry 4 h after bleaching in untreated roots (*E* and *F*) compared with the vacuolar accumulation of PIN2-mCherry in PAC-treated roots (*H* and *I*). (*J* and *K*) Graphical representation of PM and vacuolar PIN2-mCherry distribution in mock (*J*) and PAC-treated (*K*) roots. Color code was used for PIN2-Dendra green and PIN2-mCherry intensity visualization. (Scale bar: 10 μm.)

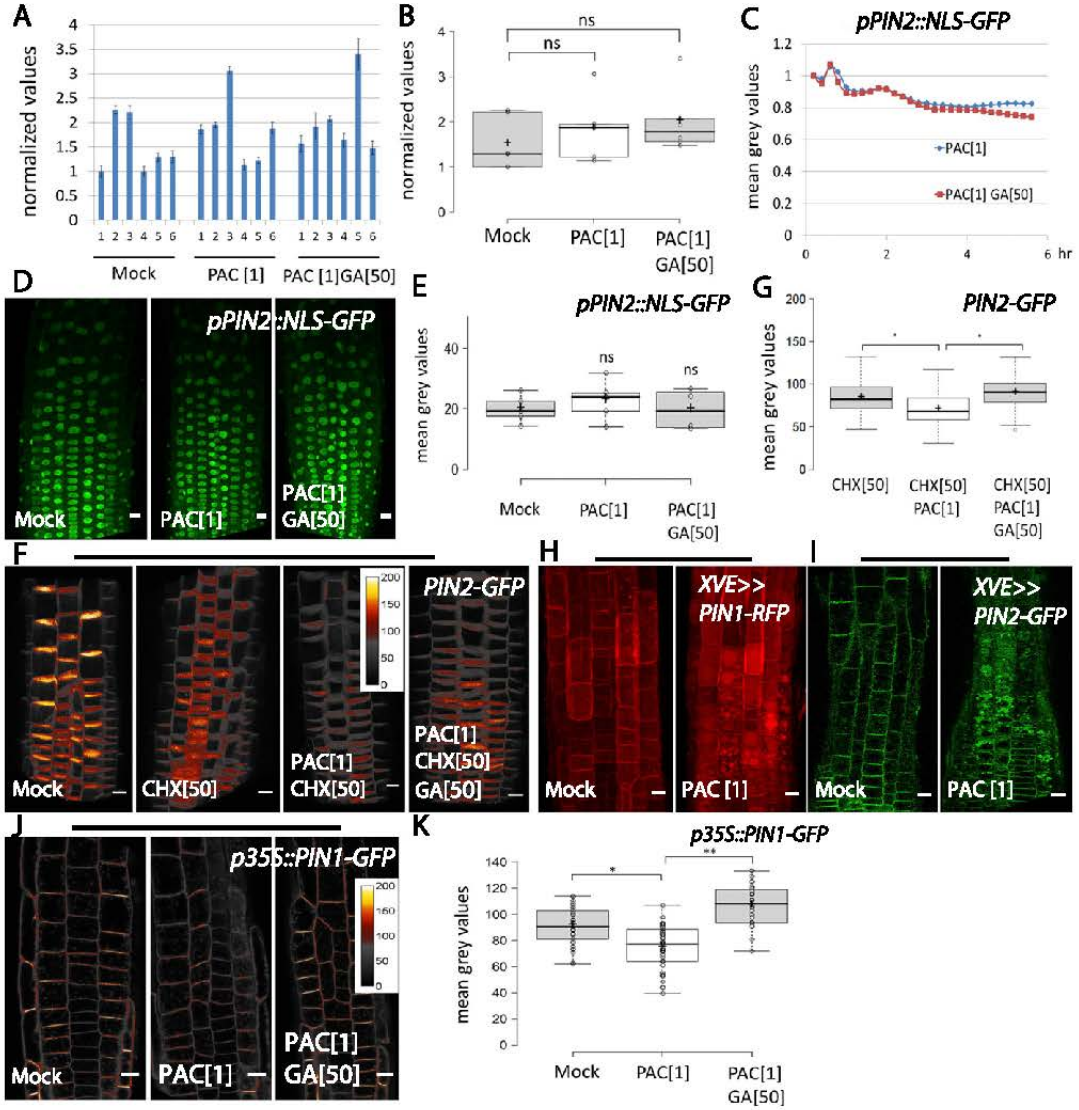


Fig. S3. GA effects on PIN-protein abundance. (*A* and *B*) qRT-PCR showed no changes in the levels of *PIN2* transcription upon PAC or GA treatments. Six independent mRNA repeats were included for each condition (*A*) and pooled together for more concise statistics (*B*). (*C–E*) GA did not affect the activity of the *PIN2* promoter. (*C*) Dynamics of *PIN2* promoter activity evaluated based on nuclear signal of pPIN2::NLS-GFP showing no differences in roots pretreated with PAC only versus PAC+GA–treated roots. (*D* and *E*) Unaffected pPIN2::NLS-GFP signal by PAC (1 d) or PAC+GA (1 d PAC+4 h GA) treatments. (*F* and *G*) Recovery of PAC-compromised PIN2 level at the PM by GA in the presence of CHX, confirming a protein synthesis-independent regulation of PIN abundance by GA. (*H–K*) GA deficiency responsiveness of PIN2 and PIN1 proteins driven by estradiol-induced (XVE>>) and 35S-promoters. This confirms a PIN-promoter–independent regulation by GA and the effect on PIN protein abundance. (*H* and *I*) Vacuolar retargeting of XVE >> PIN1-RFP and XVE >> PIN2-GFP in PAC conditions. (*J* and *K*) Decrease in membrane stability of 35S::PIN1-GFP protein upon PAC and the reverse effect by GA (*J*). Signal quantification (*K*). Color code was used for PIN2-GFP (*F*) and 35S::PIN1-GFP (*J*) intensity visualization. (Scale bar: 10 μm.)

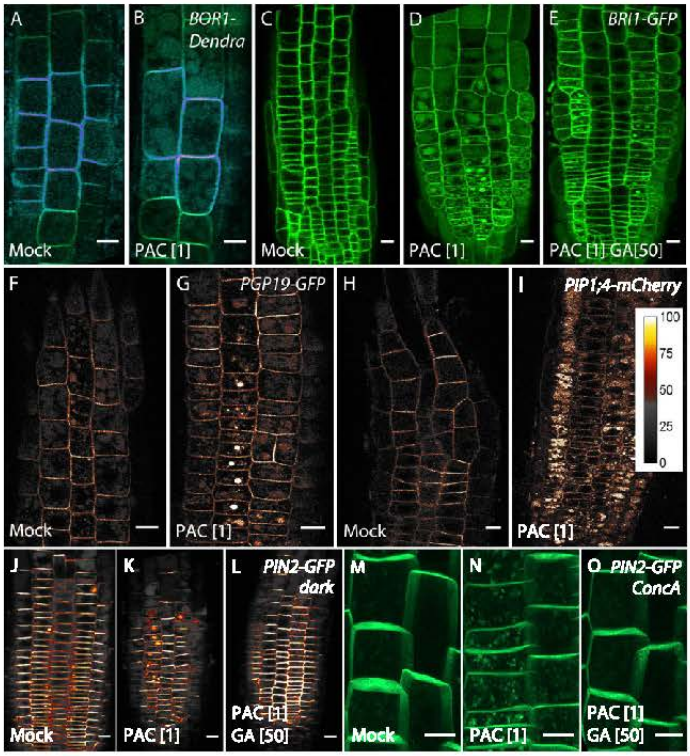
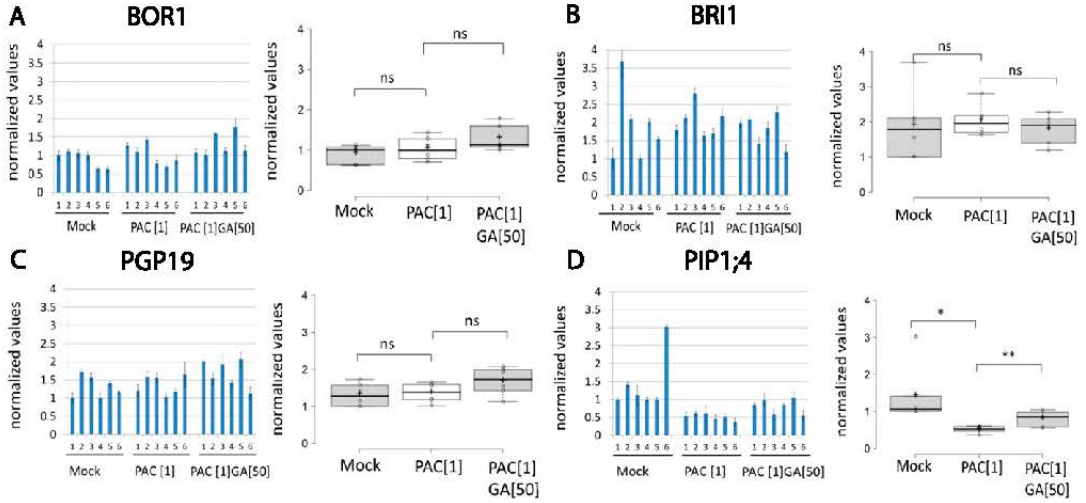


Fig. S4. GA effects on vacuolar targeting of different cargo proteins. (*A* and *B*) Increased vacuolar targeting of BOR1-Dendra in 1 μM PAC-treated seedlings (*B*) compared with untreated mock (*A*). (*C*–*E*) Vacuolar localization of BRI-GFP in 1 μM PAC-treated seedlings (*D*) compared with prevalent PM-residing BRI1-GFP in mock (*C*) and 50 μM GA-treated seedlings (*E*). (*F*–*I*) Increased vacuolar targeting of PGP19-GFP (*G*) and PIP1;4-mCherry (*I*) in PAC-treated seedlings compared with PM-accumulated PGP19-GFP (*F*) and PIP1;4-mCherry (*H*) in mock seedlings. (*J*–*O*) Visualization of increased vacuolar targeting of PIN2-GFP upon PAC treatment in dark (*K*) and 1 μM concanamycin A (*N*) conditions in comparison with mock (*J* and *M*) and GA-treatment (*L* and *O*). Color code was used for PGP19-GFP, PIP1;4-mCherry, and PIN2-GFP (in dark) intensity visualization. (Scale bar: 10 μm.)



E qRT-PCR primers

AGI code (Gene name)	Forward primer sequence	Reverse primer sequence
AT5G57090 (PIN2)	TCACGACAACCTCGCTACTAAAGC	TGCCCATGTAAGGTGACTTTCCC
AT2G47160 (BOR1)	GCTCCAGCTTTACCCTTCAATCTC	TCTCCTCTGCTTCGGGTCATAA
	TCACGGCTGTTCAAACCTTAGC	GGCTCTGCAACACCGAGAATAAG
AT4G39400 (BRI1)	TGGCGATGGGATTGTTGTTCTC	TCTCCAACTCCGCCTCTTTCT
	GACGAGCGGCTTCTTGTGTATG	GCCGTGTGGACCAGTTTAGTTT
AT3G28860 (PGP19)	GGATGGCTAAAGGGTTGGGTTTAG	GCCTTTCCTCCATCGGTTTGT
	TCCAGCAGAAGCAGAGAAGAAGA	GCACCAAGAGAACCAACGAACA
AT4G00430 (PIP1;4)	AGTCCACCGACAAGGACTACAA	ACTCAGCTATTCCGGCTCTGT
	GCAATGTCTTGGAGCCATCTGT	GTAGCCATGAGCAACGGTGTTAG
AT4G05320 (UBQ)	CACACTCCACTTGGTCTTGCG	TGGTCTTTCCGGTGAGAGTCTTCA
AT1G13320 (PP2A)	TAACGTGGCCAAAATGATGC	GTTCTCCACAACCGCTTGGT

Fig. S5. qRT-PCR results of selected cargoes mostly unaffected by PAC or GA treatments. (*A–C*) Insignificantly different levels of mRNA of *BOR1* (*A*), *BRI1* (*B*), and *PGP19* (*C*) in mock, PAC, or GA-optimized conditions. (*D*) GA-dependent mRNA levels of *PIP1;4*. Six independent mRNA repeats were performed for each condition and pooled together for statistics. (*E*) Primers used for qRT-PCR of *PIN2* and other protein cargoes.

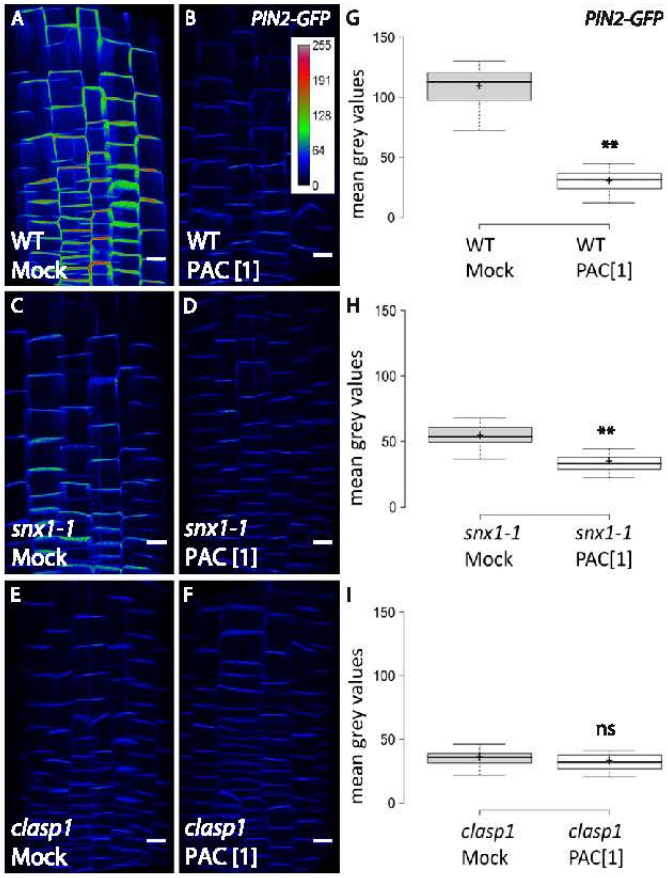


Fig. S6. Mutants compromised in SNX1 and CLASP1 proteins are less sensitive to PAC application. Decrease in PIN2-GFP PM levels was statistically significant but much less profound in *snx1-1* mutant plants treated with PAC (*C*, *D*, and *H*) compared with WT plants (*A*, *B*, and *G*). No significant changes in PIN2-GFP in *clasp1* mutant lines (*E*, *F*, and *I*). Color code was used for PIN2-GFP intensity visualization. (Scale bar: 10 μm.)

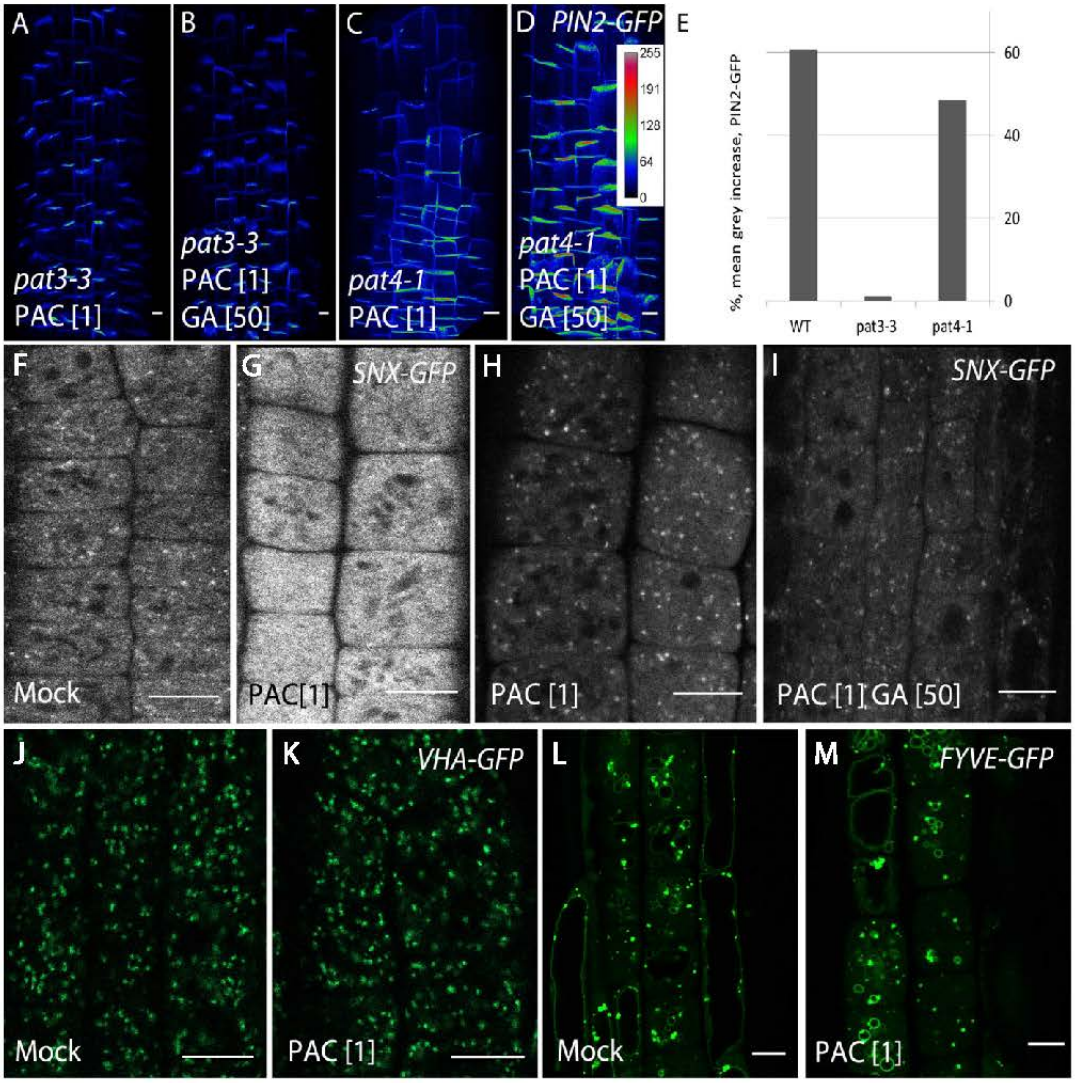


Fig. S7. GA targeting of a trafficking step upstream of the retromer-involving protein degradation. (*A–E*) Unrestored PIN2 at the PM after application of 50 μM GA to the *pat3-3* roots pretreated with 1 μM PAC (*A* and *B*) compared with efficiently restored amount of PIN2 at the PM in *pat4-1* after a similar treatment (*C* and *D*). Quantifications (*E*). (*F* and *G*) Increased cytosolic amount of SNX1-GFP in seedlings treated with 1 μM PAC (*G*) compared with nontreated mock (*F*). (*H* and *I*) Decreased amount of abnormal endosomes within several hours of GA treatment (*I*) compared with PAC-treated seedlings (*H*). (*J–M*) GA deficiency lacking effects on the endosomal compartments labeled with VHA-GFP and FYVE-GFP, in comparison with SNX1-GFP. Unaffected endosomal localization of VHA-GFP (*K*) and FYVE-GFP (*M*) after 1 μM PAC treatment compared with nontreated seedlings (*J* and *L*). Color code was used for PIN2-GFP signal visualization. (Scale bar: 10 μm.)

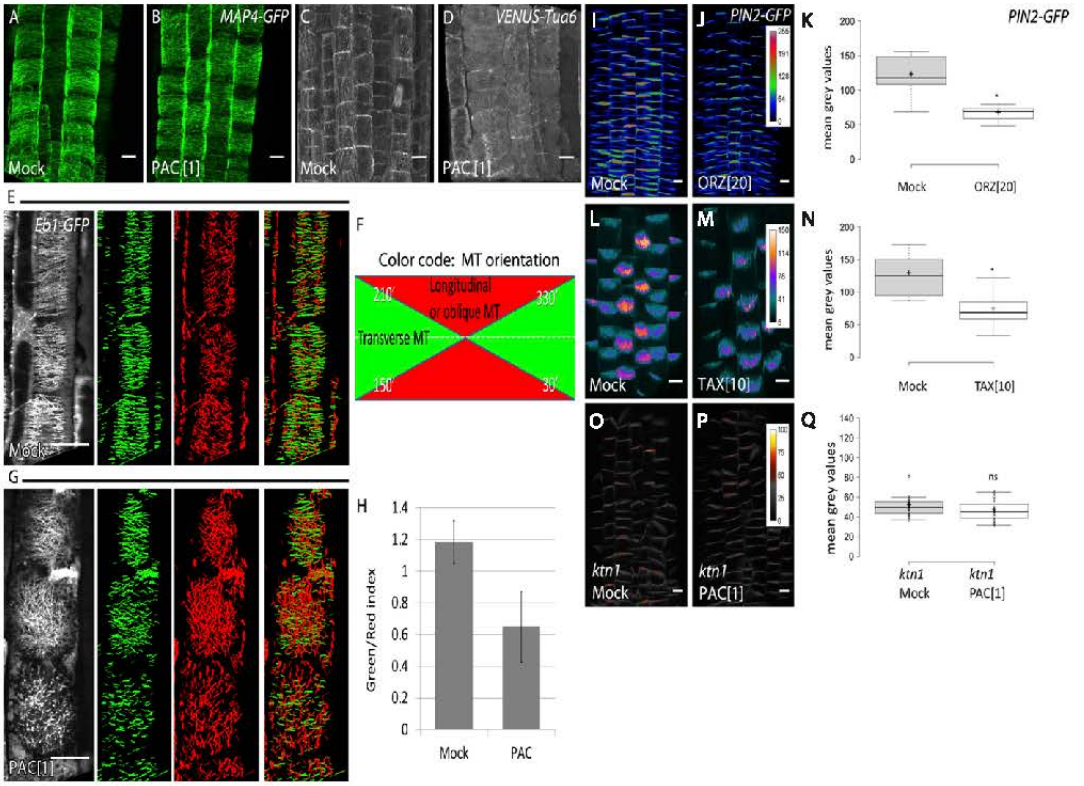


Fig. S8. MT are essential for GA action on PIN2 trafficking. (*A* and *B*) GA effect on MT. More randomized network of MTs in MAP4-GFP seedlings after treatment with 1 μM PAC (*B*) compared with nontreated seedlings (*A*). (*C* and *D*) Confocal images of VENUS-TUA6 after prolonged PAC treatment of roots show an overall decrease in the MT network and increase in the fluorescent signal in the cytoplasm. (*E*–*H*) Reoriented microtubules labeled with Eb1b-GFP show enrichment in longitudinal or oblique direction (red color) upon PAC treatment (*G*) compared with more transversely oriented MTs in GA conditions (*E*). MT orientation was determined based on the angle of MTs toward the horizontal axis and color-coded accordingly (*F*). Green/red index indicates the ratio of transversally oriented MTs to oblique or longitudinal orientation in mock and PAC conditions (*H*). (*I*–*Q*) Depolymerization and stabilization of MTs affect PIN2 abundance. (*I* and *J*) Decrease in PIN2-GFP signal at PM after depolymerization of MTs with 20 μM oryzalin. (*L* and *M*) Taxol-mediated stabilization of MTs leads to a significant drop of PIN2-GFP at PM. (*O* and *P*) No significant changes of PIN2-GFP in the *ktn1* mutant line upon PAC. (*K*, *N*, and *Q*) Quantifications of PIN2-GFP signal after ozyralin (*K*) and taxol (*N*) treatments and in *ktn1* mutant after PAC treatment (*Q*). Color code was used for PIN2-GFP signal visualization. (Scale bar: 10 μm.)

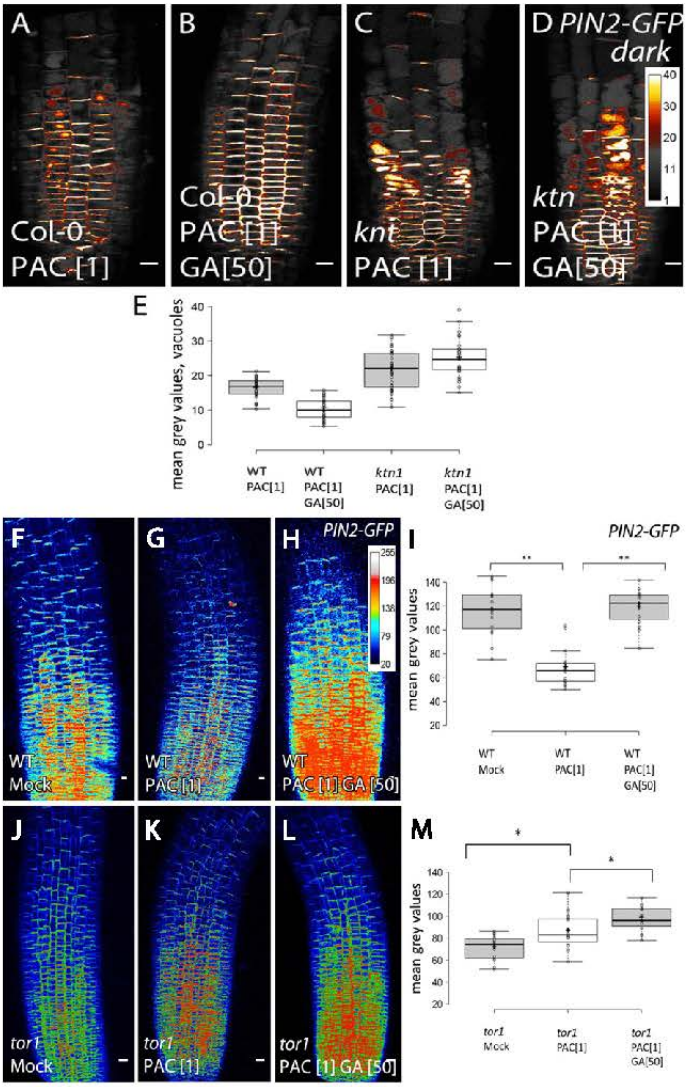


Fig. S9. *ktn1* and *tor1* mutants are insensitive to GA status. (*A–D*) Inability of *ktn1* mutant roots pretreated with PAC to decrease vacuolar PIN2 degradation after GA application (*C* and *D*) compared with GA in Col-0 plants (*A* and *B*). (*E*) Quantifications. (*F–M*) The decrease in PIN2-GFP signal, which was consistently observed in WT roots and rescued by GA application (*F–I*), was not observed in *tor1* mutant (*J–M*). On the contrary, a slight increase in PIN2-GFP level was observed on PAC-containing media in *tor1* roots (*K*). Color code was used for PIN2-GFP signal visualization. (Scale bar: 10 μm.)

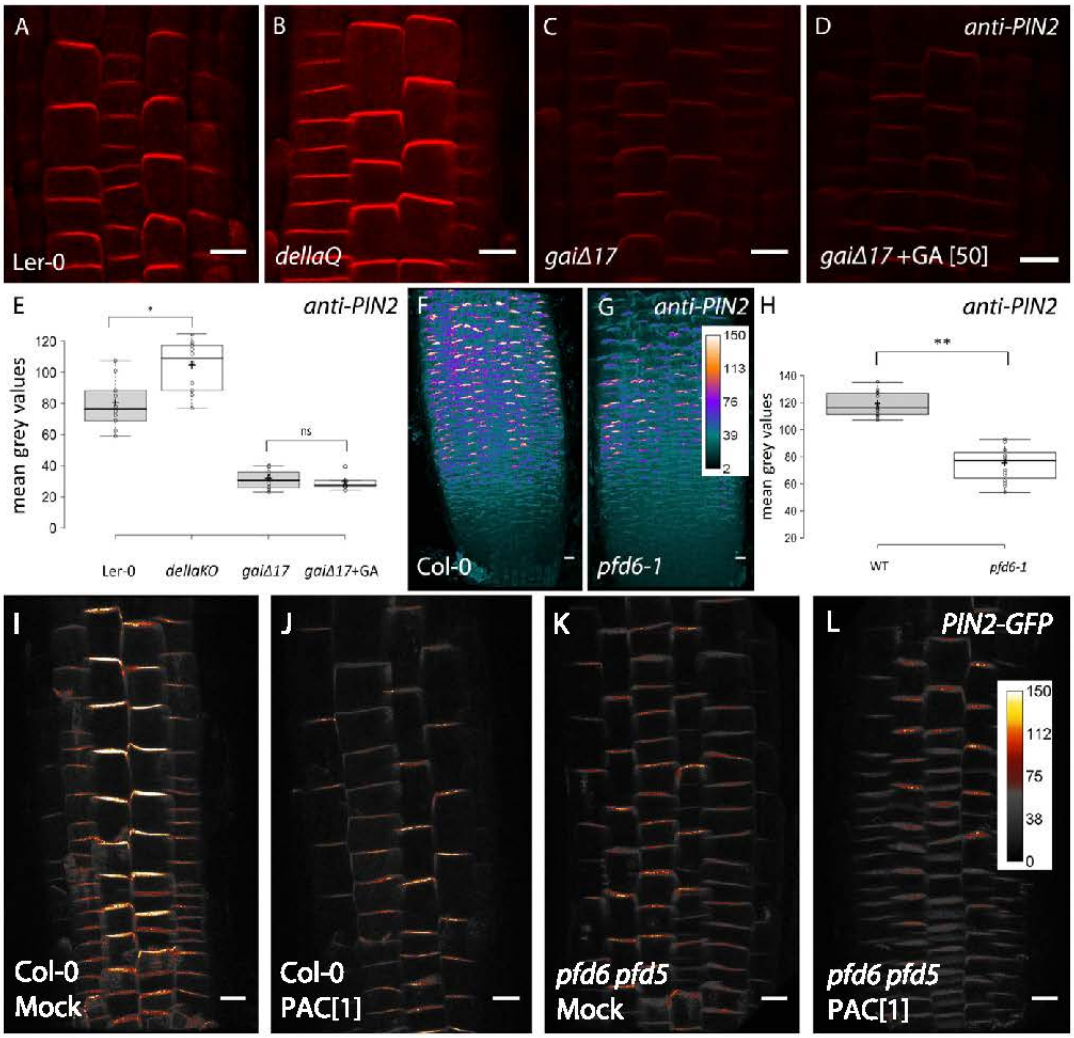


Fig. S10. DELLA and Prefoldin proteins are necessary for PIN2 level regulation. (*A–D*) Immunolocalization of PIN2 at the PM shows an increase of protein in *della* knockout seedlings (*B*) and a decrease in dominant-negative *gaiΔ17* mutants (*C*) compared with *Landsberg erecta-0* wild-type seedlings (*A*). (*D*) Insensitivity of *gaiΔ17* mutants to GA. (*E*) Quantifications. (*F–H*) Reduced PIN2 protein level in the *pfd6-1* mutant seedlings (*G*) compared with wild-type (*F*) seedlings by Z-stack maximum projection analysis of PIN2 immunolocalized samples. (*H*) Quantifications. (*I–L*) Mutants compromised in Prefoldin proteins are less sensitive to PAC application. No significant decrease in PIN2-GFP PM levels was detected in double *pfd5 pfd6* mutant plants treated with PAC (*K* and *L*) compared with WT plants (*I* and *J*). Color code was used for anti-PIN2 CY3 and PIN2-GFP signal visualization. (Scale bar: 10 μm.)

nature plants

LETTERS

https://doi.org/10.1038/s41477-018-0190-1

Rapid and reversible root growth inhibition by TIR1 auxin signalling

Matyáš Fendrych[1,2], Maria Akhmanova[1], Jack Merrin[1], Matouš Glanc[1,2], Shinya Hagihara[3], Koji Takahashi[3], Naoyuki Uchida[3], Keiko U. Torii[3,4] and Jiří Friml[1*]

The phytohormone auxin is the information carrier in a plethora of developmental and physiological processes in plants[1]. It has been firmly established that canonical, nuclear auxin signalling acts through regulation of gene transcription[2]. Here, we combined microfluidics, live imaging, genetic engineering and computational modelling to reanalyse the classical case of root growth inhibition[3] by auxin. We show that *Arabidopsis* roots react to addition and removal of auxin by extremely rapid adaptation of growth rate. This process requires intracellular auxin perception but not transcriptional reprogramming. The formation of the canonical TIR1/AFB–Aux/IAA co-receptor complex is required for the growth regulation, hinting to a novel, non-transcriptional branch of this signalling pathway. Our results challenge the current understanding of root growth regulation by auxin and suggest another, presumably non-transcriptional, signalling output of the canonical auxin pathway.

Plant roots are positively gravitropic[4]. This is essential for plants to colonize land and for water and nutrient uptake. The columella cells of the root tip perceive gravity[5,6], and following gravistimulation redirect the flux of the phytohormone auxin to the lower side of the root[7]. In response to auxin, epidermal cells inhibit their elongation[3,8]. The differential auxin distribution and cell elongation thus leads to bending of the root[8] along the gravity vector (Fig. 1a). Root growth inhibition in response to auxin therefore forms the basis for the gravitropic bending enabling land plants to anchor in soil and utilize its resources. The effect of auxin on root growth has been instrumental to identifying the auxin signalling mechanism. Canonical auxin signalling starts with auxin binding to the TIR1/AFB–Aux/IAA co-receptor complex[9], leading to ubiquitination and degradation of Aux/IAA proteins[2] that act as transcriptional repressors; the TIR1/AFB–Aux/IAA pathway thus acts via modulation of gene transcription. In the shoot, this nuclear signalling cascade seems to be sufficient to regulate auxin-mediated growth promotion and upward growth towards the light[10,11]. Components of the TIR1/AFB–Aux/IAA pathway are also crucial for the root growth inhibition by auxin[12–14], with roots of corresponding mutants being largely resistant to auxin. A decades-long controversy has argued that auxin's effect on root growth is too rapid[15,16] to be explained by the TIR1-mediated transcriptional regulation. A current model attempting to reconcile this contradiction is that auxin is perceived by an unknown cell surface receptor that mediates the rapid, non-transcriptional growth inhibition, which is later reinforced by the TIR1-mediated transcriptional regulation[1,16]. Thus, the mechanism of auxin action on root growth remains unknown. Here, we established an extensive experimental toolkit including a vertical microfluidic confocal microscopy setup to re-examine the auxin-induced growth inhibition with high time resolution, minimal interference and superior control of experimental conditions.

To enable quantitative analysis of root growth response to auxin, roots need to grow along the gravity vector, and any treatment must be extremely gentle to avoid stress that would perturb root growth. We developed a vertical vRootChip (Fig. 1b; Supplementary Fig. 1a), a microfluidic device with pressure-actuated microvalves derived from the RootChip device[17], and performed the experiments using a vertical-stage confocal laser scanning microscope setup[18] (Supplementary Fig. 1b). Roots of *Arabidopsis thaliana* grew vigorously in the microfluidic channels, and in response to the natural auxin indole-3-acetic acid (IAA) inhibited growth seemingly very rapidly (Fig. 1c,d; Supplementary Video 1). Growth inhibition was triggered by nanomolar concentrations of IAA (Fig. 1e) and the rapid response showed a dose response similar to that of roots grown in the presence of IAA over longer periods of time (Supplementary Fig. 3a), suggesting that both might involve one and the same mechanism. Timing of the growth response was comparable to what was reported for calcium and surface pH response[15]. These low concentrations match well the physiological levels of IAA that act during gravitropic bending[19]. The DII-Venus auxin reporter[20] reacted to addition of auxin with very similar dynamics to the growth response (Fig. 1c; Supplementary Fig. 1c); however, the epidermal cells of the elongation zone that are key in auxin reaction did not accumulate this marker in sufficient intensities, and so the DII-Venus dynamics could not be easily compared to the growth response.

Gravitropism is a dynamic process requiring a transient response, and so the ability to recover from the growth inhibition is crucial. Therefore, we analysed the roots' reaction to withdrawal of auxin from the medium. Surprisingly, following IAA removal from the medium, the roots started to resume the growth rate without any detectable lag phase (Fig. 1c,f; Supplementary Video 1). The roots reacted to repetitive addition and removal of IAA by repetitive growth inhibition and resumption, respectively, with very reproducible dynamics (Fig. 1f). In summary, the growth rate of roots is an extremely sensitive and rapid readout of IAA presence in the medium.

Further, we analysed the response to 10 nM IAA addition and removal in a high temporal resolution. For this, we added a fluorescent tracer to determine exactly the moment when IAA reaches the root surface. This approach unequivocally determined that roots initiated growth inhibition in less than 30 s after auxin reached the root surface (Fig. 2a). Following auxin removal, roots started

[1]Institute of Science and Technology (IST) Austria, Klosterneuburg, Austria. [2]Department of Experimental Plant Biology, Faculty of Science, Charles University, Prague, Czechia. [3]Institute of Transformative Biomolecules (WPI-ITbM) and Graduate School of Science, Nagoya University, Chikusa, Nagoya, Japan. [4]Howard Hughes Medical Institute and Department of Biology, University of Washington, Seattle, WA, USA. *e-mail: jiri.friml@ist.ac.at

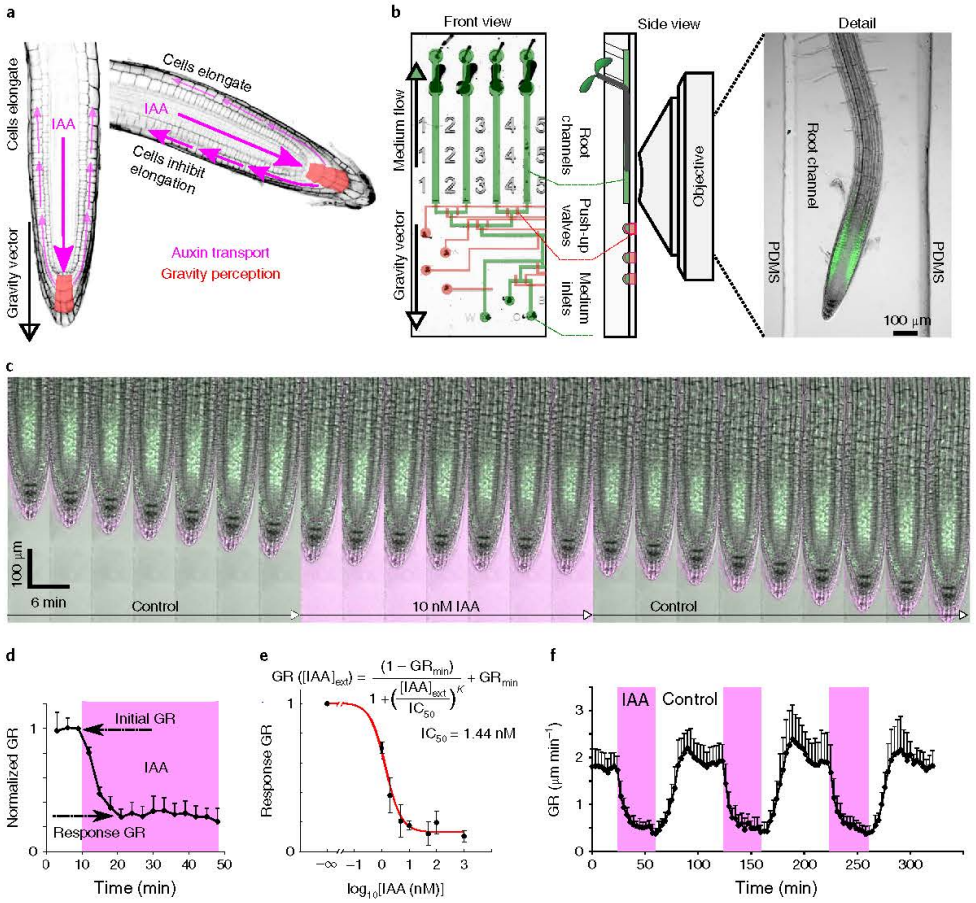


Fig. 1 | Nanomolar concentrations of auxin reversibly inhibit root growth. a, Schematics of auxin fluxes in the root tip during gravitropism. **b**, The vRootChip device with flow channels and pressure valves coloured in green and red, respectively (left). The side view of the device positioned in the vertical microscope (middle) and a root growing in the channel (right). **c**, A timelapse of a DII-Venus root treated with 10 nM IAA; IAA medium contains a fluorescent tracer shown in magenta. **d**, Quantification of root growth rate (GR) during addition of 10 nM IAA, shown in magenta. Normalized growth rate precedent to IAA addition, mean of four roots + s.d. **e**, The dependence of the response growth rate on $[IAA]_{ext}$. See **d** for 'response GR'. Data points are means of $N = 3, 8, 9, 3, 16, 7, 16$ roots for $[IAA]_{ext} = 1, 2, 5, 10, 50, 100, 1{,}000$ nM ± s.d. Best fit (red): $IC_{50} = 1.44$ nM, $GR_{min} = 0.13$. **f**, Quantification of a repetitive treatment of roots with 10 nM IAA (magenta). Mean of seven roots + s.d.

to resume their growth rate within 2 min after the medium was replaced by the auxin-free one (Fig. 2b). Even though the resuming response was more variable than the reaction to IAA application, it was very rapid and faster than previously assumed[3]. We extended the treatment up to 80 min of constant auxin exposure (Fig. 2c,d), and still roots reacted by rapid (less than 3 min) growth resumption when auxin was removed from the medium. These observations do not support any long-term reprogramming of root growth by auxin but suggest a rapidly reversible mechanism of growth regulation.

The speed of the reaction effectively rules out the possibility that transcription and translation of auxin-induced genes participate in the response, as RNA polymerization, messenger RNA processing, transport and translation require minutes in eukaryotes[21] and, accordingly, the earliest auxin-induced mRNA could be detected approximately 5 min after auxin addition[22]. To directly compare the dynamics of TIR1 transcriptional response with the growth reaction, we harnessed the synthetic auxin-responsive promoter DR5 driving the firefly luciferase enzyme[23]. The earliest TIR1-dependent gene expression response could be detected approximately 15 min after addition of auxin to the roots (Fig. 2e) with a full activation only after 40–80 min of the treatment (Fig. 2f). Thus, the dynamics of auxin-mediated regulation of root growth did not at all temporally correlate with transcriptional activation, therefore arguing against the involvement of transcriptional reprogramming in the growth inhibition response. This contrasts with the situation in the hypocotyl, where the DR5::luciferase response matches perfectly with the growth response[10].

To further test the requirement of new protein synthesis for the growth inhibition response, we inhibited protein synthesis by the drug cycloheximide. This experiment needed optimization because cycloheximide on its own influenced root growth (Supplementary Fig. 2a,b), which can be attributed to its reported rapid effect on ion uptake and respiration in plant tissues[24] and to the importance of short-lived proteins in sustaining root growth. Nonetheless, in the presence of lower concentrations of cycloheximide, which were still sufficient to almost completely inhibit the DR5::luciferase

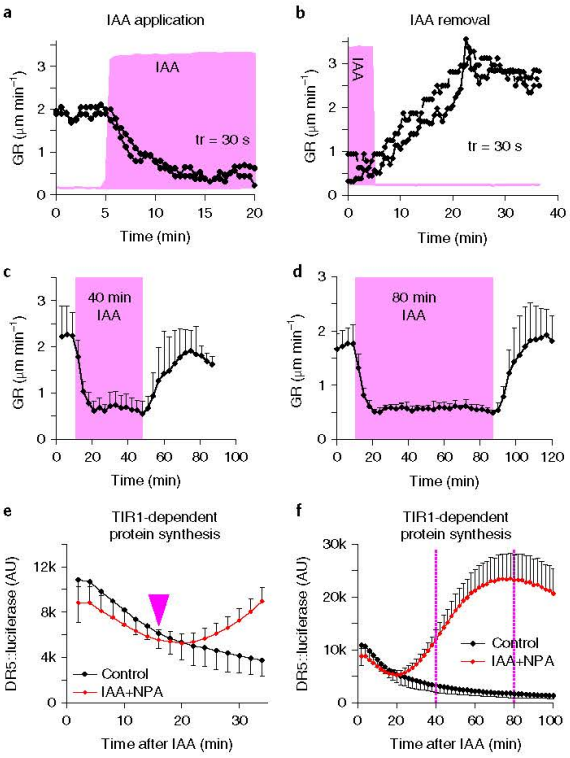


Fig. 2 | Roots rapidly adapt growth rate to auxin application and removal. **a**,**b**,The reaction of two individual roots to the application (**a**) and removal (**b**) of 10 nM IAA. tr, temporal resolution. The presence of IAA is shown as the intensity of the fluorescent tracer (magenta). **c**,**d**, Roots rapidly resume the growth rate after 40 min (**c**) and 80 min (**d**) of 10 nM IAA treatment. Means of four and six roots + s.d. for **c** and **d**, respectively. **e**,**f**, TIR1-dependent protein synthesis in root tips was determined by the luminescence intensity of DR5::luciferase. AU, arbitrary units. The first detectable increase in the signal is marked by an arrowhead (**e**). At 40 and 80 min (dotted lines) the transcriptional response is fully activated (**f**). At time point 0, 100 nM IAA with 1 μM NPA was added. **e**, zoomed region from **f**; means of five root tips ± s.d.

response, auxin was fully capable of rapidly inhibiting root growth (Supplementary Fig. 2b–e). These results show that auxin-mediated growth inhibition does not involve transcriptome reprogramming, not only during the initiation of the response, but also during its duration, which enables a very rapid reversal of the response when auxin concentration decreases. This means that the rapid growth inhibition response is conceptually different from what we thought: it has no distinct 'fast' and 'slow' components; instead, auxin acts as a constantly fast, non-transcriptional growth brake, on the timescale of tens of seconds to hours. It is important to note that protein synthesis is absolutely required for root growth as such (Supplementary Fig. 2a,b), and it is probable that the components of the rapid growth response are under control of the transcriptional auxin pathway[25] that will lead to alteration of the response sensitivity on longer timescales.

Next, we addressed where in the cell the auxin that mediates root growth inhibition is perceived. IAA is transported into cells by influx carriers and partly by diffusion; export out of the cell requires efflux carriers[7] (Fig. 3a). AUX1 influx carrier is expressed in the cells that execute gravitropic bending (Fig. 3b)[26], and roots that lack AUX1 are agravitropic and resistant to auxin-mediated growth inhibition in the long term[27]. In our setup, the *aux1* was almost completely insensitive to low IAA concentrations, while it showed a control-like reaction to higher concentrations (Fig. 3c; Supplementary Video 2). Thus, the *aux1* mutant's dose response was shifted to higher IAA concentrations (Fig. 3d), similarly to the classical experiment on agar surface (Supplementary Fig. 3a). As expected, the *aux1* mutant showed a normal reaction to the membrane-permeable auxin analogue NAA[28] (Fig. 3e; Supplementary Fig. 3b), confirming that the mutant is capable of auxin response, but defective in IAA import. These results show that auxin must pass the plasma membrane to trigger the growth inhibition response. To test whether it is the auxin flux across the membrane itself or the intracellular accumulation of auxin that triggers the response, we pharmacologically inhibited auxin efflux[7] (Fig. 3a). This resulted in a rapid growth inhibition, similar to IAA application but delayed by approximately 3 min (Fig. 3f). It was recently claimed that H^+-IAA symport through AUX1 carriers contributes to membrane depolarization or signalling in the root hair cells[29]. We cannot exclude that the very initial phase of the growth inhibition might be connected directly with flux of the auxin molecules across the plasma membrane; however, altogether the results with the *aux1* mutant, membrane permeable NAA, and auxin efflux inhibitor point to intracellular auxin concentration ($[IAA]_{cell}$) as the basis for growth inhibition.

To understand the dynamics of IAA accumulation, we constructed a computational model of auxin transport in the epidermal cells (Supplementary Fig. 4a–c; Supplementary Text), which incorporated known auxin transport properties of the plasma membrane and capacities of auxin carriers. After IAA addition to the exterior of the modelled wild-type root, the $[IAA]_{cell}$ rapidly reached a steady state concentration approximately 30× higher than the external auxin concentration ($[IAA]_{ext}$), and removal of auxin from the medium resulted in a rapid decrease of $[IAA]_{cell}$ (Fig. 3g; Supplementary Fig. 4d–f). The timing of IAA accumulation was faster than the growth response, making $[IAA]_{cell}$ a plausible input for the response (Fig. 3g). Further, we removed the AUX1 influx carriers to simulate the *aux1* mutant. The model predicted steady state $[IAA]_{cell}$ in *aux1* being only ~2 × $[IAA]_{ext}$ (Supplementary Fig. 4g,h; Supplementary Video 3), which implies that *aux1* growth inhibition should be equal to control if $[IAA]_{ext}$ is 30:2 times higher. This prediction matches well the dose response shift of *aux1* (11.8 ± 3.8), which we determined experimentally (Fig. 3d). This explains why at low $[IAA]_{ext}$ *aux1*' growth is largely insensitive, while at $[IAA]_{ext}$ approximately ≥50 nM *aux1* accumulates enough IAA to react similarly to control roots (Supplementary Text): the response is already close to saturation at these concentrations. This also clarifies the discrepancy with previous reports that stated that *aux1* reacted to IAA almost normally[15,16].

Finally, we used the model and fitted dose-response curves to test whether $[IAA]_{cell}$ exactly maps to the growth rate at any time point (Fig. 3h; Supplementary Text). However, theoretical slopes of growth inhibition and resumption were always steeper than experimental curves, both for *aux1* and control, indicating a short delay between signalling and the full execution of the response. Collectively, these results demonstrate that the rapid auxin-mediated root growth inhibition depends on intracellular IAA accumulation. The auxin receptor that triggers the growth inhibition must therefore be located inside the cell.

Our observations show that the auxin-triggered growth inhibition is a process that starts with intracellular auxin perception but does not involve transcriptome reprogramming, typically associated with the nuclear, TIR1-mediated pathway. However, previous work clearly shows that the TIR1/AFB–Aux/IAA signalling module is required for auxin-mediated root growth inhibition; the key components of this pathway were even identified based on the auxin-insensitivity of the root growth in the corresponding mutants[12–14].

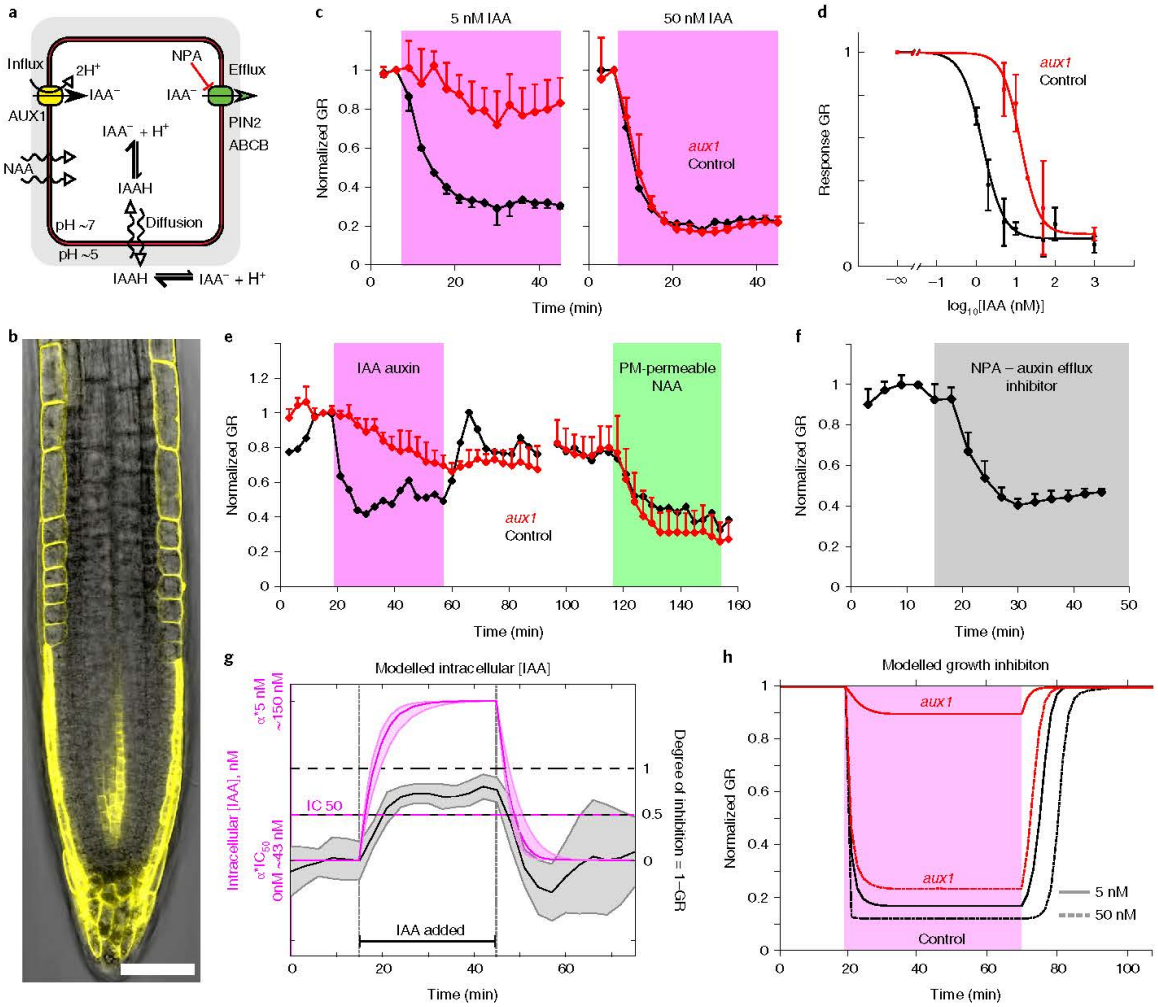


Fig. 3 | Rapid root growth inhibition depends on auxin levels inside the cell. a, A schematic of auxin fluxes in a root epidermal cell. **b**, Auxin influx carrier AUX1-YFP is expressed in the root epidermal cells. Scale bar, 50 µm. **c**, The *aux1* mutant is resistant to 5 nM IAA but reacts to 50 nM IAA. Mean normalized values of 3 (5 nM), 2 (50 nM control) and 5 (50 nM aux1) roots ± s.d. **d**, The dose response of *aux1* is shifted towards higher IAA concentrations by approximately tenfold (control is the same as in Fig. 1e). Fit: $IC_{50}^{aux1} = 17.2\,nM = 11.8 * IC_{50}^{col}$. Data points are means of $N = 10, 4, 2, 9, 7$ roots for $[IAA]_{ext} = 5, 10, 20, 50, 1{,}000$ nM, respectively, ± s.d.; the 1,000 nM was done on an agar plate. **e**, The *aux1* mutant reacts little to 5 nM IAA (magenta) but its reaction to membrane-permeable NAA (100 nM, green) is comparable to control roots. Mean normalized values of five (*aux1*) and two (control) roots ± s.d. **f**, The auxin efflux inhibitor NPA (5 µM, grey) triggers root growth inhibition. Mean normalized values of five roots + s.d. **g**, Auxin accumulation (magenta, simulated) is faster than growth inhibition during application of 5 nM IAA (grey, mean experimental values of 1-GR). Note time delay between $[IAA]_{cell} = \alpha^{col} \cdot IC_{50}$ and (1–GR) = 0.5. Accumulation ratio $\alpha^{col} \cong 30$ (Supplementary Text). Shaded regions correspond to 1 s.d. (grey, $n = 6$ roots) or variation due to s.d. of parameter values (magenta, simulation results). **h**, The modelled theoretical inhibition for *aux1* and control roots.

How do these facts fit together? We analysed the auxin response of *tir1-1/afb2-1/afb3-1* triple mutant (*tir triple*)[30] that lacks three of the six auxin co-receptors, but whose roots still grow rather well. In the vRootChip, the *tir triple* mutant had a less steep immediate response to IAA (Fig. 4a) and showed a dose response shift towards higher IAA concentrations (Fig. 4b, Supplementary Fig. 3a), hinting to a direct involvement of TIR1/AFB in the rapid response to auxin. This was not due to the lack of auxin import, because the *tir triple* mutant was resistant to the membrane-permeable auxin analogue NAA as well (Supplementary Fig. 3b). We further took advantage of the auxin antagonist PEO-IAA[31] that binds TIR1 and blocks the formation of the TIR1–auxin–Aux/IAA complex. Addition of PEO-IAA to growing roots resulted in an increase in growth rate (Supplementary Fig. 5a). However, the most striking effect was observed in roots where growth was partially inhibited by low concentration of IAA: addition of PEO-IAA caused rapid increase in growth rate (Fig. 4c). Parallel monitoring of the dynamics of the DII-Venus marker and root growth revealed a direct correlation between the formation of the TIR1/AFB–auxin–Aux/IAA complex and root growth rate (Figs. 1c and 4c). These observations hint at an unexpected involvement of TIR1-based auxin signalling in the non-transcriptional regulation of root growth.

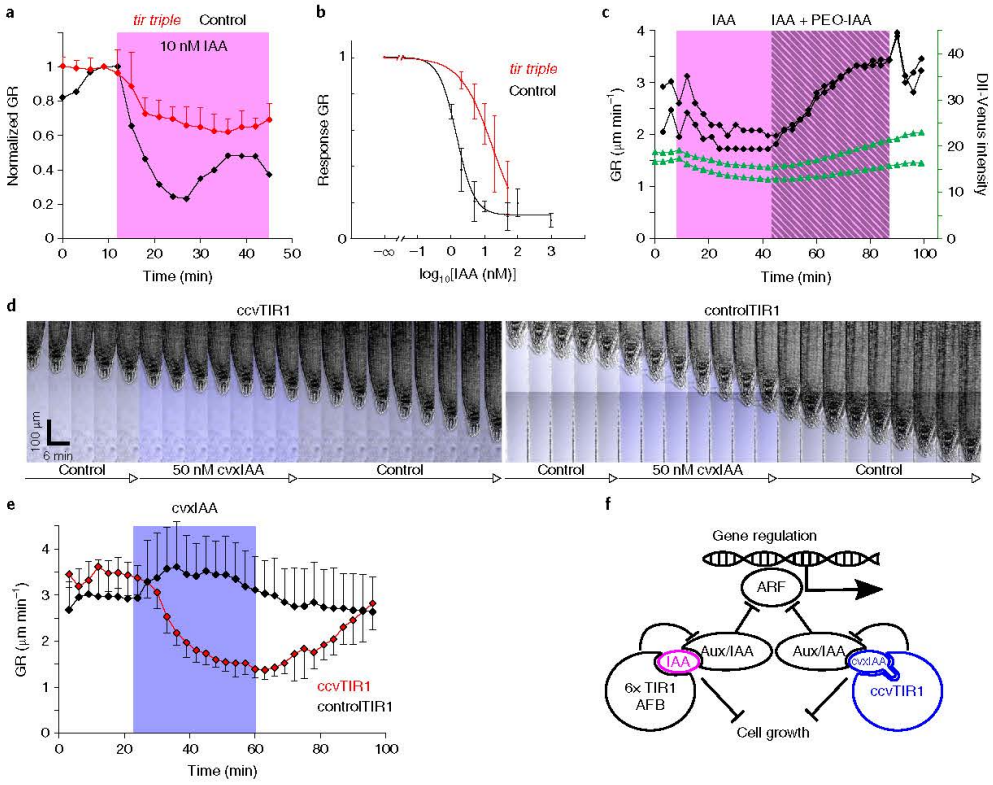


Fig. 4 | Root growth inhibition requires the TIR1/AFB–Aux/IAA auxin co-receptor. a, *tir triple* mutant shows a defect in the response to 10 nM IAA (compare with Fig. 1d,f). Mean normalized growth rate, five and two roots for *tir triple* and control + s.d. **b**, The dose response of the *tir triple* mutant is shifted towards higher IAA concentrations: IC_{50} = 17.8 nM (control is the same as in Fig. 1e). Data points are means of N = 4, 5, 4, 8, 9 roots for $[IAA]_{ext}$ = 2, 5, 10, 20, 50 nM, respectively, ± s.d. **c**, Addition of PEO-IAA results in a rapid reversion of the growth inhibition and an increase in the DII-Venus marker intensity. IAA 1 nM is shaded in magenta; addition of PEO-IAA (10 µM) is marked by grey stripes. DII-Venus intensity (green) was measured in the lateral root cap cells. Growth rates and DII-Venus intensities of two independent roots are shown. **d**, cvxIAA causes root growth inhibition only in the synthetic ccvTIR1 line. Addition of cvxIAA (50 nM) is marked by the tracer fluorescence in blue. **e**, Quantification of the ccvTIR1 (red) and controlTIR1 (black) roots to 50 nM cvxIAA (blue). Means of five roots for each genotype ± s.d. **f**, The formation of the TIR1/AFB–auxin–Aux/IAA complex negatively regulates root growth, probably by a signalling branch that is distinct from the transcriptional regulation function. The synthetic ccvTIR1 receptor and the cvxIAA ligand are shown in blue.

To definitively test the involvement of the TIR1 receptor mechanism in the growth inhibition response directly, we used a synthetic biology approach in which an artificial ligand, convexIAA (cvxIAA), binds to an engineered concave TIR1 (ccvTIR1)[11]. The cvxIAA has no other binding site in the cell, and the ccvTIR1 receptor is unable to bind the natural auxin IAA. Indeed, application of cvxIAA to control roots caused no growth inhibition but cvxIAA application to the *ccvTIR1* roots resulted in growth inhibition very similar to the native IAA-control situation (Fig. 4d, Supplemental Video 4). The cvxIAA was effective at higher concentration (Supplementary Fig. 5b) and both the inhibition and resuming response were somewhat delayed (approximately 3 min) and more gradual (Fig. 4e), presumably due to the expected lower affinity of the cvxIAA towards the auxin transporters as compared with native IAA. Regardless, this shows that the growth inhibition could be triggered directly from the synthetic cvxIAA–ccvTIR1 pair, demonstrating that specific activation of the TIR1/AFB–Aux/IAA co-receptor is sufficient to mediate the rapid root growth inhibition.

This study reconciles a long-standing controversy about the rapid versus slow, transcriptional versus non-transcriptional auxin signalling mechanism regulating growth. Our vRootChip-based analysis revealed that the root growth response to auxin is a constant, reversible and rapid non-transcriptional brake proportional to the intracellular auxin levels. This growth brake is mediated by the formation of the nuclear TIR1/AFB–auxin–Aux/IAA co-receptor complex, which has been so far associated with auxin-mediated transcriptional regulation[1]. It implies that this canonical signalling pathway regulates root growth via an unknown, non-transcriptional signalling branch (Fig. 4f). Recently, rapid, auxin-dependent depolarization of plasma membrane in root hair cells has been shown also to require AUX1 auxin import, functional TIR1/AFB–Aux/IAA pathway and the CNGC14 channel[29]. It was shown previously that rapid auxin response in the root that triggers pH changes and calcium signalling also requires the CNGC14 channel[16], but apparently not the TIR1/AFB receptor[15]. Therefore, it remains to be confirmed whether these distinct rapid auxin effects are mediated by the same non-transcriptional signalling branch triggered from the TIR1/AFB–Aux/IAA receptor.

With the exception of the extremely low concentrations of auxin that were shown to promote growth[3], root growth rate is negatively correlated with the formation of the TIR1/AFB–auxin–Aux/IAA complex, and therefore we speculate that free Aux/IAA proteins

promote root growth, ubiquitinated Aux/IAA proteins inhibit it, or there is an unknown interactor or substrate of the TIR1/AFB receptor that might regulate growth in either direction. There has been an ongoing debate over 'fast and slow' TIR1-dependent and independent auxin responses[1]. Our observations reveal that the classical auxin-mediated process, root growth inhibition, involves fast and TIR1-dependent mechanisms at the same time and force us to broaden our understanding of (nuclear) auxin signalling.

Methods

Plant materials and growth conditions. *Arabidopsis thaliana* Col-0 was used as control background; in the vRootChip experiments, DII-Venus was often used as control. The following lines originate from these publications: DII-Venus[20], DR5::luciferase[22], AUX1::AUX1-YFP[32], *tir triple*[30], ccvTIR1 and controlTIR1[11]. *aux1* is the *aux1-100* transfer DNA insertion line that was genotyped using these primers: AGCTGCGCATCTAACCAAGT, GTTTCACACCTTCCGCCTAA and the SALK LBb1.3 primer.

For the vRootChip experiments, seeds were surface-sterilized with chlorine gas and sown in cut pipette tips (5 mm long) filled with 1/2MS medium with 1% sucrose and 0.8% plant agar that were placed in a round petri dish, according to ref. [33]. Sown seeds were stratified for 2 days in 4 °C, and then placed for 4 days in a growth room with 21 °C, long-day conditions. Afterwards, those seedlings that were just reaching the opening of the pipette tip were placed in the prepared vRootChip (see below). In the chip, 1/4MS, 1/2MS or full MS medium without sucrose (to avoid contamination) was used overnight to 24 h; during this time, the roots grew into the microfluidic channels. One to two hours before the experiment, the medium was supplemented with 0.1% sucrose to increase the growth of the roots. During the experiments, medium was flowed against the roots with a pressure of 0.2–0.4 bar and the seedlings were illuminated with a blue and red light-emitting diode (LED) light source, as described[18].

For other experiments, surface-sterilized seeds were sown on the surface of 1/2MS agar with 1% sucrose and 0.8% agar in square petri dishes, stratified for 2 days in 4 °C and then placed vertically for 4 days in a growth room with 21 °C, long-day conditions. For growth measurements over the course of 6 h, seedlings were transferred to 1/2MS with 1% sucrose and 1.5% phytagel and the appropriate treatment and imaged using a flatbed scanner placed vertically, as described[34].

Treatments. Treatments in the microfluidic device were achieved by alternating the control medium with a medium with the desired drug or hormone. During the experiments, roots were continuously flushed with medium to ensure constant composition of the solution and concentration of the treatment molecule (otherwise the roots quickly change the solution and use up the treatment molecule due to the small volume of the channel). The treatment solution was supplemented with a cell-impermeable dextranated fluorescent dye, mostly tetramethylrhodamine isothiocyanate–dextran, average molecular weight 20,000 (Sigma). The 10 mg ml^{-1} water stock of the dye was diluted 500–1,000× so that it was weakly visible with low 561 nm excitation laser intensities. IAA and 1-naphthaleneacetic acid (NAA) were from Sigma and were used as 10 mM EtOH stocks; PEO-IAA (Olchemim) used as 10 mM EtOH or DMSO stock. 1-*N*-naphthylphthalamic acid (NPA) (Sigma), cvxIAA[11] and cycloheximide (Sigma) were used as 10, 10 and 50 mM DMSO stocks, respectively.

Imaging and image analysis. The vRootChip was imaged on a vertical-stage laser scanning confocal Zeiss 700, described in ref. [18]. Most images were taken with a 20×/0.8 Plan-Apochromat M27 objective; the dextranated reference dye was excited by the 561 nM, Venus and YFP with the 488 nm laser line.

Root growth measurements were performed using a vertically positioned flatbed scanner, EPSON perfection v370, as described in ref. [34]. Luciferase bioluminescence was analysed as described in detail in ref. [34].

Root growth rate was measured automatically by stabilizing the drift of the root tip and calculating the growth from the drift vector using MATLAB and Fiji programs. Growth rate in the time point n is thus the distance that the root tip travelled between time points n-1 and n. DII-Venus intensity was measured in a region of interest drawn around the lateral root cap and stele cells in image series stabilized for growth drift using the StackReg Fiji plugin in the 'translation' or 'rigid body' option[35]. All images and videos were viewed, processed and analysed using Fiji[36,37]. Data were analysed in Microsoft Excel, figures were assembled in Inkscape and boxplots were made by BoxPlotR (http://shiny.chemgrid.org/boxplotr/).

vRootChip fabrication protocol. *Photomasks.* Photomask designs were exported to DXF from CorelDraw X8 and converted to Gerber using Linkcad 9. We used high-resolution transparency photomasks ~10 μm (JD Photo, UK). Valve crossovers had a size of 20 μm. We used a custom-made mask aligner with a 365 nm ultraviolet LED (Thor Labs) and beam expander. We routinely aligned within 10 μm. We used 200×200 μm^2 Quake style valves.

Protocols for SU8. The root channels were 110 μm high in SU8. GM-1075 SU8 photoresist (Gersteltec, Switzerland) was spin coated at 1,530 r.p.m. for 100 s resulting in 110 μm, baked at 40 °C for 30 min, baked at 120 °C for 2 min and exposed to ultraviolet for 15 min. Post bake was 95 °C for 30 min. Twenty-five-micrometre valves were made with Microchem SU8-3025 using the standard procedure.

Protocols for AZ-40XT. The mould for rounded fluid layer channels was made with AZ-40XT. We first spin coated hexamethyldisilazane (HMDS) at 3,000 r.p.m. for 30 s, baked at 110 °C for 1 min, spin coated AZ-40XT at 3,000 r.p.m. for 30 s baked at 110 °C for 5 min, exposed ~1 J cm^{-2} and post exposure baked for 2 min at 110 °C. We developed in 327 MIF for 5 min and rinsed in water. Reflow for several minutes was done at 130 °C followed by inspection under the microscope to observe parabolic channels. The height of the channel in the centre was roughly 26 μm using a profilometer.

Silane treatment. Wafers were treated in a vacuum desiccator with Trichloro(1*H*,1*H*,2*H*,2*H*-perfluorooctyl)silane (Sigma) for 1 h. The treatment need only be applied once.

Polydimethylsiloxane (PDMS) device protocol. We weighed approximately 60 g 5:1 RTV 615 and 21 g 20:1 RTV 615. We used a Thinky ARE-250 mixer with 2,000 r.p.m. mixing and 2 min at 2,000 r.p.m. degassing, and made an aluminium foil dish for the wafer. We poured the 5:1 PDMS onto the fluid layer and degassed one last time for approximately 10 min to remove bubbles in the photoresist. We then spin coated the 20:1 PDMS at 2,000 r.p.m. for 30 s. The 5:1 layer was baked for 1 h at 80 °C and the spin-coated layer was baked for 40 min at 80 °C. The thick layer was cooled off and cut into pieces and holes were punched (0.5 mm puncher for the flow inlets and 1.25 mm for the root inlets). Scotch tape was then applied to remove particles, and the pieces were aligned by hand under the stereomicroscope. An additional 2 h of bonding was done at 80 °C in the oven. The pieces were then cut out and the final holes for the control valves were punched out (0.5 mm puncher). Scotch tape was applied. Glass slides were prepared by sonication briefly in isopropanol. The devices were plasma bonded for 1 min at medium power in a Harrick plasma cleaner (pdc-02). After sealing, the devices were baked at 100 °C for 1 h on a hotplate and then placed back in the oven overnight at 80 °C; they were then ready to use and solidly bonded.

Valve electronics. We used an adaptation of the Rafael Gomez circuit board design to control 16 Festo valves, but used an Arduino to control the valves. The control software was programmed in Arduino and operated by serial communication of commands that control the valve states. The Auto-It scripting language can be used to make automated sequences of programs by interfacing with the serial communication window. The program changes the sequences of media applied and which roots or group of roots the media is directed to.

Growing plants in chip and chip usage. The vRootChip was mounted in a custom-made aluminium sealable holder the size of the 96-well plate that fitted the microscope inset. The valve layer was first filled with sterile water, the flow layer was filled with growth medium, all inlets were closed using 3M tape, 0.2 bar pressure was applied and then we waited until all of the bubbles were removed from the system. Then, the tape was removed, seedlings in the pipette tips were transferred to root inlets, the holder was sealed and placed under a blue-red LED lamp to support photosynthesis of the plants overnight to 24 h and the flow was sustained by ~0.1 bar. The entire setup was then transferred to the microscope and connected to pressure control and medium, and experiments were performed. Good chips were reused by flowing with 70% EtOH, enabling pulling out of shrunken roots followed by cleaning with sterile water.

Statistics and reproducibility. Number of experiments with similar results from which the illustrative microscopy images or individual measurements were selected: Fig. 1c: more than 3×; Fig. 2a: more than 3×; Fig. 2b: 2×; Fig. 3b: more than 3×; Fig. 4c: 2×; Fig. 4d: more than 3×.

Reporting summary. Further information on experimental design is available in the Nature Research Reporting Summary linked to this article.

Data availability. All source data for the results in the manuscript are provided in the Supplementary Data 1.

Received: 16 March 2018; Accepted: 1 June 2018;
Published online: 25 June 2018

References

1. Leyser, O. Auxin signaling. *Plant Physiol.* **176**, 465–479 (2018).
2. Gray, W. M., Kepinski, S., Rouse, D., Leyser, O. & Estelle, M. Auxin regulates SCFTIR1-dependent degradation of AUX/IAA proteins. *Nature* **414**, 271–276 (2001).
3. Evans, M. L., Ishikawa, H. & Estelle, M. A. Responses of *Arabidopsis* roots to auxin studied with high temporal resolution—Comparison of wild-type and auxin-response mutants. *Planta* **194**, 215–222 (1994).

4. Knight, T. A. On the direction of the radicle and germen during the vegetation of seeds. *Philos. Trans. R. Soc. Lond. B. Biol. Sci.* **96**, 99–108 (1806).
5. Darwin, C. *The Power of Movement in Plants* (John Murray, London, 1880).
6. Nemec, B. Ueber die art der wahrnehmung des schwek—Raftreizes bei den pflanzen. *Ber. Dtsch. Bot. Ges.* **18**, 241–245 (1900).
7. Adamowski, M. & Friml, J. PIN-dependent auxin transport: Action, regulation, and evolution. *Plant Cell* **27**, 20–32 (2015).
8. Went, F. & Thimann, K. *Phytohormones* (Macmillan, New York, 1937).
9. Tan, X. et al. Mechanism of auxin perception by the TIR1 ubiquitin ligase. *Nature* **446**, 640–645 (2007).
10. Fendrych, M., Leung, J. & Friml, J. TIR1/AFB–Aux/IAA auxin perception mediates rapid cell wall acidification and growth of *Arabidopsis* hypocotyls. *eLife* 5, e19048 (2016).
11. Uchida, N. et al. Chemical hijacking of auxin signaling with an engineered auxin-TIR1 pair. *Nat. Chem. Biol.* **14**, 299–305 (2018).
12. Leyser, H. M. O., Pickett, F. B., Dharmasiri, S. & Estelle, M. Mutations in the AXR3 gene of *Arabidopsis* result in altered auxin response including ectopic expression from the SAUR-AC1 promoter. *Plant J.* **10**, 403–413 (1996).
13. Ruegger, M. et al. The TIR1 protein of *Arabidopsis* functions in auxin response and is related to human SKP2 and yeast grr1p. *Genes Dev.* **12**, 198–207 (1998).
14. Scheitz, K., Lüthen, H. & Schenck, D. Rapid auxin-induced root growth inhibition requires the TIR and AFB auxin receptors. *Planta* **238**, 1171–1176 (2013).
15. Monshausen, G. B., Miller, N. D., Murphy, A. S. & Gilroy, S. Dynamics of auxin-dependent Ca2 + and pH signaling in root growth revealed by integrating high-resolution imaging with automated computer vision-based analysis. *Plant J.* **65**, 309–318 (2011).
16. Shih, H. W., Depew, C. L., Miller, N. D. & Monshausen, G. B. The cyclic nucleotide-gated channel CNGC14 regulates root gravitropism in *Arabidopsis thaliana*. *Curr. Biol.* **25**, 3119–3125 (2015).
17. Grossmann, G. et al. The RootChip: An integrated microfluidic chip for plant science. *Plant Cell* **23**, 4234–4240 (2011).
18. von Wangenheim, D. et al. Live tracking of moving samples in confocal microscopy for vertically grown roots. *eLife* **6**, e26792 (2017).
19. Band, L. R. R. et al. Root gravitropism is regulated by a transient lateral auxin gradient controlled by a tipping-point mechanism. *Proc. Natl Acad. Sci. USA* **109**, 4668–4673 (2012).
20. Brunoud, G. et al. A novel sensor to map auxin response and distribution at high spatio-temporal resolution. *Nature* **482**, 103–106 (2012).
21. Hoyle, N. P. & Ish-Horowicz, D. Transcript processing and export kinetics are rate-limiting steps in expressing vertebrate segmentation clock genes. *Proc. Natl Acad. Sci. USA* **110**, E4316–E4324 (2013).
22. McClure, B. A., Hagen, G., Brown, C. S., Gee, M. A. & Guilfoyle, T. J. Transcription, organization, and sequence of an auxin-regulated gene cluster in soybean. *Plant Cell* **1**, 229–39 (1989).
23. Moreno-Risueno, M. A. et al. Oscillating gene expression determines competence for periodic *Arabidopsis* root branching. *Science* **329**, 1306–1311 (2010).
24. Macdonald, I. R. & Ellis, R. J. Does cycloheximide inhibit protein synthesis specifically in plant tissues?. *Nature* **222**, 791–792 (1969).
25. Okushima, Y. et al. Functional genomic analysis of the AUXIN RESPONSE FACTOR gene family members in *Arabidopsis thaliana*. *Plant Cell* **17**, 444–463 (2005).
26. Swarup, R. et al. Root gravitropism requires lateral root cap and epidermal cells for transport and response to a mobile auxin signal. *Nat. Cell Biol.* **7**, 1057–1065 (2005).
27. Bennett, M. J. et al. Arabidopsis AUX1 gene: A permease-like regulator of root gravitropism. *Science* **273**, 948–950 (1996).
28. Delbarre, A., Muller, P., Imhoff, V. & Guern, J. Comparison of mechanisms controlling uptake and accumulation of 2,4-dichlorophenoxy acetic acid, naphthalene-1-acetic acid, and indole-3-acetic acid in suspension-cultured tobacco cells. *Planta* **198**, 532–541 (1996).
29. Dindas, J. et al. AUX1-mediated root hair auxin influx governs SCFTIR1/AFB-type Ca2 + signaling. *Nat. Commun.* **9**, 1174 (2018).
30. Dharmasiri, N. et al. Plant development is regulated by a family of auxin receptor F box proteins. *Dev. Cell* **9**, 109–119 (2005).
31. Hayashi, K. et al. Rational design of an auxin antagonist of the SCF(TIR1) auxin receptor complex. *ACS Chem. Biol.* **7**, 590–598 (2012).
32. Swarup, R. et al. Structure-function analysis of the presumptive *Arabidopsis* auxin permease AUX1. *Plant Cell* **16**, 3069–3083 (2004).
33. Grossmann, G. et al. Time-lapse fluorescence imaging of *Arabidopsis* root growth with rapid manipulation of the root environment using the RootChip. *J. Vis. Exp.* **65**, e4290 (2012).
34. Li, L., Krens, S. F. G., Fendrych, M. & Friml, J. Real-time analysis of auxin response, cell wall pH and elongation in *Arabidopsis thaliana* hypocotyls. *Bio-Protoc.* **7**, 1–10 (2018).
35. Thévenaz, P., Ruttimann, U. E., U., M., Thevenaz, P., Ruttimann, U. E. & Unser, M. A pyramid approach to subpixel registration based on intensity. *IEEE Trans. Image Process.* **7**, 27–41 (1998).
36. Schneider, Ca, Rasband, W. S. & Eliceiri, K. W. NIH Image to ImageJ: 25 years of image analysis. *Nat. Methods* **9**, 671–675 (2012).
37. Schindelin, J. et al. Fiji: An open-source platform for biological-image analysis. *Nat. Methods* **9**, 676–682 (2012).

Acknowledgements

The authors thank R. Hauschild for help with image analysis. M.F. was supported by the Austrian Science Fund (FWF) (M 2128-B21), and in the final stages of the project by the Czech Science Foundation (18-10116Y). M.A. was supported by the Austrian Science Fund (FWF) (M2379-B28). Additional funding for M.G. was received from the Ministry of Education of the Czech Republic/MŠMT project NPUI-LO1417. N.U. received MEXT/JSPS KAKENHI JP16H01462, S.H. received JP17H06350, K.T. received JP26440140 and K.U.T. received JP16H01237. K.U.T. is supported by GBMF Grant No. 3035. S.H. is a JST PRESTO Investigator and K.U.T. is an HHMI-GBMF Investigator. J.F. acknowledges the ERC Advanced Grants (ETAP).

Author contributions

M.F. initiated the project, acquired funding, performed the experiments, analysed the data and wrote the manuscript. M.A. created the computational model of auxin fluxes and wrote the manuscript. J.M. designed, optimized and fabricated the microfluidic devices. M.G. performed experiments and edited the manuscript. S.H., K.T., N.U. and K.U.T. designed, synthesized and developed the engineered cvxIAA–ccvTIR1 system and edited the manuscript. J.F. initiated the project, acquired funding and wrote the manuscript.

Competing interests

The authors declare no competing interests.

Additional information

Supplementary information is available for this paper at https://doi.org/10.1038/s41477-018-0190-1.

Reprints and permissions information is available at www.nature.com/reprints.

Correspondence and requests for materials should be addressed to J.F.

Publisher's note: Springer Nature remains neutral with regard to jurisdictional claims in published maps and institutional affiliations.

nature research

Corresponding author(s): FRIML

Reporting Summary

Nature Research wishes to improve the reproducibility of the work that we publish. This form provides structure for consistency and transparency in reporting. For further information on Nature Research policies, see Authors & Referees and the Editorial Policy Checklist.

Statistical parameters

When statistical analyses are reported, confirm that the following items are present in the relevant location (e.g. figure legend, table legend, main text, or Methods section).

n/a	Confirmed	
☐	☒	The exact sample size (*n*) for each experimental group/condition, given as a discrete number and unit of measurement
☒	☐	An indication of whether measurements were taken from distinct samples or whether the same sample was measured repeatedly
☒	☐	The statistical test(s) used AND whether they are one- or two-sided *Only common tests should be described solely by name; describe more complex techniques in the Methods section.*
☒	☐	A description of all covariates tested
☒	☐	A description of any assumptions or corrections, such as tests of normality and adjustment for multiple comparisons
☒	☐	A full description of the statistics including central tendency (e.g. means) or other basic estimates (e.g. regression coefficient) AND variation (e.g. standard deviation) or associated estimates of uncertainty (e.g. confidence intervals)
☒	☐	For null hypothesis testing, the test statistic (e.g. *F*, *t*, *r*) with confidence intervals, effect sizes, degrees of freedom and *P* value noted *Give P values as exact values whenever suitable.*
☒	☐	For Bayesian analysis, information on the choice of priors and Markov chain Monte Carlo settings
☒	☐	For hierarchical and complex designs, identification of the appropriate level for tests and full reporting of outcomes
☒	☐	Estimates of effect sizes (e.g. Cohen's *d*, Pearson's *r*), indicating how they were calculated
☐	☒	Clearly defined error bars *State explicitly what error bars represent (e.g. SD, SE, CI)*

Our web collection on statistics for biologists may be useful.

Software and code

Policy information about availability of computer code

Data collection	Image data was collected using the Zeiss Zen (version 2010) software, the root chip was controlled via the Arduino (Uno rev3)and AutoIt (v 3.3) programs. For preparation of the photomasks, CorelDraw (X8) and Linkcad (9) were used.
Data analysis	Images were analyzed using Fiji (2017 release) and MATLAB (R2014 and R2015a). Data was processed in MATLAB (R2015a) and MS Excel (2010 and 2013). Model was created in Comsol Multiphysics (5.2a). Boxplots were created using BoxPlotR (http://shiny.chemgrid.org/boxplotr/). Figures and movies were prepared using Fiji and Inkscape (0.92).

For manuscripts utilizing custom algorithms or software that are central to the research but not yet described in published literature, software must be made available to editors/reviewers upon request. We strongly encourage code deposition in a community repository (e.g. GitHub). See the Nature Research guidelines for submitting code & software for further information.

Data

Policy information about availability of data

All manuscripts must include a data availability statement. This statement should provide the following information, where applicable:

- Accession codes, unique identifiers, or web links for publicly available datasets
- A list of figures that have associated raw data
- A description of any restrictions on data availability

All source data for the results in the manuscript are provided in the Supplementary Data 1 file

Field-specific reporting

Please select the best fit for your research. If you are not sure, read the appropriate sections before making your selection.

☒ Life sciences ☐ Behavioural & social sciences ☐ Ecological, evolutionary & environmental sciences

For a reference copy of the document with all sections, see nature.com/authors/policies/ReportingSummary-flat.pdf

Life sciences study design

All studies must disclose on these points even when the disclosure is negative.

Sample size	This study analyzes growth of individual roots inside the microfluidic device that has 8 channels for 8 independent treatments of individual roots. Therefore the sample size was physically limited by the number of roots that entered the microfluidic channel and could be successfully flown by the treatment media. In case of comparing genotypes, control was included on the same chip - further the maximum sample size for the experiment. For the other growth experiments, we used approximately 7 roots per treatment and genotype, because this number still fits one one treatment plate.
Data exclusions	The individual roots were excluded from analysis if 1) the root did not grow or grew extremely slowly 2) if the respective microfluidic channel was blocked and therefore had no flow in it.
Replication	The results were replicated in technically independent replications.
Randomization	In case of comparing two genotypes, these were grown alongside on the same microfluidic chip. In case of studying the treatment effect, the pre-treatment state was takes as a baseline.
Blinding	Blinding was not relevant for this study because the growthrates of roots were determined using image analysis, not manually.

Reporting for specific materials, systems and methods

Materials & experimental systems

n/a	Involved in the study
☐	☒ Unique biological materials
☒	☐ Antibodies
☒	☐ Eukaryotic cell lines
☒	☐ Palaeontology
☒	☐ Animals and other organisms
☒	☐ Human research participants

Methods

n/a	Involved in the study
☒	☐ ChIP-seq
☒	☐ Flow cytometry
☒	☐ MRI-based neuroimaging

Unique biological materials

Policy information about availability of materials

Obtaining unique materials	The origin of the biological material used in the study is described in the Methods; there are no restrictions on the availability of the materials used.

nature plants

SUPPLEMENTARY INFORMATION

https://doi.org/10.1038/s41477-018-0190-1

In the format provided by the authors and unedited.

Rapid and reversible root growth inhibition by TIR1 auxin signalling

Matyáš Fendrych[1,2], Maria Akhmanova[1], Jack Merrin[1], Matouš Glanc[1,2], Shinya Hagihara[3], Koji Takahashi[3], Naoyuki Uchida[3], Keiko U. Torii[3,4] and Jiří Friml[1]*

[1]Institute of Science and Technology (IST) Austria, Klosterneuburg, Austria. [2]Department of Experimental Plant Biology, Faculty of Science, Charles University, Prague, Czechia. [3]Institute of Transformative Biomolecules (WPI-ITbM) and Graduate School of Science, Nagoya University, Chikusa, Nagoya, Japan. [4]Howard Hughes Medical Institute and Department of Biology, University of Washington, Seattle, WA, USA. *e-mail: jiri.friml@ist.ac.at

© 2018 Macmillan Publishers Limited, part of Springer Nature. All rights reserved.

Title: Rapid root growth brake by TIR1 auxin signaling

Supplementary Material

Contents

Supplementary Text: 1
Supplementary Figures 7
Supplementary Tables 12
Supplementary References 16

Supplementary Text:

Model of IAA transport from media into the root

1. Model description

To assess temporal dynamics of intracellular auxin accumulated from the media into the elongating root cells, we simulated auxin transport in the root tip. Our model follows the framework used in the previous models of auxin transport[12–14]: root tip comprises a multicellular structure with isolated intracellular compartments and extracellular compartment (the cell wall), within which auxin can diffuse freely. Auxin transport between the adjacent compartments is governed by its concentration gradient and membrane permeability. There are three distinct paths for auxin molecule to permeate the cell membrane: diffusion, influx carriers and efflux carriers. As shown previously, major governing factor for auxin transport is the distribution of membrane permeabilities for auxin through these paths, which depend on localization of the carrier proteins (AUX1, PINs and others)[12–14]. Our model contains also a media compartment around the root to simulate external auxin concentration.

Model Geometry

Presenting the root tip as an array of rectangular cells has computational advantages and provided useful quantitative results in the past[12,14,15]. We draw 2D rectangular geometry of the half of a root tip, containing cells of the root apex: meristematic zone, elongation zone and the beginning of the differentiation zone (where cells are no longer elongating) (Fig. S4A). Total root geometry is~ 1500μm in length, 80μm in width. Right outmost domain represents media. As auxin distribution depends on individual cell sizes[14], it is crucial to recapitulate cellular dimensions as close to the real root as possible. Most important is to preserve the cell volume distribution in the real root. To fulfill this requirement and facilitate assigning of membrane permeabilities in the same time, the widths of the cell files in our model correspond to those in elongation zone, taken from segmented confocal images[16]. The heights of the cells are also taken from segmented confocal images. Lateral root cap is drawn as an additional cell file on the outer side of meristematic zone. Cell wall thickness is set to 200 nm.

The 3D structure is obtained by rotating 2D geometry around the central axis. Assuming auxin concentrations and dynamics to be axisymmetric (neglecting variations around the roots circumference) enables us to capture the 3D structure of the root tip without significantly increasing simulation time. However, this approach eliminates lateral cell membranes, which are parallel to the rotating plane (perpendicular to the circumference). In our model we compensate for these missing membranes by proportional increase in permeability of the rest of the cell contour.

Parameters governing auxin transport; specifying the carrier distributions.

Bulk diffusion. Diffusion coefficients inside the cell and in the media are assumed to be equal to diffusion in water at the room temperature $D_c = D_m = 600\ \mu m^2/s$ [12]; in the wall $D_w = 32\ \mu m^2/s$ based on measurements [17].

Carrier distribution. Membrane transport of auxin has three components: 1) diffusion of the IAAH, protonated form of auxin, 2) influx of anion IAA^- from the wall into the cell via influx carriers, 3) efflux of IAA^- from the cell into the wall via efflux carriers. Diffusional permeability is the same for all cell boundaries. Carrier-mediated membrane permeabilities depend on carrier density and on the specific permeability of the unit density of a carrier. Carrier densities are assigned for each cell boundary following the carrier localization schemes presented in *Simuplant,* default settings[16]: based on the fluorescence staining of the main known auxin transporters in the root (AUX1, LAX2 and LAX3 influx transporters; PIN1, PIN2, PIN3, PIN4 and PIN7 efflux transporters) it has been assumed that either carrier is present on the membrane and its density equals 1 or it is absent with the density equal 0 (Fig. S4A). Most cells containing influx carriers have them localized on all sides of the cell membrane[13]. AUX1 is localized mostly in outward cell layer: lateral root cap (LRC) and epidermis (Fig.3B, Fig. S4A). PIN proteins are polarized in most cells (QC is an exception, where PINs are on all boundaries) and each cell has the prevailing PIN type expressed. This results in the characteristic distribution of PINs within the root[13], proved to cause the reverse auxin fountain: the downward auxin flux in the stele and upward auxin flux in the outer cell layer[14]. Other non-polar efflux transporters (NPEs) are not yet characterized well, but they are not polarized as PINs and are thought to have much less permeability[16]. In the main model we neglect non-polar efflux carriers (NPEs), but sensitivity of the solution for their presence on all cell boundaries is calculated (Table S2). We simulate *aux1* mutant lacking AUX1 carrier by setting AUX1 density to 0 in the outer layer (epidermis and LRC).

Measured permeability values. Permeability values have been measured separately for diffusion, influx and efflux carriers in a number of studies[18,19]. Rutschow et al. provide diffusion permeability for Arabidopsis root protoplasts ($P_{IAAH} = 0.35 \pm 0.22\ \mu m/s$), which is close to the values provided by[19] for tobacco cells. Influx permeability in AUX1-positive root protoplasts was determined[18] as: $P_{AUX1} = 0.35 \pm 0.07 \mu m/s$. We assume $P_{LAX2,3} = P_{AUX1}$ [13]. Permeability for PINs has been previously estimated as ~ $0.3 \mu m/s$ [12]. One way to estimate the PIN efflux permeability in epidermis is from the auxin transport velocity in the shoot direction, that corresponds to polar transport[19]. Measured auxin velocities in the Arabidopsis root are in the range of $0.3 \div 3 \mu m/s$ [20]. To get upward auxin flux in the epidermis ~ $1\ \mu m/s$ in our model, we set the efflux permeability of PIN2, which is polarized shootward in epidermis and solely defines the shootward IAA transport: $P_{PIN2} = 0.5 \pm 0.2 \mu m/s$. This is close to the value estimated by[18]. We assume that all PINs-containing cells have the same P_{PIN} disregarding the PIN type and number of different PINs. This assumption is rough, however, as we aim to calculate $[IAA]_{cell}$ mainly in epidermis, we choose P_{AUX1} and P_{PIN2} to be the reference values.

Other assumptions:
(i) Saturation of the auxin transporters is not considered, because concentrations tested in the model are below saturation level: $K_{D(AUX1)} \cong 2\mu M$, $K_{D(PINS)} \cong 6\mu M$ [21], whereas 1nM≤$[IAA]_{ext}$≤50nM and calculated $[IAA]_{cell} < 3\mu M$.
(ii) Auxin synthesis and degradation are neglected in the model. It is not known precisely, what is auxin synthesis rate in the root and what fraction of auxin present in the root is transported from the shoot. Nevertheless, E. Kramer and E. Ackelsberg estimated that synthesis contributes to less than 1% of the auxin amount present in the fast transporting tissues such as root[22]. Auxin degradation is also a slow process compared to transport[16,22]. As we have an infinite pool of auxin (coming from shoot and media), degradation can be assumed negligible.

For the complete list of the parameters used in the model see Tables S2 and S3.

Equations for diffusion within compartments and membrane auxin fluxes.

Dynamic auxin distribution is calculated by solving a system of Partial Differential Equations (PDEs) that describe how the auxin concentration IAA(x,t) within each compartment evolve due to bulk auxin diffusion (Fick's law) and mass conservation law:

$$\frac{\partial [IAA]_{c/w/m}}{\partial t} = D_{c/w/m} \cdot \Delta [IAA]_{c/w/m}. \quad \text{(Eq.1.)}$$

Normal diffusive auxin flux at the boundaries of compartments equals to auxin flux across membrane between compartments:

$$J_{boundary} = -D_{c/w/m} \cdot \nabla [IAA]_{c/w/m} = J_{through\ PM}$$

(=molecules passed through membrane per unit time per unit area), which is governed by membrane permeabilities:

$$J_{wall \to cell} = J_{diff} + J_{influx} + J_{efflux}\ , \quad \text{(Eq.2)}$$
$$J_{diff} = P_{IAAH}(A_1 \cdot [IAA]_{wall} - B_1 \cdot [IAA]_{cell}) \quad \text{(Eq.3)}$$
$$J_{influx} = P_{AUX1\ or\ LAX2,3}(A_2 \cdot [IAA]_{wall} - B_2 \cdot [IAA]_{cell}) \quad \text{(Eq.4)}$$
$$J_{efflux} = P_{PIN}(A_3 \cdot [IAA]_{wall} - B_3 \cdot [IAA]_{cell}), \quad \text{(Eq.5)}$$

where A_i, B_i are coefficients that depend on pH_{wall}, pH_{cell}, pK of auxin and membrane potential V_m. Total IAA concentration is a sum of protonated form and anion form: $[IAA] = IAAH + IAA^-$. Expressions for A_i, B_i account for IAAH and IAA^- ratio in solution due to pH and also for electric potential gradient across the membrane (Fig. S4B). Derivation of A_i, B_i is provided in detail in[16] and[12]. For $pH_{wall} = 5.3$, $pH_{cell} = 7.2, V_m = -120mV$, typical for the root, these constants have the following values:

$$J_{diff} = P_{IAAH}(0.24 \cdot [IAA]_{wall} - 0.004 \cdot [IAA]_{cell}) \quad \text{(Eq.3')}$$
$$J_{influx} = P_{AUX1\ or\ LAX2,3}(3.57 \cdot [IAA]_{wall} - 0.045 \cdot [IAA]_{cell}) \quad \text{(Eq.4')}$$
$$J_{efflux} = P_{PIN}(0.034 \cdot [IAA]_{wall} - 4.68 \cdot [IAA]_{cell}), \quad \text{(Eq.5')}$$

Numerical procedure
PDEs are solved in finite element software Comsol Multiphysics 5.2a: domains of the 2D geometry are discretized by constructing a mesh of 41702 triangular elements. Variables are defined in vertices and computed over time. Time steps are determined by solver.

External boundary conditions (Fig.S4A). On the upper boundary of the stele the IAA concentration is set to constant C_{shoot}, that corresponds to the supply of auxin from the shoot.

On the upper boundary of the epidermis the sink is set also by IAA concentration condition: C_{epi}=0. The external boundary of the media compartment has concentration equal to applied auxin: C_{ext}=IAA_{ext}. The rest of the external boundaries have "no flux" boundary condition. We tested that auxin accumulation into epidermal cells from the media doesn't depend on C_{epi} because it is governed by concentration in the media and the upward flux by PINs. To define C_{shoot} we take into account the average [IAA] in the intact root tip of 1mm length, which has been experimentally found to be ~200nM[23,24]. C_{shoot} =400nM gives the same average [IAA] without auxin application (C_{ext}=0).

Initial conditions. First, we calculate steady state solution for the C_{ext}=0 (Fig. S4C): this endogenous $[IAA]_{cell}$ and $[IAA]_{wall}$ distribution in the root serves as initial conditions for further numerical analysis of IAA accumulation (for Fig. S4D-H). The initial auxin concentration in epidermis before auxin application is $[IAA]_{cell0}$~=5nM in the control and $[IAA]_{cell0}$~=1.4nM in *aux1*.

Starting from initial concentrations our model calculates $[IAA]_{cell}$ and $[IAA]_{wall}$ change in time due to accumulation and eventually comes to constant: a *steady state* solution. In a steady state net fluxes through membranes are also constant, but not zero: auxin can be pumped into the cell at one boundary and pumped out at the other boundary while keeping $[IAA]_{cell}$ constant.

2. Results

Control

We use the model to calculate steady state and temporal dependence of the auxin accumulation after application of $[IAA]_{ext}$. Cell-average $[IAA]_{cell}$ in epidermal cells rises after external auxin application and establishes an ascendant gradient along the elongation zone because auxin is pumped up by efflux carriers (Fig.S4E). We will further present $[IAA]_{cell}$ for the 5th epidermal cell above the lateral root cap for simplicity (see Fig.S4E,F), as its value correspond to the volume-average $[IAA]_{cell}$ of all epidermal cells in the elongation zone.

For 1nM<$[IAA]_{ext}$ <50nM auxin steady state accumulation can be described by a single parameter: $\alpha=[IAA]_{cell}/[IAA]_{ext}$ – accumulation ratio (Fig.S4DE). In control α^{Col}~=30±12 (error is due to parameter variation (Table S2) and to slight difference for different $[IAA]_{ext}$ (Fig.S4D)).

From α^{Col} and experimental IC_{50} that causes half growth inhibition we can find the intracellular auxin concentration that causes half growth inhibition, namely $IAA_{cell50}^{col} = \alpha^{col} \cdot IC_{50}^{col} = 43 \pm 18nM$. Assuming that *tir triple* mutant accumulates IAA as much as the control, one can calculate auxin concentration that causes half growth inhibition when there are not enough receptors present: $IAA_{cell50}^{tir} = \alpha^{col} \cdot IC_{50}^{tir} = 275 \pm 115nM$. It gives an estimate of affinity between TIR1/ABF-Aux/IAA and auxin given that it is a primary receptor in the growth inhibition pathway[25]. Affinities measured for some of the TIR1/ABF-Aux/IAA pairs indeed fall in this range[26].

Temporal dynamics of auxin accumulation is shown on Fig.S4E: time to reach half maximum concentration $t_{1/2}$~=150s. ($t_{1/2}$~= 60s to 200s depending on cell location and on parameter variation as shown in Fig.3G.) It is instructive to estimate t_{IC50} - time to reach intracellular concentration $IAA_{cell50}^{col} = \alpha^{col} \cdot IC_{50}^{col}$, that causes half growth inhibition. (This time doesn't depend on α^{Col}, which acts as a common scale factor for both half inhibitory concentration and for the steady state concentration.) Comparison of t_{IC50} to the half inhibition time of GR, τ_{GR50}, provides information about timing for signaling cascade. Even for $[IAA]_{ext}$=5nM t_{IC50}~*70sec* is much shorter than $\tau_{GR50} = 6min$, giving an estimate of *5min* characteristic time

for the full response execution (reaching *responseGR*). At higher $[IAA]_{ext}$, IAA_{cell50}^{col} is reached faster, and thus reduces the total response time, which is consistent with experimental data for $[IAA]_{ext}$=50nM. We conclude, that auxin uptake alone cannot explain temporal dependence of GR inhibition, and that signaling pathway should contain few fast reaction steps.

Influx mutant *aux1*

Auxin accumulation ratio $\alpha^{aux1\sim}$=1.9±0.5, that gives

$$\frac{\alpha^{col}}{\alpha^{aux1}} = 15.9 \pm 5.5 \qquad \text{(Eq.6.)}$$

$[IAA]_{cell}$ in *aux1* reaches steady state faster than in the control: $t_{1/2}{}^{\sim}$=100s (Fig.S4G).

Notes on assumption of zero influx permeability in aux1. Measurements of auxin fluxes in the null mutant *aux1*-22 show, that it's influx permeability can be up to 15% of that in control[18]. If we account for such influx carrier activity in the *aux1* mutant (in the outer cell layer), we get $\frac{\alpha^{col}}{\alpha^{aux1}} = 6$ in our model. Thus, influx permeability in the mutant, if present, reduces difference between control and *aux1* and makes it lower than the experimental value. It is possible, however, that non-zero influx in *aux1*-22 in those experiments is caused by LAX transporters, that are not present in epidermis. Thus, epidermal cells, which are the focus of our analysis, can indeed have no influx activity in *aux1*. In our experiments we use *aux1*-100, which is also null mutant, but for which no permeability measurements are available. Not having more precise experimental values, we assume that influx permeability in the outer cell layer of *aux1* mutant is lowest possible: $P_{AUX1} = 0$.

Sensitivity of accumulation ratios on parameter variations is presented in Table S2. Changing permeability values within the range of their standard deviations gives maximum error of the solution, presented in the Table S4.

Simplified 1D model to estimate ratio between control and *aux1* accumulation $\alpha^{Col}/\alpha^{aux1}$

Auxin accumulation ratio in epidermis in our numerical model depends only slightly on the transport properties of the other cells composing the root. Thus, considering these cells in the model doesn't change the result much. We can simplify our model even further and not account for PIN polarity, assuming that efflux carriers are distributed around the epidermal membrane evenly. Then the steady state concentration can be found simply from the balance of the auxin fluxes across any segment of the membrane:

$$J_{wall\to cell} = J_{diff} + J_{influx} + J_{efflux} = 0 \qquad \text{(Eq.7.)}$$

From Eq.3'-5 ' in control:

$$\alpha^{col} = \frac{[IAA]_{cell}}{[IAA]_{wall}} = \frac{P_{IAAH}\cdot 0.24 + P_{AUX1}\cdot 3.57 + P_{PIN}\cdot 0.034}{P_{IAAH}\cdot 0.004 + P_{AUX1}\cdot 0.045 + P_{PIN}\cdot 4.6}, \qquad \text{(Eq.8.)}$$

and in *aux1* ($P_{AUX1} = 0$):

$$\alpha^{aux1} = \frac{[IAA]_{cell}}{[IAA]_{wall}} = \frac{P_{IAAH}\cdot 0.24 + 0 + P_{PIN}\cdot 0.034}{P_{IAAH}\cdot 0.004 + 0 + P_{PIN}\cdot 4.6}. \qquad \text{(Eq.9.)}$$

Introducing values of permeabilities (Table S2) allows to approximate:

$$\frac{\alpha^{col}}{\alpha^{aux1}} = \frac{P_{IAAH}\cdot 0.24 + P_{AUX1}\cdot 3.57}{P_{PIN}\cdot 4.6} \cdot \frac{P_{PIN}\cdot 4.6}{P_{IAAH}\cdot 0.24} = 13.3 \pm 3.5 \qquad \text{(Eq.10.)}$$

In this simple model ratio between control and *aux1* doesn't depend on efflux permeability, which is cancelled, but solely on the diffusive and influx permeabilities, that are measured in

the root quite precisely[18]. We conclude, that the root geometry and PIN polarity only slightly contribute to the observed difference between control and *aux1* growth inhibition.

II. Fitting procedures

Calculation of response growth rate from experimental growth curves.
We normalize growth inhibition curves by the growth rate immediately preceding auxin application (*initGR*). Using MATLAB, we fitted individual normalized growth inhibition curves with an exponentially descending function that gives us the steady state growth rate, reached by the root after a while: *responseGR*. At high $[IAA]_{ext}$ *responseGR* saturates: roots do not fully stop; the minimal responseGR, GR_{min}, is about 13% in control (consistent with previous reports[27]). Surprisingly, we didn't find any correlation between *initGR* and GR_{min}: fast roots that grow at *initGR*~7 μm/min reduce their growth rate to 13% as well as slow roots with *initGR*~1 μm/min. Nor we observed any correlation between *initGR* and *responseGR* for any $[IAA]_{ext}$. Thus, normalization to *initGR* is justified.

Hill-equation fit of *responseGR*. Dependence of *responseGR* on the dose, $\log_{10}([IAA]_{ext})$, has sigmoidal shape, characteristic for dose-effect curves (Fig.1E, Fig.3D, Fig.4B). Dose-effect curves are usually fitted by Hill equation[28]. For normalized *GR* equation takes the form:

$$GR([IAA]_{ext}) = \frac{1-GR_{min}}{1+\left(\frac{[IAA]_{ext}}{IC_{50}}\right)^{k}} + GR_{min}, \qquad \text{(Eq.12)}$$

where maximum growth rate equals 1, GR_{min} is minimal growth rate, IC_{50} is half inhibitory concentration of $[IAA]_{ext}$ and k characterizes steepness of the slope.
Fitting was performed in MATLAB. Fitted coefficient values are listed in Table S1.

Theoretical growth rate response (Fig.3H). We use the same Hill equation to predict growth inhibition in time on the assumption that cells react instantaneously to the $[IAA]_{cell}$ reached at the moment:

$$GR^{i}(t) = \frac{1-GR_{min}}{1+\left(\frac{[IAA]^{i}_{cell}(t)}{\alpha^{i}\cdot IC^{i}_{50}}\right)^{k}} + GR_{min}, \qquad \text{(Eq.12)}$$

where i=control, *aux1*.
GR_{min}, k, α^{i}, IC^{i}_{50} values are listed in Tables S1 and S4. Calculated $GR^{i}(t)$ are shown in Fig.3H for $[IAA]_{ext}$=5nM and $[IAA]_{ext}$=50nM. Fig.3H illustrates difference between reaction to particular $[IAA]_{ext}$ in control and *aux1*. It also shows that for higher $[IAA]_{ext}$ GR inhibition should become more steep and the curve becomes more asymmetric: inhibition and resumption parts are symmetric only when steady state $[IAA]_{cell}$ doesn't considerably exceed the half maximal inhibitory concentration. That is why curves for *aux1* are more symmetric than for control, which accumulates much more.

Notably, the slopes of all theoretical curves are steeper than experimental GR(t), indicating that a delay between signaling and the execution of the response is present also in *aux1*.

Supplementary Figures

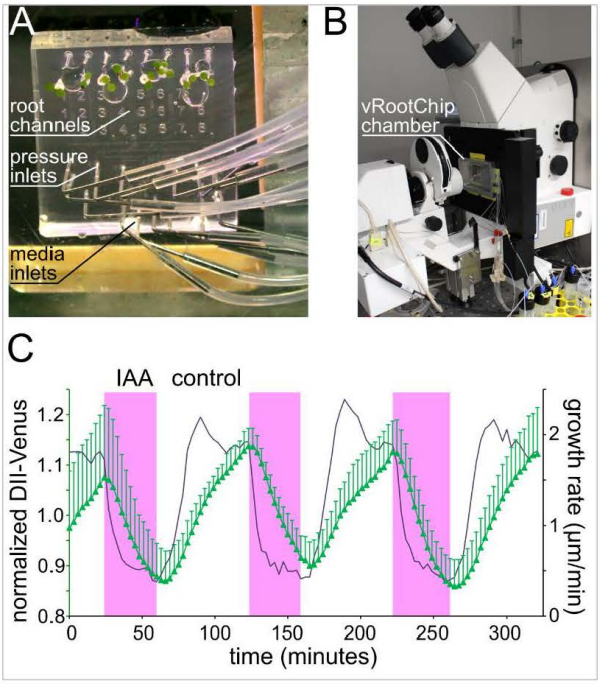


Fig. S1. A) Photo of vRootChip with Arabidopsis seedlings and connected tubing for pressure control and media influx. B) Photo of the assembled vRootChip device on the vertical confocal microscope. C) DII-Venus intensity dynamics (green line) during a repetitive treatment with 10nM IAA is closely correlated with the growth rate dynamics (black line, the same data as in Fig.1F). DII-Venus was measured in the lateral root cap and stele, and was normalized to the mean value over the course of the experiment for each root. Mean intensity of 8 roots +SD.

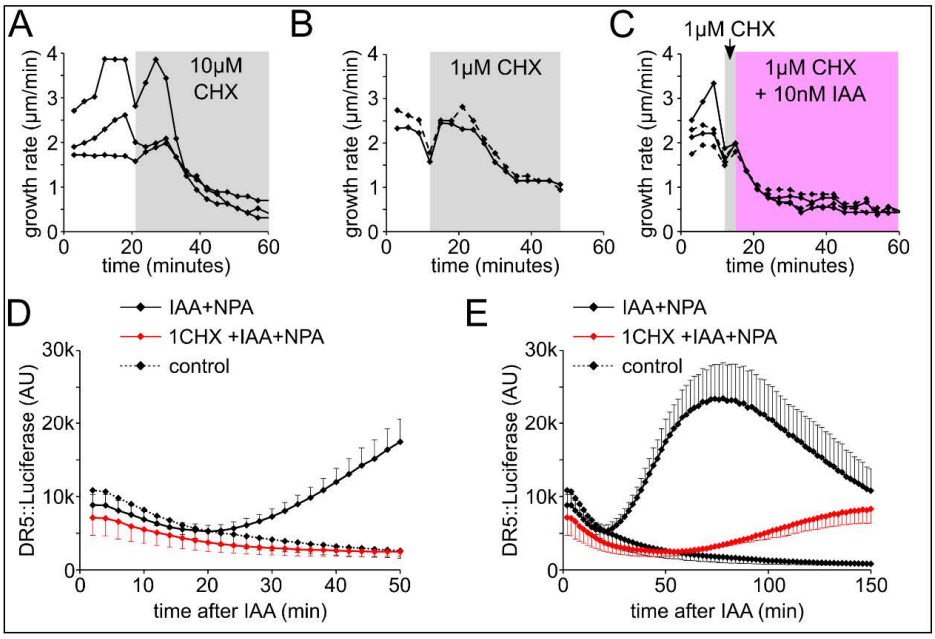


Fig. S2. A) Effect of 10µM cycloheximide (shaded in grey) on root growth of three individual roots. B) Effect of 1µM cycloheximide (shaded in grey) on root growth of two individual roots. C) Pretreatment with 1µM cycloheximide (grey) does not prevent the IAA-triggered (magenta) root growth inhibition. Time course of four individual roots. D) Addition of 1µM cycloheximide inhibits the IAA-triggered increase in DR5::luciferase intensity (D). After 50 minutes, DR5::luciferase starts to be expressed due to dilution of the inhibitor into the medium (E). The data of control and IAA+NPA correspond to Figure 2EF, and represent the mean ±SD of 5 root tips for each condition; D is a zoom of E.

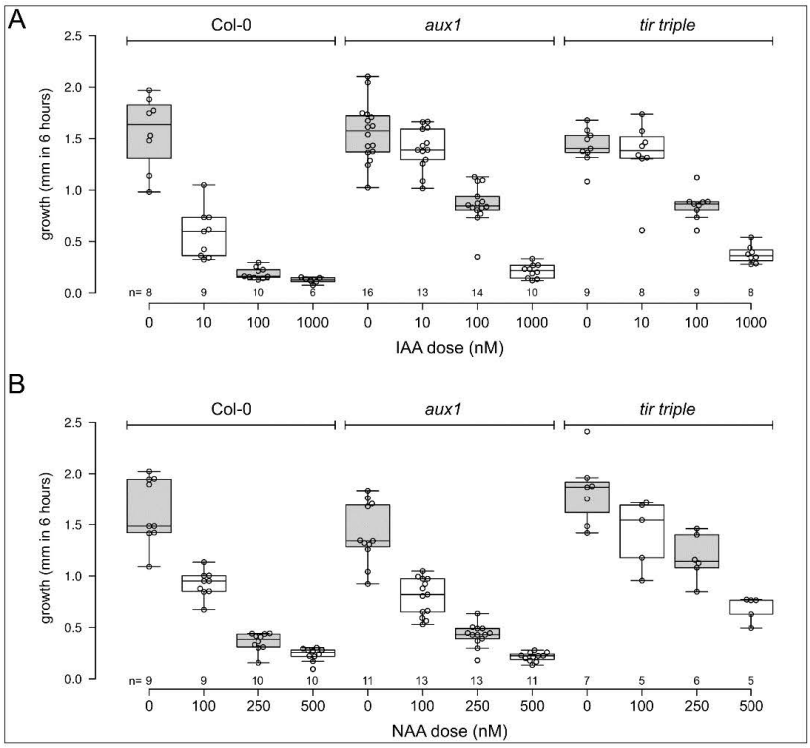


Fig. S3. A,B) Growth of control Col-0, *aux1* and *tir triple* mutant roots on the surface of media supplemented with increasing concentration of IAA or NAA. Growth was measured as the displacement of the root tip during a six-hour experiment. In the boxplots, center lines show the medians; box limits indicate the 25th and 75th percentiles as determined by R software; whiskers extend 1.5 times the interquartile range from the 25th and 75th percentiles, individual datapoints are represented by dots, n is indicated below each boxplot.

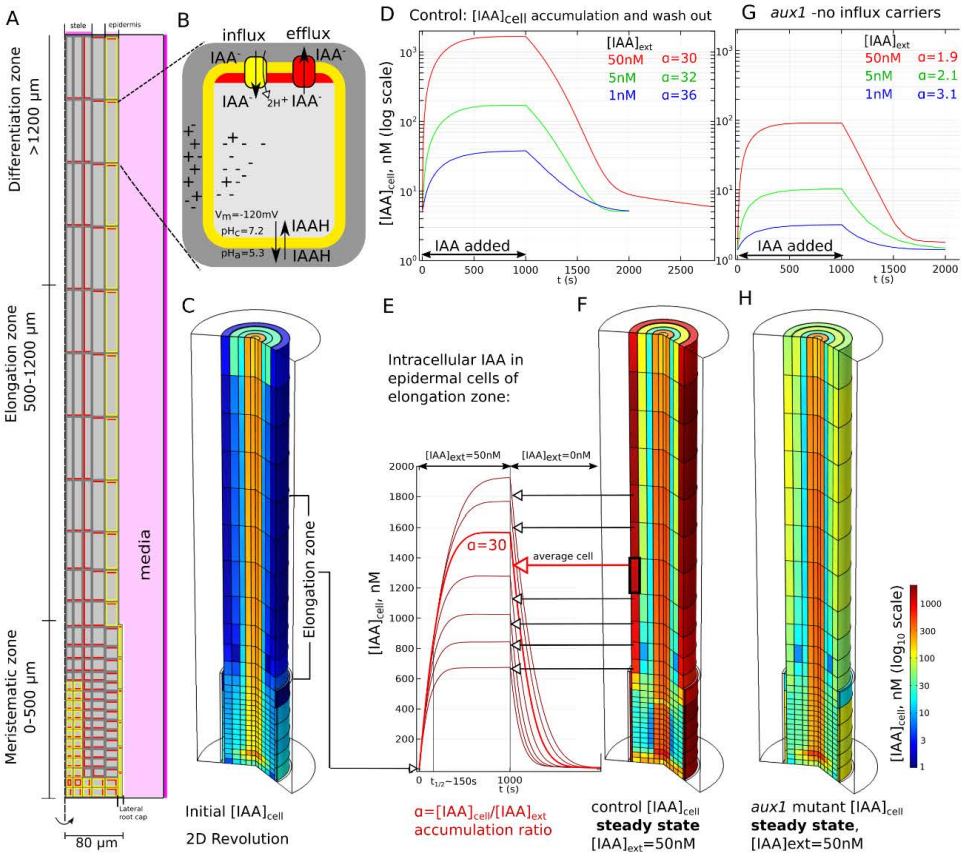


Fig. S4. A) Model geometry: intracellular domains (light gray), cell wall domain (dark gray), media (magenta). Magenta lines indicate boundaries with auxin concentration condition. Localization of influx (yellow) and efflux (red) transporters. B) Scheme of one cell showing three paths for IAA transport through membrane, that determine IAA flux. C) IAA concentration in the modeled root at $[IAA]_{ext} = 0$, that is used as initial condition in D. Scale bar in the right low corner is the same for C,F,H. D) Control root $[IAA]_{cell}$ accumulation for different $[IAA]_{ext}$ and wash out upon $[IAA]_{ext}$ removal (log scale). E) $[IAA]_{cell}$ accumulation and removal in control for $[IAA]_{ext}$ =50nM, volume-average for individual cells of elongation zone. The 5th cell above LRC accumulates average $[IAA]_{cell}$ of all cells. F) Control steady state auxin pattern at $[IAA]_{ext}$ =50nM, reached at ~1000s. G) aux1 root $[IAA]_{cell}$ accumulation for different $[IAA]_{ext}$ and wash out upon $[IAA]_{ext}$ removal (log scale). H) *aux1* steady state auxin pattern at $[IAA]_{ext}$ =50nM, reached at ~500s.

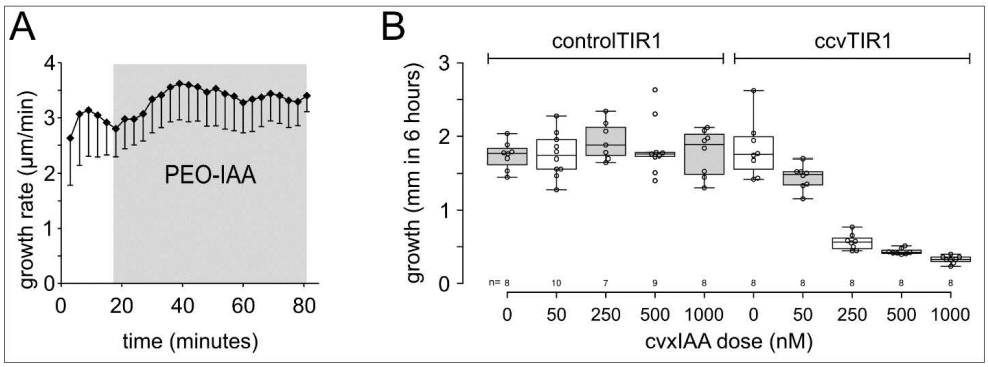


Fig. S5. A) PEO-IAA addition stimulates root growth. 5µM PEO addition is shaded grey. Mean of 9 roots, -SD. B) Growth of controlTIR1 and ccvTIR1 roots on medium with increasing concentrations of cvxIAA. Growth was measured as the displacement of the root tip during a six-hour experiment. In the boxplots, center lines show the medians; box limits indicate the 25th and 75th percentiles as determined by R software; whiskers extend 1.5 times the interquartile range from the 25th and 75th percentiles, individual datapoints are represented by dots, n is indicated below each boxplot.

Supplementary Tables

Table S1. Coefficients in Hill equations (Eq.12) fitted to experimental dose-response (Fig.1E, Fig.3D, Fig.4B), (±95% confidence bounds).

	IC_{50} , nM	GR_{min}	k
Control	1.44 (±0.23)	0.13 (±0.03)	1.63 (±0.43)
aux1	17.2 (±4.7)	0.14 (±0.03)	1.88 (±0.87)
tir triple	17.8 (± 2.01)	0	0.89 (±0.07)

Table S2. Permeability values and variation used in the model.

Parameter	**Value in the model, [μm/s]**	**Reference, reference value**	**Sensitivity of accumulation ratio α to permeabilities** [change in α per 0.1 μm/s]	
			α^{Col}=30.3	α^{aux1}=1.9
P_{AUX1} (permeability of influx carriers)	0.7±0.15 *	$P_{AUX1} \cdot A_2 = 1.5 \pm 0.3$ μm$/s$ => $P_{AUX1} = 0.35 \pm 0.07\ \mu m/s$ (Rutschow et al., 2014)	5.96	0
P_{PIN} (permeability of PIN efflux carriers)	0.5±0.2 **	$P_{PIN} \cdot B_3 = 2\ \mu m/s$ => $P_{PIN} = 0.43\ \mu m/s$ (Rutschow et al., 2014)	-3.17	- 0.49
P_{IAAH} (diffusive permeability for IAAH)	0.8±0.4 *	$P_{IAAH} = 0.35 \pm 0.22\ \mu m/s$ (Rutschow et al., 2014)	0.226	0.5
P_{NPE} (permeability of non-PIN-efflux carriers)	0	$P_{NPE} \leq 0.3 \cdot P_{PIN}$ (Band et al., 2014)	-149	- 2.88

* Permeabilities for influx carriers and diffusion are 2 times higher than the reference value to account for the lateral membranes, not included in the model geometry, which have area approximately equal to the area of membranes present in the model and also have the same permeabilities (Fig.S15C in (Band et al., 2014)).

** Efflux permeability doesn't account for the lateral membranes because efflux transporters are not present on these membranes.

Table S3. Other parameter values used in the model.

Parameter	Value	Reference
pH_{cell}	5.3	(Band et al., 2014)
pH_{wall}	7.2	(Band et al., 2014)
pK (IAA dissociation constant)	4.8	(Band et al., 2014)
D_c (IAA diffusion in cell)	$600\ \mu m^2/s$	(Swarup et al., 2005)
D_m (IAA diffusion in media)	$600\ \mu m^2/s$	(Swarup et al., 2005)
D_w (IAA diffusion in wall)	$32\ \mu m^2/s$	(Kramer et al., 2007)
V_m (membrane potential)	-120 mV	(Band et al., 2014)
Cell wall thickness	$0.2\ \mu m$	rounded from (Band et al., 2014)

Table S4. Accumulation ratios $\alpha=[IAA]_{cell}/[IAA]_{ext}$ for Control and *aux1* mutant , ± maximum variation based on variation of permeability values (see Table S2).

	3D numerical model	**simple 1D model, not accounting for PIN polarity**	**$(IC_{50}^{aux1})/(IC_{50}^{Col})$ from experimental fit (±95% confidence bounds)**
control α^{Col}	30.3 ±12.5	5.3 ±2.5	
aux1 α^{aux1}	1.9 ±0.5	0.4 ±0.2	
$\alpha^{Col}/\alpha^{aux1}$	**15.9 ± 5.5**	**13.3 ± 3.5**	**11.8 ± 3.77**

Supplementary References

1. Brunoud, G. *et al.* A novel sensor to map auxin response and distribution at high spatio-temporal resolution. *Nature* **482,** 103–6 (2012).
2. Moreno-Risueno, M. A. *et al.* Oscillating gene expression determines competence for periodic Arabidopsis root branching. *Science* **329,** 1306–11 (2010).
3. Swarup, R. *et al.* Structure-Function Analysis of the Presumptive Arabidopsis Auxin Permease AUX1. *Plant Cell* **16,** 3069–3083 (2004).
4. Dharmasiri, N. *et al.* Plant development is regulated by a family of auxin receptor F box proteins. *Dev. Cell* **9,** 109–119 (2005).
5. Uchida, N. *et al.* Chemical hijacking of auxin signaling with an engineered auxin–TIR1 pair. *Nat. Chem. Biol.* (2018). doi:10.1038/nchembio.2555
6. Grossmann, G. *et al.* Time-lapse Fluorescence Imaging of Arabidopsis Root Growth with Rapid Manipulation of The Root Environment Using The RootChip. *J. Vis. Exp.* e4290–e4290 (2012). doi:10.3791/4290
7. von Wangenheim, D. *et al.* Live tracking of moving samples in confocal microscopy for vertically grown roots. *Elife* **6,** (2017).
8. Li, L., Krens, S. F. G., Fendrych, M. & Friml, J. Real-time Analysis of Auxin Response, Cell Wall pH and Elongation in Arabidopsis thaliana Hypocotyls. *Bio-Protocol* **7,** 1–10 (2018).
9. P. Thévenaz, U.E. Ruttimann, M. U., Thevenaz, P., Ruttimann, U. E. & Unser, M. A Pyramid Approach to Subpixel Registration Based on Intensity. *IEEE Trans. Image Process.* **7,** 27–41 (1998).
10. Schneider, C. a, Rasband, W. S. & Eliceiri, K. W. NIH Image to ImageJ: 25 years of image analysis. *Nat. Methods* **9,** 671–675 (2012).
11. Schindelin, J. *et al.* Fiji: an open-source platform for biological-image analysis. *Nat. Methods* **9,** 676–682 (2012).
12. Swarup, R. *et al.* Root gravitropism requires lateral root cap and epidermal cells for transport and response to a mobile auxin signal. *Nat. Cell Biol.* **7,** 1057–1065 (2005).
13. Band, L. R. *et al.* Systems analysis of auxin transport in the Arabidopsis root apex. *Plant Cell* **26,** 862–875 (2014).
14. Grieneisen, V. A., Xu, J., Marée, A. F. M., Hogeweg, P. & Scheres, B. Auxin transport is sufficient to generate a maximum and gradient guiding root growth. *Nature* **449,** 1008–1013 (2007).
15. Van Den Berg, T., Korver, R. A., Testerink, C. & Ten Tusscher, K. H. W. J. Modeling halotropism: a key role for root tip architecture and reflux loop remodeling in redistributing auxin. *Development* **143,** 3350–3362 (2016).
16. Band, L. R. *et al.* Systems analysis of auxin transport in the Arabidopsis root apex. *Plant Cell* **26,** 862–875 (2014).
17. Kramer, E. M., Frazer, N. L. & Baskin, T. I. Measurement of diffusion within the cell wall in living roots of Arabidopsis thaliana. *J. Exp. Bot.* **58,** 3005–3015 (2007).
18. Rutschow, H. L., Baskin, T. I. & Kramer, E. M. The carrier AUXIN RESISTANT (AUX1) dominates auxin flux into Arabidopsis protoplasts. (2014).
19. Delbarre, A., Muller, P., Imhoff, V. & Guern, J. Comparison of mechanisms controlling uptake and accumulation of 2,4-dichlorophenoxy acetic acid, naphthalene-1-acetic acid, and indole-3-acetic acid in suspension-cultured tobacco cells. *Planta* **198,** 532–541 (1996).
20. Kramer, E. M., Rutschow, H. L. & Mabie, S. S. AuxV: a database of auxin transport velocities. *Trends Plant Sci.* **16,** 461–463 (2011).
21. Carrier, D. J. *et al.* The binding of auxin to the Arabidopsis auxin influx transporter AUX1. *Plant Physiol.* **148,** 529–35 (2008).

22. Kramer, E. M. & Ackelsberg, E. M. Auxin metabolism rates and implications for plant development. *Front. Plant Sci.* **6,** 150 (2015).
23. Band, L. R. *et al.* Root gravitropism is regulated by a transient lateral auxin gradient controlled by a tipping-point mechanism. *Proc. Natl. Acad. Sci. U. S. A.* **109,** 4668–4673 (2012).
24. Swarup, R. *et al.* Localization of the auxin permease AUX1 suggests two functionally distinct hormone transport pathways operate in the Arabidopsis root apex. *Genes Dev.* **15,** 2648–53 (2001).
25. Katzung, B. G. & Trevor, A. J. *Basic and clinical pharmacology*. (2012).
26. Calderón Villalobos, L. I. A. *et al.* A combinatorial TIR1/AFB-Aux/IAA co-receptor system for differential sensing of auxin. *Nat. Chem. Biol.* **8,** 477–85 (2012).
27. Evans, M. L. & Ishikawa, H. Responses of Arabidopsis roots to auxin studied with high temporal resolution : Comparison of wild type and auxin-response mutants. (1994).
28. Giraldo, J., Vivas, N. M., Vila, E. & Badia, A. Assessing the (a)symmetry of concentration-effect curves: Empirical versus mechanistic models. *Pharmacol. Ther.* **95,** 21–45 (2002).

International Journal of
Molecular Sciences

MDPI

Article

Relative Contribution of PIN-Containing Secretory Vesicles and Plasma Membrane PINs to the Directed Auxin Transport: Theoretical Estimation

Sander Hille [1,†], Maria Akhmanova [2,†], Matouš Glanc [2,3], Alexander Johnson [2] and Jiří Friml [2,*]

1 Mathematical Institute, Faculty of Science, Leiden University, 2333 CA Leiden, The Netherlands; shille@math.leidenuniv.nl
2 Institute of Science and Technology (IST) Austria, Am Campus 1, 3400 Klosterneuburg, Austria; axmahoba@gmail.com (M.A.); matous.glanc@gmail.com (M.G.); alexander.johnson@ist.ac.at (A.J.)
3 Department Experimental Plant Biology, Faculty of Science, Charles University, 12843 Prague, Czech Republic
* Correspondence: jiri.friml@ist.ac.at; Tel.: +43-2243-9000-5401
† These authors contributed equally to this work.

Received: 17 September 2018; Accepted: 4 November 2018; Published: 12 November 2018



Abstract: The intercellular transport of auxin is driven by PIN-formed (PIN) auxin efflux carriers. PINs are localized at the plasma membrane (PM) and on constitutively recycling endomembrane vesicles. Therefore, PINs can mediate auxin transport either by direct translocation across the PM or by pumping auxin into secretory vesicles (SVs), leading to its secretory release upon fusion with the PM. Which of these two mechanisms dominates is a matter of debate. Here, we addressed the issue with a mathematical modeling approach. We demonstrate that the efficiency of secretory transport depends on SV size, half-life of PINs on the PM, pH, exocytosis frequency and PIN density. 3D structured illumination microscopy (SIM) was used to determine PIN density on the PM. Combining this data with published values of the other parameters, we show that the transport activity of PINs in SVs would have to be at least 1000× greater than on the PM in order to produce a comparable macroscopic auxin transport. If both transport mechanisms operated simultaneously and PINs were equally active on SVs and PM, the contribution of secretion to the total auxin flux would be negligible. In conclusion, while secretory vesicle-mediated transport of auxin is an intriguing and theoretically possible model, it is unlikely to be a major mechanism of auxin transport *in planta*.

Keywords: auxin; polar auxin transport; PIN transporters; secretion; 3D-SIM microscopy; mathematical modeling

1. Introduction

The plant hormone auxin (indole-3-acetic acid; IAA) is subject to intercellular polar auxin transport (PAT) mediated by diffusion and the action of efflux and influx carriers. PAT generates local auxin maxima that are crucial for a plethora of developmental processes [1]. Therefore, studies into the mechanism of auxin transport and its regulation have had a prominent place in the auxin field. Auxin maxima-driven developmental events depend on the activity of the PIN-formed (PIN) IAA efflux carriers, which provide directionality to intercellular IAA transport through their asymmetric subcellular localization [1–3]. The PIN proteins constitutively cycle between the plasma membrane (PM) and endosomal compartments [4–6], and the developmental importance of this energetically demanding phenomenon has not been unequivocally explained. Three hypotheses have been suggested [7] to explain the requirement of PIN recycling: (1) recycling enables rapid relocation

of PINs and thereby the rapid redirection of auxin transport; (2) PINs serve as IAA transceptors (transporters and receptors at the same time) and their recycling is important for the process of signal transduction; and (3) the PIN-containing secretory vesicles (SVs) are filled with auxin, which is released into the apoplast upon fusion of the SV with the PM. This process is analogous to neurotransmitter release in animals, and is important for the transport of auxin as suggested by previous reports [7,8] (Figure 1).

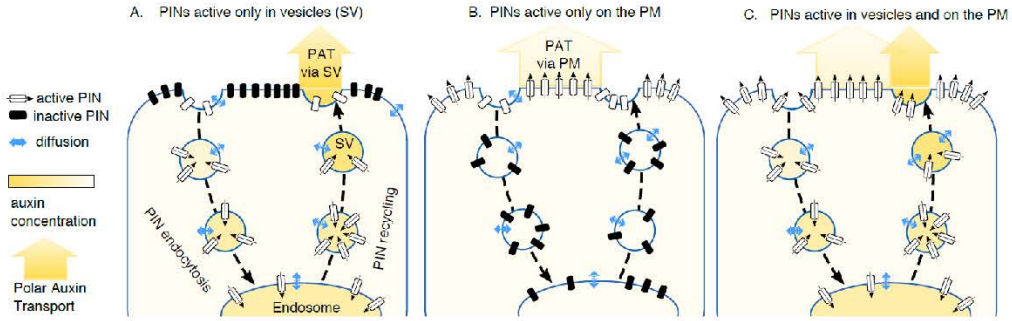


Figure 1. (**A**–**C**) chematics of PIN-formed (PIN) endomembrane trafficking and possible auxin transport mechanisms.

Several studies claimed to have proven the vesicular transport of IAA [9–11]. However, the validity of the evidence presented in most of these studies has been questioned by many researchers in the field, and thus the hypothesis of vesicular transport of auxin remains controversial [12,13]. A major reason this controversy exists is the inability to uncouple vesicular trafficking from PIN occurrence at the PM using existing cell biology methods. For example, if one could genetically or pharmacologically completely and specifically block the movement of PIN-containing secretory vesicles, it would be impossible to conclude whether the resulting reduction in auxin transport was caused by the lack of IAA secreting vesicles or by the lack of PINs at the PM.

Here, we have constructed a simple mathematical model to estimate the parameters under which auxin transport by intracellular vesicles could explain the measured net flux values of PAT. We show that a vesicular transport model would require at least 1000 times greater PIN activity than the conventional PM transport model to generate the same net flux values.

2. Results

2.1. Model Assumptions: PINs Can Be Active on the Endomembrane Vesicles Exclusively or in Addition to Their Activity on the Plasma Membrane (PM)

PAT is characterized by the sustained velocity of auxin over long distances (several millimeters, which is much greater than a typical cell length). The magnitude of this velocity is in the range of $1-10\frac{\mu m}{s}$ for different species and different types of plant tissue [14]. Arabidopsis root epidermal cells serve as a useful example because many of the physiological parameters that influence the PAT, and thus used in our calculations, have been experimentally measured in this cell type. Furthermore, vesicular auxin transport has been proposed to play a role in the transition zone of the root [9]. Thus, we chose to apply our model to this tissue. In the roots, auxin is transported towards the root tip inside the central cells (stele), whereas in the outer cell layer (lateral root cap cells and epidermal cells) it is transported in the reverse direction: from the root tip towards the shoot [15]. The velocity of this directed transport in *Arabidopsis* roots was found to be in a range $2-3\frac{\mu m}{s}$ [16]. We therefore assume that $v_{PAT} \geq 1\frac{\mu m}{s}$ in the epidermal cells in the root transition zone and estimated the permeability of PINs needed to yield this value.

In our model we consider only secretory/recycling vesicles (SVs) that fuse with the PM, and consider these secretory vesicles as the method of PIN delivery from the endosome to the PM.

For such auxin-transporting vesicles we considered two hypothetical scenarios: (1) PINs transport auxin exclusively in these endomembrane vesicles, which we compare to the case when PINs are active only on the PM (published results) [17–19]; and (2) PINs transport auxin both in the vesicles and on the PM. The auxin permeability of a PIN-containing membrane (P_{PIN}) remains undetermined. However, P_{PIN} has been calculated previously for a scenario when PINs are active solely on the PM (P_{PIN}^{PM}) [17,18]. Therefore, the permeability of PINs in vesicles P_{PIN}^{v} is a readout rather than input to our calculations. We calculated (1) the relative values of permeability P_{PIN}^{v} and the individual activity of PINs proteins needed for the vesicular transport model to generate the same net flux as the PM model and (2) the relative contribution of the vesicular transport to the net flux, assuming that PINs activity is the same in the vesicles and in the PM. A plan of the model and performed calculations is presented in Figure 2A.

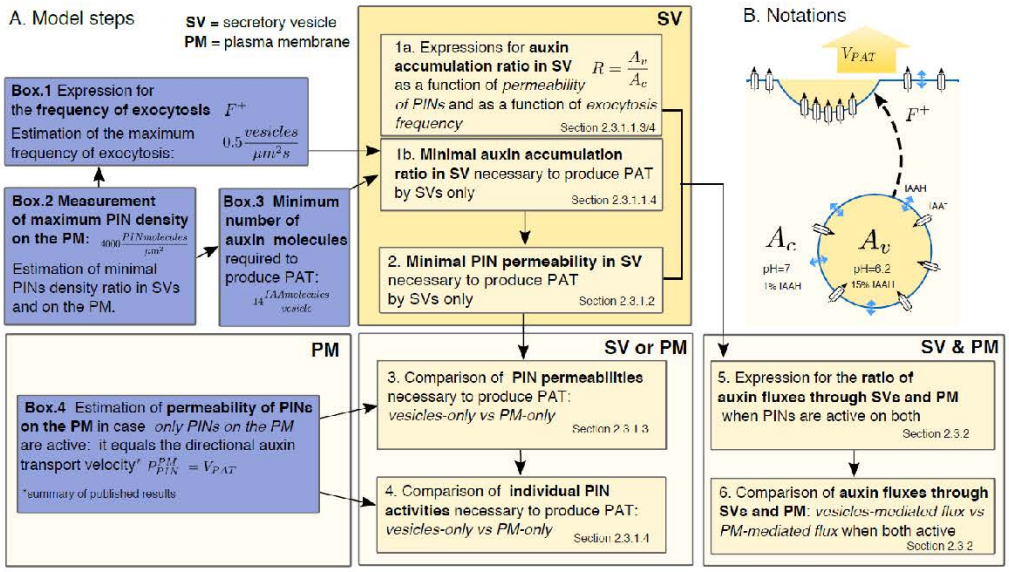


Figure 2. (**A**) Map of the model steps and usage of results from side-calculations presented in boxes; (**B**) scheme of the auxin transport into the secretory vesicle (SV) and illustration of variables used in the model.

2.2. *Short Summary of Model Results*

(1) For the case when only vesicular PINs are actively transporting auxin, we derived equations for auxin concentration inside the vesicles, which depends on the permeability of the vesicle membrane to auxin due to PINs (P_{PIN}^{v} $[\frac{\mu m}{s}]$, the measure of how many auxin molecules per second are transported through 1 μm^2 area of a membrane when it is unit auxin concentration ($1\frac{mol}{\mu m^2}$) outside the vesicle). At the same time, intravesicular auxin concentration determines the amount of auxin released into the cell wall. Therefore, we related macroscopic auxin transport velocity (v_{PAT} $[\frac{\mu m}{s}]$) to P_{PIN}^{v} and calculated the coefficient of proportionality between these variables for the physiological values of the other parameters: $\boldsymbol{P_{PIN}^{v\text{-}only} \geq 42 \cdot v_{PAT}}$.

However, if PINs are only active on the PM, then PINs permeability $\boldsymbol{P_{PIN}^{PM\text{-}only} \simeq v_{PAT}}$ [17]. Thus, for the minimal velocity $v_{PAT} = 1\frac{\mu m}{s}$, as observed in epidermal root cells [14], the lowest possible value of permeability is $P_{PIN}^{v\text{-}only} \simeq 42\frac{\mu m}{s}$ for vesicular transport, which is much higher than the permeability required for PM transport $P_{PIN}^{PM\text{-}only} \simeq 1\frac{\mu m}{s}$.

As the permeability is proportional to the density of PINs (the number of PIN molecules per unit area of the membrane), we generalized our equations via dividing permeability values by the density of PINs. The resulting quantity is the activity of individual PINs. We show that on the vesicle

membrane PINs' activity has to be 3 orders of magnitude higher than in the scenario where they are active only on the PM, in order to produce the same PAT velocity:

$$\frac{\text{PINs activity on SV only}}{\text{PINs activity on PM only}} > 4200. \quad (1)$$

(2) For the case when PINs are active both in vesicles and on the PM, our model provides the ratio of auxin amount passing through these two mechanisms depending on individual activities of PIN molecules in these domains:

$$\frac{\text{Auxin flux through PM}}{\text{Auxin flux through SV}} = \mathbf{4200} \cdot \frac{\text{PINs activity on PM}}{\text{PINs activity on SV}}. \quad (2)$$

Thus, if activities are equal, auxin flux through SVs contributes no more than 0.02% of the total flux.

Conclusion: The transport of auxin by vesicles is ~1000 times less efficient than through PINs active on the PM. Permeability values of PINs (P^{v}_{PIN} and P^{PM}_{PIN}) still await direct measurements, but values as high as $P^{v}_{PIN} = 42\frac{\mu m}{s}$, as estimated in our study, are unlikely. Therefore, this argues against vesicular transport of auxin in SVs as a major mechanism of directional auxin transport.

2.3. Detailed Model Description

2.3.1. PINs Active Only in Vesicles. Comparison to the Case When PINs are Active Only on PM

List of parameters used in the model is provided in the Table 1. Assumptions taken throughout the model description are listed in Table 2.

2.3.1.1. How Much Auxin Should a Vesicle with Active PIN Contain to Produce the PAT?

(1) Size of a Vesicle

The size of exocytotic vesicles that are considered to perform auxin transport is well known; they are spherical in shape and their diameter was reported to be $d = 0.06 - 0.08$ µm [20] (see Table 1 for corresponding surface area and volume).

Table 1. Values of parameters used in this study.

Parameter	Description	Value/Range	Ref.
d	Typical diameter of a vesicle	0.06–0.08 μm	[20]
$S_v = \pi d^2$	Surface area of a vesicle	1.1–2.0 $\times 10^{-2}$ μm^2	
$V_v = (1/6)\pi d^3$	Volume of a vesicle	1.1–2.7 $\times 10^{-4}$ μm^3	
pH_v	pH in the lumen of the trans-Golgi network/early endosome (TGN/EE)-derived vesicle	5.5–6.5	[21,22]
pH_c	pH in the cytoplasm	7	[21,22]
v_{PAT}	Speed of directional plant hormone auxin (IAA) transport in epidermal cells of Arabidopsis root tip	2–3 μm/s	[14,16]
$\tau_{1/2}$	Half-life of PINs on the plasma membrane (PM)	1.3 $\times 10^4$ s	[23]
$(\rho_v)_{min}$	Minimum PIN density in a vesicle	$50 \frac{1}{\mu m^2}$	One molecule per vesicle
$(\rho_{PM})_{max}$	Maximum PIN density on a plasma membrane	$2 \times 10^4 \frac{1}{\mu m^2}$ $4 \times 10^3 \frac{1}{\mu m^2}$	Close-packing of equal spheres of 4 nm radius. Estimate based on experimental data, this study.
P_{diff}(IAAH)	Diffusional permeability of IAA through membrane	0.5 μm/s	[18,24]

Table 2. List of assumptions *.

	Assumption	Effect on Efficiency of SVs to Transport Auxin	Effect on Efficiency of PM to Transport Auxin
1	Steady state/homogeneity: auxin fluxes and parameters that influence auxin fluxes are constant in time. Note, that experimentally measured values of parameters used in the model were also assumed to be constant when measured (Table 1): size of SV, pH in the cell and in SV, and listed below:		
1.1	PINs density on the PM equals an average density of PINs, being constant and homogenous along the whole polar side of the PM.		
1.2	PINs density on SVs is constant, all SV are identical and contain the same density of PINs.		
1.3	Intracellular auxin concentration near the PM is constant and homogenous.		
1.4	Intravesicular auxin concentration is homogenous.		
1.5	Removal of PINs from the PM is proportional to the PINs concentration on the PM and is a constant process in time, characterized by constant half-life of PINs on the PM. It doesn't depend on the exocytosis rate.	Less efficient	No effect
2	SVs fuse with the PM and deliver all PIN proteins that they contain to the PM.	Less efficient	No effect
3	SV fills with auxin to its maximum concentration and then all auxin inside the SV is released outside the cell.	More efficient	No effect
4	Diffusion of anion form (IAA^-) through the membrane (PM and SV) is negligible.	More efficient	-
5	PINs transport auxin (IAA^-) only in one direction (inside the vesicle, outside the cell on the PM).	More efficient	More efficient
6	Non-polar auxin transport is neglected when equating auxin flux through PM or via SVs and directional auxin transport rate	More efficient, magnitude of correction is the same for PM and SVs	

* Validation of each assumption is provided in the text; most assumptions favor vesicular transport (increase auxin efflux mediated by SVs) and are taken to estimate minimal requirements for vesicular auxin transport.

(2) Biochemical Constituents and Transport Processes, Equation for Auxin Concentration inside the Vesicle

The total concentration of auxin (IAA) is the mixture of anions IAA^- and protonated form (IAAH), and the ratio between them depends on pH of the solution:

$pH_c = 7$ in cytoplasm, ~99% of IAA^-, 1% of IAAH

$pH_v = 5.5$ *to* 6.5 in vesicle, ~83–98% of IAA^-, 17–2% of IAAH

$pK_a = 4.8$ for IAA.

The fractions of IAA in anion form in cytosol and vesicle are denoted by f_{ac} and f_{av} respectively. The values were computed using:

$$f_{av} = \frac{1}{1 + 10^{pK_a - pH_v}}, \tag{3}$$

$$f_{ac} = \frac{1}{1 + 10^{pK_a - pH_c}}. \tag{4}$$

Thus, $(1 - f_{av})$ and $(1 - f_{ac})$ are fractions of IAAH in vesicle and cytosol, respectively (see Figure 2B and Table 3 for IAA^- fractions depending on pH).

We denote:

A_c—cytoplasmic concentration of auxin [mol/L],

A_v—concentration of auxin inside the vesicle [mol/L].

Fast diffusion in the cytoplasm ($D \cong 670$ μm^2/s [17,25]) ensures fast mixing of IAA inside the small vesicle, that takes $\tau_{diff} \leq 10^{-6}$ s in vesicles of diameter $d \leq 100$ nm. Thus, IAA concentration inside the vesicle can be considered homogenous and increases proportionally to the flux through the membrane:

$$\frac{dA_v}{dt} = \frac{1}{V_v} J_{in}^{net}, \tag{5}$$

where J_{in}^{net} is the net influx of IAA into vesicle (units [mol/s]), which has two components: transport of anions IAA^- by PINs and transport of IAA^- and $IAAH$ by diffusion through the membrane:

$$J_{in}^{net} = J_{PIN}^{IAA^-} + J_{diff}. \tag{6}$$

PINs transport anions IAA^- and are presumed to be permeable only in one direction (into vesicle) resulting in the unknown permeability P_{PIN}^{v} of the vesicular membrane. We neglect dependence of PIN-mediated influx on intravesicular auxin concentration and assume that reverse permeability is zero. By doing so, we make PINs more efficient in our considerations than they can possibly be in reality. This approach is acceptable because our aim is to find the lower bound of the permeability of PINs which is able to produce the physiologically observed PAT transport.

Thus, PIN-mediated transport is simplified to:

$$J_{PIN}^{IAA^-} = P_{PIN}^{v} S_v f_{ac} A_c. \tag{7}$$

Diffusive flux across the membrane is governed by Fick's law:

$$J_{diff} = J_{diff}^{IAAH} + J_{diff}^{IAA^-} = P_{diff}^{IAAH} S_v ((1 - f_{ac}) A_c - (1 - f_{av}) A_v) + P_{diff}^{IAA^-} S_v (f_{ac} A_c - f_{av} A_v). \tag{8}$$

Diffusional permeability for IAAH is known: $P_{diff}^{IAAH} = 0.5$ μm/s [18,24]. IAAH is assumed to have the same diffusional permeability P_{diff}^{IAAH} in both directions.

Anion diffusion permeability is estimated to be much lower: $P_{diff}^{IAA^-} \leq \frac{P_{diff}(\text{IAAH})}{100}$ [24]. However, at $pH_v = 7$, concentration of $[IAA^-] \cong 165 \cdot [IAAH]$ and thus diffusional flux of IAA^-. can be of the same order of magnitude as IAAH flux. Nevertheless, to simplify the equations we omit the term for IAA^- diffusion. As diffusion of IAA^- acts against PINs-mediated transport, this simplification also favors auxin accumulation into vesicles.

Combining Equations (7) and (8) and neglecting $J_{diff}^{IAA^-}$ result in the following expression for the net total flux:

$$J_{in}^{net} = P_{PIN}^{v} S_v f_{ac} A_c + P_{diff}^{IAAH} S_v ((1 - f_{ac}) A_c - (1 - f_{av}) A_v). \quad (9)$$

Thus, Equation (5) can be rewritten as:

$$\frac{dA_v}{dt} = A_c \cdot \alpha - \lambda \cdot A_v, \quad (10)$$

where,

$$\alpha = \frac{P_{PIN}^{v} S_v}{V_v} f_{ac} + \frac{P_{diff}^{IAAH} S_v}{V_v} (1 - f_{ac}), \quad (11)$$

$$\lambda = \frac{P_{diff}^{IAAH} S_v}{V_v} (1 - f_{av}). \quad (12)$$

(3) Maximum Loading of Vesicles with Auxin is Proportional to the Permeability of PINs

We assume that vesicles exist in the cytoplasm long enough that the internal vesicular auxin concentration reaches its maximum: steady state concentration A_v. The analytical solution of Equation (10) reads:

$$A_v(t) = A_c \frac{\alpha}{\lambda} \left(1 - e^{-\lambda t}\right) + e^{-\lambda t} A_v(0). \quad (13)$$

Thus, characteristic time to load vesicle from zero concentration till $A_v = A_c \cdot \frac{\alpha}{\lambda} \left(1 - \frac{1}{e}\right)$ is $\tau_{load} = \frac{1}{\lambda} =$ 4.6 s for $pH_v = 7$ (and faster for $pH_v < 7$). For times $t \gg \tau_{load}$ vesicles will be fully filled. We consider fully filled vesicles because our aim is to find the *minimal* requirements for the vesicular transport, and partly filled vesicles would require *higher* permeability values to produce the PAT.

At steady state, when $\frac{dA_v}{dt} = 0$, Equation (10) simplifies to:

$$A_c \cdot \alpha = \lambda \cdot A_v. \quad (14)$$

Thus, the number of IAA molecules (in moles) in one vesicle:

$$N_v^{max} = A_v^{max} \cdot V_v = A_c \cdot V_v \frac{\alpha}{\lambda}. \quad (15)$$

Substituting α and λ by their expressions gives:

$$N_v^{max} = A_c \cdot V_v \left[\frac{P_{PIN}^{v}}{P_{diff}^{IAAH}} \cdot \frac{f_{ac}}{1 - f_{av}} + \frac{1 - f_{ac}}{1 - f_{av}} \right], \quad (16)$$

that shows that the number of auxin molecules loaded inside the vesicle is proportional to P_{PIN}^{v}.

We can also rewrite this equation in the form:

$$N_v^{max} = A_c \cdot V_v \cdot R, \quad (17)$$

where,

$$R = \frac{A_v^{max}}{A_c} = \frac{P_{PIN}^{v}}{P_{diff}^{IAAH}} \cdot \frac{f_{ac}}{1 - f_{av}} + \frac{1 - f_{ac}}{1 - f_{av}} \quad (18)$$

is the accumulation ratio—the ratio of intravesicular IAA concentration to that in the cytoplasm surrounding the vesicle. Expressions for accumulation ratio and maximum loading of vesicles for different pH_v are presented in Table 3.

Table 3. Dependence of the accumulation ratio **R** (Equation (18)) and maximum number of molecules in the vesicle N_v^{max} (Equation (15)) on pH in the vesicle. The last column provides the lower bounds for $\frac{P_{PIN}^{v\text{-}only}}{P_{diff}^{IAAH}}$, required to yield directional transport of auxin v_{PAT} depending on pH_v. $f_{Hv/c}$ —fraction of IAA^- in the vesicle/cytoplasm, $(1 - f_{av/c})$ —fraction of IAAH in the vesicle/cytoplasm.

pH_v	f_{av}	$1-f_{av}$	R *	N_v^{max}	$\frac{P_{PIN}^{v\text{-}only}}{P_{diff}^{IAAH}}$
5.5	0.833	0.167	$6.0 \cdot \frac{P_{PIN}^{v}}{P_{diff}} + 0.036$ **	$0.096 \cdot \frac{P_{PIN}^{v}}{P_{diff}}$	$\geq 2330 \frac{s}{\mu m} \cdot v_{PAT}$
6.2	0.962	0.038	$26.2 \cdot \frac{P_{PIN}^{v}}{P_{diff}} + 0.16$ **	$0.42 \cdot \frac{P_{PIN}^{v}}{P_{diff}}$	$\geq 535 \frac{s}{\mu m} \cdot v_{PAT}$
6.5	0.980	0.020	$49.7 \cdot \frac{P_{PIN}^{v}}{P_{diff}} + 0.3$ **	$0.80 \cdot \frac{P_{PIN}^{v}}{P_{diff}}$	$\geq 280 \frac{s}{\mu m} \cdot v_{PAT}$
7.0	$0.994 = f_{ac}$	$0.006 = 1 - f_{ac}$	$166 \cdot \frac{P_{PIN}^{v}}{P_{diff}} + 1$ **	$2.7 \cdot \frac{P_{PIN}^{v}}{P_{diff}}$	$\geq 84 \frac{s}{\mu m} \cdot v_{PAT}$

* For lower pH_v accumulation ratios R have lower coefficient in front of $\frac{P_{PIN}^{v\text{-}only}}{P_{diff}^{IAAH}}$ because diffusion from the vesicle, that acts against PIN-mediated influx, is higher for lower pH_v. ** the right terms are always much smaller than the left terms and can be neglected, because $v_{PAT} \geq 1 \frac{\mu m}{s}$ and thus $\frac{P_{PIN}^{v}}{P_{diff}} > 84$.

(4) Lower Bound for Accumulation Ratio Necessary to Produce the PAT

In this section we estimated the auxin accumulation ratio R in vesicles, which is necessary to produce v_{PAT} if auxin is transported via vesicles *only*. Auxin flux density (molecules passed per unit area per second) on the polar domain of the PM that corresponds to v_{PAT} velocity is given by:

$$\Phi_{cell \to apoplast} = v_{PAT} \cdot A_c \left[\frac{mol}{\mu m^2 \cdot s} \right]. \quad (19)$$

Maximum flux of auxin, that vesicles can carry through the PM is:

$$\Phi_v = N_v^{max} \cdot F_{max}^{+} \left[\frac{mol}{\mu m^2 \cdot s} \right], \quad (20)$$

where F_{max}^{+} is the maximum exocytosis frequency (vesicles per second fusing with the unit area of cell face). This flux should be not lower than the yielded flux:

$$\Phi_v \geq \Phi_{cell \to apoplast}. \quad (21)$$

This equation takes into account that diffusion diminishes the directional transport (see Box 4 for explanation).

Thus,

$$N_v^{max} \cdot F_{max}^{+} \geq v_{PAT} \cdot A_c. \quad (22)$$

which gives, using Equation (17):

$$R \cdot A_c \cdot V_v \cdot F_{max}^{+} \geq v_{PAT} \cdot A_c. \quad (23)$$

Consequently,

$$R \geq \frac{v_{PAT}}{V_v \cdot F_{max}^{+}}. \quad (24)$$

Substituting F_{max}^{+} with its expression (see Equation (1.7) in Box 1) $F_{max}^{+} = \frac{ln2}{S_v \cdot \tau_{1/2}} \left(\frac{\rho_{PM}}{\rho_v} \right)_{max}$, we can find the lower bound of the accumulation ratio, that is required for v_{PAT} :

$$R \geq \frac{v_{PAT} \cdot S_v \cdot \tau_{1/2}}{V_v \cdot ln2} \left(\frac{\rho_v}{\rho_{PM}} \right)_{min}. \quad (25)$$

Note, that intracellular auxin concentration A_c cancels (Equation (23)), which means that the equations are valid for any A_c. Nevertheless, we checked that vesicles will contain at least one molecule of auxin for the physiological value of A_c, a condition required for auxin transport to be theoretically possible (see Box 3). We also calculated the minimum accumulation ratio required for $v_{PAT} = 1$ μm/s (Box 3).

Box 1. Expression for F^+, frequency of secretory vesicles fusing with PM, and estimation of its maximum value F^+_{max}.

In the following text we will consider only the polar domain of PM, which is the front membrane in the direction of PAT. It contains more PINs than the neighboring sides of the PM, and is visible by fluorescence microscopy [23]. The density of PINs depends on the rate of their delivery to PM by vesicles and on the rate of their removal. We assume that within the polar domain PINs are homogeneously distributed. Mass conservation for the number of PINs on a polar domain of the PM of area S_{PM} then reads:

$$\frac{dn}{dt} = n_v F^+ S_{PM} - \beta \cdot n, \tag{1.1}$$

where n —number of PINs on PM, n_v—number of PINs in one vesicle, F^+ is frequency of exocytosis. PINs come to PM via $F^+ S_{PM}$ vesicles per second. Removal of PINs is proportional to n with the decay coefficient β, which describes any possible decay mechanism (through endocytosis, diffusion to other PM domains, degradation etc.).

The decay coefficient β can be found from the following arguments. The equation for PINs that are already delivered to the PM (let us call them "old PINs") and are only removed from the PM is the same as Equation (1.1) without exocytosis term:

$$\frac{dn_{old}}{dt} = -\beta \cdot n_{old}. \tag{1.2}$$

The solution of this equation reads:

$$n_{old}(t) = n_{old}(0) e^{-\beta \cdot t}. \tag{1.3}$$

Introducing half-life $\tau_{1/2}$, time when 50% of PINs has been removed ($n_{old}(\tau_{1/2}) = n_{old}(0)/2$), gives β:

$$\beta = \frac{ln2}{\tau_{1/2}}. \tag{1.4}$$

$\tau_{1/2} = 1.3 \times 10^4$ s, which has been measured by Jásik et al. ([23]) for functional PIN2-Dendra translational fusion protein in epidermal cells of Arabidopsis root. In their experiments, Jásik et al. ([23]) visualized "old PINs" separately from newly arriving PINs by use of photoconvertion of PIN2-Dendra.

Assuming that β is constant and does not depend on the method of PINs visualization, and assuming a steady state of PINs concentration on the PM, $\frac{dn}{dt} = 0$, Equation (1.1) transforms to:

$$n_v F^+ S_{PM} = \beta \cdot n. \tag{1.5}$$

Equations (1.4) and (1.5) give us expression for F^+, the frequency of vesicle fusion with the PM:

$$F^+ = \frac{ln2}{S_{PM} \cdot \tau_{1/2}} \frac{n}{n_v}, \tag{1.6}$$

We rewrite it using $\rho_{PM} = \frac{n}{S_{PM}}$, $\rho_v = \frac{n_v}{S_v}$—densities of PINs on the PM and vesicle membrane respectively:

$$F^+ = \frac{ln2}{S_{PM} \cdot \tau_{1/2}} \frac{n}{n_v} = \frac{ln2}{S_{PM} \cdot \tau_{1/2}} \frac{\rho_{PM}}{\rho_v} \frac{S_{PM}}{S_v} = \frac{ln2}{S_v \cdot \tau_{1/2}} \frac{\rho_{PM}}{\rho_v}. \tag{1.7}$$

Finally, introducing values for S_v and $\tau_{1/2}$ gives:

$$F^+ = \frac{0.69}{1.1 \times 10^{-2}\ \mu m^2 \cdot 1.3 \times 10^4\ s} \frac{\rho_{PM}}{\rho_v} = \frac{\rho_{PM}}{\rho_v} \cdot 0.005 \frac{1}{\mu m^2\ s}, \tag{1.8}$$

Introducing an estimation of minimum value for densities ratio $\left(\frac{\rho_v}{\rho_{PM}}\right)_{min} = 0.01$ (see Box 2) into Equation (1.8) gives the upper bound for F^+:

$$F^+_{max} = 0.5 \frac{vesicles}{\mu m^2\ s}. \tag{1.9}$$

The experimentally measured endocytosis rate gives an alternative estimate of the exocytosis rate.

In accordance with the above result, the measured rate of endocytosis is $\sim 0.5 \frac{vesicles}{\mu m^2\ s}$ (Table 4). The total area of vesicles fusing with the PM in one cell has to be balanced by the area of endocytosed vesicles. Given that sizes of exocytotic and endocytotic vesicles are the same, the maximal rate of endocytosis gives a rough estimate of the maximal possible rate of exocytosis, which is in the same order of magnitude as our maximal theoretical estimate.

It is worth noting that the half-life of PINs $\tau_{1/2}$ was measured for "old" PINs and does not account for the possibility of "old" PINs being removed and brought back to the membrane via vesicles. This process would effectively reduce $\tau_{1/2}$ and allow for a higher F^+_{max}. However, based on our comparison with experimental values of endocytosis, we argue that F^+_{max} cannot be much higher than $0.5 \frac{vesicles}{\mu m^2\ s}$. This restriction comes from the physiological *in vivo* rate of endocytic vesicle formation (taking ~18–22 s per vesicle, see Table 4 [26]) and limited area of the cell membrane. Thus, as $\left(\frac{\rho_v}{\rho_{PM}}\right)_{max} = 1$, $\tau_{1/2}$ can be reduced not more than by 100.

Box 2. Estimation of minimal PINs density ratio on vesicles and the PM: $\left(\frac{\rho_v}{\rho_{PM}}\right)_{\min}$.

The lowest possible density of PINs on the vesicular membrane is one PIN molecule per vesicle: $(\rho_v)_{min} = \frac{1}{S_v} = 50\frac{1}{\mu m^2}$.

The maximum PIN density can be calculated as follows: diameter of the globular 60 kDa protein is ~8 nm. If PINs on the PM are densely packed, their density is at most $(\rho_{PM})_{max} \cong 2 \times 10^4 \frac{1}{\mu m^2}$, which is the maximum value of PIN density on the PM.

Thus,

$$\left(\frac{\rho_v}{\rho_{PM}}\right)_{min} = \frac{(\rho_v)_{min}}{(\rho_{PM})_{max}} = 0.002. \quad (2.1)$$

However, PINs probably cannot reach this maximum density *in vivo*, because numerous other proteins occupy space in the membrane. Also, quantification of PIN2-GFP in live epidermal cells of *Arabidopsis* root cells, observed using 3D structured illumination microscopy (SIM) with an x and y resolution of 106 nm and 104 nm respectively (Figure 3a), and an average acquisition speed faster than the average rate of endocytosis (see Methods & Table 4), showed that separated source-spots of GFP signal are always resolved with maximum density of $5.6\frac{\text{spots}}{\mu m^2}$ (Figure 3b). Each of the spot contains at least one PIN-GFP protein. However, most spots are large: mean area of the spots is 0.034 ± 0.002 μm^2, max area 0.098 μm^2, min area 0.01 μm^2 (corresponds to resolution limit). Thus, most spots are likely to contain many PINs, which together fill at most 1/5 part of the membrane area (as $5.6\frac{1}{\mu m^2} \cdot 0.034$ $\mu m^2 = 0.19$). This result argues that upper bound for the PIN density on PM is less than close-packing: $(\rho_{PM})_{max} \leq 4 \times 10^3 \frac{1}{\mu m^2}$. Correspondingly,

$$\left(\frac{\rho_v}{\rho_{PM}}\right)_{min} = \mathbf{0.01} \quad (2.2)$$

is a more realistic value of minimal PINs density ratio for epidermal root cells.

Box 3. How many IAA molecules should be inside of one vesicle?

Rewriting Equation (25) as inequality gives the accumulation ratio R, which is necessary for minimal PAT ($v_{PAT} = 1\frac{\mu m}{s}$):

$$R \geq \frac{\mathbf{v}_{min}\, S_v \cdot \tau_{\frac{1}{2}}}{V_v \cdot ln2}\left(\frac{\rho_v}{\rho_{PM}}\right)_{min} = \frac{1\frac{\mu m}{s}\, 2 \times 10^{-2}\mu m^2\, 1.3 \times 10^4\, s}{2.7 \times 10^{-4}\mu m^3 \cdot 0.69} 0.002 > 2800. \quad (3.1)$$

This minimal required accumulation ratio is valid for any A_c. Nevertheless, we have to check, that vesicles will contain at least one molecule. In the volume of a vesicle (maximum 2.7×10^5 nm^3) there will be initially $N_v^{t=0} = A_c \cdot V_v = 0.005$ molecules if cytoplasmic auxin concentration $A_c = 30$ nM, which is a plausible estimate for the root epidermis [29]. For the lowest possible accumulation ratio $R = 2800$, the number of molecules in one vesicle will be:

$$N_v = A_c \cdot V_v \cdot R \approx \mathbf{14}, \quad (3.2)$$

which is a minimal requirement for vesicular transport.

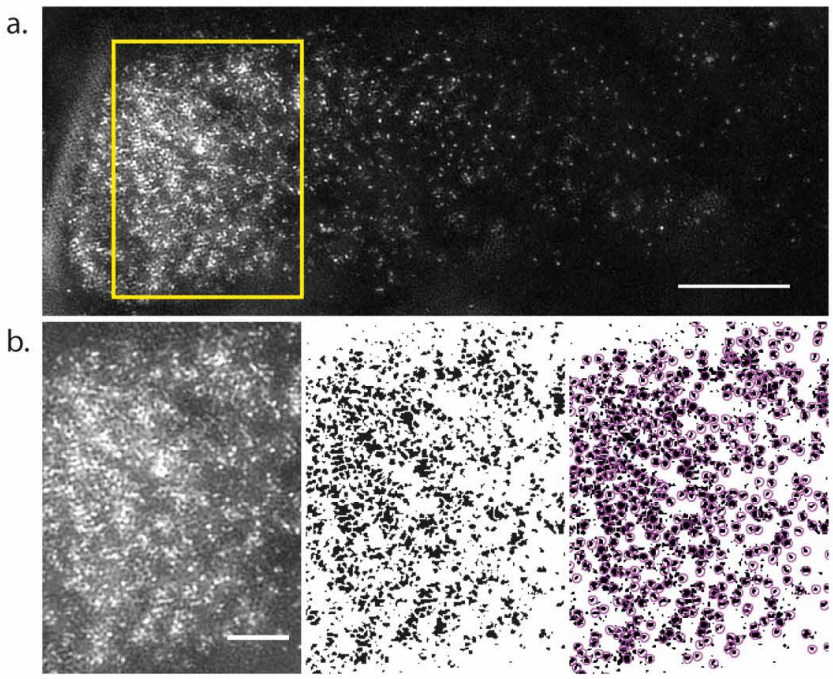


Figure 3. PIN2 translational fusion to Green Fluorescent Protein (PIN2-GFP) density measured by 3D structured illumination microscopy (SIM). (**a**) Example max projection of a 3D SIM image of the lateral membrane of root epidermal cells; (**b**) Left panel; the magnified yellow rectangle in (**a**). Middle panel; the image is made binary and subjected to watershed segmentation. Right panel; pink circles denote detected PIN2-GFP spots. Scale bars; (**a**), 5 μm, (**b**), 2 μm.

Table 4. Calculation of rate of endocytosis (based on values from [27,28]).

Endocytic Marker	DRP1C-GFP (Dynamin-Related Protein 1C-GFP)	CLC-GFP (Clathrin Light Chain-GFP)
foci per μm^2	3.54	3.48
standard deviation (SD)	0.62	0.55
average lifetime (s)	17.7	19.7
SD	8.8	6.8
foci per model cell (15 × 15 micron)	796.5	783
SD	139.5	123.75
Endocytosis events per cell per second	**DRP1C-GFP**	**CLC-GFP**
Average	45.0	39.7
max	105.2	70.3
min	24.8	24.9
Maximum rate of endocytosis per second per μm^2	**0.467**	**0.312**

2.3.1.2. Minimal Permeability of PINs in Vesicles Necessary for Vesicular Auxin Transport

By combining Equations (18) and (25) we can find the relation between vesicular PINs' permeability $P_{PIN}^{v\text{-}only}$ and the transport velocity v_{PAT} in the case that PINs are only active in vesicles and thus all PAT is produced by vesicles:

$$\frac{P_{PIN}^{v\text{-}only}}{P_{diff}^{IAAH}} \cdot \frac{f_{ac}}{1-f_{av}} + \frac{1-f_{ac}}{1-f_{av}} \geq \frac{v_{PAT}\, S_v \cdot \tau_{1/2}}{V_v \cdot ln2} \left(\frac{\rho_v}{\rho_{PM}}\right)_{min}. \quad (26)$$

Consequently,

$$P_{PIN}^{v\text{-}only} \geq P_{diff}^{IAAH}\left(\frac{\mathrm{v}_{PAT}\cdot S_v\cdot\tau_{1/2}}{V_v\cdot ln2}\left(\frac{\rho_v}{\rho_{PM}}\right)_{min}-\frac{1-f_{ac}}{1-f_{av}}\right)/\left(\frac{f_{ac}}{1-f_{av}}\right). \quad (27)$$

Thus, because $\frac{1-f_{ac}}{1-f_{av}} \leq 1$ can be neglected being much smaller than the first term $\frac{\mathrm{v}_{PAT}\cdot S_v\cdot\tau_{1/2}}{V_v\cdot ln2}\left(\frac{\rho_v}{\rho_{PM}}\right)_{min} \geq 10^4$,

$$P_{PIN}^{v\text{-}only} \geq P_{diff}^{IAAH}\cdot\frac{\mathrm{v}_{PAT}\cdot S_v\cdot\tau_{1/2}}{V_v\cdot ln2}\frac{(1-f_{av})}{f_{ac}}\left(\frac{\rho_v}{\rho_{PM}}\right)_{min}. \quad (28)$$

Grouping all parameters except v_{PAT} and $\left(\frac{\rho_v}{\rho_{PM}}\right)_{min}$ into constant K gives:

$$P_{PIN}^{v\text{-}only} \geq \mathrm{K}\cdot\mathrm{v}_{PAT}\cdot\left(\frac{\rho_v}{\rho_{PM}}\right)_{min}. \quad (29)$$

From Table 3 we find $min\left(\frac{1-f_{av}}{f_{ac}}\right) = 0.006$ for $pH_v = 7.0$, and using parameter values from Table 1, d = 0.08 μm, we calculate value:

$$\mathrm{K} = \left(\frac{P_{diff}^{IAAH}\cdot S_v\cdot\tau_{\frac{1}{2}}}{V_v\cdot ln2}\cdot\frac{1-f_{av}}{f_{ac}}\right)_{min} = \frac{10^2\cdot 6\cdot 1.3\cdot 10^4}{8\cdot 0.69}\cdot\frac{6\cdot 10^{-3}}{2} \cong 4240\,. \quad (30)$$

Using $\frac{\rho_v}{\rho_{PM}} = 0.01$ from Box 2, gives an estimate of the lower bound of PIN permeability in vesicles:

$$\boldsymbol{P_{PIN}^{v\text{-}only} \geq 42\cdot\mathrm{v}_{PAT}}\,. \quad (31)$$

For $pH_v < 7.0$ bounds for $\frac{P_{PIN}^{v\text{-}only}}{P_{diff}^{IAAH}}$ are provided in Table 3. For a pH value that we consider realistic, $pH_v = 6.2$ permeability has to be higher: $P_{PIN}^{v\text{-}only} \geq 260\cdot\mathrm{v}_{PAT}$.

2.3.1.3. Comparison to the Case when PINs are Active Only on the PM: Permeability due to PINs has to be Much Greater on the Vesicles than on PM to Produce the Same Auxin Transport Velocity

It would be informative to compare our estimate of the permeability value (Equation (30)) $P_{PIN}^{v\text{-}only} \geq \mathbf{42}\cdot\mathbf{v}_{PAT}$ with experimental measurements. Unfortunately, the permeability of PINs has never been measured directly in the intact tissues. Also measurements of the influx carrier permeability are not possible in explants like protoplasts, as PINs do not stay on the PM, but are instead internalized [18], resulting in no contribution to the efflux of auxin as in *in vivo* systems.

Fortunately, analogous estimates for PIN permeability have been done for the case when PINs are active only on the PM (see Box 4, [18]), which have shown that:

$$\boldsymbol{P_{PIN}^{PM\text{-}only} \simeq \mathrm{v}_{PAT}}. \quad (32)$$

This relation was proved in theoretical studies using simple mathematical models and confirmed by computational models of multicellular tissues (see Box 4). It is determined under the assumption that PINs are active only on the PMs and facilitate auxin transport without any action from vesicles. Consequently, in epidermal cells of *Arabidopsis* root $P_{PIN2}^{PM} \simeq 1$ μm/s .

We conclude from Equations (31) and (32) that if all other parameters are held in physiological range, to yield the same PAT velocity as PM PINs, vesicular PINs permeability has to be much higher: $\frac{P_{PIN}^{v\text{-}only}}{P_{PIN}^{PM\text{-}only}} \geq 42$. However, $P_{PIN}^{v\text{-}only}$ and $P_{PIN}^{PM\text{-}only}$ also depend on density of PINs on the membranes. To

clarify this issue, in the next section we calculated the ratio of PINs activity, which is characteristic of individual transporters and which does not depend on the densities of PINs.

Box 4. The permeability of PINs on the plasma membrane P_{PIN}^{PM} equals the directional auxin transport velocity $\mathbf{v}_{PAT}$.

P_{PIN}^{PM} can be derived from the following considerations, analogous to Equations (19)–(21). Auxin flux density due to PINs through the PM has the following expression because PINs are transporting anions IAA^- and depend only on its intracellular concentration $f_{ac} \cdot A_C$:

$$\Phi_{PM} = P_{PIN}^{PM} \cdot f_{ac} \cdot A_C, \tag{4.1}$$

that coincides with Equation (39).

It should be not lower than the PAT flux Equation (19): $\Phi_{PM} \geq \Phi_{cell \to apoplast}$, because other transport mechanisms, diffusion and non-polar transporters, are diminishing polar auxin transport velocity. The relationship between PAT velocity and the polar permeability accounting for the non-polar permeability was derived by Mitchison [17] (Equation (2)), which is discussed below in this box. Thus, an underestimate for P_{PIN}^{PM} is obtained by equating the directional transport to transport by PM-PINs:

$$P_{PIN}^{PM} \cdot f_{ac} \cdot A_C \geq \mathrm{v}_{PAT} \cdot A_c. \tag{4.2}$$

Moreover, non-polar term is at least 100 less than P_{PIN}^{PM}. Consequently, we can consider

$$P_{PIN}^{PM} \cdot f_{ac} = \mathrm{v}_{PAT}, \tag{4.3}$$

or, as $f_{ac} \cong 1$, for pH = 7

$$\boldsymbol{P_{PIN}^{PM} \cong \mathbf{v}_{PAT}}. \tag{4.4}$$

Thus, for $\mathrm{v}_{PAT} = 1$ μm/s, $P_{PIN}^{PM} \cong 1$ μm/s.

In fact, References [17,19] have shown that for a file of cells transport speed is comparable to the efflux permeability, and this conclusion was confirmed by computer simulations of multilayered tissues [17–19]. In these classical works, it has been proven that the "advection" of auxin can be just a result of combined polar membrane transport and cytoplasmic diffusion. Thus, macroscopic advection velocity is limited either by polar membrane transport or by the rate of auxin's transfer along the cell length; whichever value is lower. One can calculate that diffusion along the longest cell length (~100 μm) is faster than the measured velocity, proving that cytoplasmic transport does not limit the "macroscopic advection velocity v_{PAT}" [14]. In this case, polar membrane transport governs macroscopic velocity [17,19]. To show this, we provide derivation done by Mitchison [17].

Derivation of P_{PIN}^{PM} that would yield $\mathbf{v}_{PAT} =$ 1 μm/s from theory developed by Mitchison [17]:

Equation (2) from [17] reads:

$$\frac{1}{\mathrm{v}_{PAT}} = \frac{1}{p} + \left(1 + \frac{2q}{p}\right)\frac{L}{2D}, \tag{4.5}$$

where v_{PAT}—macroscopic auxin velocity, p—polar efflux permeability, q—non-polar permeability (by diffusion), L—cell length, D—diffusion coefficient of auxin inside the cell. Because $\frac{L}{2D} \leq \frac{1 \times 10^{-4}\,\mathrm{m}}{2 \cdot 6.7 \times \frac{10^{-10}\,\mathrm{m}^2}{\mathrm{s}}} = 7.46 \times 10^4$ s/m, $\mathrm{v}_{PAT} = 1 \times 10^{-6}$ m/s:

$$\boldsymbol{p = \frac{1 + 2q\frac{L}{2D}}{\frac{1}{\mathrm{v}_{PAT}} - \frac{L}{2D}} \geq 1.1 \cdot 10^{-6} m/s}. \tag{4.6}$$

This equation shows that the efflux permeability $p \cong \mathrm{v}_{PAT}$, because $2q\frac{L}{2D} \ll 1$ for realistic maximum value of $q = 10^{-6}$ m/s. Note, that condition $\frac{1}{\mathrm{v}_{PAT}} - \frac{L}{2D} \geq 0$ must hold, so that the value of permeability is positive, which is true for $\mathrm{v}_{PAT} \leq \frac{2D}{L} = 13.4 \times 10^{-6}$ m/s. The polar permeability value estimated in [17] is also in the order of $10^{-6} m/s$.

In principle, auxin-containing vesicles can also contribute to directional transport within the cell. However, as noted above, diffusion is already sufficient to transport auxin inside the cell, so such additional "acceleration" is not relevant for the macroscopic transport rate.

2.3.1.4. Individual Activity of PINs Has to Be Much Higher on the Vesicles than on the PM to Produce the Same Auxin Transport Velocity

To compare the efficiency of transport, it is necessary to normalize permeabilities $P_{PIN}^{v\text{-}only}$ and $P_{PIN}^{PM\text{-}only}$ to the corresponding density of PINs. Membrane permeability due to PINs is proportional to

the PINs' density and can be expressed as a product of 1) density of transporters on the membrane ρ_{PIN} $[\frac{\text{mol}}{\mu\text{m}^2}]$ and (2) individual activity of one transporter protein $p_{PIN}[\frac{\mu\text{m/s}}{\text{mol}/\mu\text{m}^2}]$, which depends on affinity to auxin, electrical potential across the membrane ([19]), phosphorylation status, and any other parameters.

$$P_{PIN} = \rho_{PIN} \cdot p_{PIN}. \tag{33}$$

The ratio of normalized permeabilities equals the ratio of the individual activity of PIN transporters situated in vesicles ($\boldsymbol{p_{v\text{-}only}}$) and on the PM ($\boldsymbol{p_{PM\text{-}only}}$): $\frac{p_{v\text{-}only}}{p_{PM\text{-}only}} = \frac{P_{PIN}^{v\text{-}only}}{\rho_v} \frac{\rho_{PM}}{P_{PIN}^{PM\text{-}only}}$.

Combining this equation and Equation (29) (equality form):

$$P_{PIN}^{v\text{-}only} = \mathrm{K} \cdot \mathrm{v}_{PAT} \frac{\rho_v}{\rho_{PM}} \tag{34}$$

gives:

$$\frac{p_{v\text{-}only}}{p_{PM\text{-}only}} = \frac{\mathrm{v}_{PAT} \cdot \mathrm{K}}{P_{PIN}^{PM\text{-}only}} \frac{\rho_v}{\rho_{PM}} \cdot \frac{\rho_{PM}}{\rho_v}. \tag{35}$$

Note that density ratio $\frac{\rho_v}{\rho_{PM}}$ cancels in this equation:

$$\frac{p_{v\text{-}only}}{p_{PM\text{-}only}} = \frac{\mathrm{v}_{PAT} \cdot \mathrm{K}}{P_{PIN}^{PM\text{-}only}}. \tag{36}$$

By calculating the minimum of the right-hand side and using the fact that $\mathrm{v}_{PAT} = P_{PIN}^{PM\text{-}only} \cdot f_{ac}$ (see Box 4), we can find the lower bound for the PINs activity ratio:

$$\frac{p_{v\text{-}only}}{p_{PM\text{-}only}} \geq \mathrm{K} \cdot f_{ac} \tag{37}$$

Introducing the minimal value of K (Equation (30)) and $f_{ac} = 0.994$:

$$\frac{\boldsymbol{p_{v\text{-}only}}}{\boldsymbol{p_{PM\text{-}only}}} > \mathbf{4200}. \tag{38}$$

For $pH_v = 6.2$, (see Table 3), the ratio is even higher: $\frac{p_{v\text{-}only}}{p_{PM\text{-}only}} > 26600$.

Conclusion I: For vesicle transport to be able to produce all of the observed IAA flux, the activity of PINs on the vesicle membrane has to be at least three orders of magnitude greater than that estimated for the case when PINs are only active on the PM. Our calculations show that transporting auxin directly through the PM is 1000 times more effective than by means of SVs. This, in our opinion, is an argument against SVs-mediated transport of auxin as a major mechanism of directional auxin transport.

2.3.2. PINs Active Both in Vesicles and on the PM

Next, we derived the expression for the ratio of auxin fluxes through both mechanisms in the case that PINs are active on vesicles and the PM. Auxin efflux density caused by (active) PINs on the PM is:

$$\Phi_{PM} = P_{PIN}^{PM} \cdot f_{ac} \cdot A_C. \tag{39}$$

Auxin efflux density caused by arriving PIN delivery vesicles (from Equation (20) using Equation (16) and omitting the term $\frac{1-f_{ac}}{1-f_{av}}$ as in Equation (28)):

$$\Phi_v = N_v \cdot F^+ \cong \frac{P_{PIN}^v}{P_{diff}^{IAAH}} \cdot \frac{f_{ac}}{1-f_{av}} \cdot V_v \cdot F^+ \cdot A_c. \tag{40}$$

Both effluxes are proportional to intracellular auxin concentration A_c, which is assumed to be the same at the PM and around SVs.

Dividing Equation (39) by Equation (40) gives the flux ratio:

$$\frac{\Phi_{PM}}{\Phi_v} = \frac{P_{PIN}^{PM} \cdot f_{ac} A_c}{\frac{P_{PIN}^{v}}{P_{diff}^{IAAH}} \cdot \frac{f_{ac}}{1-f_{av}} \cdot V_v \cdot F^+ \cdot A_c} = \frac{P_{PIN}^{PM}}{P_{PIN}^{v}} \cdot \frac{P_{diff}^{IAAH}(1-f_{av})}{V_v} \cdot \frac{1}{F^+}. \quad (41)$$

Using Equation (33),

$$\frac{\Phi_{PM}}{\Phi_v} = \frac{P_{diff}^{IAAH}(1-f_{av})}{V_v} \cdot \frac{1}{F^+} \frac{\rho_{PM}}{\rho_v} \cdot \frac{\boldsymbol{p_{PM}}}{\boldsymbol{p_v}}. \quad (42)$$

Substituting F^+ by its expression from Equation (1.7) gives:

$$\frac{\Phi_{PM}}{\Phi_v} = \frac{P_{diff}^{IAAH} \cdot (1-f_{av})}{V_v} \frac{\rho_v}{\rho_{PM}} \frac{S_v \cdot \tau_{1/2}}{ln2} \frac{\rho_{PM}}{\rho_v} \frac{\boldsymbol{p_{PM}}}{\boldsymbol{p_v}}, \quad (43)$$

where $\frac{\rho_v}{\rho_{PM}}$ cancel. Substituting with the constant K (Equation (30)) we reduce it further:

$$\frac{\Phi_{PM}}{\Phi_v} = K \cdot f_{ac} \cdot \frac{\boldsymbol{p_{PM}}}{\boldsymbol{p_v}}. \quad (44)$$

The coefficient here is the same as in Equation (38):

$$\frac{\Phi_{PM}}{\Phi_v} \geq \mathbf{4200} \cdot \frac{\boldsymbol{p_{PM}}}{\boldsymbol{p_v}}, \quad (45)$$

where $\frac{\boldsymbol{p_{PM}}}{\boldsymbol{p_v}}$ is the ratio of individual PINs activity on the PM and vesicles if PINs are active on both membranes. Note that the densities of PINs cancel out and flux distributions between the two mechanisms depend only on the activity of PINs. Also Equation (38) can be derived directly from Equation (45) by assuming $\frac{\Phi_{PM}}{\Phi_v} = 1$.

If the individual activity of PINs on the vesicle and on the PM are equal ($\boldsymbol{p_v} = \boldsymbol{p_{PM}}$), then,

$$\frac{\Phi_{PM}}{\Phi_v} \geq \mathbf{4200}, \quad (46)$$

which means that the flux through the vesicle mechanism does not contribute more than 0.02% to the total flux.

For $pH_v = 6.2$ the lower bound of the ratio is higher: $\frac{\Phi_{PM}}{\Phi_v} \geq 26600$, which implies that the contribution of the vesicular mechanism is less than 0.004%, which is negligibly small compared to PM flux.

The flux ratio $\frac{\Phi_{PM}}{\Phi_v}$ would be higher (favoring PM flux over SV-mediated flux) if:

- PINs half-life on the PM is higher;
- pH in the vesicle is lower;
- vesicles do not stay in the cytoplasm for long enough before fusing with the PM to be fully filled with IAA;
- the size of vesicles is smaller.

The opposite changes of parameter values would increase the SV-mediated contribution to the auxin flux (see Equation (43)).

Conclusion II: The activity of PIN transporters in the vesicle has to be at least 1000 times greater than on the PM to make a substantial contribution to the total directional auxin transport. When realistic physiological parameter values were used in the model, a factor greater than 10^4 was determined.

3. Discussion

The hypothesis of vesicular secretion of auxin was postulated more than 15 years ago [7,8]. While several studies have claimed to provide experimental evidence to support this concept since [9–11], their conclusions are currently greatly debated in the field [12,13]. Hence the question whether vesicular secretion significantly contributes to intercellular auxin transport remains unresolved. Here, we took a modeling approach to estimate whether such mode of auxin transport is even theoretically possible.

First, we compared individual activities of PINs active exclusively on vesicles or on the PM that are necessary to yield the same PAT velocity (Equations (37) and (38)):

$$\frac{p_{v\text{-}only}}{p_{PM\text{-}only}} \geq P_{diff}^{IAAH}\left(\frac{6\cdot\tau_{1/2}}{d\cdot ln2}\cdot\frac{1-f_{av}}{f_{ac}}\right)_{min}. \tag{47}$$

This ratio is valid for any PAT velocity and depends on the following measurable parameters: diameter of vesicles d, half-life time of PINs on the PM $\tau_{1/2}$, pH-dependent fraction of IAAH in a vesicle $(1-f_{av})$, fraction of IAA^- in cytoplasm f_{ac}. Experimental parameter values (Table 1) gave us $\frac{p_{v\text{-}only}}{p_{PM\text{-}only}} > 4200$, meaning that the individual activity of PINs on SVs (p_v) needs to be at least three orders of magnitude greater than the activity of PINs on the PM (p_{PM}) in order to produce the same auxin transport.

We also provide an estimate for the permeability of PINs in the vesicles required to yield $v_{PAT} = 1\frac{\mu m}{s}$ in epidermal root cells: $P_{PIN}^{v} \geq 42\frac{\mu m}{s}$, which is not the measure of individual transporters, but characteristic of the unit area of the membrane. This value is much higher than any measured permeabilities to date [18,24]. The measurements of permeability due to PINs either on the PM, in vesicles or in both domains will allow one to draw precise conclusions from our model.

Calculation of permeability P_{PIN}^{v} requires the knowledge of relative density of PINs proteins on vesicles and the PM. We provide measurement of PM density of PINs using SIM microscopy: $\rho_{PM} \leq 4\times10^{3}\frac{1}{\mu m^2}$, which gives an estimate of minimal possible density ratio: $\left(\frac{\rho_v}{\rho_{PM}}\right)_{min} = 0.01$ (Box 2).

Finally, we derived an expression that relates auxin flux driven by PINs on the polar domain of PM and auxin flux driven by PINs at the vesicles, if they are both active (Equation (43), using Equation (30)):

$$\frac{\Phi_{PM}}{\Phi_v} = \frac{P_{diff}^{IAAH}\cdot(1-f_{av})}{d}\cdot\frac{6\cdot\tau_{1/2}}{ln2}\cdot\frac{p_{PM}}{p_v}. \tag{48}$$

This shows that relative auxin fluxes through both mechanisms depend on: diameter of vesicles d, half-life time of PINs on the PM $\tau_{1/2}$, pH-dependent fraction of IAAH in a vesicle $(1-f_{av})$ and individual activities of PIN proteins p_{PM} and p_v.

The main parameter, namely PIN activity, has not been experimentally determined on the PM or in vesicles, which makes it impossible to find the actual ratio of fluxes *in vivo*. Nevertheless, by estimating the extreme values of the rest of parameters from available experimental data (Table 1), we were able to show that $\frac{\Phi_{PM}}{\Phi_v} > 4200\cdot\frac{p_{PM}}{p_v}$. This expression suggests that if PINs were equally active both at the PM and on the SVs, the contribution of secreted IAA to the overall net IAA flux would be less than 0.02% at pH = 7 inside vesicles of maximal size, which is the maximal possible contribution in that case.

Moreover, instead of the half-life time of PINs on the PM $\tau_{1/2}$ and vesicle diameter, other measurable parameters can be put in this equation (using Equation (1.7), as done in Equation (42)): exocytosis frequency F^+, densities of PINs $\rho_{v,PM}$, pH-dependent fraction of IAAH in a vesicle $(1-f_{av})$ and vesicular volume V_v:

$$\frac{\Phi_{PM}}{\Phi_v} = \frac{P_{diff}^{IAAH}(1-f_{av})}{V_v}\cdot\frac{1}{F^+}\frac{\rho_{PM}}{\rho_v}\frac{p_{PM}}{p_v}. \tag{49}$$

Interestingly, our theoretical estimate of maximum exocytosis rate Equation (1.7) coincides with experimentally measured maximum endocytosis rate: $F^{+}_{max} = 0.5\frac{vesicles}{\mu m^2\, s}$ (see end of Box 1), which provides additional confirmation that the chosen parameter ranges are plausible. Equation (49) shows that the restrictions on frequency of exocytosis is one of the factors that limits the capacity of vesicles to release auxin at a high rate. Also limiting for SV-mediated transport is the fact that the density of PINs on the vesicle membrane cannot be higher than the density of PINs on the PM, which is almost at its possible maximum.

Our assumptions and calculations are based on the model of a PIN2-expressing root epidermal cell. We cannot rule out that vesicular transport of auxin could prevail in different cell types or physiological contexts. However, all parameters in Equations (48) and (49) except PINs activities cannot have zero values, thus, they would have to be changed by orders of magnitude to make vesicular auxin transport the dominant mechanism, causing massive changes in cell homeostasis. Therefore, we consider this unlikely and assume that our conclusions can be extrapolated to any cell type. If experimental values of parameters in any other cell type become available in the future, our equations can be used to resolve this question.

If it was found that PINs transporters are active exclusively in vesicles and are inactive on the PM ($p_{PM} = 0$), Equations (48) and (49) would become meaningless. Then the testable relation between the individual activity of PINs and the measurable parameters is (from Equation (28)):

$$p_{v\text{-}only} = \frac{P^{v\text{-}only}_{PIN}}{\rho_v} = \frac{P^{IAAH}_{diff}}{\rho_{PM}} \cdot \frac{v_{PAT} \cdot 6 \cdot \tau_{1/2}}{d \cdot ln2} \frac{(1 - f_{av})}{f_{ac}}. \quad (50)$$

However, the individual activity of PINs remains a technically demanding value to determine experimentally. Moreover, SV localization of a member of the AGCVIII kinase family, the action of which is required for PIN activity [30], has not been reported, arguing that PINs in the SVs are possibly inactive [13]. An additional argument that PINs are active at the PM is that increasing PINs incidence at the cell surface, e.g., by inhibiting their endocytosis leads to increased auxin efflux [31,32]. Overall, methods for separate measurement or perturbation of parameters in Equations (48) and (49) are needed to unambiguously distinguish between vesicular-mediated and PM-mediated auxin fluxes.

In conclusion, we have created a simple mathematical model to calculate the efficiency of PIN-mediated vesicular secretion of auxin compared to transport across the PM. Even under the most "vesicular transport-favoring" values of the parameters the vesicular transport of auxin was still determined to be several orders of magnitude less efficient compared to the membrane transport. Our calculations showed that PINs on the PM can produce auxin transport having much less individual activity than required for PINs in the secretory vesicles (SVs). Therefore, we consider it unlikely that PINs are active only in the secretory vesicles; and in case they are active on both PM and SVs, vesicular transport would play a negligible role in PAT.

4. Materials and Methods

Measurement of PIN Density Using Structured Illumination Microscopy (SIM)

Live *Arabidopsis* roots samples were prepared as previously described by Johnson and Vert [26], where the imaging media was supplemented with 30% opti-prep and the coverslips were fixed on to the microscope slide. Cells in the elongation zone were imaged using an OMX BLAZE v4 3D SIM (Applied Precision). A 60 × 1.42 NA Oil Immersion objective and a 100 mw 488 nm laser was used. The microscope was aligned and calibrated using 100 nm tetra spark beads (Thermo Scientific) and found to have a working resolution of 106 nm and 104 nm in the x and y dimension and 336.9 nm in the z dimension. This SIM system was used due to its enhanced speed of acquisition, when compared to other systems, in order to minimize the effect of rapidly recycling proteins during acquisition. To overcome the curved and non-uniform shape of the roots, Z-stacks (with an optimal z spacing of 125 nm) were created to image the entire lateral membrane of the PIN2 polar domain. This is

particularly important when imaging the lateral membrane next to the apical face of the cell, as it curves away from the coverslip. Depending on the shape of the cell, 1.625–3 µm stacks were made of each cell to ensure the entire lateral membrane region was captured, with an average acquisition time for the total z-stack of 17.7 s, with each z position having an average dwell time of 1.08 s. Each z-position image is based on 15 images generated from 3 different angles and 5 different SIM patterns using SOFTWORX software (Applied Precision). A maximum projection of the stacks was used for analysis. Images were made binary and subjected to watershed segmentation using Fiji [33]. PIN2-GFP spots were then detected using TrackMate [34]. The density of PIN2-GFP, mean, and maximum and minimum area of the PIN2-GFP spots were calculated from 12,343 spots in 9 different cells from 3 independent roots.

Author Contributions: Conceptualization, S.H., M.G. and J.F.; Methodology, S.H., M.A., A.J.; Formal Analysis, S.H., M.A.; Investigation, S.H., M.A., M.G., A.J.; Visualization, S.H., A.J.; Funding Acquisition, S.H., J.F.; Writing—Original Draft Preparation, M.A., M.G.; Writing—Review and Editing, S.H., M.A., M.G., A.J. and J.F.

Funding: European Research Council (ERC): 742985 to Jiri Friml; M.A. was supported by the Austrian Science Fund (FWF) (M2379-B28); AJ was supported by the Austria Science Fund (FWF): I03630 to Jiri Friml.

Acknowledgments: We cordially thank František Baluška, Kees Boot, Bert van Duijn, Geneviève Hines, Kees Libbenga and Eric Kramer for their valuable input to the initial discussions that led to this work. These took place at the "Quantitative Biology of Auxin Transport" workshop at the Lorentz Center, Leiden, Netherlands, 12–16 January 2015, and we would therefore also like to acknowledge the organizers of this workshop. We acknowledge the Advanced Microscopy Facility (advMICRO) of the Vienna Biocenter Core Facilities (VBCF), member of the Vienna Biocenter (VBC) Austria, for use of the OMX v4 3D SIM microscope and Lijuan Zhang for her technical assistance. We thank Ivan Kulik for comments on the manuscript.

Conflicts of Interest: The authors declare no conflict of interest.

Abbreviations

PM	Plasma membrane
SV	Secretory vesicle
IAA	Indole-3-acetic acid = auxin
PINs	PIN-formed transporters
TGN/EE	Trans-Golgi network/ early endosome

References

1. Adamowski, M.; Friml, J. PIN-Dependent Auxin Transport: Action, Regulation, and Evolution. *Plant Cell* **2015**, *27*, 20–32. [CrossRef] [PubMed]
2. Kleine-Vehn, J.; Langowski, L.; Wisniewska, J.; Dhonukshe, P.; Brewer, P.B.; Friml, J. Cellular and Molecular Requirements for Polar PIN Targeting and Transcytosis in Plants. *Mol. Plant* **2008**, *1*, 1056–1066. [CrossRef] [PubMed]
3. Zhou, J.-J.; Luo, J. The PIN-FORMED Auxin Efflux Carriers in Plants. *Int. J. Mol. Sci.* **2018**, *19*, 2759. [CrossRef] [PubMed]
4. Geldner, N.; Friml, J.; Stierhof, Y.-D.D.; Jürgens, G.; Palme, K. Auxin Transport Inhibitors Block PIN1 Cycling and Vesicle Trafficking. *Nature* **2001**, *413*, 425–428. [CrossRef] [PubMed]
5. Dhonukshe, P.; Aniento, F.; Hwang, I.; Robinson, D.G.; Mravec, J.; Stierhof, Y.-D.D.; Friml, J.J. Clathrin-Mediated Constitutive Endocytosis of PIN Auxin Efflux Carriers in Arabidopsis. *Curr. Biol.* **2007**, *17*, 520–527. [CrossRef] [PubMed]
6. Adamowski, M.; Narasimhan, M.; Kania, U.; Glanc, M.; De Jaeger, G.; Friml, J. A Functional Study of AUXILIN-LIKE1 and 2, Two Putative Clathrin Uncoating Factors in Arabidopsis. *Plant Cell* **2018**. [CrossRef] [PubMed]
7. Friml, J.; Palme, K. Polar Auxin Transport—Old Questions and New Concepts? *Plant Mol. Biol.* **2002**, *49*, 273–284. [CrossRef] [PubMed]
8. Baluška, F.; Šamaj, J.; Menzel, D. Polar Transport of Auxin: Carrier-Mediated Flux across the Plasma Membrane or Neurotransmitter-like Secretion? *Trends Cell Biol.* **2003**, *13*, 282–285. [CrossRef]

9. Mancuso, S.; Marras, A.M.; Mugnai, S.; Schlicht, M.; Zársky, V.; Li, G.; Song, L.; Xue, H.-W.; Baluska, F. Phospholipase Dzeta2 Drives Vesicular Secretion of Auxin for Its Polar Cell-Cell Transport in the Transition Zone of the Root Apex. *Plant Signal. Behav.* **2007**, *2*, 240–244. [CrossRef] [PubMed]
10. Mettbach, U.; Strnad, M.; Mancuso, S.; Baluška, F. Immunogold-EM Analysis Reveal Brefeldin a-Sensitive Clusters of Auxin in Arabidopsis Root Apex Cells. *Commun. Integr. Biol.* **2017**, *10*, e1327105. [CrossRef] [PubMed]
11. Schlicht, M.; Strnad, M.; Scanlon, M.J.; Mancuso, S.; Hochholdinger, F.; Palme, K.; Volkmann, D.; Menzel, D.; Baluska, F. Auxin Immunolocalization Implicates Vesicular Neurotransmitter-like Mode of Polar Auxin Transport in Root Apices. *Plant Signal. Behav.* **2006**, *1*, 122–133. [CrossRef] [PubMed]
12. Alpi, A.; Amrhein, N.; Bertl, A.; Blatt, M.R.; Blumwald, E.; Cervone, F.; Dainty, J.; De Michelis, M.I.; Epstein, E.; Galston, A.W.; et al. Plant Neurobiology: No Brain, No Gain? *Trends Plant Sci.* **2007**, *12*, 135–136. [CrossRef] [PubMed]
13. Robinson, D.G.; Hawes, C.; Hillmer, S.; Jürgens, G.; Schwechheimer, C.; Stierhof, Y.-D.; Viotti, C. Auxin and Vesicle Traffic. *Plant Physiol.* **2018**, *176*, 1884–1888. [CrossRef] [PubMed]
14. Kramer, E.M.; Rutschow, H.L.; Mabie, S.S. AuxV: A Database of Auxin Transport Velocities. *Trends Plant Sci.* **2011**, *16*, 461–463. [CrossRef] [PubMed]
15. Petrášek, J.; Friml, J. Auxin Transport Routes in Plant Development. *Development* **2009**, *136*, 2675–2688. [CrossRef] [PubMed]
16. Rashotte, A.M.; Poupart, J.; Waddell, C.S.; Muday, G.K. Transport of the Two Natural Auxins, Indole-3-Butyric Acid and Indole-3-Acetic Acid, in Arabidopsis. *Plant Physiol.* **2003**, *133*, 761–772. [CrossRef] [PubMed]
17. Mitchison, G.J. The Dynamics of Auxin Transport. *Proc. R. Soc. B Biol. Sci.* **1980**, *209*, 489–511. [CrossRef]
18. Rutschow, H.L.; Baskin, T.I.; Kramer, E.M. The Carrier AUXIN RESISTANT (AUX1) Dominates Auxin Flux into Arabidopsis Protoplasts. *New Phytol.* **2014**, *204*, 536–544. [CrossRef] [PubMed]
19. Goldsmith, M.H.; Goldsmith, T.H.; Martin, M.H. Mathematical Analysis of the Chemosmotic Polar Diffusion of Auxin through Plant Tissues. *Proc. Natl. Acad. Sci. USA* **1981**, *78*, 976–980. [CrossRef] [PubMed]
20. Pimpl, P.; Movafeghi, A.; Coughlan, S.; Denecke, J.; Hillmer, S.; Robinson, D.G. In Situ Localization and in Vitro Induction of Plant COPI-Coated Vesicles. *Plant Cell* **2000**, *12*, 2219–2236. [CrossRef] [PubMed]
21. Luo, Y.; Scholl, S.; Doering, A.; Zhang, Y.; Irani, N.G.; Di Rubbo, S.; Neumetzler, L.; Krishnamoorthy, P.; Van Houtte, I.; Mylle, E.; et al. V-ATPase Activity in the TGN/EE Is Required for Exocytosis and Recycling in Arabidopsis. *Nat. Plants* **2015**, *1*, 15094. [CrossRef] [PubMed]
22. Shen, J.; Zeng, Y.; Zhuang, X.; Sun, L.; Yao, X.; Pimpl, P.; Jiang, L. Organelle PH in the Arabidopsis Endomembrane System. *Mol. Plant* **2013**, *6*, 1419–1437. [CrossRef] [PubMed]
23. Jásik, J.; Boggetti, B.; Baluška, F.; Volkmann, D.; Gensch, T.; Rutten, T.; Altmann, T.; Schmelzer, E. PIN2 Turnover in Arabidopsis Root Epidermal Cells Explored by the Photoconvertible Protein Dendra2. *PLoS ONE* **2013**, *8*, e61403. [CrossRef] [PubMed]
24. Delbarre, A.; Muller, P.; Imhoff, V.; Guern, J. Comparison of Mechanisms Controlling Uptake and Accumulation of 2,4-Dichlorophenoxy Acetic Acid, Naphthalene-1-Acetic Acid, and Indole-3-Acetic Acid in Suspension-Cultured Tobacco Cells. *Planta* **1996**, *198*, 532–541. [CrossRef] [PubMed]
25. Swarup, R.; Kramer, E.M.; Perry, P.; Knox, K.; Leyser, H.M.O.; Haseloff, J.; Beemster, G.T.S.S.; Bhalerao, R.; Bennett, M.J.; Leyser, O.; et al. Root Gravitropism Requires Lateral Root Cap and Epidermal Cells for Transport and Response to a Mobile Auxin Signal. *Nat. Cell Biol.* **2005**, *7*, 1057–1065. [CrossRef] [PubMed]
26. Johnson, A.; Vert, G. Single Event Resolution of Plant Plasma Membrane Protein Endocytosis by TIRF Microscopy. *Front. Plant Sci.* **2017**, *8*, 612. [CrossRef] [PubMed]
27. Konopka, C.A.; Bednarek, S.Y. Comparison of the Dynamics and Functional Redundancy of the Arabidopsis Dynamin-Related Isoforms DRP1A and DRP1C during Plant Development. *Plant Physiol.* **2008**, *147*, 1590–1602. [CrossRef] [PubMed]
28. Konopka, C.A.; Backues, S.K.; Bednarek, S.Y. Dynamics of Arabidopsis Dynamin-Related Protein 1C and a Clathrin Light Chain at the Plasma Membrane. *Plant Cell Online* **2008**, *20*, 1363–1380. [CrossRef] [PubMed]
29. Fendrych, M.; Akhmanova, M.; Merrin, J.; Glanc, M.; Hagihara, S.; Takahashi, K.; Uchida, N.; Torii, K.U.; Friml, J. Rapid and Reversible Root Growth Inhibition by TIR1 Auxin Signalling. *Nat. Plants* **2018**, *4*, 453–459. [CrossRef] [PubMed]

30. Zourelidou, M.; Absmanner, B.; Weller, B.; Barbosa, I.C.; Willige, B.C.; Fastner, A.; Streit, V.; Port, S.A.; Colcombet, J.; de la Fuente van Bentem, S.; et al. Auxin Efflux by PIN-FORMED Proteins Is Activated by Two Different Protein Kinases, D6 PROTEIN KINASE and PINOID. *Elife* **2014**, *3*, e02860. [CrossRef] [PubMed]
31. Paciorek, T.; Zazímalová, E.; Ruthardt, N.; Petrásek, J.; Stierhof, Y.-D.; Kleine-Vehn, J.; Morris, D.A.; Emans, N.; Jürgens, G.; Geldner, N.; et al. Auxin Inhibits Endocytosis and Promotes Its Own Efflux from Cells. *Nature* **2005**, *435*, 1251–1256. [CrossRef] [PubMed]
32. Simon, S.; Kubeš, M.; Baster, P.; Robert, S.; Dobrev, P.I.; Friml, J.; Petrášek, J.; Zažímalová, E. Defining the Selectivity of Processes along the Auxin Response Chain: A Study Using Auxin Analogues. *New Phytol.* **2013**, *200*, 1034–1048. [CrossRef] [PubMed]
33. Schindelin, J.; Arganda-Carreras, I.; Frise, E.; Kaynig, V.; Longair, M.; Pietzsch, T.; Preibisch, S.; Rueden, C.; Saalfeld, S.; Schmid, B.; et al. Fiji: An Open-Source Platform for Biological-Image Analysis. *Nat. Methods* **2012**, *9*, 676–682. [CrossRef] [PubMed]
34. Tinevez, J.-Y.; Perry, N.; Schindelin, J.; Hoopes, G.M.; Reynolds, G.D.; Laplantine, E.; Bednarek, S.Y.; Shorte, S.L.; Eliceiri, K.W. TrackMate: An Open and Extensible Platform for Single-Particle Tracking. *Methods* **2017**, *115*, 80–90. [CrossRef] [PubMed]



© 2018 by the authors. Licensee MDPI, Basel, Switzerland. This article is an open access article distributed under the terms and conditions of the Creative Commons Attribution (CC BY) license (http://creativecommons.org/licenses/by/4.0/).

9.5 Contributions to manuscripts

A Functional Study of AUXILIN-LIKE1 and 2, Two Putative Clathrin Uncoating Factors in Arabidopsis. *Adamowski, M., Narasimhan, M., Kania, U.,* ***Glanc, M****., De Jaeger, G., and Friml, J.* Plant Cell 30, 700–716 (2018)

I designed, performed and analyzed the experiments presented in Figures 5D, S2B, S5, S6 and S8. I also participated in designing the experiment presented in Figure 4B.

Mechanistic framework for cell-intrinsic re-establishment of PIN2 polarity after cell division. ***Glanc, M****., Fendrych, M., and Friml, J.* Nature Plants, in press (2018)

I designed all experiments with valuable contributions from M.F. and J.F. I performed all experiments and analyzed the data, with the exception of statistical analysis presented in Figure S6, which was done by M.F. I assembled the figures and wrote the manuscript with substantial input from M.F. and J.F.

Generation of PIN2 polarity in the absence of functional cytoskeleton. ***Glanc, M****., Fendrych, M., and Friml, J.* In preparation

I designed all experiments with input from M.F. and J.F. I performed and analyzed all experiments except for statistical analysis in Fig. 1g, which was done by M.F. I wrote the manuscript with input from M.F. and J.F.

Arabidopsis MAB4/MEL proteins mediate PIN polarity maintenance and root gravitropism by reducing PIN lateral diffusion. ***Glanc, M****., Domjan, D., Abas, L., Hörmayer L., Včelařová, L., Hauschild, R., Tan, S., Rodriguez-Solovey, L., Fendrych, M., and Friml, J.* In preparation

I designed, performed and analyzed all experiments with the following exceptions: molecular cloning (performed in cooperation with D.D. and L.V.); Fig. 2c (designed in cooperation with D.D. and S.T., performed and analyzed by D.D.); Fig. 2d-e (analyzed in cooperation with R.H.); Fig. S1a-b (performed and analyzed by D.D.); Fig. S1c (designed in cooperation with M.F.); Fig. S2a (designed, performed and analyzed by L.A.), Fig. S2b-c (designed in cooperation with D.D. and L.R.-S., performed in cooperation with D.D., analyzed in cooperation with R.H.). I assembled the figures and together with J.F. wrote the manuscript.

Strong morphological defects in conditional Arabidopsis abp1 knock-down mutants generated in absence of functional ABP1 protein. *Michalko, J.*,* ***Glanc, M****.*, Perrot-Rechenmann, C., and Friml, J.* F1000Research 5, 86 (2016) *Equal contributions

I participated in designing the experiments. J.M. and I contributed equally to performing the experiments and analyzing data. I assembled the figures. I contributed to writing the manuscript equally to J.M., with substantial contributions from C.P.-R. and J.F.

Gibberellin DELLA signaling targets the retromer complex to redirect protein trafficking to the plasma membrane. *Salanenka, Y., Verstraeten, I., Löfke, C., Tabata, K., Naramoto, S.,* ***Glanc, M.****, and Friml, J.* Proc. Natl. Acad. Sci. 115, 3716–3721 (2018)

I generated the line and participated in designing the experiments presented in Figure S3c-e. I contributed to finalizing the figures and text during revision.

Rapid and reversible root growth inhibition by TIR1 auxin signaling. *Fendrych, M., Akhmanova, M., Merrin, J.,* ***Glanc, M.****, Hagihara, S., Takahashi, K., Uchida, N., Torii, K.U., and Friml, J.* Nat. Plants 4, 453-459 (2018)

I performed and analyzed the experiments presented in Fig. 3b,c and contributed to finalizing the manuscript.

Relative contribution of PIN-containing secretory vesicles and plasma membrane PINs to the directed auxin transport: theoretical estimation. *Hille, S.*, Akhmanova, M.*,* ***Glanc, M.****, Johnson, A., and Friml., J.* IJMS 19, 3566 (2018) *Equal contributions

I participated in conceiving the rationale of the model and determining the parameter values to be used. I wrote the Abstract, Introduction and part of the Discussion sections with contributions from all authors and contributed to finalizing the manuscript.

9.6 Curriculum Vitae

Personal information

Born 4.1.1988 in Prague, Czech Republic; married, one child born 2017

matous.glanc@gmail.com; +420 777 086 826

Education

2014 – 2019: PhD in Plant Physiology and Cell Biology

Faculty of Science, Charles University; supervisor prof. Jiří Friml

2012 –2013: ERASMUS practical internship

Karlsruhe Institute of Technology, supervisor prof. Peter Nick

2009 – 2014: MSc in Plant Physiology and Cell Biology

Faculty of Science, Charles University; supervisor ass. prof. Viktor Žárský

1999 – 2007: High school

PORG - elite private high school in Prague

2002 – 2003: Exchange year in USA

Urban Academy - progressive high school in New York City, NY

Employment

2014 - 2019: IST Austria

Institue of Science and Technology Austria

External PhD student in the Friml group (Developmental and Cell Biology of Plants)

2011 –2014: Jules a Jim, o.s.

NGO focused on primary prevention, experiential education and teambuilding

Experiential education instructor; 2013-2014 Production and event manager

2009 –2014: Ramus, o.s.

NGO focused on free time activities for young people with special needs

Co-founder and project coordinator; 2009 – 2012 chariman

Awards & Fellowships

Poster prize New Phytologist Next Generations Scientists Symposium, 2017

AKTION scholarship Austria- Czech Republic, 2016

OEAD scholarship for undergraduates, graduates and postgraduates, 2015

Summa cum laude graduation, 2014

Publications

Glanc, M., Fendrych, M., and Friml, J. *Mechanistic framework for cell-intrinsic re-establishment of PIN2 polarity after cell division.* Nature Plants 2018, *in press*

Hille, S.*, Akhmanova, M.*, **Glanc, M**., Johnson, A., and Friml., J. *Relative Contribution of PIN-Containing Secretory Vesicles and Plasma Membrane PINs to the Directed Auxin Transport: Theoretical Estimation.* IJMS 2018
* equal contributions

Fendrych, M., Akhmanova, M., Merrin, J., **Glanc, M.**, Hagihara, S., Takahashi, K., Uchida, N., Torii, K.U., and Friml, J. *Rapid and reversible root growth inhibition by TIR1 auxin signalling.* Nature Plants, 2018

Adamowski, M., Narasimhan, M., Kania, U., **Glanc, M.**, De Jaeger, G., and Friml, J. *A Functional Study of AUXILIN-LIKE1 and 2, Two Putative Clathrin Uncoating Factors in Arabidopsis.* Plant Cell, 2018

Salanenka, Y., Verstraeten, I., Löfke, C., Tabata, K., Naramoto, S., **Glanc, M.**, and Friml, J. *Gibberellin DELLA signaling targets the retromer complex to redirect protein trafficking to the plasma membrane.* PNAS, 2018

Michalko, J.*, **Glanc, M.***, Perrot-Rechenmann, C., and Friml, J. *Strong morphological defects in conditional Arabidopsis abp1 knock-down mutants generated in absence of functional ABP1 protein.* F1000Research, 2016
*** equal contributions**

Kulich, I., Vojtíková, Z., **Glanc, M.**, Ortmannová, J., Rasmann, S., and Žárský, V. *Cell Wall Maturation of Arabidopsis Trichomes Is Dependent on Exocyst Subunit EXO70H4 and Involves Callose Deposition.* Plant Physiology, 2015

Conference presentations

ENPER Vienna 2018, *poster*

ACPD Prague 2018, *oral presentation*

ENPER Prague 2017, *oral presentation*

New Phytologist Next Generation Scientists Norwich 2017; *poster*

Auxin Get-together Brno 2016; *oral presentation*

ENPER Bordeaux 2016; *oral presentation*

Quantitative Biology of Auxin Transport Leiden 2015; *oral presentation*

ENPER Lecce 2014; *poster*

New Phytologist Next Generation Scientists Norwich 2014; *poster*